THE CYTOSKELETON IN T CELL MIGRATION AND ACTIVATION

EDITED BY: Jerome Delon, Manish Butte and Jens Volker Stein
PUBLISHED IN: Frontiers in Immunology

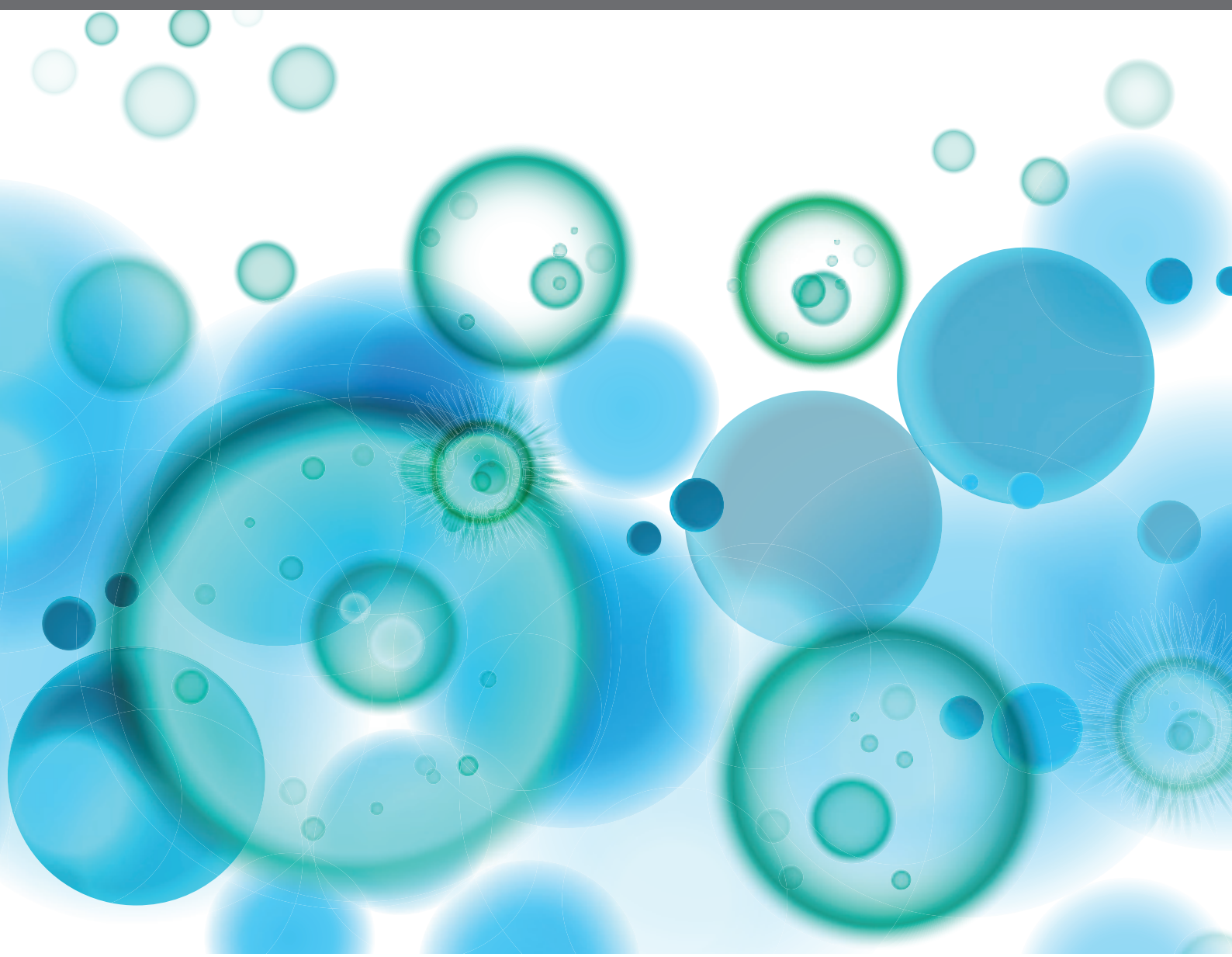

frontiers Research Topics

frontiers

ISSN 1664-8714
ISBN 978-2-83250-625-7
DOI 10.3389/978-2-83250-625-7

About Frontiers

Frontiers is more than just an open-access publisher of scholarly articles: it is a pioneering approach to the world of academia, radically improving the way scholarly research is managed. The grand vision of Frontiers is a world where all people have an equal opportunity to seek, share and generate knowledge. Frontiers provides immediate and permanent online open access to all its publications, but this alone is not enough to realize our grand goals.

Frontiers Journal Series

The Frontiers Journal Series is a multi-tier and interdisciplinary set of open-access, online journals, promising a paradigm shift from the current review, selection and dissemination processes in academic publishing. All Frontiers journals are driven by researchers for researchers; therefore, they constitute a service to the scholarly community. At the same time, the Frontiers Journal Series operates on a revolutionary invention, the tiered publishing system, initially addressing specific communities of scholars, and gradually climbing up to broader public understanding, thus serving the interests of the lay society, too.

Dedication to Quality

Each Frontiers article is a landmark of the highest quality, thanks to genuinely collaborative interactions between authors and review editors, who include some of the world's best academicians. Research must be certified by peers before entering a stream of knowledge that may eventually reach the public - and shape society; therefore, Frontiers only applies the most rigorous and unbiased reviews.
Frontiers revolutionizes research publishing by freely delivering the most outstanding research, evaluated with no bias from both the academic and social point of view. By applying the most advanced information technologies, Frontiers is catapulting scholarly publishing into a new generation.

What are Frontiers Research Topics?

Frontiers Research Topics are very popular trademarks of the Frontiers Journals Series: they are collections of at least ten articles, all centered on a particular subject. With their unique mix of varied contributions from Original Research to Review Articles, Frontiers Research Topics unify the most influential researchers, the latest key findings and historical advances in a hot research area! Find out more on how to host your own Frontiers Research Topic or contribute to one as an author by contacting the Frontiers Editorial Office: frontiersin.org/about/contact

THE CYTOSKELETON IN T CELL MIGRATION AND ACTIVATION

Topic Editors:
Jerome Delon, INSERM U1016 Institut Cochin, France
Manish Butte, University of California, Los Angeles, United States
Jens Volker Stein, Université de Fribourg, Switzerland

Citation: Delon, J., Butte, M., Stein, J. V., eds. (2022). The Cytoskeleton in T Cell Migration and Activation. Lausanne: Frontiers Media SA.
doi: 10.3389/978-2-83250-625-7

Table of Contents

frontiers | Frontiers in Immunology

TYPE Editorial
PUBLISHED 14 October 2022
DOI 10.3389/fimmu.2022.1057533

OPEN ACCESS

EDITED AND REVIEWED BY
Eilon Sherman,
Hebrew University of Jerusalem, Israel

*CORRESPONDENCE
Jérôme Delon
jerome.delon@inserm.fr

SPECIALTY SECTION
This article was submitted to T Cell Biology, a section of the journal Frontiers in Immunology

RECEIVED 29 September 2022
ACCEPTED 06 October 2022
PUBLISHED 14 October 2022

CITATION
Butte MJ, Stein JV and Delon J (2022) Editorial: The cytoskeleton in T cell migration and activation. *Front. Immunol.* 13:1057533. doi: 10.3389/fimmu.2022.1057533

Editorial: The cytoskeleton in T cell migration and activation

Manish J. Butte[1], Jens V. Stein[2] and Jérôme Delon[3]*

[1]Department of Pediatrics, David Geffen School of Medicine, University of California, Los Angeles, Los Angeles, CA, United States, [2]Department of Oncology, Microbiology and Immunology, University of Fribourg, Fribourg, Switzerland, [3]Université Paris Cité, Institut Cochin, Inserm, Centre National de la Recherche Scientifique (CNRS), Paris, France

KEYWORDS

T cells, migration, activation, cytoskeleton, Rho (Rho GTPase), mechanical properties

Editorial on the Research Topic
The cytoskeleton in T cell migration and activation

Cytoskeletal elements and factors that regulate them are necessary for proper T cell-mediated immune responses. In this Research Topic, we gather reviews and original articles that emphasise the signalling pathways and mechanisms that regulate the T cell cytoskeleton during migration and activation.

One of the major signalling pathways that regulates the cytoskeleton are small GTPases of the Rho family (1). Although the roles of RhoA, Rac1 and Cdc42 in actin polymerization have been first reported in fibroblasts thirty years ago, the involvement of other less studied Rho members, including in immune cells, is less clear. In this Research Topic, Mokhtar et al. review the role of RhoG in T cells and provide evidence based on human patients devoid of RhoG function for a negative role of RhoG in T cell activation. Furthermore, Rho GTPases are activated by guanine nucleotide exchange factors (GEFs) such as DOCK2, which is the major Rac activator in T cells stimulated by the chemokine receptor CCR7. Here, Thelen et al. show that CCR7-driven intranodal T cell motility also involves to a minor extent the Tec kinase Itk downstream of PI3Kγ, whereas it does not require the Rac GEF Tiam1. Finally, the role of Rho GTPases in T cell biology extends far beyond their impact on actin polymerization, since they also control the activities of the actin cross-linkers ezrin/radixin/moesin (ERM) proteins. Moesin is the main member of this family expressed in T cells and a particular missense variant is responsible for a primary immunodeficiency disease in humans. In order to better understand the origin of this pathology, Avery et al. report here a mouse model of X-linked moesin-associated immunodeficiency (X-MAID) that shows severe defects in thymic T cell maturation and motility in response to sphingosine-1-phosphate but not in response to CCR7.

Two additional articles focus more specifically on proteins that increase actin polymerization downstream the LAT and SLP76 signalosomes triggered upon T-cell receptor engagement. First, Waldman et al. study Enabled/vasodilator-stimulated phosphoprotein (Ena/VASP) proteins which are a family of cytoskeletal effector proteins responsible for actin polymerization. Ena/VASP proteins contribute to T cell actin remodelling during T cell-APC interactions, which promotes the initiation of stable

T cell conjugates during APC scanning. Therefore, Ena/VASP proteins are required for efficient activation and expansion of T cells *in vivo*. Second, Joshi and Morley summarise how the actin-bundling protein L-plastin (LPL) regulates T-cell activation and migration. LPL enhances F-actin polymerization and also directly binds to the β2 chain of the integrin LFA-1 to support intercellular adhesion and immunological synapse (IS) formation in human and murine T cells. T cells lacking LPL migrate slowly in response to chemoattractants such as CXCL12 and CCL19, and poorly polarise towards ICAM-1. Loss of LPL also impairs thymic egress and motility within lymph nodes. Thus, different actin modulators exhibit some degrees of redundancy to favour actin polymerisation and control the triggering of immune responses.

Furthermore, one particular property of T cells essential to fulfil their functions is their ability to polarise receptors, cytoskeletal components and organelles towards the antigen-presenting cell during assembly of the IS. In this Research Topic, Cassioli and Baldari review recent evidence regarding the presence of a puzzling network of actin filaments that surrounds the centrosome in resting T cells. Upon T-cell activation, centrosomal actin is depleted, allowing for centrosome detachment from the nucleus and its polarisation towards the immune synapse. This work reviews the clearance of actin by a centrosome-associated proteasome and the Bardet-Biedl syndrome 1 (BBS1) protein. In addition, González-Mancha et al. also report a role for the Sorting nexin 27 (SNX27) protein in centrosome and secretory machinery translocation to the immune synapse. In the absence of SNX27 expression, T cells show marked alteration in cytoskeleton architecture including a failure in the organisation of the microtubule network and defects in actin clearance at the IS. The possibility of a cooperation between BBS1 and SNX27 in order to regulate the same cytoskeletal phenomena remains elusive. Nevertheless, the polarity process that builds up during IS formation allows amplification and compartmentalization of signals in T-cell activation. As reviewed by Molon et al., the actin cytoskeleton together with CD28 and chemokine receptors play major roles in these events.

More recently, because the cytoskeleton can be considered as a soft material that confers cells a particular rigidity, physicists have been attracted towards this field and have thus embarked in studying the mechanical properties of immune cells using new tools and quantitative methods (2). In this Research Topic, Mustapha et al. introduce the method of Traction Force Microscopy for studying the forces that T cells apply onto their surrounding environment. For T cells to move within diverse tissues, blood and lymphatic vessels (3), which impose different types of physical constraints, T lymphocytes need to sense and adapt to their mechanical environments. T lymphocytes largely exert forces onto their environment through the LFA-1 integrin. Using optical tweezers, McDonald et al. report here the role of the LFA-1 partner kindlin-3 in its ability to regulate the adhesion of LFA-1 to ICAM-1. By measuring the force needed to dissociate a bead out of contact with T cells, the authors show that T cells bearing a pathogenic mutation of kindlin-3 show defective LFA-1-mediated T cell adhesion to the bead and weak, but not absent, catch bond formation. Thus signalling through kindlin-3 plays a role in catch bond formation and activation of LFA-1. These adhesive properties are most likely involved in the process of T cell scanning of their surrounding environment using their cell surface microvilli as sensors (4), a mechanosurveillance phenomenon that Göhring et al. review here.

Altogether, the articles gathered here bring additional information to the complexity of biochemical signals that control the T cell cytoskeleton. They also point to a more recent theme of research, which is the influence of mechanical signals on the cytoskeleton. The integration of biochemical and mechanical stimuli by the T cell cytoskeleton is an exciting field for further research in order to understand how morphology changes shape T cell migration and activation.

Author contributions

JD wrote the first draft of the editorial. MB and JS edited the manuscript. All authors contributed to the article and approved the submitted version.

Funding

JS is supported by the Swiss National Foundation project grants 31003A_172994 and 310030_200406, the Novartis foundation for medical-biological Research 21C171 and the San Salvatore Foundation. JD is supported by Inserm, Agence Nationale de la Recherche (ANR 2019 RIDES), Ligue contre le Cancer, and Idex Program Université Paris Cité.

Conflict of interest

The authors declare that the research was conducted in the absence of any commercial or financial relationships that could be construed as a potential conflict of interest.

Publisher's note

References

1. El Masri R, Delon J. RHO GTPases: from new partners to complex immune syndromes. *Nat Rev Immunol* (2021) 21(8):499–513. doi: 10.1038/s41577-021-00500-7

2. Du H, Bartleson JM, Butenko S, Alonso V, Liu WF, Winer DA, et al. Tuning immunity through tissue mechanotransduction. *Nat Rev Immunol* (2022) 16:1–15. doi: 10.1038/s41577-022-00761-w

3. Stein JV, Ruef N, Wissmann S. Organ-specific surveillance and long-term residency strategies adapted by tissue-resident memory $CD8^+$ T cells. *Front Immunol* (2021) 12:626019. doi: 10.3389/fimmu.2021.626019

4. Cai E, Marchuk K, Beemiller P, Beppler C, Rubashkin MG, Weaver VM, et al. Visualizing dynamic microvillar search and stabilization during ligand detection by T cells. *Science* (2017) 356(6338):pii: eaal3118. doi: 10.1126/science.aal3118

frontiers in Immunology

ORIGINAL RESEARCH
published: 09 September 2021
doi: 10.3389/fimmu.2021.716405

The Tec Kinase Itk Integrates Naïve T Cell Migration and *In Vivo* Homeostasis

Flavian Thelen[1], *Stefanie Wissmann*[2], *Nora Ruef*[2] *and Jens V. Stein*[2]*

[1] Department of Medical Oncology and Hematology, University of Zürich and University Hospital Zürich, Zürich, Switzerland,
[2] Department of Oncology, Microbiology and Immunology, University of Fribourg, Fribourg, Switzerland

Naïve T cells (T_N) constitutively recirculate through secondary lymphatic organs (SLOs), where they scan dendritic cells (DCs) for cognate peptide-loaded major histocompatibility complexes (pMHC). Continuous trafficking between SLOs not only enables rapid clonal selection but also ensures T_N homeostasis by providing access to prosurvival signals from TCR, IL-7R, and the chemokine receptor CCR7. Inside the lymphoid tissue, CCR7-mediated T_N motility is mainly driven by the Rac activator DOCK2, with a separate contribution by a phosphoinositide-3-kinase γ (PI3Kγ)-dependent pathway. Tec tyrosine kinases and the Rac activator Tiam1 constitute prominent downstream effectors of PI3K signaling. Yet, the precise role of Tec kinase versus Tiam1 signaling during CCR7-mediated T_N migration and homeostasis remains incompletely understood. Here, we examined the function of the Tec family member interleukin-2-inducible T-cell kinase (Itk) and Tiam1 during T_N migration *in vitro* and *in vivo* using intravital microscopy. Itk deficiency caused a mild decrease in CCR7-triggered T_N migration, mirroring observations made with PI3Kγ$^{-/-}$ T cells, while lack of Tiam1 did not affect T_N motility. *In silico* modeling suggested that reduced migration in the absence of Itk does not result in a substantial decrease in the frequency of T_N encounters with DCs within the lymphoid tissue. In contrast, Itk was important to maintain *in vivo* homeostasis of $CD4^+$ T_N, also in MHCII-deficient hosts. Taken together, our data suggest that Itk contributes to T_N migration and survival by integrating chemokine receptor and TCR signaling pathways.

Keywords: T cell trafficking, chemokine, signal transduction, Tec kinase, CCL21/CCR7 axis, intravital 2-photon microscopy

OPEN ACCESS

Edited by:
Alexandre M. Carmo, Universidade do Porto, Portugal

Reviewed by:
Nicole Boucheron, Medical University of Vienna, Austria
Jacques A. Nunes, INSERM U1068 Centre de Recherche en Cancérologie de Marseille (CRCM), France

***Correspondence:**
Jens V. Stein
jens.stein@unifr.ch

Specialty section:
This article was submitted to T Cell Biology, a section of the journal Frontiers in Immunology

Received: *28 May 2021*
Accepted: *19 August 2021*
Published: *09 September 2021*

Citation:
Thelen F, Wissmann S, Ruef N and Stein J V (2021) The Tec Kinase Itk Integrates Naïve T Cell Migration and In Vivo Homeostasis. Front. Immunol. 12:716405. doi: 10.3389/fimmu.2021.716405

INTRODUCTION

Naïve T cells (T_N) continuously roam secondary lymphoid organs (SLOs) including peripheral lymph nodes (PLNs) to scan for the presence of cognate peptide-loaded major histocompatibility complex (pMHC) on dendritic cells (DCs). The chemokine receptor CCR7 on T_N and its ligands CCL19 and CCL21 expressed by SLO stromal cells fulfill a key function in this process (1). CCL21 is central for recruitment of blood-borne T_N *via* high endothelial venules into the PLN parenchyma (2), where CCR7 ligands contribute to fast T_N motility of ~15 μm/min on a scaffold of fibroblastic reticular cells (FRCs) (3–7). This process enables efficient T_N scanning of pMHC presented on DC

surfaces (8, 9). In addition to providing an "antigen library" that mirrors the immune status of their surveilled area, SLOs provide critical factors for T_N homeostasis. First, FRCs are a main source of the prosurvival cytokine IL-7 (10). Second, tonic signaling by self-pMHC binding to the T cell receptor (TCR) on migrating T cells induces a baseline phosphorylation of the TCR complex ζ; chain important for responsiveness to foreign pMHC (11) and $CD4^+$ T cell survival (12, 13). Third, CCR7 ligands themselves constitute prosurvival signals for circulating T_N (10). Accordingly, the expression of CCR7, the PLN homing receptor CD62L, and the IL-7 receptor CD127 are transcriptionally coordinated in T_N (14).

On a molecular level, CCR7 activation triggers an increase in F-actin polymerization, mainly *via* the Rac guanine exchange factor (GEF) DOCK2 that catalyzes the formation of Rac-GTP at the cell's leading edge. This, in turn, activates the actin nucleator Arp2/3 complex *via* the nucleation promoting factor Scar/WAVE (15, 16). DOCK2-Rac-Scar/WAVE-Arp2/3-driven retrograde (i.e., from the cell front to the rear) F-actin flow imprints the characteristic amoeboid shape of migrating T_N and forms the basis for rapid cellular translocation by force-coupling of cortical actin to the extracellular substrate *via* transmembrane receptors, mainly LFA-1 (17).

In addition to DOCK2 activation, chemokine receptors activate a phosphoinositide-3-kinase (PI3K) pathway in T cells (18). In T_N, CCR7 signaling activates the p110γ isoform through its interaction with Gβγ subunits that dissociate from $G\alpha_i$ after ligand binding (19). While pharmacological or genetic inhibition of this pathway does not affect the major DOCK2-Rac-Arp2/3 axis, PI3K blockade induces a minor but significant decrease in T_N migration *in vitro* and *in vivo* (19, 20). To date, the downstream signals that transmit PI3K signals for CCR7-mediated T_N migration remain incompletely understood. PI3K-generated phosphoinositide-3,4,5-triphosphate (PIP3) at the inner plasma membrane is recognized by proteins containing pleckstrin homology (PH) domains, such as the Rac GEF Tiam1, which has been implicated in T cell trafficking (21, 22). Additionally, Tec proteins constitute a well-characterized PH-domain-containing nonreceptor tyrosine kinase family that plays key regulatory functions in lymphocyte development, activation, and effector differentiation. The Tec family is composed of five members, of which Itk and Rlk are expressed in T_N (23). Itk signals from multiple surface receptors, such as TCR, the costimulatory receptor CD28, and chemokine receptors (23–25). In accordance with this, Itk-deficient and Itk/Rlk double-deficient T cells show reduced chemotaxis to CXCL12 (26, 27). Itk activation of Vav1, a GEF for the small GTPases Rac1 and Cdc42, is important for actin reorganization and adhesion (23, 28–30). Yet, the precise roles of Itk and Tiam1 during CCR7-triggered DOCK2- versus PI3K-dependent T_N migration and their impact on physiological T_N motility and homeostasis have not been assigned thus far.

Here, we investigated the role of Itk and Tiam1 in CCR7-driven T_N motility and survival after adoptive transfer. Our data uncover a role for Itk but not Tiam1 downstream PI3K-dependent *in vitro* T_N polarization and migration in response to the CCR7 ligand CCL21, with a concomitant decrease in homing capacity to SLOs. While intravital imaging confirmed that *in vivo* T cell motility is reduced in the absence of Itk, *in silico* track modeling suggests only a minor impact on the efficacy to encounter DCs in the LN parenchyma. In contrast, significantly fewer Itk-deficient $CD4^+$ T cells were recovered from blood and SLOs 8–14 days after adoptive transfer into WT and MHCII-deficient recipients, supporting a role for this Tec family member for T_N homeostasis even in the absence of tonic TCR signaling.

RESULTS

CCL21-Induced T Cell Polarization and Migration Are Impaired in the Absence of Itk

We first examined the impact of Itk deficiency on CCR7-triggered rapid F-actin polymerization. Akin to PI3Kγ$^{-/-}$ T cells (19), we detected a small but consistent reduction of F-actin polymerization in Itk$^{-/-}$ T cells immediately after CCL21 addition (**Figures 1A, B**). This difference disappeared when WT cells were pretreated with Wortmannin (Wn), a broad PI3K inhibitor, whereas the same treatment on Itk$^{-/-}$ cells caused no further decrease in F-actin polymerization (**Figures 1A, B**). This is in line with results showing that Itk acts downstream of PI3K and contributes to F-actin polymerization upon chemokine receptor activation in T cells (23). Given the close causal relation between F-actin treadmilling and T cell shape (17), we examined the impact of Itk on chemokine-induced polarization. T cells were allowed to adhere to fibronectin-coated glass slides and stimulated with CCL21 for 20 min, followed by immunofluorescent analysis of PKCζ and CD44 as markers for leading edge and uropod, respectively (**Figure 1C**). Itk$^{-/-}$ T cells showed reduced cellular polarization as compared to WT T cells and resembled PI3Kγ$^{-/-}$ T cells or WT T cells treated with the pan-PI3K inhibitor Wortmannin (Wn) (**Figure 1D**). Taken together, our data suggest that a PI3K-Itk pathway contributes to F-actin polymerization and T cell polarization upon stimulation with CCR7 ligands.

Itk$^{-/-}$ mice display a defect in thymic positive selection and show an increased ratio of "memory-like" $CD44^{high}$ to $CD44^{low}$ T_N in SLOs (31, 32) (**Figure S1A**). To exclude this as cause of reduced Itk$^{-/-}$ T cell response to CCL21, we enriched $CD62L^{high}CD44^{low}$ *bona fide* T_N by depleting $CD44^{high}$ T cells using titrated amounts of anti-CD44 mAb-coated magnetic beads as described (33) and applied bead sorting to both WT and Itk$^{-/-}$ T cells (**Figure S1B**). As reported for migration to CXCL12 (26, 27), *bona fide* Itk$^{-/-}$ T_N migration toward increasing concentrations of CCL21 showed a minor but significant and consistent reduction (**Figure 1E**).

In contrast to Itk, DOCK2 activity in lymphocytes is regulated in a PI3K-independent manner (19) and plays a pivotal role in chemokine-induced migration (15). Accordingly, we observed reduced migration of both WT and Itk$^{-/-}$ T_N with the specific DOCK2 inhibitor CPYPP (34) in a dose-dependent manner

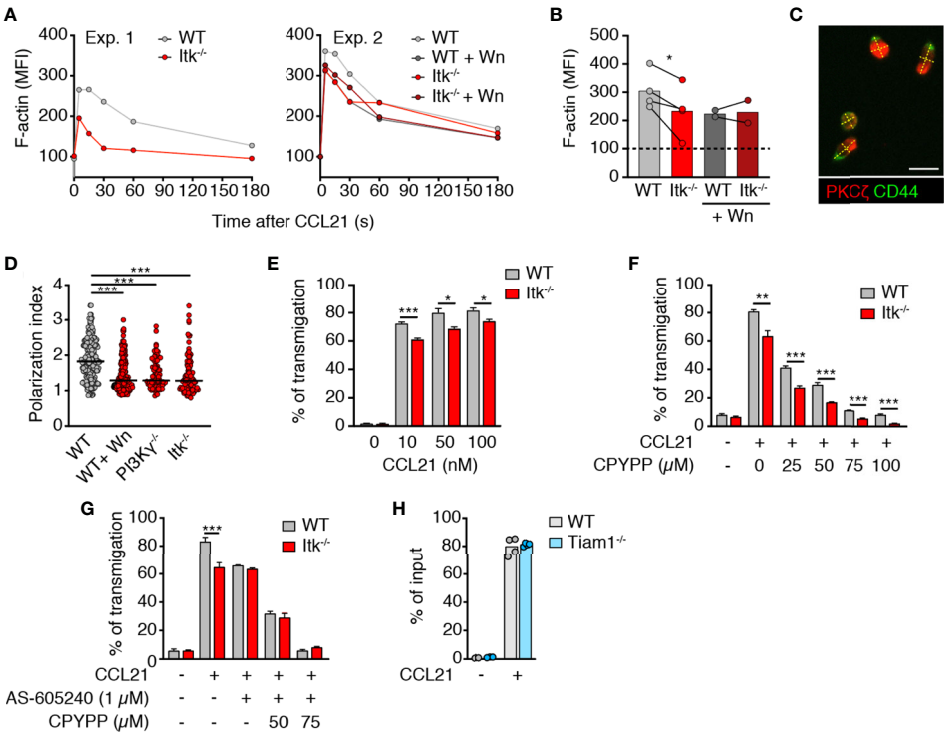

FIGURE 1 | Itk enhances CCL21-induced polarization and migration of T cells. **(A)** MFI of F-actin after CCL21 stimulation with and without Wn treatment. **(B)** Summary of normalized F-actin MFI at 30 s post CCL21 addition (100 = baseline). Experiments performed on the same day (i.e., same flow cytometer settings) are linked with a line. **(C)** Image of CCL21-stimulated T cells on fibronectin-coated glass dish. Scale bar, 10 μm. **(D)** Quantification of cell polarization as measured by the ratio between the length and the width of the cellular body (dotted yellow lines in C). **(E)** Chemotaxis of WT and Itk$^{-/-}$ CD4$^+$ T_N to indicated CCL21 concentrations. **(F, G)** Chemotaxis of WT and Itk$^{-/-}$ CD4$^+$ T_N pretreated with CPYPP **(F)** and/or AS-605204 **(G)** toward 50 nM CCL21. Graph shows percentage of transmigrated cells. **(H)** Chemotaxis of WT and Tiam1$^{-/-}$ CD4$^+$ T cells toward 50 nM CCL21. Graph shows percentage of transmigrated cells. Data in **(B)** were analyzed using a paired t-test. Data in **(D–H)** are pooled from at least two independent experiments and analyzed by Kruskal–Wallis test **(D)** or unpaired Student's t-test **(E–H)**. *p < 0.05; **p < 0.01; ***p < 0.001.

(**Figure 1F**). The migratory difference between WT and Itk$^{-/-}$ CD4$^+$ T cells was maintained during CPYPP treatment, confirming that Itk-dependent migration is uncoupled from DOCK2-induced motility. In line with this, treatment of WT CD4$^+$ T_N with the specific PI3Kγ inhibitor AS-605240 reduced migration to the same level as of Itk$^{-/-}$ CD4$^+$ T_N, while this treatment did not have an impact on Itk$^{-/-}$ CD4$^+$ T_N chemotaxis (**Figure 1G**). Consistent with the abolished chemotaxis of DOCK2 x PI3Kγ-double deficient T cells (19), combined CPYPP + AS-605240 treatment completely abrogated T_N migration to CCL21 (**Figure 1G**). Similarly, migration toward CXCL12 was partially reduced in WT T_N by either CPYPP or AS-605240 treatment, while combined CPYPP + AS-605240 treatment abolished T_N chemotaxis (**Figure S1C**). In contrast, Itk$^{-/-}$ T_N migration to CXCL12 was not affected by AS-605240, whereas CPYPP treatment severely impaired chemotaxis toward CXCL12 (**Figure S1C**). These data suggested that the dual engagement of DOCK2- and PI3Kγ-dependent signaling affects other chemokine receptors as well. Inhibitor treatment did not affect the viability of T_N, as assessed by PI staining (>90% viability after double inhibitor treatment).

Itk has been reported to be constitutively associated with the Rac/Cdc42 GEF Vav1, which mediates its effects on the actin cytoskeleton (30). In addition to Vav1, the Rac GEF Tiam1 becomes activated downstream of PI3K signaling (35), and Tiam1 has been previously shown to mediate T cell polarization and migration to CXCL12 and CCL21 *via* the Par complex (22, 36). We therefore examined whether Tiam1$^{-/-}$ T cells were impaired in their motility to CCL21. However, Tiam1$^{-/-}$ CD4$^+$ T cells showed no defect in chemotaxis (**Figure 1H**). Taken together, these results confirm that DOCK2 plays a dominant function in CCL21-dependent T_N migration, while a PI3Kγ-Itk axis contributes to optimal cell polarity and chemokine responsiveness, potentially by regulating the activity of Vav1 or other GEFs.

Itk Supports T_N Migration in LN Parenchyma

Rlk/Itk-double-deficient naïve T cells display impaired *in vivo* homing to spleen and PLNs (27). We confirmed this observation after adoptive transfer of WT and Itk$^{-/-}$ CD4$^+$ T_N, since we recovered fewer Itk-deficient T cells in spleen and other SLOs at

2 h post transfer, while these cells were more abundant in blood (**Figure 2A**). Since CCR7 contributes to T_N motility inside the LN parenchyma (3, 5, 6, 17, 37), we set out to assess the impact of Itk deficiency on *in vivo* T cell scanning behavior. We adoptively transferred fluorescently labeled CD4$^+$ WT and Itk$^{-/-}$ T_N into C57BL/6 recipients and performed intravital imaging of the popliteal LN 16-24 h post transfer. We detected a minor but significant reduction in Itk$^{-/-}$ CD4$^+$ versus WT T_N speeds (13.2 ± 0.3 and 11.9 ± 0.3 μm/min for WT and Itk$^{-/-}$ T_N, respectively; mean ± SEM; **Figure 2B**) without affecting the turning angles as a readout for directionality (38) (**Figure 2C**). As a result, the motility coefficient (MC), which represents a measure of the average scanned area per time, was reduced from 64 μm^2/min for WT to 36 μm^2/min for Itk$^{-/-}$ CD4$^+$ T_N (**Figure 2D**). In contrast, parenchymal CD4$^+$ T cell speeds were unaffected by Tiam1 deficiency (**Figure 2E**), in line with *in vitro* chemotaxis data.

Based on the measured *in vivo* motility data, we modeled how T_N encounters with abundant (10^4) or rare (50) DCs would be affected by Itk deficiency using *in silico* generated tracks in an artificial 3D volume representing the T cell zone (39) (**Figure 2F**). Both cell types efficiently intercepted highly abundant DCs (**Figure 2G**). In contrast to the reported reduction of T cell–DC encounters in the absence of DOCK2 (39), the absence of Itk only had a minor impact on the ability of migrating T_N to encounter rare cognate pMHC-bearing DCs (20.1 ± 4.9% and 13.8 ± 4.3% of WT and Itk$^{-/-}$ *in silico* T cell tracks, respectively, engaging in DC encounters in 8-h simulations with a total of 50 DCs/T cell zone; mean ± SD; **Figure 2G**). Taken together, Itk signaling makes a minor but detectable contribution to *in vivo* T cell migration akin to observations made with PI3Kγ$^{-/-}$ T cells (40), yet without causing a substantial decrease in the likelihood of T cell–DC encounters.

Itk Contributes to Circulating T_N Homeostasis

CD4$^+$ T_N continuously homes to SLO to receive pro-survival factors provided in part by TCR and CCR7 signaling. We therefore investigated whether Itk promotes T_N homeostasis by facilitating homing and integration of prosurvival signals from pMHC and/or CCR7. We transferred fluorescently labeled WT and Itk$^{-/-}$ CD4$^+$ T_N at a 1:1 ratio into age- and sex-matched recipients as described (10). After 10–14 days, we isolated SLOs and blood to determine the ratio of recovered WT and Itk$^{-/-}$ CD4$^+$ T_N (**Figure 3A**). In all organs tested, we detected an approximately 30% reduction in the frequency of CD4$^+$ T_N lacking Itk$^{-/-}$ expression in comparison to their WT counterparts (**Figure 3B**). In contrast to the short-term homing experiment (**Figure 2A**), we now observed fewer Itk$^{-/-}$ T_N in blood as compared to their WT counterparts. In contrast, we recovered a similar ratio of Tiam1$^{-/-}$: WT T cells from all tissues at 14 days post transfer (**Figure 3C**).

To examine whether reduced recovery of Itk$^{-/-}$ T cells is owing due to impaired homeostatic TCR signaling (24), we transferred Itk$^{-/-}$and WT CD4$^+$ T_N into MHCII$^{-/-}$ recipients in a 1:1 ratio as above. On 8 days post transfer, we collected SLOs and measured the ratio of recovered WT: Itk$^{-/-}$ CD4$^+$ T cells. Similar to WT recipients, Itk$^{-/-}$ CD4$^+$ T_N were underrepresented in blood and most SLOs except spleen (**Figure 3D**). Taken

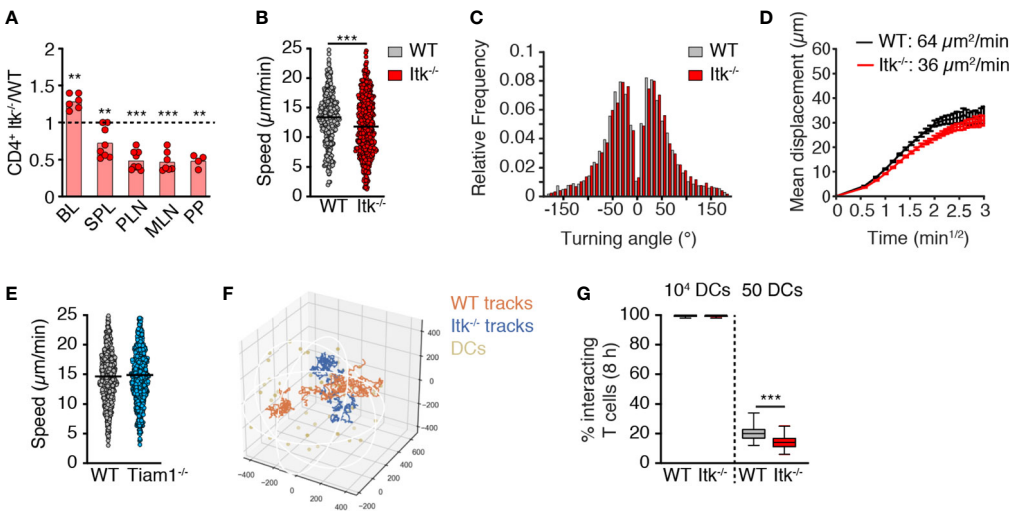

FIGURE 2 | Itk contributes to *in vivo* T_N homing and motility. **(A)** Ratio of Itk$^{-/-}$ to WT CD4$^+$ T_N in blood (BL), spleen (SPL), PLN, mesenteric LN (MLN), and Peyer's patches (PP) at 2 h post adoptive transfer. **(B, C)** Speeds **(B)** and frequency of turning angles **(C)** of WT and Itk$^{-/-}$ CD4$^+$ T_N in LN parenchyma. **(D)** Mean displacement of T cells as a function of the square root of time. **(E)** Speeds of WT and Tiam1$^{-/-}$ T_N in LN parenchyma. **(F)** Representative 8-h-long *in silico* WT and Itk$^{-/-}$ CD4$^+$ T cell tracks with 50 dispersed DCs. Numbers indicate μm. **(G)** Percentage of 100 *in silico* WT and Itk$^{-/-}$ CD4$^+$ T cell tracks encountering 1 in 10^4 or 50 DCs in 50 8-h simulations. All data were pooled from at least two independent experiments (except PP in A; n = 4 mice from one exp.). Data in **(A)** were analyzed by a one-sample t-test against the theoretical value of "1" (= equal recovery); data in **(B, E, G)** were analyzed using an unpaired Student's t-test, and data in **(C)** using Mann–Whitney test. **p < 0.01; ***p < 0.001.

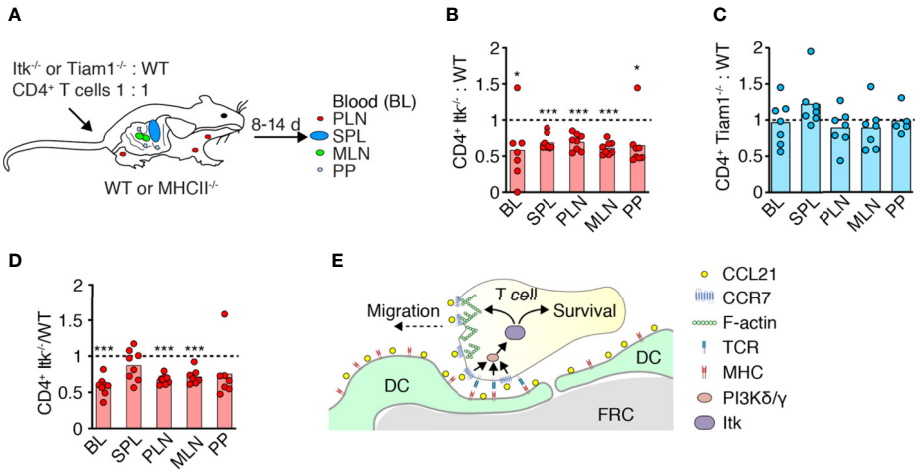

FIGURE 3 | Itk supports physiological T_N homeostasis. **(A)** Experimental layout. Fluorescently labeled WT and Itk$^{-/-}$ or Tiam1$^{-/-}$ CD4$^+$ T_N were transferred in a 1:1 ratio into WT or MHCII$^{-/-}$ recipients, and blood (BL), spleen (SPL), PLN, mesenteric LN (MLN), and Peyer's patches (PP) were analyzed 8–14 days post transfer (p.t.) by flow cytometry. **(B–D)** Itk$^{-/-}$ or Tiam1$^{-/-}$ to WT CD4$^+$ T_N ratio recovered 10–14 days p.t. into WT **(B, C)** or 8 days p.t. into MHCII$^{-/-}$ recipients **(D)**, normalized to input. **(E)** Scheme of Itk function in T_N migration and survival. Data in **(B–D)** are from two independent experiments and analyzed by a one-sample t-test against the theoretical value of "1" (= equal recovery). *$p < 0.05$; ***$p < 0.001$.

together, these data suggest a role for Itk in mediating T_N homeostasis beyond TCR signal transduction, presumably by signal transmission *via* CCR7 or other chemoattractant receptors (**Figure 3E**).

DISCUSSION

T_N uses two separate signaling modules for CCR7-triggered motility, a major DOCK2-dependent and a minor PI3Kγ-dependent pathway (19, 40). While the DOCK2-Scar/WAVE-Arp2/3-Rac signaling cascade is well characterized, it has remained unclear which molecules act downstream PI3K after CCR7 activation. Here we report a role for the Tec kinase Itk in optimizing PI3K-dependent T_N polarization and migration. In line with the limited contribution of PI3K signaling for homeostatic T_N migration, we find that Itk deficiency had only a minor effect on CCR7-induced motility *in vitro* and T_N scanning behavior *in vivo*. In contrast, Itk deficiency impaired short-term T_N homing to SLOs and precipitated a loss of T_N recovery after 1–2 weeks post transfer. Thus, Itk integrates PI3K-dependent motility and homeostasis of circulating T_N.

Unlike in neutrophils (41), DOCK2 activation in T cells occurs independently of PIP3 and might involve additional phospholipids such as phosphatidic acid (42). Given that PI3K activation is a universal hallmark of chemokine receptors including CCR7 (18), there is, to date, remarkably little knowledge on the physiological impact of this pathway in primary T cells. Tec kinases act at the crossroads of TCR and chemokine receptor signaling and have well-characterized effects on the actin cytoskeleton in multiple cell types, with a wide-ranging impact on T cell development, activation, and differentiation (23, 24). Here we focused on the role of Itk, since its activity is regulated by PIP3 binding to its PH domain, in contrast to the other Tec family member expressed in naïve T cells, Rlk (23) (**Figure S2**). While we identify a role for Itk in CCR7-triggered PI3K-dependent T_N migration, our findings suggest a more prominent role of Itk for long-term T_N survival. Our data further indicate that Itk-dependent homeostasis is not solely driven by TCR signaling, as evidenced by reduced recovery of Itk$^{-/-}$ T_N in MHC II-deficient hosts as compared to WT T_N. As TCR stimulates the PI3Kδ isoform in T cells, while CCR7 activates PI3Kγ, Itk is in a key position to integrate both baseline PIP3 signals generated during homeostatic T_N recirculation into a prosurvival program (**Figure 3E**). One caveat is that the I-Aa$^{-/-}$ recipients we used as MHCII-deficient might still retain residual expression of noncanonical MHC molecules (12, 43).

In contrast to previous publications (22, 36), we were unable to assign a role for Tiam1 in CCR7-driven, PI3K-mediated T_N migration *in vitro* and *in vivo*. While the reason for this discrepancy might be due to the different mouse strain background used in both studies, our findings reflect the lack of Tiam1 expression in C57BL/6 T_N (www.immgen.org). Similarly, Tiam2 was not expressed in naïve CD4$^+$ T cells (**Figure S2**). Furthermore, recent work suggests that the Tiam1 PH domain binds with a lower affinity to PIP3 as compared to other membrane lipids such as phosphoinositide-5-phosphate (44). Taken together, our data assign a role for Itk during CCR7-mediated signaling in T cells, leading to enhanced actin polymerization, polarization, and migration. Yet, the most relevant impact of Itk is in promoting T_N homeostasis, presumably by facilitating SLO homing and integration of prosurvival pMHC and CCR7 signals.

MATERIAL AND METHODS

Mouse Lines

C57BL/6 mice were purchased from Janvier labs. Itk$^{-/-}$ (31) and Tiam1$^{-/-}$ mice (45) were obtained from P. Schwartzberg (NIH, Bethesda, MD, USA) and J. van Buul (Sanquin Research Center, The Netherlands), respectively. PI3Kγ$^{-/-}$ and H2-Aa^{tm1Blt} (MHCII$^{-/-}$) were described (46, 47). Mice were bred at the Department of Clinical Research of the University of Bern and at the University of Fribourg. Experiments were approved by the Cantonal authorities and performed in accordance with the Swiss Federal Veterinary Office guidelines.

T Cell Isolation

Spleens, PLNs, and mesenteric LNs (MLNs) were harvested and homogenized using a 70-µm cell strainer and a syringe plug. T cells or CD4$^+$ T cells were isolated with an EasySep Mouse negative selection kit according to the manufacturer's protocol (STEMCELL Technologies). For depletion of CD44^{high} CD4$^+$ T cells, 2.5 µg of biotinylated anti-CD44 mAb (BD Biosciences) was added per 10^7 cells. Cells were incubated for 20 min on ice. CD44^{low} *bona fide* T_N was negatively isolated using an EasySep™ Streptavidin RapidSpheres™ Isolation kit according to the manufacturer's protocol (STEMCELL Technologies). Purity was typically >95%.

Flow Cytometry

Single cell suspensions from SLOs were isolated and homogenized using 70-µm cell strainers. Fc receptors were blocked with purified anti-CD16/CD32 mAb (2.4G2) in a FACS buffer (PBS with 1% FCS and 0.05% NaN3) for 10 min. Cells were stained with fluorochrome-conjugated mAbs against CD8 (53-6.7), CD62L (Mel-14; 4°C for 30 min), CD4 (RM4-5; all Biolegend), and CD44 (IM7; BD Bioscience) with appropriate isotype controls and analyzed by flow cytometry (BD Biosciences).

F-Actin Polymerization, Cell Polarization, and Chemotaxis

For F-actin polymerization, T cells from Itk$^{-/-}$, PI3Kγ$^{-/-}$, and WT mice were starved for 1.5 h in a serum-free medium. Where noted, cells were pretreated with 0.5 µM Wortmannin (Calbiochem) for 1 h at 37°C. CCL21 (100 nM; Peprotech) was added to 2 x 10^6 cells/ml in a 37°C water bath, and cells were fixed at indicated time points in 4% cold PFA. Cells were permeabilized and labeled with FITC-Phalloidin (Invitrogen) as described (19). For polarization assays, T cells were added on 1 µg/ml fibronectin-coated glass slides before the addition of CCL21 (100 nM) and fixation after 20 min with 2% PFA. After permeabilization with 0.1% Triton X-100 (5 min), cells were incubated with anti-protein kinase ζ; (PKCζ) (H-1; Santa Cruz Biotechnology) and biotin-labeled anti-CD44 (IM7; BD Pharmingen) mAbs. Primary antibodies were detected with a Cy3-labeled anti-mouse Ab (Jackson ImmunoResearch Laboratories) and Alexa488-labeled avidin (Molecular Probes). For chemotaxis assays, T_N was pretreated with inhibitors for DOCK2 (CPYPP) and PI3Kγ (AS-605240; both Tocris) as indicated for 1 h at 37°C, and 0.5 x 10^6 T_N/well were added to Transwell chambers (5-µm pore size; Costar) to migrate to 50 nM CCL21 for 1.5 h at 37°C in the presence of the inhibitors. Cell viability was assessed by PI staining at the end of the experiment. Input and migrated T cells were enumerated by flow cytometry.

Intravital Microscopy of Popliteal LN

(5-(and−6)-(((4-chloromethyl) benzoyl) amino) tetramethylrhodamine) (CMTMR, CellTracker orange) and Chloromethyl-coumarin (CMAC, CellTracker blue)-labeled WT, Itk$^{-/-}$ or Tiam1$^{-/-}$ CD4$^+$ T_N (3 x 10^6) were injected i.v. into sex-matched C57BL/6 mice 24–32 h prior to imaging. The right popliteal LN of recipient mice was surgically prepared as previously described (48). 2PM imaging was performed using a TrimScope 2PM system (LaVision Biotec) and a 20X objective (NA 0.95; Olympus). 16-slice z stacks with 4-µm spacing of 250 x 250 µm field of views were acquired every 20 s for 20 min. Imaging was performed in the T cell zone as identified by the presence of high endothelial venules (labeled with Alexa Fluor 633–coupled MECA-79; 10 µg/mouse). Volocity software (PerkinElmer) was used to generate volume-rendered 4D movies and for semiautomated tracking of cell motility. Mean single cell track speeds were calculated from the x,y,z coordinates of cell centroids using Matlab (The MathWorks) (49).

Estimation of T Cell–DC Encounters

We simulated 200 8-h-long WT and Itk$^{-/-}$ T cell tracks by sampling from control and Itk$^{-/-}$ T cell tracks acquired by 2PM. As steps at higher velocities tend to have smaller turning angles, we drew combinations of speed, turning angle, and plane angle from the same step instead of drawing speed, turning angle, and plane angle separately. To additionally account for the correlation of velocity and turning angle, we repeatedly exchanged random steps of our samples, keeping only those exchanges that made the mean squared differences of consecutive speeds and turning angles of our synthetic track more similar to the same means of the measured tracks. We stopped exchanging when both means of the simulated track were smaller than those of the measured tracks. To simulate contact formation among a predefined number of synthetic T cells and a number of DCs, we randomly chose 100 simulated T cell tracks and moved them to starting positions normally distributed around the center of a spherical T cell zone of 1-mm diameter for 8 h as described (39). We chose the SD of 150 µm, such that half of the WT tracks resided within the T cell zone for an average half-life of 11 h (40). We considered all steps of the track within the T cell zone, including reentry as residency time. We then checked, step by step, the distance to 10'000 and 50 static DCs uniformly distributed throughout the T cell zone. We considered proximity ≥ 15 µm as a stable contact and did not allow T cells to move on. We repeated the different simulations 50 times to obtain stable distributions of outcomes. This analysis was performed using open Python libraries for scientific computing (https://github.com/germannp/lana/blob/master/lana/).

In Vivo Homing and Homeostasis

WT, Itk$^{-/-}$, or Tiam1$^{-/-}$ T_N were labeled with Carboxyfluorescein succinimidyl ester (CFSE; Life Technologies) or eFluor 670 (e670; Life Technologies) for 15–20 min at 37°C in PBS, with dyes swapped between experiments, and 3 x 10^6 cells of each were injected i.v. at a 1:1 ratio into 5- to 10-week-old C57BL/6J or MHCII$^{-/-}$ recipient mice. At the indicated time points, blood and SLOs were isolated and analyzed by flow cytometry for percentage of transferred cells among CD4$^+$ T cells. In WT recipients, we recovered between 0.22% (in PP) and 1.84% (in blood) of WT and Itk$^{-/-}$ CD4$^+$ T cells at 10 to 14 days post transfer, while in MHCII$^{-/-}$ recipients, we recovered between 0.98% (in PP) and 8.37% (in blood) of transferred cells at 8 days post transfer.

Statistical Analysis

Data were analyzed using Prism (GraphPad Software) using unpaired Student's t-test or Mann–Whitney or Kruskal–Wallis tests. P-values < 0.05 were considered significant.

DATA AVAILABILITY STATEMENT

The original contributions presented in the study are included in the article/**Supplementary Material**. Further inquiries can be directed to the corresponding author.

ETHICS STATEMENT

The animal study was reviewed and approved by Kanton of Bern and Fribourg Amt für Lebensmittelsicherheit und Veterinärwesen.

AUTHOR CONTRIBUTIONS

FT performed the experiments and analyzed the data with the help of SW. NR performed *in silico* analysis. JS designed the experiments, analyzed the data, and wrote the manuscript with input from all coauthors. All authors contributed to the article and approved the submitted version.

FUNDING

This work was funded by Swiss National Foundation (SNF) project grant 31003A_172994 and 310030-200406 and Sinergia project CRSII5_170969 (to JS).

ACKNOWLEDGMENTS

We thank Federica Moalli, Bettina Stolp, Philipp Germann, and Varsha Kumar for help with experiments and Yağmur Farsakoğlu for critical reading.

SUPPLEMENTARY MATERIAL

The Supplementary Material for this article can be found online at: https://www.frontiersin.org/articles/10.3389/fimmu.2021.716405/full#supplementary-material

Supplementary Figure 1 | CD44^{high} CD4$^+$ T cell depletion and migration to CXCL12. **(A)** Representative flow cytometry plot showing CD44 and CD62L expression on WT and Itk$^{-/-}$ CD4$^+$ and CD8$^+$ T cells. Numbers indicate percentage. **(B)** Representative flow cytometry plot of CD44 and CD62L expression on CD4$^+$ T cells before and after negative isolation with CD44-coated beads. **(C)** Chemotaxis of WT and Itk$^{-/-}$ CD4$^+$ T_N treated with either CPYPP and/or AS-605204 towards 100 nM CXCL12. Graph shows percentage of transmigrated cells. Data in C were analyzed using an unpaired t-test and pooled from two independent experiments. *p < 0.05; ***p < 0.001.

Supplementary Figure 2 | RNAseq expression level of Tec, Tiam and Vav family members in spleen CD4$^+$ T_N. Data are from Immgen database (www.immgen.org).

REFERENCES

1. Förster R, Davalos-Misslitz AC, Rot A. CCR7 and Its Ligands: Balancing Immunity and Tolerance. *Nat Rev Immunol* (2008) 8:362–71. doi: 10.1038/nri2297
2. Stein JV, Rot A, Luo Y, Narasimhaswamy M, Nakano H, Gunn MD, et al. The CC Chemokine Thymus-Derived Chemotactic Agent 4 (TCA-4, Secondary Lymphoid Tissue Chemokine, 6Ckine, Exodus-2) Triggers Lymphocyte Function-Associated Antigen 1-Mediated Arrest of Rolling T Lymphocytes in Peripheral Lymph Node High Endothelial Venules. *J Exp Med* (2000) 191:61–76. doi: 10.1084/jem.191.1.61
3. Woolf E, Grigorova I, Sagiv A, Grabovsky V, Feigelson SW, Shulman Z, et al. Lymph Node Chemokines Promote Sustained T Lymphocyte Motility Without Triggering Stable Integrin Adhesiveness in the Absence of Shear Forces. *Nat Immunol* (2007) 8:1076–85. doi: 10.1038/ni1499
4. Krummel MF, Bartumeus F, Gérard A. T Cell Migration, Search Strategies and Mechanisms. *Nat Rev Immunol* (2016) 16:193–201. doi: 10.1038/nri.2015.16
5. Okada T, Cyster JG. CC Chemokine Receptor 7 Contributes to Gi-Dependent T Cell Motility in the Lymph Node. *J Immunol* (2007) 178:2973–8. doi: 10.4049/jimmunol.178.5.2973
6. Worbs T, Mempel TR, Bölter J, Andrian von UH, Förster R. CCR7 Ligands Stimulate the Intranodal Motility of T Lymphocytes *In Vivo*. *J Exp Med* (2007) 204:489–95. doi: 10.1084/jem.20061706
7. Bajénoff M, Egen JG, Koo LY, Laugier JP, Brau F, Glaichenhaus N, et al. Stromal Cell Networks Regulate Lymphocyte Entry, Migration, and Territoriality in Lymph Nodes. *Immunity* (2006) 25:989–1001. doi: 10.1016/j.immuni.2006.10.011
8. Katakai T, Habiro K, Kinashi T. Dendritic Cells Regulate High-Speed Interstitial T Cell Migration in the Lymph Node *via* LFA-1/ICAM-1. *J Immunol* (2013) 191:1188–99. doi: 10.4049/jimmunol.1300739
9. Moreau HD, Bogle G, Bousso P. A Virtual Lymph Node Model to Dissect the Requirements for T-Cell Activation by Synapses and Kinapses. *Immunol Cell Biol* (2016) 94:680–8. doi: 10.1038/icb.2016.36
10. Link A, Vogt TK, Favre S, Britschgi MR, Acha-Orbea H, Hinz B, et al. Fibroblastic Reticular Cells in Lymph Nodes Regulate the Homeostasis of Naive T Cells. *Nat Immunol* (2007) 8:1255–65. doi: 10.1038/ni1513
11. Štefanová I, Dorfman JR, Germain RN. Self-Recognition Promotes the Foreign Antigen Sensitivity of Naive T Lymphocytes. *Nature* (2002) 420:429–34. doi: 10.1038/nature01146
12. Martin B, Bécourt C, Bienvenu B, Lucas B. Self-Recognition is Crucial for Maintaining the Peripheral CD4+ T-Cell Pool in a Nonlymphopenic Environment. *Blood* (2006) 108:270–7. doi: 10.1182/blood-2006-01-0017
13. Boyman O, Krieg C, Homann D, Sprent J. Homeostatic Maintenance of T Cells and Natural Killer Cells. *Cell Mol Life Sci* (2012) 69:1597–608. doi: 10.1007/s00018-012-0968-7

14. Kerdiles YM, Beisner DR, Tinoco R, Dejean AS, Castrillon DH, DePinho RA, et al. Foxo1 Links Homing and Survival of Naive T Cells by Regulating L-Selectin, CCR7 and Interleukin 7 Receptor. *Nat Immunol* (2009) 10:176–84. doi: 10.1038/ni.1689
15. Fukui Y, Hashimoto O, Sanui T, Oono T, Koga H, Abe M, et al. Haematopoietic Cell-Specific CDM Family Protein DOCK2 Is Essential for Lymphocyte Migration. *Nature* (2001) 412:826–31. doi: 10.1038/35090591
16. Goley ED, Welch MD. The ARP2/3 Complex: An Actin Nucleator Comes of Age. *Nat Rev Mol Cell Biol* (2006) 7:713–26. doi: 10.1038/nrm2026
17. Hons M, Kopf A, Hauschild R, Leithner A, Gaertner F, Abe J, et al. Chemokines and Integrins Independently Tune Actin Flow and Substrate Friction During Intranodal Migration of T Cells. *Nat Immunol* (2018) 19:606–16. doi: 10.1038/s41590-018-0109-z
18. Ward SG, Marelli-Berg FM. Mechanisms of Chemokine and Antigen-Dependent T-Lymphocyte Navigation. *Biochem J* (2009) 418:13–27. doi: 10.1042/BJ20081969
19. Nombela-Arrieta C, Lacalle RA, Montoya MC, Kunisaki Y, Megías D, Marqués M, et al. Differential Requirements for DOCK2 and Phosphoinositide-3-Kinase Gamma During T and B Lymphocyte Homing. *Immunity* (2004) 21:429–41. doi: 10.1016/j.immuni.2004.07.012
20. Stein JV, Soriano SF, M'Rini C, Nombela-Arrieta C, de Buitrago GG, Rodríguez-Frade JM, et al. CCR7-Mediated Physiological Lymphocyte Homing Involves Activation of a Tyrosine Kinase Pathway. *Blood* (2003) 101:38–44. doi: 10.1182/blood-2002-03-0841
21. Grönholm M, Jahan F, Marchesan S, Karvonen U, Aatonen M, Narumanchi S, et al. TCR-Induced Activation of LFA-1 Involves Signaling Through Tiam1. *J Immunol* (2011) 187:3613–9. doi: 10.4049/jimmunol.1100704
22. Gérard A, Mertens AEE, van der Kammen RA, Collard JG. The Par Polarity Complex Regulates Rap1- and Chemokine-Induced T Cell Polarization. *J Cell Biol* (2007) 176:863–75. doi: 10.1083/jcb.200608161
23. Gomez-Rodriguez J, Readinger JA, Viorritto IC, Mueller KL, Houghtling RA, Schwartzberg PL. Tec Kinases, Actin, and Cell Adhesion. *Immunol Rev* (2007) 218:45–64. doi: 10.1111/j.1600-065X.2007.00534.x
24. Andreotti AH, Schwartzberg PL, Joseph RE, Berg LJ. T-Cell Signaling Regulated by the Tec Family Kinase, Itk. *Cold Spring Harb Perspect Biol* (2010) 2:a002287. doi: 10.1101/cshperspect.a002287
25. Schwartzberg PL, Finkelstein LD, Readinger JA. TEC-Family Kinases: Regulators of T-Helper-Cell Differentiation. *Nat Publishing Group* (2005) 5:284–95. doi: 10.1038/nri1591
26. Fischer AM, Mercer JC, Iyer A, Ragin MJ, August A. Regulation of CXC Chemokine Receptor 4-Mediated Migration by the Tec Family Tyrosine Kinase ITK. *J Biol Chem* (2004) 279:29816–20. doi: 10.1074/jbc.M312848200
27. Takesono A, Horai R, Mandai M, Dombroski D, Schwartzberg PL. Requirement for Tec Kinases in Chemokine-Induced Migration and Activation of Cdc42 and Rac. *Curr Biol* (2004) 14:917–22. doi: 10.1016/j.cub.2004.04.011
28. Tybulewicz VLJ. Vav-Family Proteins in T-Cell Signalling. *Curr Opin Immunol* (2005) 17:267–74. doi: 10.1016/j.coi.2005.04.003
29. Vicente-Manzanares M. Control of Lymphocyte Shape and the Chemotactic Response by the GTP Exchange Factor Vav. *Blood* (2005) 105:3026–34. doi: 10.1182/blood-2004-07-2925
30. Dombroski D, Houghtling RA, Labno CM, Precht P, Takesono A, Caplen NJ, et al. Kinase-Independent Functions for Itk in TCR-Induced Regulation of Vav and the Actin Cytoskeleton. *J Immunol* (2005) 174:1385–92. doi: 10.4049/jimmunol.174.3.1385
31. Liao XC, Littman DR. Altered T Cell Receptor Signaling and Disrupted T Cell Development in Mice Lacking Itk. *Immunity* (1995) 3:757–69. doi: 10.1016/1074-7613(95)90065-9
32. Hu J, August A. Naive and Innate Memory Phenotype CD4+ T Cells Have Different Requirements for Active Itk for Their Development. *J Immunol* (2008) 180:6544–52. doi: 10.4049/jimmunol.180.10.6544
33. Köchl R, Thelen F, Vanes L, Brazão TF, Fountain K, Xie J, et al. WNK1 Kinase Balances T Cell Adhesion Versus Migration *In Vivo*. *Nat Immunol* (2016) 17:1075–83. doi: 10.1038/ni.3495
34. Nishikimi A, Uruno T, Duan X, Cao Q, Okamura Y, Saitoh T, et al. Blockade of Inflammatory Responses by a Small-Molecule Inhibitor of the Rac Activator DOCK2. *Chem Biol* (2012) 19:488–97. doi: 10.1016/j.chembiol.2012.03.008
35. Cain RJ, Vanhaesebroeck B, Ridley AJ. The PI3K P110alpha Isoform Regulates Endothelial Adherens Junctions *via* Pyk2 and Rac1. *J Cell Biol* (2010) 188:863–76. doi: 10.1083/jcb.200907135
36. Gérard A, van der Kammen RA, Janssen H, Ellenbroek SI, Collard JG. The Rac Activator Tiam1 Controls Efficient T-Cell Trafficking and Route of Transendothelial Migration. *Blood* (2009) 113:6138–47. doi: 10.1182/blood-2008-07-167668
37. Asperti-Boursin F, Real E, Bismuth G, Trautmann A, Donnadieu E. CCR7 Ligands Control Basal T Cell Motility Within Lymph Node Slices in a Phosphoinositide 3-Kinase-Independent Manner. *J Exp Med* (2007) 204:1167–79. doi: 10.1084/jem.20062079
38. Sumen C, Mempel TR, Mazo IB, Andrian von UH. Intravital Microscopy: Visualizing Immunity in Context. *Immunity* (2004) 21:315–29. doi: 10.1016/j.immuni.2004.08.006
39. Ackerknecht M, Gollmer K, Germann P, Ficht X, Abe J, Fukui Y, et al. Antigen Availability and DOCK2-Driven Motility Govern CD4+ T Cell Interactions With Dendritic Cells *In Vivo*. *J Immunol* (2017) 199:520–30. doi: 10.4049/jimmunol.1601148
40. Nombela-Arrieta C, Mempel TR, Soriano SF, Mazo I, Wymann MP, Hirsch E, et al. A Central Role for DOCK2 During Interstitial Lymphocyte Motility and Sphingosine-1-Phosphate-Mediated Egress. *J Exp Med* (2007) 204:497–510. doi: 10.1084/jem.20061780
41. Kunisaki Y, Nishikimi A, Tanaka Y, Takii R, Noda M, Inayoshi A, et al. DOCK2 Is a Rac Activator That Regulates Motility and Polarity During Neutrophil Chemotaxis. *J Cell Biol* (2006) 174:647–52. doi: 10.1083/jcb.200602142
42. Nishikimi A, Fukuhara H, Su W, Hongu T, Takasuga S, Mihara H, et al. Sequential Regulation of DOCK2 Dynamics by Two Phospholipids During Neutrophil Chemotaxis. *Science* (2009) 324:384–7. doi: 10.1126/science.1170179
43. Madsen L, Labrecque N, Engberg J, Dierich A, Svejgaard A, Benoist C, et al. Mice Lacking All Conventional MHC Class II Genes. *Proc Natl Acad Sci U S A* (1999) 96:10338–43. doi: 10.1073/pnas.96.18.10338
44. Viaud J, Lagarrigue F, Ramel D, Allart S, Chicanne G, Ceccato L, et al. Phosphatidylinositol 5-Phosphate Regulates Invasion Through Binding and Activation of Tiam1. *Nat Commun* (2014) 5:4080–17. doi: 10.1038/ncomms5080
45. Malliri A, van der Kammen RA, Clark K, van der Valk M, Michiels F, Collard JG. Mice Deficient in the Rac Activator Tiam1 are Resistant to Ras-Induced Skin Tumours. *Nature* (2002) 417:867–71. doi: 10.1038/nature00848
46. Hirsch E, Katanaev VL, Garlanda C, Azzolino O, Pirola L, Silengo L, et al. Central Role for G Protein-Coupled Phosphoinositide 3-Kinase Gamma in Inflammation. *Science* (2000) 287:1049–53. doi: 10.1126/science.287.5455.1049
47. Köntgen F, Süss G, Stewart C, Steinmetz M, Bluethmann H. Targeted Disruption of the MHC Class II Aa Gene in C57BL/6 Mice. *Int Immunol* (1993) 5:957–64. doi: 10.1093/intimm/5.8.957
48. Moalli F, Cupovic J, Thelen F, Halbherr P, Fukui Y, Narumiya S, et al. Thromboxane A2 Acts as Tonic Immunoregulator by Preferential Disruption of Low-Avidity CD4+ T Cell-Dendritic Cell Interactions. *J Exp Med* (2014) 211:2507–17. doi: 10.1084/jem.20140137
49. Mempel TR, Henrickson SE, Andrian von UH. T-Cell Priming by Dendritic Cells in Lymph Nodes Occurs in Three Distinct Phases. *Nature* (2004) 427:154–9. doi: 10.1038/nature02238

Conflict of Interest: The authors declare that the research was conducted in the absence of any commercial or financial relationships that could be construed as a potential conflict of interest.

Publisher's Note: All claims expressed in this article are solely those of the authors and do not necessarily represent those of their affiliated organizations, or those of the publisher, the editors and the reviewers. Any product that may be evaluated in this article, or claim that may be made by its manufacturer, is not guaranteed or endorsed by the publisher.

frontiers in Immunology

ORIGINAL RESEARCH
published: 06 January 2022
doi: 10.3389/fimmu.2021.726406

A Murine Model of X-Linked Moesin-Associated Immunodeficiency (X-MAID) Reveals Defects in T Cell Homeostasis and Migration

Lyndsay Avery[1,2], *Tanner F. Robertson*[1,2], *Christine F. Wu*[1,2], *Nathan H. Roy*[1,2], *Samuel D. Chauvin*[1,2], *Eric Perkey*[3], *Ashley Vanderbeck*[4], *Ivan Maillard*[4] *and Janis K. Burkhardt*[1,2]*

[1] Department of Pathology and Laboratory Medicine, Children's Hospital of Philadelphia Research Institute, Philadelphia, PA, United States, [2] Perelman School of Medicine, University of Pennsylvania, Philadelphia, PA, United States, [3] Graduate Program in Cellular and Molecular Biology and Medical Scientist Training Program, University of Michigan, Ann Arbor, MI, United States, [4] Division of Hematology/Oncology, Department of Medicine and Abramson Family Cancer Research Institute, Perelman School of Medicine, University of Pennsylvania, Philadelphia, PA, United States

OPEN ACCESS

Edited by:
Jerome Delon,
U1016 Institut Cochin (INSERM), France

Reviewed by:
Andres Alcover,
Institut Pasteur, France
Jonathan Soboloff,
Temple University, United States
Sharon Celeste Morley,
Washington University School of Medicine in St. Louis, United States

***Correspondence:**
Janis K. Burkhardt
jburkhar@pennmedicine.upenn.edu

Specialty section:
This article was submitted to T Cell Biology, a section of the journal Frontiers in Immunology

Received: 16 June 2021
Accepted: 13 December 2021
Published: 06 January 2022

Citation:
Avery L, Robertson TF, Wu CF, Roy NH, Chauvin SD, Perkey E, Vanderbeck A, Maillard I and Burkhardt JK (2022) A Murine Model of X-Linked Moesin-Associated Immunodeficiency (X-MAID) Reveals Defects in T Cell Homeostasis and Migration. Front. Immunol. 12:726406. doi: 10.3389/fimmu.2021.726406

X-linked moesin associated immunodeficiency (X-MAID) is a primary immunodeficiency disease in which patients suffer from profound lymphopenia leading to recurrent infections. The disease is caused by a single point mutation leading to a R171W amino acid change in the protein moesin (moesin^{R171W}). Moesin is a member of the ERM family of proteins, which reversibly link the cortical actin cytoskeleton to the plasma membrane. Here, we describe a novel mouse model with global expression of moesin^{R171W} that recapitulates multiple facets of patient disease, including severe lymphopenia. Further analysis reveals that these mice have diminished numbers of thymocytes and bone marrow precursors. X-MAID mice also exhibit systemic inflammation that is ameliorated by elimination of mature lymphocytes through breeding to a Rag1-deficient background. The few T cells in the periphery of X-MAID mice are highly activated and have mostly lost moesin^{R171W} expression. In contrast, single-positive (SP) thymocytes do not appear activated and retain high expression levels of moesin^{R171W}. Analysis of *ex vivo* CD4 SP thymocytes reveals defects in chemotactic responses and reduced migration on integrin ligands. While chemokine signaling appears intact, CD4 SP thymocytes from X-MAID mice are unable to polarize and rearrange cytoskeletal elements. This mouse model will be a valuable tool for teasing apart the complexity of the immunodeficiency caused by moesin^{R171W}, and will provide new insights into how the actin cortex regulates lymphocyte function.

Keywords: T cell, immunodeficiency, actin, moesin, migration, cytoskeleton, hematopoiesis, development

INTRODUCTION

Protective immune responses depend on regulated actin cytoskeletal dynamics, which direct cell migration, adhesion and signaling (1–5). The importance of these processes is highlighted by the existence of several primary immunodeficiency diseases linked to mutations in actin regulatory proteins like WASp, WIPF1, Rac2, Hem1, and Dock2 (6–8). Recently, a new primary immunodeficiency disorder was described and attributed to mutations in the actin binding protein moesin (9–12). Unlike other actin regulatory proteins linked to immunodeficiency, moesin does not regulate actin filament growth. Instead, it reversibly links the cortical actin cytoskeleton to plasma membrane lipids and proteins, thereby providing structural rigidity to the cell, controlling cell shape changes, and organizing specialized membrane domains (13, 14).

Moesin is a member of the ezrin/radixin/moesin (ERM) protein family. One or more members of this highly homologous group of proteins is expressed in most cell types; T cells express high levels of moesin, moderate levels of ezrin, and little to no radixin (15). These proteins are comprised of an N-terminal 4.1-ezrin-radixin-moesin (FERM) domain, a flexible linker, and a C-terminal actin binding domain (ABD). In the active conformation, the FERM domain of moesin associates with the plasma membrane by binding to phosphatidylinositol bisphosphate (PIP_2) and to the cytoplasmic tails of membrane proteins such as CD43, while the ABD interacts with actin filaments that lie just beneath the membrane. Moesin can also assume an inactive conformation, in which intramolecular interaction of the FERM and ABD domains (16) masks the binding sites for plasma membrane components and actin. PIP_2 binding and phosphorylation at T558 residue disrupt the autoinhibited fold, activating linker activity (17–21). Engagement of antigen or chemokine receptors leads to transient ERM protein dephosphorylation and loss of linker activity, allowing molecular rearrangements and cell shape changes associated with T cell activation and migration (22–24). When overexpressed in cells, constitutively active mutants of ezrin or moesin prevent appropriate cytoskeletal rearrangement. Lymphocytes expressing these mutants are abnormally rigid, polarize poorly, and display defective migratory responses *in vitro* and *in vivo* (22, 23, 25, 26). Interestingly, however, cells lacking ERM proteins or lymphocyte-oriented kinase (LOK), the kinase that activates linker activity, polarize well and migrate relatively normally in response to conventional chemokines (27, 28). Nonetheless, moesin knockout mice exhibit profound lymphopenia, due in large part to defective migratory responses to sphingosine-1-phosphate (29). Though T cells express both ezrin and moesin, deletion of ezrin in the T cell compartment has little effect on T cell trafficking (15), and the effect of deleting both ezrin and moesin is only slightly more severe than deleting moesin alone (29), indicating that moesin is the most important ERM family member in T cells.

Recently, a dozen patients worldwide have been diagnosed with a novel combined immunodeficiency disease known as X-linked moesin-associated immunodeficiency (X-MAID) (9–12). Remarkably, eleven of the twelve patients have the same single point mutation within the moesin FERM domain (R171W). Disease is characterized by severe lymphopenia, fluctuating neutropenia, and recurrent viral and bacterial infections. Most patients also exhibit eczema and other autoimmune phenotypes. Disease severity is variable; some patients required bone marrow transplantation although most patients have responded well to IVIG, prophylactic antibodies, and/or G-CSF (9, 11, 12). Little is known about the cell biological basis for pathology in X-MAID, though analysis of patient PBMCs shows evidence of defects in proliferation and migration (11). Furthermore, data from patient cells point to complex phenotypic changes related to patient age and lymphocyte activation status. In order to better understand this disease, we used CRISPR technology to generate mice with germline expression of moesin^{R171W} (note that murine and human moesin are 99% identical at the amino acid level, and 100% identical within the FERM domain where the mutation lies). This X-MAID mouse model recapitulates key aspects of the human disease including profound lymphopenia and susceptibility to opportunistic infections. X-MAID mice exhibit diminished numbers of thymocytes and bone marrow precursors, and systemic inflammation that can be ameliorated by mature lymphocyte deletion. The few peripheral T cells that are present are highly activated and have lost moesin expression, whereas SP thymocytes express high levels of the mutant protein. Functional analysis of X-MAID thymocytes reveals defects in migration traceable to an inability to undergo appropriate chemoattractant-induced cell shape changes. This mouse model provides novel insights into the mechanisms underlying moesin-based immunodeficiency.

MATERIALS AND METHODS

Mice

Moesin knockout (MKO) mice on the C57BL/6 background were described previously (28–30). Mice homozygous for Rag1^{tm1mom} (RagKO) were obtained from Jackson Laboratories and bred in house. CRISPR mice in which the murine moesin gene was edited to contain the R171W mutation found in the majority of X-MAID patients (X-MAID mice) were generated by the CRISPR/Cas9 Mouse Targeting Core Facility, together with the Transgenic and Chimeric Mouse Facility at the University of Pennsylvania, following protocols published in (31). Briefly, Cas9 mRNA, gRNA, and ssDNA oligos containing the R171W X-MAID point mutation were designed and injected into C57BL/6J zygotes. Embryos were then transferred into pseudopregnant mice, creating the F0 chimeric generation. All founder mice were screened for chimerism and bred to determine germline transmission of the mutation. X-MAID mice were backcrossed to C57BL/6J mice (Jackson Laboratories) for at least 4 generations. Results from two independent founder lines were in agreement. All mice were bred in-house under SPF conditions and used at 3-5 weeks of age, all in accordance with protocols approved by the Institutional Animal Care and Use Committee of the Children's Hospital of Philadelphia Research Institute. Exclusively male mice were used of every genotype, with WT mice being littermates to X-MAID mice.

Histology

Upon necropsy, mice were perfused with 10% formalin *via* the pulmonary artery to inflate and fix the lung tissue. Tissues were collected into 10% formalin and processed by the Pathology Core Facility at the Children's Hospital of Philadelphia. Briefly, tissue was paraffin embedded and then five-micron sections were cut and stained with hematoxylin and eosin. Slides were digitally scanned at 20× magnification on a Leica DM4000B upright imaging scope with a Spot RT/SE Slider Camera.

Flow Cytometry

Single cell suspensions were prepared from spleens, thymi, and bone marrow while peripheral blood mononuclear cells were isolated with Lymphoprep (STEMCELL). For surface labeling, the following reagents from Tonbo Biosciences were used: Ghost Dye (Live/Dead) in v510, CD44 (IM7) in APC-Cy7, CD62L (MEL-14) in APC, TCRβ (H57-597) in PE or FITC, CD25 (PC61.5) in PE-Cy7, NK1.1 (PK136) in FITC, and Ly6G (1A8) in PerCP-Cy5.5. Antibodies to CD8 (53-6.7) in BV711, and CD4 (GK1.5) in BUV395 were from BD Biosciences, and antibodies to CD69 (H1.2F3) in APC, CD19 (6D5) in BV785, CD11b (M1/70) in AlexaFluor700, Ly6C (HK1.4) in Pacific Blue, CD29 (HMβ1-1) in FITC, LFA-1 (H155-78) in PE, Flt3 (A2F10) in APC, Ckit (ACK2) in APC-Cy7 or APC, CD150 (TC15-12F12.2) in PE-Cy7, CD48 (HM48-1) in FITC, IL7Rα (A7R34) in v450, CD41 (MWReg30) in APC-Cy7, FcγRII/III (93) in BV711, Sca1 (D7) in PerCP-Cy5.5, and CD105 (MJ7/18) in v450 were from Biolegend. In addition, the lineage dump gate included antibodies for CD3, CD8α, CD11b, CD11c, CD19, B220, TCRβ, TCRγδ, GR-1, NK1.1, and Ter119 all in PE conjugate format from Biolegend. For intracellular staining, surface staining was followed by fixation/permeabilization with the FoxP3 fix/perm kit (eBioscience), then cells were labeled for 30 minutes at room temperature with rabbit anti-moesin (Q480, Cell Signaling Technologies) followed by anti-rabbit AlexaFluor 647 secondary antibody (Invitrogen), and/or with anti-FoxP3 (FJK-16s) in PerCP-Cy5.5 from eBioscience. For flow cytometric analysis of F-actin polymerization, cells were stimulated with CCL19 (100 ng/ml) and fixed with 3% paraformaldehyde in PBS at the indicated times. Cells were then permeabilized with PSG (PBS, 0.01% saponin, 0.25% fish skin gelatin) and labeled with phalloidin AlexaFluor 488 (Invitrogen). All samples were analyzed on an LSRII (BD Biosciences) equipped with FACSDiva software (BD Biosciences). Data were analyzed using FlowJo software (v.10.4.2).

Western Blotting

CD4 SP thymocytes from WT and X-MAID mice were isolated by negative selection using a magnetic $CD4^+$ T cell isolation kit (Miltenyi). Cells were starved for 4 hours in serum-free DMEM (Corning) before stimulation 100ng/ml CCL19 (R&D Systems) for the indicated times. Cells were then lysed with 1% Triton X100, 50 mM Tris-HCl, 50 mM NaCl, 5 mM EDTA, 50 mM NaF, 30 mM $Na_4P_2O_7$, 50 mM β-glycerophosphate, with Roche Complete protease inhibitors. Proteins were separated by SDS/PAGE (4-12% NuPAGE bis-tris gel, Invitrogen) transferred to nitrocellulose membranes, blocked with Odyssey buffer (Licor) and probed for the indicated proteins. Antibodies to pERK1/2 (Thr202/Tyr204) and pAkt (Ser473) were from Cell Signaling Technologies. GAPDH was used as a loading control, and was detected with Clone 6C5 antibody, from Sigma. Primary antibodies were detected with fluorescent secondary antibodies (anti-rabbit AlexaFluor 800 or anti-mouse AlexaFluor 680, from Invitrogen). Blots were imaged using an Odyssey fluorescence-based imaging system (Licor) and prepared for publication using ImageLite Software (Licor).

Transwell Assays

CD4 SP thymocytes from WT and X-MAID mice were isolated by negative selection using a magnetic $CD4^+$ T cell isolation kit (Miltenyi) and resuspended in DMEM with 10% charcoal stripped FBS (Gibco). $2x10^5$ cells per well were placed in the top chambers of a 24 well transwell plate (5μm pore size, Corning) and allowed to settle at 37°C for 10 minutes. The top chambers were then placed on top of bottom chambers containing 100ng/ml CCL19, and incubated for 2 hours at 37°C. Top chambers were then removed and cells in the bottom chambers were counted using a hemocytometer. Percent migration was calculated based on input cell numbers.

Microscopy

Live cell imaging was conducted essentially as described previously (32). Eight-well chamber slides (Lab-Tek) were coated with 2μg/ml of murine ICAM-1-Fc (R&D Systems). CD4 SP thymocytes were placed in Leibovitz's L-15 media (Gibco) supplemented with 2mg/ml glucose and 0.1% FBS and incubated for 20 minutes. Cells were then added to ICAM-1 coated chambers, allowed to settle for 10 minutes, then imaged using a DIC 10× lens on a Zeiss Axiovert 200M microscope and ORCA-ER CCD camera (Hamamatsu). Time-lapse images were collected every 30s for 10 minutes using Slidebook 6 software (Intelligent Imaging Innovations). Migration was quantified using the manual tracking plugin in ImageJ. Cells that were not alive, not attached to the glass, or left the frame during the time frame were excluded from analysis. For each cell that met the criteria for inclusion, the total distance traversed was determined, as was the net displacement (defined as the distance between the final and starting coordinates of the cell). The percentage of migrating cells was calculated based on counting cells with a net displacement of at least 10 microns, divided by the total number of live cells that were attached to the cover glass.

Cell polarization was assessed based on immunofluorescence microscopy of fixed cells. CD4 SP thymocytes were stimulated in suspension with 100ng/ml CCL19 for indicated times, after which they were fixed with 4% paraformaldehyde in PBS and attached to coverslips coated with poly-L lysine. Cells were then permeabilized using PSG and stained with phalloidin AlexaFluor 488 and rat anti-tubulin (clone YL1/2, Millipore/Sigma) followed by goat anti-rat AlexaFluor 647 secondary antibody (Invitrogen). Slides were mounted in Mowiol and images were collected on an Axiovert 200M (Zeiss) with a spinning disk confocal system (UltraVIEW ERS6; Perkin Elmer) equipped with an ORCA-Flash 4.0 CMOS camera (Hamamatsu) and a 63× 1.4 NA

Planapo objective. Images were acquired using Volocity v6.3 software (Perkin Elmer) and were prepared for publication using ImageJ. Roundness was defined by first outlining cells in ImageJ using the wand tool, then choosing the shape descriptors option. The software determined cell roundness by the following formula: $4 \times \frac{[Area]}{\pi \times [Major\ \ axis]^2}$.

mRNA Quantification

Single cell suspensions were made from spleens of WT, X-MAID, or MKO male mice. 1 WT, 1 MKO, and 4-5 X-MAID spleens were used for each experiment. Cells were enriched by negative selection using rat anti-CD8 hybridoma supernatant (Clone 53-6.7) and anti-MHC II (BioXCell) antibodies followed by anti-rat magnetic beads (Qiagen). $CD4^+$ T cells were further purified by flow sorting using CD4-APC (Biolegend) with the FACSJazz (BD). RNA isolation was completed using the PureLink RNA mini kit (Invitrogen). Equal amounts of RNA were reverse transcribed from each group using the High Capacity RT-PCR kit (Applied Biosystems). The resulting cDNA was used for qPCR using *Msn*, *Ezr*, and *Gapdh* PrimeTime qPCR primers (IDT) and SYBR Green mastermix (Applied Biosystems). qPCR Ct was quantified on the 7500 Standard (Applied Biosystems). Data are represented as ΔCT^{-1} defined as the inverse of Ct of the primer of interest minus the *Gapdh* Ct for that sample. Technical duplicates were run for each sample.

Statistical Analysis

Unless specified otherwise, data were analyzed using a 2-sided Student's *t* test with alpha = 0.05. All analysis was conducted using GraphPad Prism Software, v. 9.1.2.

RESULTS

X-MAID Mice Exhibit Opportunistic Infections and Lymphocyte-Dependent Inflammation

A novel combined immunodeficiency disease termed X-MAID has recently been described in patients bearing a specific point mutation in the actin linker protein moesin (9–12). To better understand the mechanistic basis of this disease, we generated CRISPR knock-in mice bearing the causative mutation (R171W, hereafter called X-MAID mice). Both male X-MAID mice and heterozygous females were born at normal Mendelian sex-linked ratios. Female heterozygotes were normal and fertile, although an increased rate of dystocia was noted. In contrast, hemizygous males exhibited partial (approximately 30%) perinatal lethality. The surviving mutant males developed numerous opportunistic infections in the skin, eye, and nasal cavity, as well as inflammatory infiltrates in multiple tissues, succumbing by 7-10 weeks of age. In order to minimize secondary effects of infection, we focused further analysis on young mice (3-5 weeks of age), before mice exhibit signs of infection. At this early age, X-MAID mice were runted and spleens were enlarged (**Figures 1A–C**). The elevated spleen-to-body-weight ratio observed in X-MAID mice is consistent with systemic inflammation. In addition, histological analysis of the lung and liver showed granulocytic infiltration and evidence of extra-medullary hematopoiesis (**Figure 1D**).

To ask if the inflammatory phenotype observed in X-MAID mice is attributable to primary defects in the lymphoid compartment, X-MAID mice were bred to $Rag1^{-/-}$ (RagKO) mice, to generate X-MAID mice lacking mature lymphocytes. As shown in **Figure 1E**, this ameliorates the inflammation of non-lymphoid tissues, indicating that lymphocytes are key drivers of pathology in X-MAID. In addition, X-MAID/RagKO mice survived as long as their RagKO counterparts (data not shown). We therefore focused our analysis on the lymphoid compartment, giving special attention to T cells, where defects in X-MAID patients are observed (9–12).

Peripheral T Cell Numbers Are Reduced and Remaining Cells Are Highly Activated

X-MAID patients exhibit reduced numbers of blood T and B cells (9–12). Consistent with this, X-MAID mice showed profound lymphopenia in both spleen and blood, and lymph nodes were nearly undetectable (**Figures 2A, B**, **S1**, and data not shown). Proportions of other immune cell types (NK cells, monocytes, and neutrophils) were elevated in the spleen, although this effect was largely due to the loss of lymphocytes; the absolute numbers of these cell types were either normal or modestly reduced in X-MAID mice (**Figure S1A** and data not shown). Similar results were obtained for these populations in the blood, except that circulating neutrophil numbers were clearly elevated in X-MAID mice (**Figures S1B, C**). Histological analysis revealed a lack of splenic architecture (**Figure 2C**). Further analysis of splenic T cells from X-MAID mice reveals increased CD4:CD8 ratios and a highly activated ($CD44^+CD62L^-$) phenotype for both $CD4^+$ and $CD8^+$ T cells (**Figures 2D**, **S2**). This activated phenotype, which is also observed in X-MAID patients, may be due to homeostatic proliferation induced by lymphopenia. However, regulatory T cells (T_{regs}) were nearly undetectable in X-MAID spleens (**Figure 2E**), and this may also contribute to effector T cell activation. Note that although moesin has been implicated in iT_{reg} development (33), the lack of peripheral T_{regs} in X-MAID mice is not attributable to an inability to produce nT_{regs}, as thymic nT_{regs} were readily detectable (**Figure 2E**).

Thymocyte Numbers Are Low, but Development and Activation State Are Grossly Normal

Closer examination of thymi from X-MAID mice at weaning age showed significantly reduced cellularity as compared with WT littermates (**Figure 3A**). Proportions of DN and SP populations were elevated in thymi from X-MAID mice, while the proportion of DP cells was reduced (**Figures 3B, C**). However, because of the decreased cellularity, the absolute number of all thymic populations was reduced in X-MAID mice (**Figure 3D**). Histological analysis revealed reduced cortical area, consistent with the loss of DP cells (**Figure 3E**). Further flow cytometric analysis of DN populations based on CD44 and CD25 expression

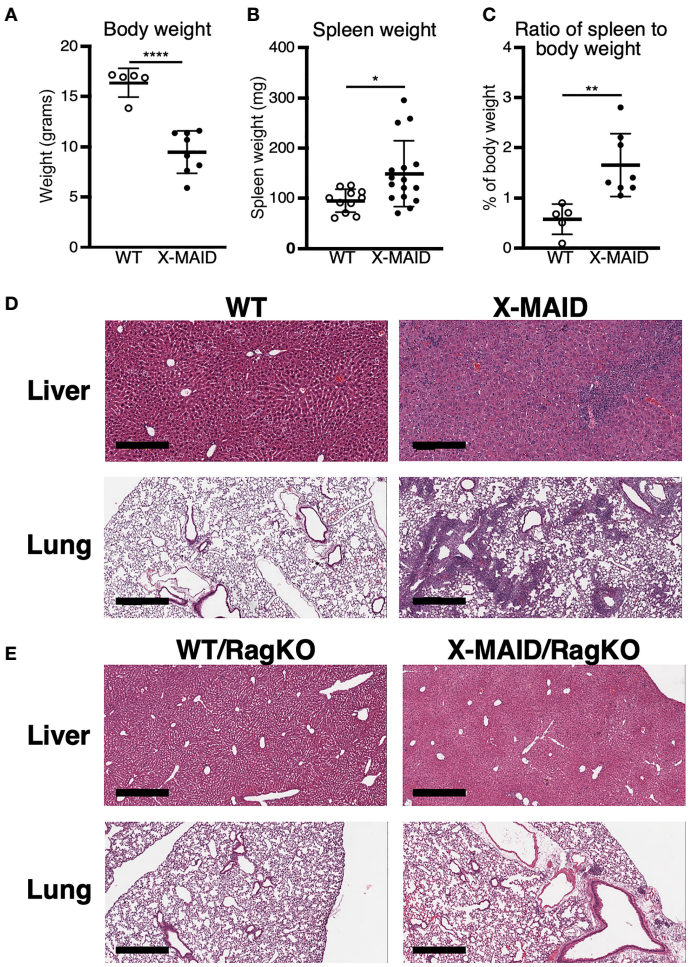

FIGURE 1 | X-MAID mice exhibit systemic inflammation ameliorated by lymphocyte deletion. WT or X-MAID male mice at 3-4 weeks old were measured for **(A)** body weight and **(B)** spleen weight. **(C)** The ratio of spleen to body weight was calculated. **(D, E)** H&E stains of sections from liver and lung of the indicated mouse strains, all at 3-4 weeks of age. Scale bars = 600μm. Note the granulocytic infiltration in X-MAID tissues, which is absent in tissues from X-MAID/RagKO mice. Data in **(A–C)** represent means ± StDev, with each point representing an individual mouse. Statistics were calculated using a Student's *t* test, *p < 0.05, **p < 0.01, ****p < 0.0001.

showed increased proportions of the DN1 population and decreased proportions of the DN3 population (**Figures 3F, G**). Notably, however, there was no significant accumulation of DN4 cells. Furthermore, analysis of DP thymocytes revealed an elevation in the proportion of $CD24^+/CD69^+$ population in X-MAID (**Figure 3H**), consistent with intact activation of these cells. Taken together, these findings suggest that the X-MAID mutation does not lead to gross defects in positive selection. Additional analysis will be required to definitively test this point and to determine any effects on the thymic repertoire.

Since peripheral $CD4^+$ T cells from X-MAID mice exhibit high basal expression of activation markers, we asked if this process begins in the thymus. CD25 and CD69 expression was analyzed in freshly isolated CD4 SP thymocytes without stimulation, and after stimulation for 24h with anti-CD3 and anti-CD28. As shown in **Figure 3I**, baseline levels of surface CD25 and CD69 were normal. After stimulation, upregulation of these activation markers was similar to that in WT thymocytes, both in terms of the number of positive cells and the levels of surface marker expression. X-MAID thymocytes did exhibit diminished ability to upregulate the late-activation marker CD44; this appeared to be largely due to reduced surface expression levels. Since CD44 is known to interact directly with moesin (34), this may reflect an effect on CD44 trafficking rather than an impact on T cell activation status.

X-MAID Mice Show Defects in Bone Marrow Precursor Populations

One of the most prominent features of X-MAID mice is overall paucity of thymocytes. To explore the basis of this defect, we conducted a series of pilot experiments using different bone marrow chimera models. Regardless of the experimental conditions, we found very few thymocytes in mice receiving X-MAID bone marrow (data not shown). This observation led

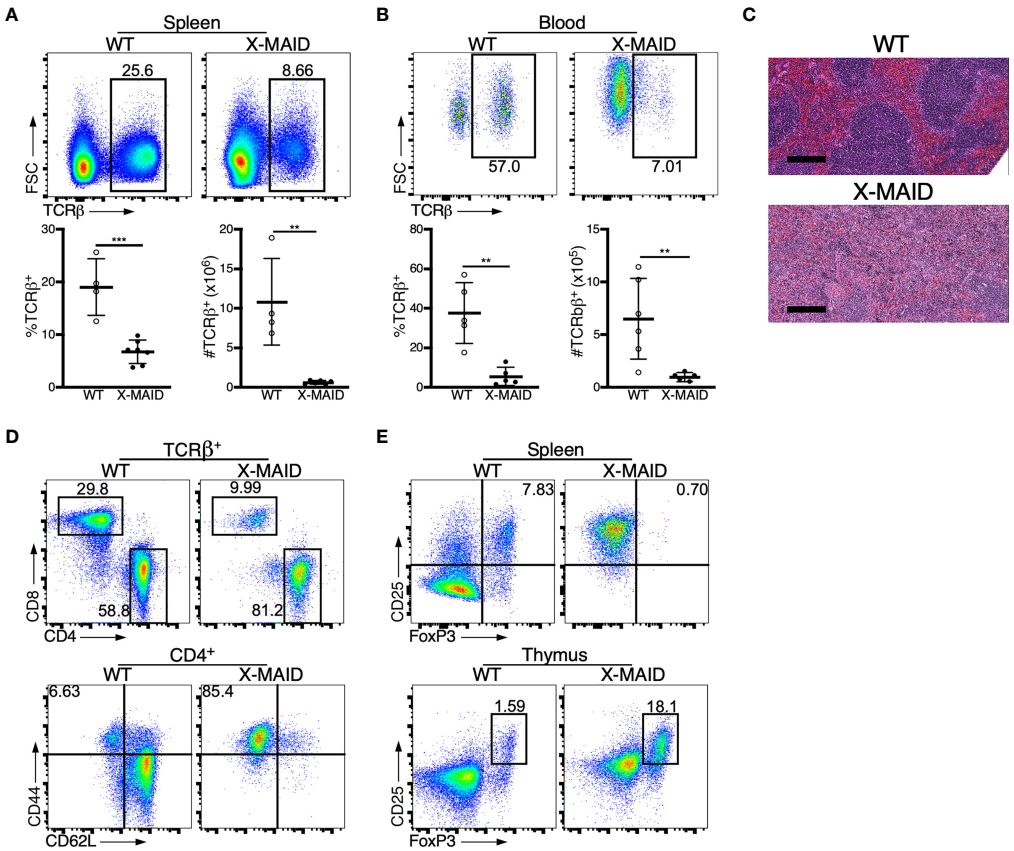

FIGURE 2 | Dysregulation of T cell populations in peripheral lymphoid organs of X-MAID mice. WT or X-MAID male mice were sacrificed at 3-5 weeks old, and the indicated tissues were harvested for analysis. **(A, B)** Using flow cytometry, gated on live single cells, the proportion and absolute number of TCR β^+ cells were determined from **(A)** spleen or **(B)** blood. **(C)** H&E staining from spleen sections shows a loss of follicle structure. Scale bars = 200μm. **(D)** Representative flow plots of $CD4^+$ and $CD8^+$ T cell subsets gated on TCR β^+ live single cells from the spleens of WT or X-MAID mice (top). Further analysis of CD44 and CD62L expression on $CD4^+$ T cells reveals elevated activation status (bottom). **(E)** $CD25^+FoxP3^+$ cells from the spleen (top) or thymus (bottom) of WT or X-MAID male mice gated on CD4 SP live single cells. Data in C-E are representative of results from at least 6 individual mice. Data in **(A, B)** represent means ± StDev, with each point representing an individual mouse. Statistics were calculated using a Student's *t* test, $^{**}p < 0.01$, $^{***}p < 0.005$.

us to examine bone marrow populations in X-MAID donors. Interestingly, we found that although the HSC population (as defined in (35), see also **Figure S3A**) appears relatively normal in X-MAID mice (**Figure 4A**), the absolute numbers and proportion of common lymphoid progenitors (CLPs) were severely reduced (**Figure 4B**). In contrast, we observed an increased proportion of granulocyte/macrophage progenitors (GMPs), although the absolute numbers of these cells were slightly lower than normal (**Figure 4C**). Based on these findings, we examined the lymphoid-primed multipotent progenitor (LMPP) population, which gives rise to CLPs and found significantly fewer cells in this population (**Figure S3D**). However, the multipotent progenitor (MPP) population, which gives rise to LMPPs as well as GMPs, was intact (**Figure S3C**) (36). Therefore, defects in cell numbers were first evident at the LMPP stage. Notably, there are also significantly fewer megakaryocyte precursors (MkP), but not erythroid progenitors [EryP (37)] in X-MAID bone marrow (**Figures S3E, F**). At present, almost nothing is known about the expression patterns and functional role of moesin with bone marrow precursor populations. Thus, additional work will be needed to understand why the moesin^{R171W} mutant protein is deleterious for LMPP cells, and whether this effect is cell-autonomous or indirect. Nonetheless, since LMPPs and CLPs are the primary precursor populations that exit the bone marrow and settle in the thymus, it seems likely that the low number of these precursor cells is at least partially responsible for the dearth of thymocytes in X-MAID mice.

Moesin^{R171W} Is Highly Expressed in the Thymus and Lost in the Periphery

The immunodeficiency and inflammatory phenotypes that we observe in X-MAID mice differ dramatically from subtle abnormalities seen in mice bearing a germline deletion of moesin (MKO mice) (28–30). This suggests that in X-MAID, expression of the mutant moesin protein is important for disease. In keeping with this view, in X-MAID patients, the mutant protein is expressed in some peripheral T cells, but is selectively

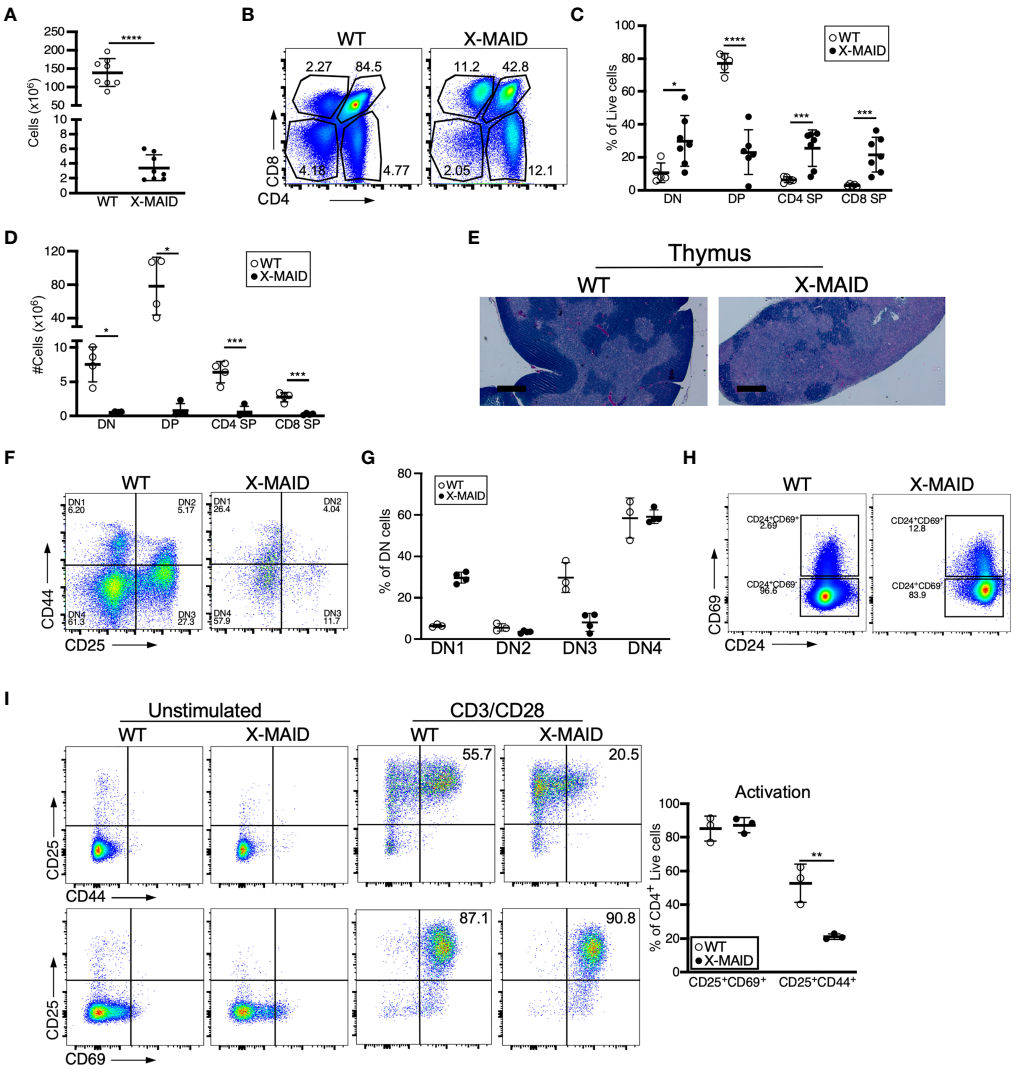

FIGURE 3 | Thymocyte numbers are reduced in X-MAID mice, but development and activation are grossly normal. Thymi from 3-4 week-old WT or X-MAID male mice were harvested and single cell suspensions were generated. **(A)** Total thymocyte number **(B)** Representative flow plots of thymocyte populations, gated on live single cells. Proportions **(C)** and absolute numbers **(D)** of thymocyte subsets were quantified, with each point representing an individual mouse. **(E)** H&E staining of the thymi from WT and X-MAID mice (representative of 4 mice for each genotype). Scale bars = 400μm. **(F)** Representative flow plots of thymocytes prepared as in A-C stained with CD44 and CD25 and gated on the $CD4^{-}CD8^{-}$ (DN) live population. **(G)** The proportion of each DN population (DN1-DN4) is quantified with each point representing an individual mouse. **(H)** Representative flow plots of thymocytes prepared as in A-C stained with CD69 and CD24 gated on $CD4^{+}CD8^{+}$ live population. **(I)** CD4 SP Thymocytes from WT or X-MAID male mice were left unstimulated or stimulated overnight with CD3/CD28 and stained for CD25, CD69, and CD44. Representative plots are gated on CD4 SP live single cells (left) and the proportion of activated cells was quantified (right). Representative of 3 independent experiments. Data in **(A, C, D, G, I)** represent means ± StDev. Statistics were calculated using a Student's *t* test, * p< 0.05, **p < 0.01, ***p < 0.005, ****p < 0.001.

lost with time and/or activation (9, 11). To ask if expression and loss of the mutant protein is recapitulated in the X-MAID mouse model, we compared the expression levels of moesin in peripheral leukocytes from X-MAID, MKO and WT mice. Analysis of blood T cells from X-MAID mice revealed a pattern of protein loss similar to that described in humans (**Figure 5A**). Moesin expression was also reduced in $CD19^{+}$ B cells but this effect was much more modest than in T cells. Analysis of splenic T and B cells revealed more profound loss of expression; most splenic T cells and a subset of B cells had extinguished expression altogether (**Figure 5B**). Loss of moesin expression was specific to B and T cells; $moesin^{R171W}$ expression was retained at WT levels in other immune populations, including natural killer cells, monocytes, and granulocytes (**Figures 5A, B**, and data not shown). Interestingly, although expression of $moesin^{R171W}$ is silenced in peripheral lymphocytes, expression levels are elevated in thymic populations (**Figure 5C**). This is particularly clear starting at the DP stage, a time when we have previously shown that moesin expression is upregulated (15).

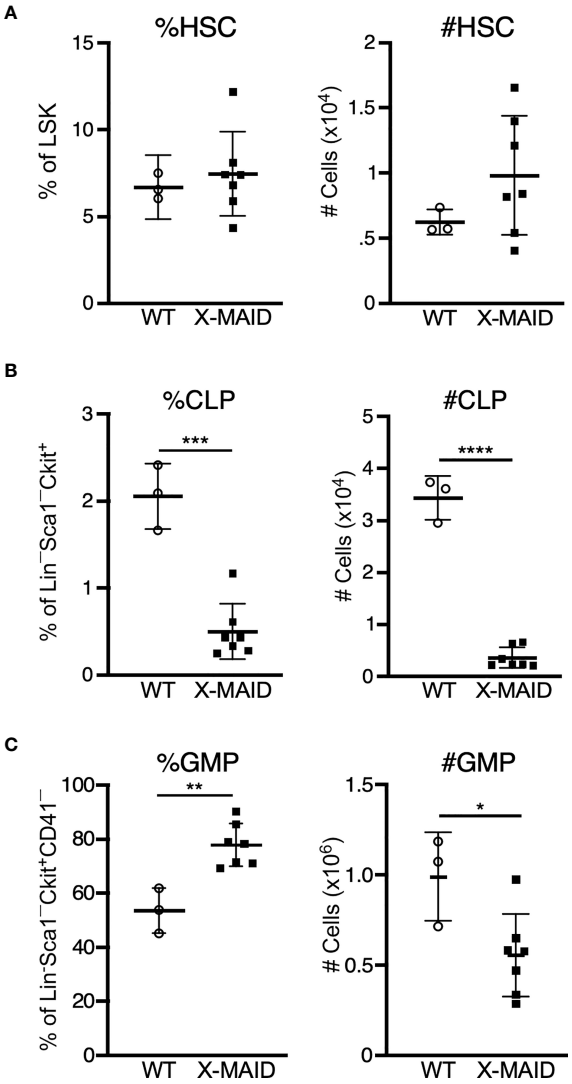

FIGURE 4 | Bone marrow of X-MAID mice shows a depleted lymphocyte progenitor population. Bone marrow cells from 3-5 week-old WT or X-MAID male mice were harvested, counted, and processed for flow cytometry. **(A)** Proportion and absolute number of hematopoietic stem cells (HSC) ($CD150^+CD48^-$) displayed as gated on $Lin^-Sca1^+Ckit^+$ (LSK) population. **(B)** Proportion and absolute number of common lymphoid progenitors (CLP) ($Flt3^+IL7R\alpha^+$) displayed are gated on $Lin^-Sca1^{LOW}Ckit^{LOW}$. **(C)** Proportion and absolute number of granulocyte/macrophage progenitors (GMP) ($\%Fc\gamma RII/III^+CD150^-$) displayed are gated on $Lin^-Sca1^-Ckit^+CD41^-$. Data represent means ± StDev, with each point representing an individual mouse. Statistics were calculated using a Student's *t* test, *p < 0.05, **p < 0.01, ***p < 0.005, ****p < 0.001.

To better understand the striking downregulation of moesin expression that takes place in peripheral T cells, we asked if moesin mRNA levels are affected by conducting qPCR analysis on splenic $CD4^+$ T cells from WT, MKO, and X-MAID mice. As shown in **Figure 5D**, moesin mRNA levels were significantly reduced in T cells from X-MAID mice. Indeed, the levels were just above the baseline set by MKO cells. Unexpectedly, we found that ezrin mRNA levels were also significantly reduced in X-MAID T cells. This contrasts with MKO T cells, where ezrin mRNA is expressed at WT levels. Taken together, these data show that the $moesin^{R171W}$ gene encodes a protein that is expressed in leukocytes but is selectively downregulated in peripheral lymphocytes, and that downregulation occurs at the mRNA level. The fact that downregulation depends on cell type and developmental stage makes it unlikely that the moesin mutation directly impairs transcriptional efficiency or message stability. Instead, it seems possible that expression of the mutant protein has deleterious effects on cell function, which pressures cells to downregulate expression of the mutant protein. Since the ezrin locus is also affected, this feedback mechanism may involve common transcriptional regulatory factors.

X-MAID T Cells Have Broad Migration Defects Due to the Inability to Polarize

The selective loss of $moesin^{R171W}$ in mature lymphocytes suggests that expression of the mutant protein is particularly deleterious for these cells. One known function of moesin in T cells is as an organizer of cell migration. Indeed, either deletion of moesin or expression of constitutively active ERM proteins causes defects in lymphocyte migration *in vitro* and *in vivo* (22, 25, 26, 28). We therefore asked if expression of the X-MAID point mutant disrupts cell migration. Because CD4 SP thymocytes are the most mature population that still express the mutant protein in most cells, we used this population for analysis. We first asked if CD4 SP thymocytes could migrate toward the chemoattractant CCL19 using a transwell assay system. As shown in **Figure 6A**, significantly fewer X-MAID thymocytes showed chemotactic responses in this assay. The failure of X-MAID thymocytes to chemotax efficiently does not reflect an inability of these cells to sense chemokine or signal through the receptor, because stimulation with CCL19 induced actin polymerization as well as phosphorylation of ERK and Akt in mutant thymocytes (**Figures 6B, C**). Indeed, CCL19-induced ERK phosphorylation was consistently elevated in X-MAID thymocytes. The reason for this remains unclear, though it may reflect dysregulation of inositol lipid homeostasis and Ras signaling responses.

We next used live cell imaging to better define the migratory phenotype of X-MAID thymocytes. Since chemokine signaling is intact, we hypothesized that these cells exhibit general defects in motility. To test this, we imaged cells undergoing random migration on surfaces coated with integrin ligands. CD4 SP thymocytes from WT and X-MAID mice were observed while migrating on the LFA-1 ligand, ICAM-1, using live cell microscopy. In agreement with the transwell data, we found that whereas about 50% of WT thymocytes migrated in this assay (defined as having a net displacement of at least 10μm), only about 10% of X-MAID thymocytes met this criterion (**Figure 7A**). Moreover, even the motile subset of X-MAID thymocytes traveled a much shorter distance than WT cells, as measured by net displacement and total track length (**Figures 7B, C**). By observing the tracks of individual cells, the difference in migratory behavior between WT and X-MAID thymocytes is readily observed. Whereas a subset of WT

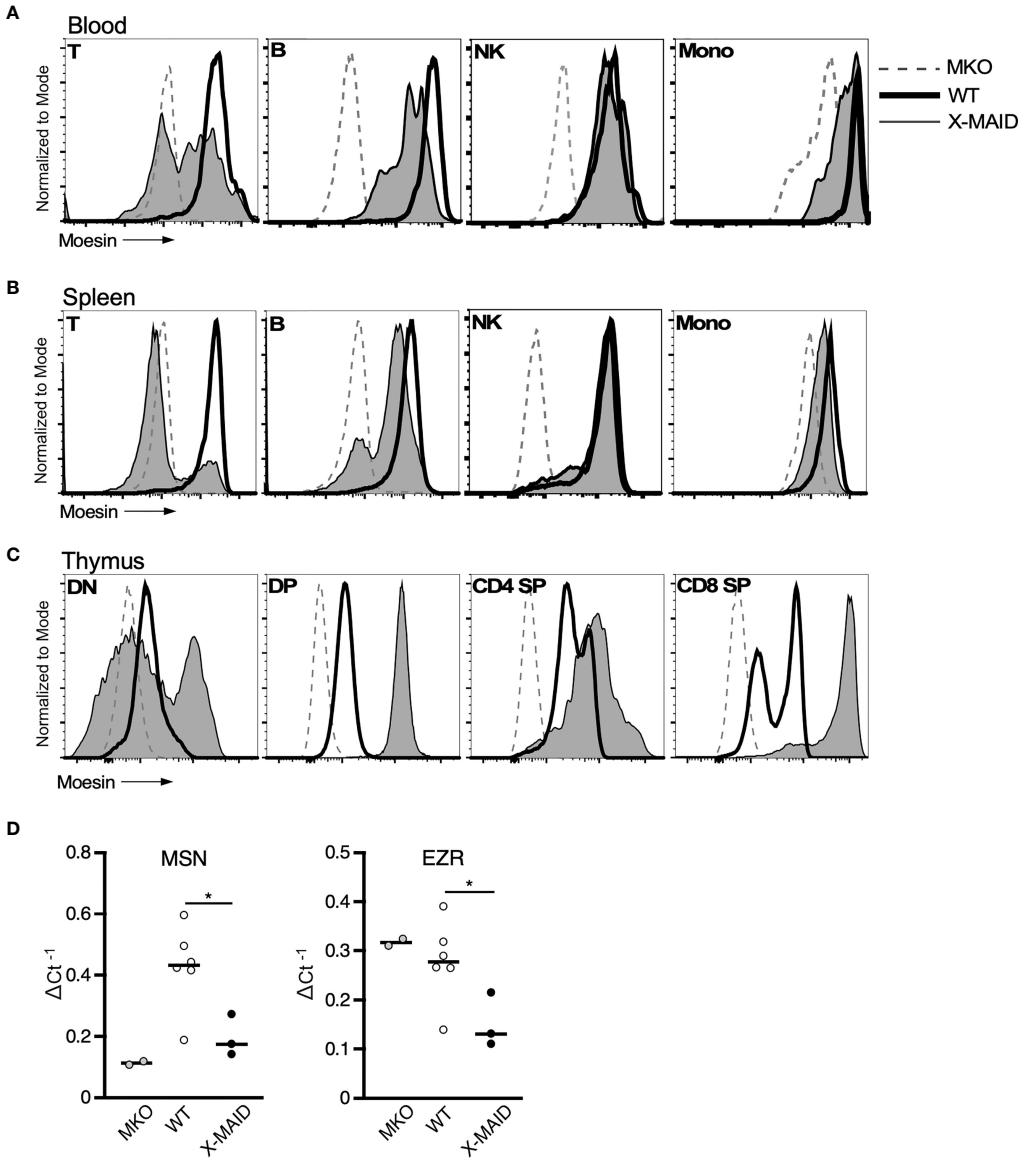

FIGURE 5 | Moesin^{R171W} expression is selectively lost in peripheral T cells. 3-4 week-old WT, X-MAID, or MKO male mice were sacrificed and the indicated tissues were harvested and processed for single cell suspensions. Cells were labeled for surface markers, and for intracellular moesin. For blood **(A)** and spleen **(B)**, populations were gated on live single cells, followed by TCRβ$^+$ (T), CD19$^+$ (B), NK1.1$^+$ (NK), and CD11b$^+$Ly6C$^+$ (Mono). For thymus **(C)**, populations were gated on live single cells, followed by CD4$^-$CD8$^-$ (DN), CD4$^+$CD8$^+$ (DP), CD4 SP, or CD8 SP. **(D)** Relative *Msn* (left) and *Ezr* (right) mRNA expression in CD4$^+$ splenic T cells from WT, X-MAID, or MKO male mice. Expressed as the inverse of the Ct of indicated gene subtracted from that of *Gapdh*. Bars in D represent means. Statistics between WT and X-MAID groups were calculated using a Student's *t* test, *p < 0.05.

thymocytes traveled significant distances along relatively linear paths, the motile X-MAID thymocytes showed only wobbling movement around their starting positions (**Figure 7D** and **Supplemental Movies 1**, **2**). We confirmed that this reduction in migration on ICAM-1 is not due to differences in integrin expression (**Figure S4**).

In order to migrate properly on integrin ligands, T cells must first polarize to form an elongated shape, with an actin-rich leading edge and a trailing, tubulin-rich uropod. In the course of analyzing our DIC movies, we frequently observed this type of polarized morphology in the WT thymocyte population, whereas the X-MAID cells seemed to maintain a rounded shape. To ask if X-MAID cells fail to elongate and undergo proper polarization of cytoskeletal elements, CD4 SP thymocytes from WT or X-MAID mice were left untreated or treated in solution with CCL19, fixed, and labeled with phalloidin and anti-tubulin antibodies. Cells were then observed by fluorescence microscopy and polarity was quantified as detailed in Materials and Methods. As shown in **Figure 7E**, unstimulated WT and X-MAID thymocytes were mostly quite round, with F-actin distributed over of the

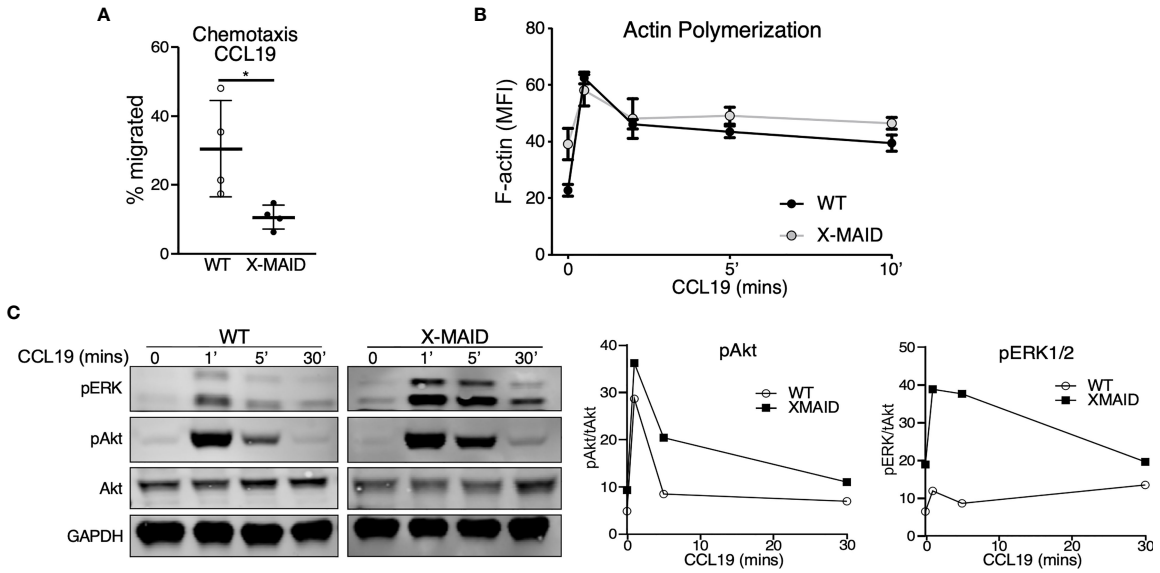

FIGURE 6 | X-MAID thymocytes are unable to properly chemotax despite intact signaling. WT or X-MAID CD4 SP thymocytes were **(A)** placed in the upper chamber of a 5 μm pore transwell with 100ng/ml CCL19 in the media of the bottom chamber and incubated at 37 degrees for 2 hours. Cells in the bottom chamber were counted and percent migrated calculated. Graph shows results from 4 independent experiments, with each data point representing an average of three technical replicates from one experiment. Each experiment used pooled cells from 3-5 X-MAID mice, and cells from one matched WT littermate control. Data represent means ± StDev. Statistics were calculated using a Student's *t* test, *p < 0.05. **(B)** WT or X-MAID CD4 SP thymocytes were left unstimulated, or stimulated with 100ng/ml CCL19 for the indicated times, permeabilized and stained with phalloidin to assess polymerized F-actin by flow cytometry. **(C)** Thymocytes stimulated as in B were fixed, lysed, and immunoblotted for pAkt (Ser473), pERK (Thr202/204), and total Akt and GAPDH as loading controls (left). WT and X-MAID samples were handled and analyzed in parallel. Blots were quantified by densitometry, and relative values were calculated after normalization to total Akt (right). For **(B, C)**, each experiment used pooled cells from 3-5 X-MAID mice, and cells from one matched littermate control. Results are representative of 3 independent experiments.

circumference of the cell, and the microtubule organizing center (MTOC) located at a random spot. After exposure to CCL19, a high proportion of WT cells become polarized, forming a clear actin-rich leading edge (arrowheads) and an opposing uropod marked by the MTOC (arrows). This segregation of cytoskeletal elements was accompanied by overall cell elongation, measured as a decrease in roundness (**Figure 7F**). In contrast, CCL19 stimulated X-MAID thymocytes looked very similar to unstimulated controls, with no clear rearrangement of actin and tubulin, and no reduction in roundness. A similar defect was observed in X-MAID thymocytes undergoing polarization in response to integrin engagement in the absence of chemokine (**Figure 7F**). While X-MAID thymocytes did show some elongation under these conditions, the response was blunted significantly. Taken together, these findings demonstrate that X-MAID thymocytes are unable to undergo appropriate morphological rearrangements necessary for motility, resulting in a general defect in cell migration.

DISCUSSION

Here, we describe a new mouse model that faithfully reflects many key features of human X-MAID immunodeficiency disease. Like their human counterparts, X-MAID mice exhibit profound lymphopenia and suffer from multiple opportunistic infections. The few T cells that are present in the periphery have a highly activated phenotype, and most have lost moesin expression. It seems likely that the extensive lymphocyte activation that we observe arises due to homeostatic proliferation occurring in response to severe lymphopenia, together with the profound loss of peripheral Tregs. Along with defects in lymphocytes, X-MAID patients also typically exhibit fluctuating neutropenia (9–12). We did not observe this in our mouse model. In fact, we observed an increased proportion of neutrophils in the blood and spleen at 4-5 weeks of age (**Figure S1C**). It remains unclear whether the apparent lack of neutropenia reflects a real difference between mice and humans, or if it is due to other factors, such as the lack of genetic variability in laboratory mice, housing in an SPF-facility, or timing of analysis (we did not analyze neutrophil numbers in a single mouse over time). Additionally, the opportunistic infections can induce neutrophilia that may not be seen in patients receiving prophylactic antibiotics.

Using the X-MAID mouse model, we could examine tissues that are inaccessible in the patients. Analysis of peripheral lymphoid organs revealed a loss of tissue architecture in the spleen, and an almost complete absence of lymph nodes. In the thymus, all developmental populations were present, suggesting that progression through thymic development occurs relatively normally. We did note a significant increase in the proportion SP thymocytes, possibly reflecting a defect in egress similar to that

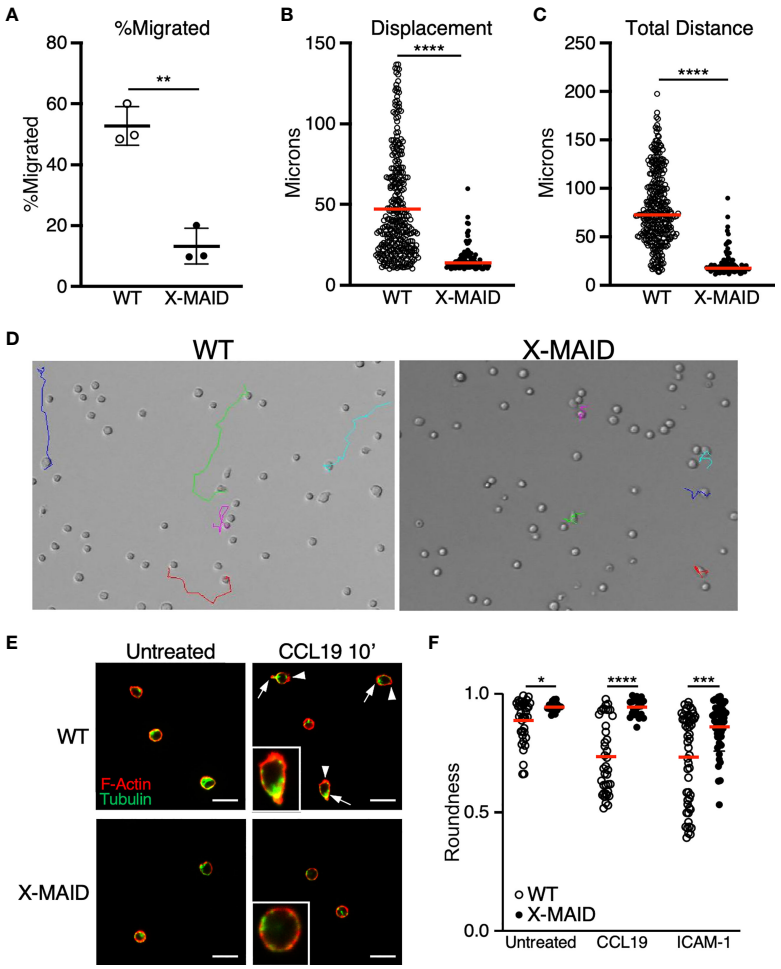

FIGURE 7 | Reduced migratory capability is associated with lack of polarization in X-MAID T cells. **(A–D)** WT or X-MAID CD4 SP thymocytes were placed on ICAM-1 coated glass surfaces and imaged live using DIC optics every 30 seconds for 10 minutes. Cells were tracked using the manual tracking plugin on ImageJ. **(A)** % migrated was calculated as any cell moving more than 10μm and remaining in view for the entirety of the movie. Each point represents a field of at least 100 cells. Data represent means ± StDev. **(B)** Displacement and **(C)** Total distance traveled were calculated from first frame to final frame. **(D)** Representative images of the final frame with colored tracks from individual cells. **(E)** CD4 SP thymocytes were left untreated or stimulated with 100ng/ml CCL19 for 10 minutes, then fixed to a poly-L coated surface and stained for F-actin and tubulin to visualize actin leading edge (arrowheads) and tubulin-rich uropods (arrows). Representative images are shown for each condition, insets show higher magnification views of typical cells. Scale bars = 20μm **(F)** Images like those in **(D, E)** were used to measure roundness of cells using ImageJ software as detailed in the Materials and Methods. Means ± StDev are shown. **(A–D)** show data from one experiment (performed using cells pooled from 3-5 mice). This experiment was done twice with separate pools of mice, with similar outcomes. The data in **(E, F)** are pooled from two separate experiments done on different days, with each experiment using cells pooled from 3-5 mice. Data from the two experiments were in agreement, so were pooled for presentation. In **(A)**, each point represents one field of cells; In **(B, C, F)** each point represents a single cell. Red bars in **(B, C, F)** represent means. Statistics for all panels were calculated using a Student's *t* test, *p < 0.05, **p < 0.01, ***p < 0.005, ****p < 0.001.

observed in moesin-deficient mice (29). Importantly, however, absolute numbers of thymocytes were severely reduced and thymic architecture was perturbed. Although Lagresle-Peyrou et al. (11) reported that X-MAID patients appear to have normal sized thymi, the same study and several others show that X-MAID patients have abnormally low T cell receptor excision circles (TRECs) (9–11), an indicator of low thymic output (38).

Analysis of bone marrow populations in X-MAID mice revealed a decrease in progenitor populations that are responsible for seeding the thymus. Since little is known about ERM protein expression or function within the bone marrow compartment, it is unclear why specific precursor populations are selectively impacted by expression of the mutant protein. One possibility is that the mutant protein is expressed in these cells and is deleterious for their proliferation or survival. However, since systemic stress suppresses LMPPs and CLPs (39), the reduction in these lineages could be a secondary effect of systemic stress due to infection, uncontrolled autoimmune inflammation, or malnutrition. A full understanding of how the X-MAID mutant protein impacts hematopoietic development will require the generation of an inducible mouse model, but our results indicate that the peripheral lymphopenia observed in

X-MAID patients probably reflects defects in both bone marrow and thymic populations.

Another area where analysis of the X-MAID mice has proven to be illuminating concerns the regulation of protein levels. In X-MAID patients, moesin expression is lost in peripheral T and B cells, and this loss increases with patient age and cellular activation status (9, 11). Consistent with this, we observed loss of expression in peripheral lymphocytes of X-MAID mice, along with elevation of activation markers. In the mouse model, we could also analyze moesin expression in thymic populations, thereby obtaining information that is unavailable from X-MAID patients. Interestingly, we found that thymocytes express the mutant protein efficiently. Indeed, expression of the mutant protein in X-MAID thymocytes is several-fold higher than in the corresponding WT populations. QPCR analysis showed similar moesin mRNA levels in WT and X-MAID thymocytes (data not shown), so overexpression likely occurs at the protein level. We are currently testing the possibility that the mutant protein is at least partially misfolded, and that its turnover is slowed.

Unlike upregulation of moesin in the thymus, we find that downregulation in peripheral T cells occurs at the mRNA level. This finding is consistent with observations in peripheral T cells from X-MAID patients, which showed diminished moesin mRNA levels (9, 11). Since this loss is dependent on cell type and differentiation state, it seems likely that mRNA downregulation involves feedback inhibition rather than direct effects of the moesin mutation on transcriptional rates or message stability. This is further supported by our finding of diminished ezrin mRNA levels in X-MAID T cells. While ezrin mRNA levels have not been reported for X-MAID patients, it has been noted that that these patients do not exhibit compensatory upregulation of ezrin protein, and it appears that ezrin protein levels are sometimes lower than in healthy donors (11). The mechanistic basis for the coordinate downregulation of ezrin and moesin in X-MAID lymphocytes remains to be determined. Since the two genes are located on different chromosomes, cis-acting regulatory mechanisms can be ruled out. Little is known about the transcriptional control of these genes, but it seems likely that they share common transcriptional regulators that are downmodulated in response to functional defects in X-MAID T cells.

Although the processes that control expression levels of moesin^{R171W} are unknown, it is clear that protein levels drop precipitously during the transition from SP thymocyte to mature peripheral T cell. This observation points to toxicity of moesin^{R171W} and selective pressure to silence protein expression. Exactly what drives this selective pressure remains to be determined. Since expression is specifically lost in peripheral T cells (and to a lesser extent in peripheral B cells), it appears that the mutant protein interferes with one or more cellular processes that are particularly important for mature lymphocytes. We considered the possibility that loss of moesin^{R171W} is needed to allow thymic egress. However, we consistently observe a population of peripheral T cells that retain high moesin expression, so egress cannot be completely blocked. Going forward, it will be important to know if the peripheral T cells that retain moesin expression are recent thymic emigrants. A definitive answer to this question will require breeding to RAG-GFP reporter mice. In mature T cells, there are multiple processes that may be impaired by expression of the mutant protein. In addition to migration, T cell activation, proliferation or survival may be affected. With respect to activation, we found that early activation markers are upregulated normally in X-MAID SP thymocytes stimulated with TCR ligands, but we have not tested TCR sensitivity or cytokine production. Even if activation proves to be intact, the mutant protein may perturb mitosis or apoptosis, since ERM proteins are known to be involved in both processes (40–43).

Despite the extensive lymphopenia in X-MAID mice, we show that lymphocytes are key drivers of pathology in this disease. When X-MAID mice were bred onto a RagKO background, systemic inflammation was dramatically reduced. This effect was clear; whereas all X-MAID mice die by 7-10 weeks of age, X-MAID/RagKO mice survive as long as RagKO littermate controls (data not shown). It is interesting to consider how lymphocytes could drive pathology in light of the changes in moesin^{R171W} expression during T cell development. Presumably, pathology is driven by cells that express the mutant protein because MKO mice do not have overt disease (28, 44). One possibility is that recent thymic emigrants still expressing the mutant protein drive disease. Mature B cells, most of which still express significant levels of the mutant protein, may also play a role. Breeding to mice that delete T or B cells at specific points in development, and experiments in which WT Tregs are transferred into neonatal X-MAID mice will be needed to determine which populations drive disease.

One of the most interesting and important questions going forward is how the R171W mutation affects moesin's linker activity, and how expression of this protein perturbs lymphocyte function. R171 is located within the FERM domain of the protein, in a region that makes contact with the ABD to form the autoinhibited conformation. The substitution of a bulky tryptophan residue may tend to disrupt moesin autoinhibition driving the protein toward the activated conformation. In keeping with this idea, we find that upon exposure to CCL19 or binding to integrin ligands, X-MAID thymocytes fail to undergo shape changes needed for polarized migration. The behavior of X-MAID thymocytes is reminiscent of the phenotype of B cells expressing a phospho-mimetic ezrin mutant that constitutively activates linker activity. Such cells are very round and rigid, and they fail to migrate properly both *in vitro* and *in vivo* (25, 26). Notably, defective chemotactic responses have also been reported in peripheral T cells from X-MAID patients, however the basis for these defects may differ, since moesin expression is mostly lost in these populations (11). Our work on peripheral T cells from MKO mice demonstrates the importance of characterizing the nature of migratory defects; these cells undergo normal lamellipodial-based migration in response to conventional chemokines like CCL19 and CXCL12, but exhibit defects in bleb-based motile responses to the lipid chemoattractant sphingosine-1-phosphate (29). Based on these comparisons, it seems likely that the migratory defects seen in X-MAID patients are multifaceted; thymocyte motility (and possibly also motility of bone marrow precursors) may be

poisoned by overexpression of a hypermorphic mutant protein, while migration of peripheral lymphocytes may be impaired by loss of moesin expression.

Given the complex nature of moesin function in the immune cells, pathology in X-MAID patients will almost certainly prove to involve dysregulation of several important immunological processes. The murine model described here will be invaluable as we tease apart the basis of disease at the molecular, cell biological, and organismal levels.

DATA AVAILABILITY STATEMENT

The original contributions presented in the study are included in the article/**Supplementary Material**. Further inquiries can be directed to the corresponding author.

ETHICS STATEMENT

The animal study was reviewed and approved by Institutional Animal Care and Use Committee of the Children's Hospital of Philadelphia Research Institute.

AUTHOR CONTRIBUTIONS

LA conceived, performed and analyzed the experiments. TR performed and analyzed experiments involving immunoblotting and immunofluorescence microscopy. CW performed analysis of cell signaling and migration. NR performed and analyzed experiments involving live cell microscopy. SC performed and analyzed experiments involving qPCR. EP and AV assisted with analysis of bone marrow populations, with guidance and oversight from IM. JB conceived the project and oversaw its execution. LA and JB wrote the paper with critical input from all authors. All authors contributed to the article and approved the submitted version.

FUNDING

This work was supported by seed funds from the University Research Foundation and the Foerderer Foundation to JB and by NIH K12GM081259 to LA. SC was supported by NIH Medical Scientist Training Program T32 GM007170. Additional support was from NIAID (R01-AI091627 to IM, F30-AI136325 to EP, F30-AI161873 to AV, T32-AI070077 to AV).

ACKNOWLEDGMENTS

The authors thank the Flow Cytometry and Pathology core facilities at the Children's Hospital of Philadelphia for their assistance with this work. We also thank Drs. Jorge Henao-Mejia and Leonel Joannas for assistance with the design and generation of X-MAID CRISPR mice, and the CRISPR/Cas 9 mouse targeting core and the Transgenic and Chimeric Mouse Facility at University of Pennsylvania for generation of the X-MAID mice. Our gratitude to Mackenzie Schade for her attentive care of the X-MAID and other mouse colonies. We thank Dr. Paula Oliver for valuable advice, members of the Burkhardt lab for critical conversations and reading of the manuscript, and Christopher Davis for expert administrative assistance.

SUPPLEMENTARY MATERIAL

The Supplementary Material for this article can be found online at: https://www.frontiersin.org/articles/10.3389/fimmu.2021.726406/full#supplementary-material

Supplementary Figure 1 | Analysis of additional cell populations in X-MAID mice. 3-5 week-old WT and X-MAID male mice were sacrificed and spleen **(A)** and blood **(B)** were collected and processed for flow cytometry. Cells were gated on live single cells then $CD19^+$ (B cells), $NK1.1^+$ (NK cells), $CD11b^+Ly6C^+$ (Monocytes), $CD11b^+Ly6G^+$ (Neutrophils), and the proportion of cells in each population was determined. Each point represents an individual mouse. **(C)** Representative flow plot of neutrophil populations in the blood of WT or X-MAID mice. Data in A and B represent means ± StDev. Statistics were calculated using a Student's *t* test $^{**}p < 0.01$, $^{***}p < 0.005$, $^{****}p < 0.001$.

Supplementary Figure 2 | $CD8^+$ T cells in the spleen of X-MAID mice have an activated phenotype. 3-5 week-old WT and X-MAID male mice were sacrificed and splenocytes were analyzed by flow cytometry. CD44 and CD62L were analyzed gated on live, single, $CD8^+$ cells. Data are representative of results from at least 6 individual mice.

Supplementary Figure 3 | Detailed analysis of bone marrow precursor populations in WT and X-MAID mice. **(A)** Diagram of precursor populations, with markers used for analysis. **(B-F)** Bone marrow from 3-5 week-old WT or X-MAID mice was harvested, counted, and analyzed by flow cytometry after labeling with the antibody panels outlined in A. **(B)** Proportion and absolute number of LSK (% $Sca1^+cKit^+$) populations are displayed; gated on Lin^- population. **(C)** Proportion and absolute number of multipotent progenitor (MPP) (%CD48–$CD150^-$) are displayed; gated on $Lin^-Sca1^+cKit^+$. **(D)** Proportion and absolute number of lymphoid-primed multipotent progenitor (LMPP) (%$Flt3^-IL7R\alpha^+$) are displayed; gated on $Lin^-Sca1^+cKit^+$. **(E)** Proportion and absolute number of megakaryocyte precursors (MkP) (%$CD150^+CD41^+$) are displayed; gated on $Lin^-Sca1^-cKit^+$. **(F)** Proportion and absolute number of erythroid progenitors (EryP) (%$CD105^+$ $CD150^+$) are displayed; gated on $Lin^-Sca1^-cKit^+Fc\gamma RII/III^-CD41^-$. Note that this population is equivalent to the pre-CFU-E population (37). Data in **(B-F)** represent means ± StDev, with each point representing an individual mouse. Statistics were calculated using a Student's *t* test $^{**}p < 0.01$, $^{***}p < 0.005$, $^{****}p < 0.001$.

Supplementary Figure 4 | Integrin expression is normal or slightly elevated on X-MAID thymocytes. 3 week-old WT or X-MAID male mice were sacrificed and thymocytes were labeled for flow cytometry. Cells were gated on live, single cells then CD4 SP or CD8 SP. Surface levels of CD29 (the β1 chain of VLA-4) and CD18/CD11a (LFA-1) were as high or higher than on WT cells. Data are representative of results from three individual mice.

Supplemental Movie 1 | WT CD4 SP thymocytes were placed on ICAM-1 coated glass surfaces and live imaged using DIC optics every 30 seconds for 10 minutes. Cells were tracked using the manual tracking plugin on ImageJ. Color tracks follow individual cells over time.

Supplemental Movie 2 | X-MAID CD4 SP thymocytes were placed on ICAM-1 coated glass surfaces and live imaged using DIC optics every 30 seconds for 10 minutes. Cells were tracked using the manual tracking plugin on ImageJ. Color tracks follow individual cells over time.

REFERENCES

1. Beemiller P, Krummel MF. Regulation of T-Cell Receptor Signaling by the Actin Cytoskeleton and Poroelastic Cytoplasm. *Immunol Rev* (2013) 256:148–59. doi: 10.1111/imr.12120
2. Burkhardt JK, Carrizosa E, Shaffer MH. The Actin Cytoskeleton in T Cell Activation. *Annu Rev Immunol* (2008) 26:233–59. doi: 10.1146/annurev.immunol.26.021607.090347
3. Kumari S, Curado S, Mayya V, Dustin ML. T Cell Antigen Receptor Activation and Actin Cytoskeleton Remodeling. *Biochim Biophys Acta* (2014) 1838:546–56. doi: 10.1016/j.bbamem.2013.05.004
4. Le Floc'h A, Huse M. Molecular Mechanisms and Functional Implications of Polarized Actin Remodeling at the T Cell Immunological Synapse. *Cell Mol Life Sci* (2015) 72:537–56. doi: 10.1007/s00018-014-1760-7
5. Mattila PK, Batista FD, Treanor B. Dynamics of the Actin Cytoskeleton Mediates Receptor Cross Talk: An Emerging Concept in Tuning Receptor Signaling. *J Cell Biol* (2016) 212:267–80. doi: 10.1083/jcb.201504137
6. Moulding DA, Record J, Malinova D, Thrasher AJ. Actin Cytoskeletal Defects in Immunodeficiency. *Immunol Rev* (2013) 256:282–99. doi: 10.1111/imr.12114
7. Janssen WJ, Geluk HC, Boes M. F-Actin Remodeling Defects as Revealed in Primary Immunodeficiency Disorders. *Clin Immunol* (2016) 164:34–42. doi: 10.1016/j.clim.2016.01.009
8. Ham H, Billadeau DD. Human Immunodeficiency Syndromes Affecting Human Natural Killer Cell Cytolytic Activity. *Front Immunol* (2014) 5:2. doi: 10.3389/fimmu.2014.00002
9. Bradshaw G, Lualhati RR, Albury CL, Maksemous N, Roos-Araujo D, Smith RA, et al. Exome Sequencing Diagnoses X-Linked Moesin-Associated Immunodeficiency in a Primary Immunodeficiency Case. *Front Immunol* (2018) 9:420. doi: 10.3389/fimmu.2018.00420
10. Delmonte OM, Biggs CM, Hayward A, Comeau AM, Kuehn HS, Rosenzweig SD, et al. First Case of X-Linked Moesin Deficiency Identified After Newborn Screening for SCID. *J Clin Immunol* (2017) 37:336–8. doi: 10.1007/s10875-017-0391-9
11. Lagresle-Peyrou C, Luce S, Ouchani F, Soheili TS, Sadek H, Chouteau M, et al. X-Linked Primary Immunodeficiency Associated With Hemizygous Mutations in the Moesin (MSN) Gene. *J Allergy Clin Immunol* (2016) 138:1681–9.e1688. doi: 10.1016/j.jaci.2016.04.032
12. Henrickson SE, Andre-Schmutz I, Lagresle-Peyrou C, Deardorff MA, Jyonouchi H, Neven B, et al. Hematopoietic Stem Cell Transplant for the Treatment of X-MAID. *Front Pediatr* (2019) 7:170. doi: 10.3389/fped.2019.00170
13. Garcia-Ortiz A, Serrador JM. ERM Proteins at the Crossroad of Leukocyte Polarization, Migration and Intercellular Adhesion. *Int J Mol Sci* (2020) 21:1502. doi: 10.3390/ijms21041502
14. Michie KA, Bermeister A, Robertson NO, Goodchild SC, Curmi PMG. Two Sides of the Coin: Ezrin/Radixin/Moesin and Merlin Control Membrane Structure and Contact Inhibition. *Int J Mol Sci* (2019) 20:1996. doi: 10.3390/ijms20081996
15. Shaffer MH, Huang Y, Corbo E, Wu GF, Velez M, Choi JK, et al. Ezrin Is Highly Expressed in Early Thymocytes, But Dispensable for T Cell Development in Mice. *PloS One* (2010) 5:e12404. doi: 10.1371/journal.pone.0012404
16. Gary R, Bretscher A. Ezrin Self-Association Involves Binding of an N-Terminal Domain to a Normally Masked C-Terminal Domain That Includes the F-Actin Binding Site. *Mol Biol Cell* (1995) 6:1061–75. doi: 10.1091/mbc.6.8.1061
17. Nakamura F, Amieva MR, Furthmayr H. Phosphorylation of Threonine 558 in the Carboxyl-Terminal Actin-Binding Domain of Moesin by Thrombin Activation of Human Platelets. *J Biol Chem* (1995) 270:31377–85. doi: 10.1074/jbc.270.52.31377
18. Nakamura F, Huang L, Pestonjamasp K, Luna EJ, Furthmayr H. Regulation of F-Actin Binding to Platelet Moesin *In Vitro* by Both Phosphorylation of Threonine 558 and Polyphosphatidylinositides. *Mol Biol Cell* (1999) 10:2669–85. doi: 10.1091/mbc.10.8.2669
19. Yonemura S, Hirao M, Doi Y, Takahashi N, Kondo T, Tsukita S, et al. Ezrin/Radixin/Moesin (ERM) Proteins Bind to a Positively Charged Amino Acid Cluster in the Juxta-Membrane Cytoplasmic Domain of CD44, CD43, and ICAM-2. *J Cell Biol* (1998) 140:885–95. doi: 10.1083/jcb.140.4.885
20. Yonemura S, Matsui T, Tsukita S, Tsukita S. Rho-Dependent and -Independent Activation Mechanisms of Ezrin/Radixin/Moesin Proteins: An Essential Role for Polyphosphoinositides *In Vivo*. *J Cell Sci* (2002) 115:2569–80. doi: 10.1242/jcs.115.12.2569
21. Fievet BT, Gautreau A, Roy C, Del Maestro L, Mangeat P, Louvard D, et al. Phosphoinositide Binding and Phosphorylation Act Sequentially in the Activation Mechanism of Ezrin. *J Cell Biol* (2004) 164:653–9. doi: 10.1083/jcb.200307032
22. Brown MJ, Nijhara R, Hallam JA, Gignac M, Yamada KM, Erlandsen SL, et al. Chemokine Stimulation of Human Peripheral Blood T Lymphocytes Induces Rapid Dephosphorylation of ERM Proteins, Which Facilitates Loss of Microvilli and Polarization. *Blood* (2003) 102:3890–9. doi: 10.1182/blood-2002-12-3807
23. Delon J, Kaibuchi K, Germain RN. Exclusion of CD43 From the Immunological Synapse Is Mediated by Phosphorylation-Regulated Relocation of the Cytoskeletal Adaptor Moesin. *Immunity* (2001) 15:691–701. doi: 10.1016/S1074-7613(01)00231-X
24. Allenspach EJ, Cullinan P, Tong J, Tang Q, Tesciuba AG, Cannon JL, et al. ERM-Dependent Movement of CD43 Defines a Novel Protein Complex Distal to the Immunological Synapse. *Immunity* (2001) 15:739–50. doi: 10.1016/S1074-7613(01)00224-2
25. Liu Y, Belkina NV, Park C, Nambiar R, Loughhead SM, Patino-Lopez G, et al. Constitutively Active Ezrin Increases Membrane Tension, Slows Migration, and Impedes Endothelial Transmigration of Lymphocytes *In Vivo* in Mice. *Blood* (2012) 119:445–53. doi: 10.1182/blood-2011-07-368860
26. Parameswaran N, Matsui K, Gupta N. Conformational Switching in Ezrin Regulates Morphological and Cytoskeletal Changes Required for B Cell Chemotaxis. *J Immunol* (2011) 186:4088–97. doi: 10.4049/jimmunol.1001139
27. Belkina NV, Liu Y, Hao JJ, Karasuyama H, Shaw S. LOK Is a Major ERM Kinase in Resting Lymphocytes and Regulates Cytoskeletal Rearrangement Through ERM Phosphorylation. *Proc Natl Acad Sci USA* (2009) 106:4707–12. doi: 10.1073/pnas.0805963106
28. Hirata T, Nomachi A, Tohya K, Miyasaka M, Tsukita S, Watanabe T, et al. Moesin-Deficient Mice Reveal a Non-Redundant Role for Moesin in Lymphocyte Homeostasis. *Int Immunol* (2012) 24:705–17. doi: 10.1093/intimm/dxs077
29. Robertson TF, Chengappa P, Gomez Atria D, Wu CF, Avery L, Roy NH, et al. Lymphocyte Egress Signal Sphingosine-1-Phosphate Promotes ERM-Guided, Bleb-Based Migration. *J Cell Biol* (2021) 220:e202007182. doi: 10.1083/jcb.202007182
30. Doi Y, Itoh M, Yonemura S, Ishihara S, Takano H, Noda T, et al. Normal Development of Mice and Unimpaired Cell Adhesion/Cell Motility/Actin-Based Cytoskeleton Without Compensatory Up-Regulation of Ezrin or Radixin in Moesin Gene Knockout. *J Biol Chem* (1999) 274:2315–21. doi: 10.1074/jbc.274.4.2315
31. Henao-Mejia J, Williams A, Rongvaux A, Stein J, Hughes C, Flavell RA. Generation of Genetically Modified Mice Using the CRISPR-Cas9 Genome-Editing System. *Cold Spring Harb Protoc* (2016) 2016:pdb prot090704. doi: 10.1101/pdb.prot090704
32. Roy NH, Kim SHJ, Buffone AJr., Blumenthal D, Huang B, Agarwal S, et al. LFA-1 Signals to Promote Actin Polymerization and Upstream Migration in T Cells. *J Cell Sci* (2020) 133::jcs248328. doi: 10.1242/jcs.248328
33. Ansa-Addo EA, Zhang Y, Yang Y, Hussey GS, Howley BV, Salem M, et al. Membrane-Organizing Protein Moesin Controls Treg Differentiation and Antitumor Immunity *via* TGF-Beta Signaling. *J Clin Invest* (2017) 127:1321–37. doi: 10.1172/JCI89281
34. Serrador JM, Alonso-Lebrero JL, del Pozo MA, Furthmayr H, Schwartz-Albiez R, Calvo J, et al. Moesin Interacts With the Cytoplasmic Region of Intercellular Adhesion Molecule-3 and Is Redistributed to the Uropod of T Lymphocytes During Cell Polarization. *J Cell Biol* (1997) 138:1409–23. doi: 10.1083/jcb.138.6.1409
35. Oguro H, Ding L, Morrison SJ. SLAM Family Markers Resolve Functionally Distinct Subpopulations of Hematopoietic Stem Cells and Multipotent Progenitors. *Cell Stem Cell* (2013) 13:102–16. doi: 10.1016/j.stem.2013.05.014
36. Pronk CJH, Bryder D. Immunophenotypic Identification of Early Myeloerythroid Development. *Methods Mol Biol* (2018) 1678:301–19. doi: 10.1007/978-1-4939-7346-0_13

37. Pronk CJ, Rossi DJ, Mansson R, Attema JL, Norddahl GL, Chan CK, et al. Elucidation of the Phenotypic, Functional, and Molecular Topography of a Myeloerythroid Progenitor Cell Hierarchy. *Cell Stem Cell* (2007) 1:428–42. doi: 10.1016/j.stem.2007.07.005
38. Baker MW, Grossman WJ, Laessig RH, Hoffman GL, Brokopp CD, Kurtycz DF, et al. Development of a Routine Newborn Screening Protocol for Severe Combined Immunodeficiency. *J Allergy Clin Immunol* (2009) 124:522–7. doi: 10.1016/j.jaci.2009.04.007
39. Pietras EM, Mirantes-Barbeito C, Fong S, Loeffler D, Kovtonyuk LV, Zhang S, et al. Chronic Interleukin-1 Exposure Drives Haematopoietic Stem Cells Towards Precocious Myeloid Differentiation at the Expense of Self-Renewal. *Nat Cell Biol* (2016) 18:607–18. doi: 10.1038/ncb3346
40. Kunda P, Pelling AE, Liu T, Baum B. Moesin Controls Cortical Rigidity, Cell Rounding, and Spindle Morphogenesis During Mitosis. *Curr Biol* (2008) 18:91–101. doi: 10.1016/j.cub.2007.12.051
41. Roubinet C, Decelle B, Chicanne G, Dorn JF, Payrastre B, Payre F, et al. Molecular Networks Linked by Moesin Drive Remodeling of the Cell Cortex During Mitosis. *J Cell Biol* (2011) 195:99–112. doi: 10.1083/jcb.201106048
42. Hebert M, Potin S, Sebbagh M, Bertoglio J, Breard J, Hamelin J. Rho-ROCK-Dependent Ezrin-Radixin-Moesin Phosphorylation Regulates Fas-Mediated Apoptosis in Jurkat Cells. *J Immunol* (2008) 181:5963–73. doi: 10.4049/jimmunol.181.9.5963
43. Kondo T, Takeuchi K, Doi Y, Yonemura S, Nagata S, Tsukita S. ERM (Ezrin/Radixin/Moesin)-Based Molecular Mechanism of Microvillar Breakdown at an Early Stage of Apoptosis. *J Cell Biol* (1997) 139:749–58. doi: 10.1083/jcb.139.3.749
44. Chen EJ, Shaffer MH, Williamson EK, Huang Y, Burkhardt JK. Ezrin and Moesin Are Required for Efficient T Cell Adhesion and Homing to Lymphoid Organs. *PLoS One* (2013) 8:e52368. doi: 10.1371/journal.pone.0052368

Conflict of Interest: The authors declare that the research was conducted in the absence of any commercial or financial relationships that could be construed as a potential conflict of interest.

Publisher's Note: All claims expressed in this article are solely those of the authors and do not necessarily represent those of their affiliated organizations, or those of the publisher, the editors and the reviewers. Any product that may be evaluated in this article, or claim that may be made by its manufacturer, is not guaranteed or endorsed by the publisher.

frontiers in Immunology

ORIGINAL RESEARCH
published: 12 January 2022
doi: 10.3389/fimmu.2021.814570

Sorting Nexin 27 Enables MTOC and Secretory Machinery Translocation to the Immune Synapse

Natalia González-Mancha[1], *Cristina Rodríguez-Rodríguez*[1], *Andrés Alcover*[2] *and Isabel Merida*[1]*

[1] Department of Immunology and Oncology, Centro Nacional de Biotecnología-Consejo Superior de Investigaciones Científicas (CNB-CSIC), Madrid, Spain, [2] Institut Pasteur, Université de Paris, Unité Biologie Cellulaire des Lymphocytes, INSERM U1224, Ligue Nationale Contre le Cancer, Équipe Labellisée Ligue-2018, Paris, France

OPEN ACCESS

Edited by:
Jens Volker Stein, Université de Fribourg, Switzerland

Reviewed by:
Francisco Sanchez-Madrid, Autonomous University of Madrid, Spain
Jeremie Rossy, Biotechnology Institute Thurgau, Switzerland

***Correspondence:**
Isabel Merida
imerida@cnb.csic.es

Specialty section:
This article was submitted to T Cell Biology, a section of the journal Frontiers in Immunology

Received: *13 November 2021*
Accepted: *20 December 2021*
Published: *12 January 2022*

Citation:
González-Mancha N, Rodríguez-Rodríguez C, Alcover A and Merida I (2022) Sorting Nexin 27 Enables MTOC and Secretory Machinery Translocation to the Immune Synapse. Front. Immunol. 12:814570. doi: 10.3389/fimmu.2021.814570

Sorting nexin 27 (SNX27) association to the retromer complex mediates intracellular trafficking of cargoes containing PSD95/Dlg1/ZO-1 (PDZ)-binding C-terminal sequences from endosomes to the cell surface, preventing their lysosomal degradation. Antigen recognition by T lymphocyte leads to the formation of a highly organized structure named the immune synapse (IS), which ensures cell-cell communication and sustained T cell activation. At the neuronal synapse, SNX27 recycles PDZ-binding receptors and its defective expression is associated with synaptic dysfunction and cognitive impairment. In T lymphocytes, SNX27 was found localized at recycling endosomal compartments that polarized to the IS, suggesting a function in polarized traffic to this structure. Proteomic analysis of PDZ-SNX27 interactors during IS formation identify proteins with known functions in cytoskeletal reorganization and lipid regulation, such as diacylglycerol (DAG) kinase (DGK) ζ, as well as components of the retromer and WASH complex. In this study, we investigated the consequences of SNX27 deficiency in cytoskeletal reorganization during IS formation. Our analyses demonstrate that SNX27 controls the polarization towards the cell-cell interface of the PDZ-interacting cargoes DGKζ and the retromer subunit vacuolar protein sorting protein 26, among others. SNX27 silencing abolishes the formation of a DAG gradient at the IS and prevents re-localization of the dynactin complex component dynactin-1/p150^{Glued}, two events that correlate with impaired microtubule organizing center translocation (MTOC). SNX27 silenced cells show marked alteration in cytoskeleton organization including a failure in the organization of the microtubule network and defects in actin clearance at the IS. Reduced SNX27 expression was also found to hinder the arrangement of signaling microclusters at the IS, as well as the polarization of the secretory machinery towards the antigen presenting cells. Our results broaden the knowledge of SNX27 function in T lymphocytes by showing a function in modulating IS organization through regulated trafficking of cargoes.

Keywords: T lymphocytes, polarization, immune response, centrosome, diacylglycerol kinase ζ, retromer, SNX27

INTRODUCTION

Precise regulation of intracellular transport and vesicle fusion is of great importance in polarized cells, which depend on the delivery of cargoes to specialized areas of the plasma membrane to carry out their functions (1–3). In T cells, intracellular trafficking plays an essential role in the establishment of the immune synapse (IS), allowing the transport of surface receptors, signaling, adhesion, and scaffold molecules towards the cell-cell contact site, as well as their removal from there (4–8). Moreover, this process favors the polarized secretion of cytokines, lytic proteins and additional cargoes towards the antigen presenting cell (APC), modulating cell-cell communication (9–13). In this context, the rapid repositioning of the microtubule-organizing center (MTOC) is functionally linked to polarized trafficking. Although the regulatory mechanisms driving MTOC polarization are not fully understood, the formation of a stable diacylglycerol (DAG) gradient represents the first step for MTOC translocation (14–17).

A relevant player in the regulation of polarized trafficking is the sorting nexin (SNX) 27-retromer complex. SNX27 belongs to the SNX family of proteins, which are involved in intracellular trafficking and endosomal signaling. SNX27 is unique, as it is the only member of its family containing a N-terminal PSD95/Dlg1/ZO-1 (PDZ) domain that allows interaction with proteins bearing a C-terminal class 1 PDZ-binding motif (PDZ-bm). In addition, it can simultaneously mediate interaction with the vacuolar protein sorting protein 26 (Vps26) subunit of the retromer complex, which increases cargoes binding affinity and thus favors their recycling (8, 18). Firstly discovered in yeast, the retromer is a protein complex consisting in the association of two subcomplexes: the cargo-selection subcomplex, composed by the trimer Vps26-Vps35-Vps29, and the membrane-deforming subcomplex, which senses and induces membrane tubulation and is formed by the SNX-BAR heterodimer Vps5-Vps17 (19, 20). In mammals, the retromer trimer is conserved and includes Vps26A/Vps26B, Vps35, and Vps29 proteins (21–23). SNX-BAR heterodimers are formed by association of SNX1/SNX2 with SNX5/SNX6 (24). The retromer regulates the endosome-to-*trans* Golgi transport and the endosome-to-plasma membrane recycling, preventing cargo degradation (25–27). This tubular-based endosomal traffic is favored by retromer interaction with cytoskeleton components such as the motor dynein/dynactin complex or the Wiskott-Aldrich syndrome protein and SCAR homologue (WASH) complex, which regulates actin polymerization (8, 28, 29).

Several studies reported that SNX27-retromer function as a mediator of retrograde trafficking that contributes to sustain cell polarization. In neurons, SNX27 localizes to recycling endosomes and traffics to spines, facilitating the synaptic delivery of receptors (30). In epithelial cells, SNX27 recruits the epithelial cell-cell junction protein zonula occludens (ZO)-1/2 to recycling endosomes and distributes it to tight junctions (31). Similarly, SNX27 in T lymphocytes locates to recycling endosomes and traffics to the IS. This depends on mechanisms that require the presence of an intact PDZ domain (32, 33). However, the contributions of SNX27 and its associated cargoes to the formation of the IS has not yet been explored.

Here, we investigated the contribution of SNX27 to the polarized trafficking of cargoes and to the establishment of the IS in Jurkat T cells. We described that SNX27 controls the traffic towards the cell-cell interface of reported PDZ-interactors, including the retromer subunit Vps26 and the DAG kinase (DGK) ζ. SNX27 silencing abolishes the formation of a DAG gradient at the IS, an effect probably related to defective retrograde transport of DAG-enriched membranes to the cell-cell interface. Impaired DAG accumulation at the IS results in deficient synaptic recruitment of the motor protein dynactin-1/p150^{Glued} and the PDZ-interactor centromere protein J (CENPJ). Moreover, the absence of a proper DAG accumulation correlates with an incorrect polarization of the MTOC, the inefficient reorganization of the microtubule network, and modest defects in actin clearance at the IS. Furthermore, we observed defects in the arrangement of signaling microclusters, as well as in the polarization of the secretory machinery towards the IS. Our results strongly support a role for the SNX27-retromer-complex in IS-directed transport of associated cargoes, highlighting a critical role of SNX27 in the correct polarization of the MTOC during antigen recognition in Jurkat T cells.

MATERIALS AND METHODS

Reagents and Antibodies

Reagents used were: poly-L-lysine, bovine serum albumin (BSA), DAPI (all purchased from Sigma-Aldrich), RPMI-1640 and L-glutamine (Biowest), CMAC (CellTracker Blue 7-amino-4-chloromethylcoumarin), BODIPY 630/650, (both from Thermo Fisher), Prolong Gold (Invitrogen), and recombinant human intercellular adhesion molecule 1 (ICAM-1) (R&D systems). For antibody (Ab)-based stimulation, we used a mouse anti-human CD3 monoclonal Ab (300402, Biolegend). For immunofluorescence staining, we used anti-: β-tubulin (MAB3408, Merk Millipore), CENPJ (11517-1-AP, Proteintech), dynactin-1/p150^{Glued} (MA1-070 Thermo Fisher), SNX27 (ab77799, Abcam), pericentrin (ab4448, Abcam), phalloidin-AlexaFluor 488 (A12379, Thermo Fisher), phosphorylated CD3ζ (Y142) (558402, BD biosciences), phosphorylated ZAP70 (Tyr 319) (PA5-17815, Thermo Fisher), phosphorylated LAT (Tyr 220) (3584, Cell signaling), and Vps26 (AB181352, Abcam). The following fluorophore-conjugated secondary Ab were used: anti-rabbit IgG-AlexaFluor 488, anti-mouse IgG-AlexaFluor 488, anti-mouse IgG2a-AlexaFluor 647 (A11034, A-11029, A21241; Thermo Fisher), anti-rabbit IgG-Cy2, anti-rabbit IgG-Cy3, anti-rabbit IgG -Cy5, anti-mouse IgG1-Cy3, anti-mouse IgG-Cy3, anti-mouse IgG1-Cy5 (2338021, 111-166-046, 111-176-046, 115-165-205, 115-166-075, 115-175-166; Jackson ImmunoResearch), and anti-mouse IgG2b-FITC (2794539, Southern Biotech). For flow cytometry analysis, we used anti-mouse CD45-APC (17-0451-82, Thermo Fisher). For western blot, we used anti-SNX27 (ab77799, Abcam), anti-GAPDH (sc25778, Santa Cruz), anti-GFP (A11122, Invitrogen), anti-DGKζ

(ab105195, Abcam), and anti-p150Glued (MA1-070 Thermo Fisher). For immunoprecipitation, GFP-Trap Agarose (gta-20, ChromoTek) was employed.

Cell Lines, Culture, and Stimulation

Human leukemic Jurkat T cells were obtained from the American Type Culture Collection (TIB-152, clone E6-1). Triple parameter reporter cells (TPR) are a human Jurkat JE6.1-derived cell line transduced with NFAT-GFP, AP-1-mCherry and NF-κB-CFP generated as previously described (34).T cell stimulator (TCS) cells are Bw5147 cells (murine thymoma cell line) modified to stably express an anti-human CD3 single chain fragment anchored to the plasma membrane *via* a human CD14 stem (CD5L-OKT3scFv-CD14). A variant of TCS cells was further engineered by retroviral transduction to express high amount of human CD86 (TCS-CD86) (35). Both TPR and TCS were kindly donated by Dr. Peter Steinberger (Medical University of Vienna, Austria). Jurkat T, TPR and TCS cells were cultured in complete RPMI medium consisting on RPMI-1640 supplemented with 10% FBS and 2 mM L-glutamine.

To establish immune synapses, TCS, used as APCs, were labeled in complete RPMI medium containing 10 μM CMAC or 1 μM BODIPY 630/650 (1 h, 37°C, darkness). After being washed twice in PBS, TCS were added at 1:1 ratio on top of Jurkat T cells previously plated on poly-L-lysine-coated coverslips. Cells were incubated for the indicated times (37°C, 5% CO_2), after which immunofluorescence was performed.

For signaling microclusters, actin and microtubules immunofluorescence, Jurkat T cells in complete RPMI medium (2×10^6 cells/ml) were seeded onto poly-L-lysine-coated glass coverslips with plate-bound anti-human CD3 (2.5 μg/ml) and recombinant human ICAM-1 (1 μg/ml, 2 h, 37°C) for the depicted times.

Plasmids and Transfection

Jurkat T cells in logarithmic growth phase ($4\text{-}5 \times 10^5$ cells/ml) were electroporated using the Gene Pulser II (Bio-Rad; 270 V, 975 μF) or the Neon Transfection System (ThermoFisher; 1200 V; 10 ms pulse width; 2 pulses). For transient SNX27 silencing, double-strand oligonucleotides encompassing the interfering sequence 5′-CCAGGUAAUUGCAUUUGAA-3′ (36) and a hairpin structure were cloned in the pSuper vector (Oligoengine) (32). pSUPER-shRNAi mouse DGKα (37) was used as a transfection control. For transient protein expression, 15 μg plasmid DNA were transfected. The pEGFP-C1-hSNX27 (WT/L67-77A/H114A) (18) were a kind gift from Dr. Peter Cullen (University of Bristol, UK). mCherry-DGKζ WT, pEFbos-GFP DGKζ-ΔETAV, pEGFP-C1b-PKCθ, and pEGFP-C1-CD63 were previously described (38–40). While silenced cells were harvested 72 h post-transfection, cells with transient protein expression were processed 24 h post-transfection.

Analysis of Protein Expression by Western Blot and Immunoprecipitation

For western blot analysis, cell pellets were suspended in cold lysis buffer (10 mM HEPES pH 7.5, 15 mM KCl, 1 mM EDTA, 1 mM EGTA, 10% glycerol, and 1% Nonidet P-40) containing protease inhibitors (10 μg/ml each leupeptin and aprotinin, 1 mM phenylmethylsulfonyl fluoride, 1 mM sodium orthovanadate, 40 mM β-glycerophosphate, and 10 μM NaF), and incubated 15 min at 4°C. A constant amount per sample was run in sodium dodecyl sulfate polyacrylamide gel electrophoresis (SDS-PAGE). Fluorescent signal was visualized using the Odyssey CLx Imaging System (LI-COR). SNX27 silencing was validated for every experiment by western blot analysis of total cell lysates.

For protein-protein interaction analysis by immunoprecipitation, cells were lysed as described above and the protocol was performed according to manufacturer's instructions (GFP-Trap Agarose, Chromotek). Immunoprecipitated proteins were analyzed by western blot.

Dual-Luciferase IL-2 Reporter Assay

Jurkat cells were transfected with control or SNX27-targeting shRNAi constructs by electroporation. At 48 h post-transfection, cells were re-electroporated with 15 μg of an IL-2 promoter construct (Addgene) together with 200 ng of Renilla luciferase vector (Promega) as an internal control. After 24 h, cells were stimulated with TCS cells at a 2.5:1 ratio in 96-well plates for the indicated time points. Lastly, cells were harvested, lysed in passive lysis buffer (Promega; 20 min, 4°C) and assayed for luciferase activity using the Dual-luciferase Reporter Assay (Promega). Relative luciferase units (RLU) were calculated relative to Renilla luciferase values.

Il-2 Detection in Culture Supernatants

Jurkat T cells transfected with control or SNX27-targeting shRNAi constructs were incubated with TCS cells at 2.5:1 ratio in a flat bottom 96 well plate in triplicates for the indicated time points. Then, ELISA test was performed on the culture supernatants according to manufacturer's intructions (Human IL-2 ELISA MAX_{TM} Delux, Biolegend).

NFAT, NFkB, and AP-1 Promoter Activity Assay

TPR cells transfected with shcontrol or shSNX27 were incubated with TCS at 2.5:1 ratio for the indicated time points. Then, cocultures were stained with anti-mouse CD45-APC in PBS staining buffer (PBS, 1% FBS, 0.5% BSA, 0.01% sodium azide) (30 min, 4°C, darkness) to exclude TCS cells from analysis. Expression of NFAT-GFP, NFκB-CFP and AP-1-Cherry was determined by flow cytometry using a CytoFLEX S Flow cytometer (Beckman Cloulter). Live cells were gated using forward and side scatter parameters. All conditions were carried out in triplicates and data were analyzed using FlowJo 10 software (FlowJo, Ashland, OR) and Prism 5.

Immunostaining

For immunofluorescence labeling, cells were fixed with 2% PFA (15 min, RT). After washing twice with PBS, cells were blocked and permeabilized 30 min, RT (1% BSA, 0.1% triton in PBS). This buffer was also used throughout the procedure as staining buffer. Cells were incubated with primary antibodies (1 h, RT), PBS-washed, and incubated with the corresponding fluorophore-

conjugated secondary Ab (30 min, RT). Coverslips were washed twice in PBS and mounted on glass slides using ProLong Gold. For microtubule and signaling microclusters staining, 2% PFA fixation was performed at 37°C and this step was followed by an ice-cold methanol fixation and permeabilization (20 min, RT) prior to Ab staining.

Confocal Microscopy and Image Processing

Confocal images were acquired using: Leica TCS SP8 confocal microscope equipped with a Plan-Apochromat HCX PL APO 63 × 1.4 NA oil immersion objective, Zeiss Axiovert LSM 510-META inverted confocal microscope equipped with a Zeiss Plan-Apochromat 63 × 1.4 NA oil objective, Zeiss Axiovert LSM 700 inverted confocal microscope equipped with a Plan-Apochromat 63 × 1.4 NA oil objective, or Olympus Fluoview FV1000 confocal microscope equipped with a Plan-Apochromat 60 × 1.4 NA oil objective. Images were collected with FV10-ASW4.2 (Olympus), LAS X (Leica), or ZEN 2009 (Zeiss) acquisition softwares. Sets to be compared were acquired using the same acquisition settings.

For quantitative analysis of protein synaptic recruitment we employed two distinct methods of quantification. For membrane proteins, accumulation at the IS was compared with the other areas of the plasma membrane: in T cell/TCS conjugates, maximal intensity Z-projections of contiguous optical sections (0.2 µm-wide) that included all the three-dimensional fluorescence information were stacked. Analysis was carried out using an in-house designed plugin for Fiji software developed by Carlos Oscar Sorzano and updated by Ana Cayuela (32). This plugin measures the mean fluorescence intensity (MFI) in circular regions of interest at the background, the IS, and the plasma membrane of the T cell outside the IS. Then the IS/plasma membrane MFI ratio was calculated as: (MFI IS - MFI background)/(MFI plasma membrane – MFI background). To quantify synaptic recruitment of proteins present at internal compartments/endosomes, fluorescence accumulated at the IS was compared with total cell fluorescence. Images were acquired as explained above and were analyzed as previously described (32). Briefly: MFI of background, whole cell, and IS regions were computed. Afterwards, the IS/cell MFI ratio was calculated as: (MFI IS - MFI background)/(MFI whole cell - MFI Background). Ratio values are represented as dot plots, where each dot depicts an individual cell.

To analyze the recruitment of signaling microclusters to the IS, we carried out a previously reported quantification (41). Initially, the area of segmented cells was measured. Among each cell, microclusters present at the cell-coverslip optical section were defined as signal intensity maxima employing the "Find Maxima" method. A value of noise tolerance was arbitrarily set at each experiment according to its background. Finally, the number of clusters per cell was divided by the cell area to obtain the density of microclusters at the IS.

Microtubule network organization patterns at the IS were categorized by three researchers by observation of unlabeled images into two classes: pattern 1 (P1), radial microtubules anchoring at the periphery of the IS; pattern 2 (P2), non-radial microtubules unable to reach the periphery of the IS. Maximum intensity projections of 4 consecutive sections (0.8 µm) at the T cell-coverslip contact were generated using the Fiji software (42) and Huygens Pro software (version 14.10) was used to perform image deconvolution.

To quantify formation of the filamentous actin (F-actin) ring and its fluorescence intensity at the IS, analysis was carried out on a 1-µm-thick section at the cell-coverslip interface.Cells from multiple microscopic fields were manually defined, and their F-actin MFI was computed. To determine the F-actin phenotype at the IS, pixel intensity plots from a line across the IS were generated. Patterns were categorized in three different phenotypes. Ring: centrally depleted actin and F-actin ring at the periphery; intermediate: uneven depletion of actin with intensity dropping at the center of the IS; accumulated: F-actin all across the IS.

For centrosomal F-actin quantification, we first defined the centrosomal area. In order to do that, we carried out a radial line scan of F-actin fluorescence intensity from the MTOC of resting Jurkat T cells. The drop in fluorescence intensity was used a threshold to define the radius of the centrosomal area. Based on our results, we defined the centrosomal F-actin area as a circumference of 1 µm of radius around the MTOC. Background subtraction (rolling ball 50 pixel) on the average z-projection of the three planes above and below the MTOC was performed. Finally, the mean intensity of F-actin fluorescence in the 2 µm-diameter circle centered at the MTOC was measured.

To measure the ability of the MTOC, CENPJ, or $CD63^+$ secretory lysosomes/multivesicular bodies (MVB) to translocate to the IS, maximum intensity projections of the whole cells (0.2 µm intervals) were generated using the ImageJ. The geometric center of MTOC, CENPJ, and MVB ($MTOC^C$, $CENPJ^C$ and MVB^C) as well as the IS region were determined. The polarity index was computed diving the distance between $MTOC^C$, $CENPJ^C$ or MVB^C to the IS ("a" distance) by the distance from the IS to the distal pole of the T cell ("b" distance). This allowed polarity indexes to be normalized by cell size and shape. We considered polarization to occur when the polarity index was <0.25. Polarity index values are represented in graphs as dot plots, where each dot represents an individual cell. To analyze the relative aligned position of the mass center of the MTOC and the center of the IS, a first axis was defined by drawing a straight line along the T cell-APC contact area, which was later divided in six regions of equal length. Then, a second axis was defined with two points: the mass center of the cell and the center of the immune synapse. Parallel lines to the second axis, intersecting at the six division points of the first axis were drawn, establishing three areas at each side of the second axis. Finally, MTOC position was categorized in symmetric, intermediate or asymmetric depending on which of those three areas (closest-to-furthest to the second axis) the MTOC was found.

The distance between the MTOC and the nucleus was measured in three dimensions using the Image 3D suite plugin on ImageJ. After applying a median 3D filter, nucleus and MTOC were automatically threshold in 3D (using Otsu and

iterative thresholding, respectively). Then, the shorter distance between the edges of these two organelles was computed.

Statistical Analysis

For co-localization analysis, Pearson's correlation and Mander's overlap coefficients were calculated using the JACoP plugin (Just Another Co-localization plugin) (43) of ImageJ software.

Statistical analysis was performed with GraphPad Prism 5 software and samples were assumed to fit normality. Details about the data presentation, the experimental replication, and the adequate statistical tests used are included in the individual figure legends. Briefly, unpaired student's *t*-test was used to analyze differences between two conditions. Unless otherwise indicated, two-way ANOVA with Bonferroni post-test was applied for multiple comparisons. The level of statistical significance is represented by * p <0.05; ** p <0.01; *** p <0.001; **** p <0.0001. Data are shown as mean ± standard error of the mean (SEM) unless otherwise specified.

RESULTS

SNX27 Facilitates Vps26 Retromer Protein Polarization to the IS

The SNX27 PDZ domain engages proteins bearing a PDZ-bm and simultaneously associate the Vps26 subunit of the retromer complex (8, 18). We have previously shown that SNX27 mutants defective for either Vps26 binding (GFP-SNX27 L67-74A) or cargo interaction (GFP-SNX27 H114A) showed defective recruitment to the IS in experiments with Jurkat T cells and SEE-loaded Raji B cells (44). Although it constitutes a well stablished system to investigate IS organization upon encounter of an APC, the loading of Raji B cells with bacterial superantigens such as SEE may be heterogenous. In order to study the IS in a setting resembling physiology, we set Jurkat T cells to interact with TCS-CD86, a mouse thymoma cell line modified to express a membrane bound anti-CD3 antibody fragment and the CD86 costimulatory molecule (35). In agreement with their reported association (44), immunofluorescence analysis showed a strong colocalization between GFP-SNX27 WT and endogenous Vps26 in resting Jurkat T cells (**Figure 1A**, top). The interaction with TCS-CD86 resulted in a complete polarization of the SNX27/Vps26 positive compartment to the cell-cell contact area (**Figure 1A**, bottom). Analysis of the GFP-SNX27 L67-74A confirmed a marked reduction in the colocalization with Vps26 (**Figures 1B**, top; **1C**). A slight decrease in SNX27-Vps26 colocalization was also observed in cells expressing GFP-SNX27 H114A (**Figures 1B**, bottom; **1C**). As described (33), both mutants show defective polarization to the IS, but they affected differently the localization of endogenous Vps26 (**Figures 1D, E**). The GFP-SNX27 L67-74A mutant showed partial accumulation at the IS, although this compartment was devoid of Vps26, that showed dispersal localization (**Figure 1D**, top). On the contrary, the mutant deficient in cargo binding retained colocalization with Vps26 in compartments that failed to polarize to the contact zone (**Figure 1D**, bottom). Deficient translocation of these SNX27 mutants correlated with a reduced accumulation of VPS26 at the IS (**Figure 1F**). These results suggest that the correct assembly of the SNX27-retromer complex together with its cargoes is required for its synaptic recruitment. This is further supported by a recent publication showing that impaired cargo recognition by SNX27 reduces retromer targeting to the plasma membrane (45).

The failure of Vps26 to relocate to the IS in GFP-SNX27 H114A overexpressing cells could be the result of sequestering the endogenous Vps26 away from its natural localization. To evaluate whether SNX27 was indeed required for Vps26 recruitment to the IS, we depleted cells for SNX27 (**Figure 1G**) and examined Vps26 localization upon engagement with TCS-CD86 cells. Analysis of endogenous proteins confirmed strong colocalization between SNX27 and Vps26 at the IS in control cells (**Figure 1H**, top). SNX27 silencing prevented the polarization of Vps26 positive vesicles, that in most cells appeared dispersed and opposite to the contact zone (**Figure 1H**, bottom; **1I**). These results confirm that PDZ-dependent interaction of SNX27 with Vps26 facilitates polarized traffic of this retromer subunit to the IS.

SNX27 Regulates DAG Accumulation at the IS

Antigen recognition by T cell receptor (TCR) results in the rapid activation of retrograde traffic from the plasma membrane to the Golgi/recycling endosomes (RE), that orient to the contact area to facilitate a polarized traffic to the IS. Studies in Jurkat T cells and primary T lymphocytes have shown that the Golgi and RE are highly enriched in DAG (46). Upon T cell interaction with APCs, the rapid translocation of DAG-enriched organelles facilitates the trafficking of DAG-loaded vesicles to the IS, contributing to the accumulation of this lipid at the cell-cell junction (46). We investigated whether SNX27 silencing alters the polarization of DAG-positive compartments to the IS. As previously reported (46), Jurkat T cells overexpressing a fluorescent construct with high affinity for DAG (GFP-C1bPKCθ) presented intense fluorescence accumulation at internal compartments, which was easily visible in fluorescence density profiles (**Figure 2A**, top). SNX27 silencing abolished compact intracellular DAG staining, and the sensor appeared distributed throughout the plasma membrane (**Figure 2A**, bottom). DAG-positive compartments polarized to the cell-cell contact site upon TCS-CD86 engagement (**Figure 2B**, top). However, SNX27-silenced cells failed to accumulate DAG-positive organelles to this region(**Figure 2B**, bottom; **2C**). Previous studies from our group employing live cell imaging showed that upon cell-cell contact, a rapid burst of DAG at the IS is rapidly followed by polarization of DAG-enriched compartments to this region (46). The fast dynamics of DAG generation and traffic are difficult to capture in fixed images, as DAG is dispersed over the cell membrane after a short time after stimulation (39, 46). Nevertheless, we did observe a few control cells at initial contacts with TCS-CD86 displaying enrichment of DAG at the plasma membrane of the IS prior to the full translocation of SNX27 and DAG-enriched compartments (**Supplementary Figure 1**).

DGKζ transforms DAG into phosphatidic acid (PA), therefore contributing to the regulation of DAG content in T cells (46). DGKζ contains a PDZ-bm that provides high affinity

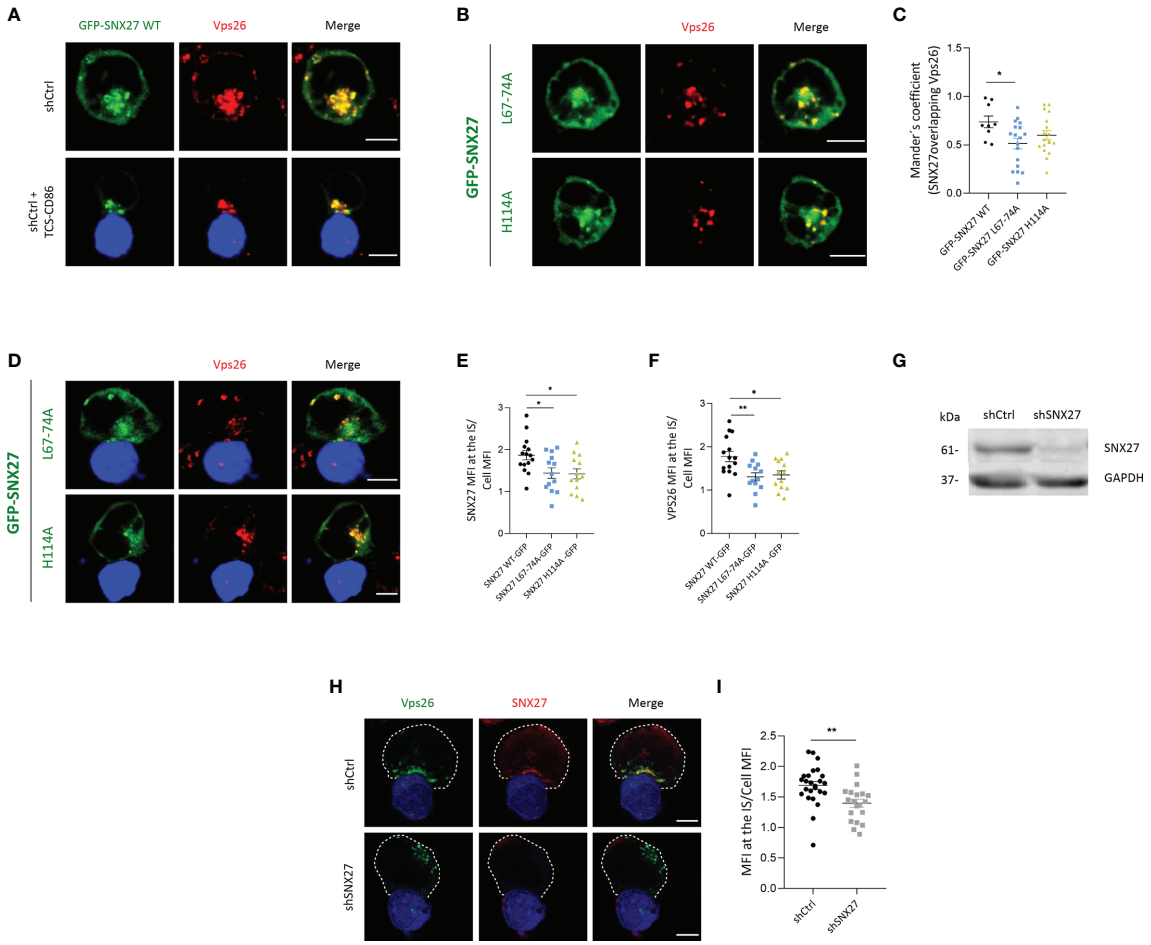

FIGURE 1 | SNX27 interacts with Vps26 and contributes to its translocation to the IS. **(A, B, D)** Representative confocal images of Jurkat T cells transfected with plasmids encoding **(A)** GPF-SNX27 WT (green), **(B, D)** GFP-SNX27 L67-74A or GFP-SNX27 H114A (green) in basal conditions (**A**, top; **B**) or after incubation with TSC-CD86 (blue) (**A**, bottom; **D**). Cells were immunostained for Vps26. **(C)** Mander´s coefficient. Data in the graph are mean ± SEM of a representative experiment of two with similar results (GFP-SNX27 WT = 9 cells; GFP-SNX27 L67-744 = 18 cells; GFP-SNX27 H114A = 18 cells). **(E)** Quantification of SNX27 or **(F)** Vps26 translocation measured as the ratio of signal intensity at the IS compared with the total signal in the cell. Ratio values are displayed as dot plots, with each dot representing a single cell. Data are shown as mean ± SEM of an experiment (GFPSNX27 WT = 15 cells; GFP-SNX27 L67-744 = 13 cells; GFP-SNX27 H114A = 13 cells). **(G)** Western blot analysis of cell lysates from shControl and shSNX27 Jurkat T cells. **(H)** Representative maximum intensity projections from confocal images of control or SNX27-silenced Jurkat T cells incubated with TCS-CD86 (blue) and stained against Vps26 and SNX27. Dashed white line indicates cell contour. **(I)** Quantification of Vps26 translocation. Data are shown as mean ± SEM of a representative experiment of three with similar results (shCtrl = 25 cells; shSNX27 = 20 cells). Scale bars = 5 µm. Significance in **(C, E, F, I)** was determined by one-way ANOVA with Bonferroni correction (*$p < 0.05$; **$p < 0.01$).

interaction with SNX27 (47). Thus, we next explored the consequences of SNX27 silencing in the subcellular localization of its cargo DGKζ. In basal conditions, mCherry-DGKζ- was distributed between the plasma membrane and internal organelles that were positive for endogenous SNX27 (**Figure 2D**, top). Upon SNX27 silencing, this internal localization was lost and mCherry- DGKζ was mainly observed at the plasma membrane (**Figure 2D**, bottom). GFP-DGKζ ΔETAV, a DGKζ mutant lacking the last four amino acids of its PDZ-bm, showed a localization mainly restricted to the plasma membrane both in the presence and in the absence of SNX27 (**Figure 2E**). These data confirm the PDZ-dependent engagement of DGKζ with SNX27 and demonstrate that this interaction is indispensable for retrograde traffic of DGKζ to the Golgi/RE in basal conditions. Upon incubation with TCS-CD86 cells, control Jurkat T cells displayed strong accumulation of mCherry-DGKζ- at the IS (**Figure 2F**, top). Nevertheless, DGKζ accumulation at the cell-cell interface was impaired in SNX27-silenced cells and this DGK isoform remained randomly distributed at the plasma membrane (**Figure 2F**, bottom; **2G**). These data suggest that retrograde traffic of DGKζ to internal compartments is indispensable for this lipid kinase to reach the IS and support a non-previously reported role for SNX27 in the spatial localization of DGKζ, which could affect its functions.

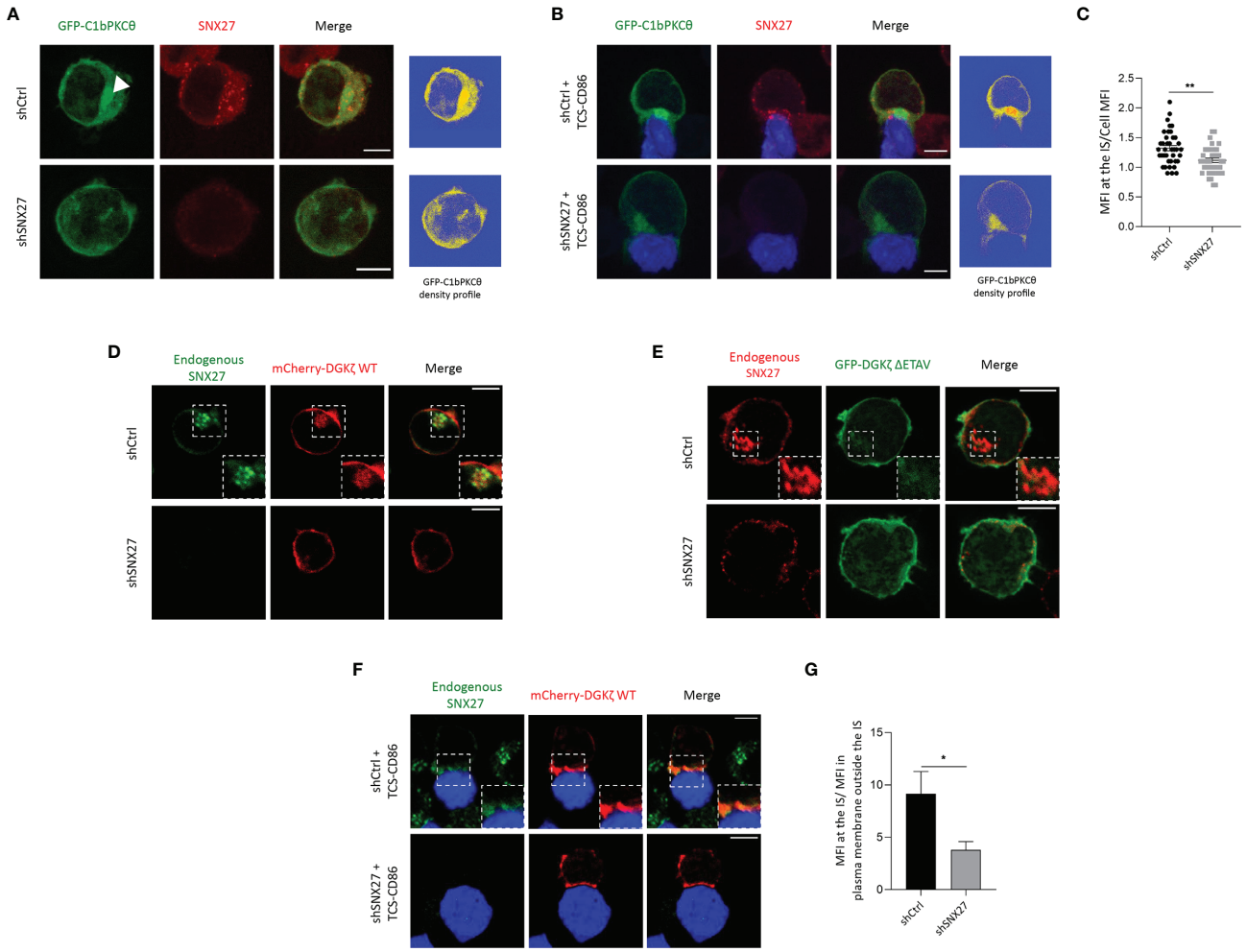

FIGURE 2 | SNX27 controls DGKζ and DAG translocation to the IS. **(A, B)** Representative maximum intensity projections from confocal images of control or SNX27-silenced Jurkat T cells transfected with the C1 domain of PKCθ fused to GFP construct (GFP-C1bPKCθ, green) in basal conditions **(A)** or after incubation with TCS-CD86 (blue) **(B)**. Arrowhead points DAG in intracellular compartment. A single medial optical section from a representative experiment out of three is shown. Right panels represent the density profiles of DAG fluorescence obtained from the medial optical section. Color scale goes from blue (zero) to yellow (intermediate) to red (maximal). **(C)** Quantification of GFP-C1bPKCθ translocation measured as the ratio of signal intensity at the IS compared with total GFP-C1bPKCθ. Ratio values are displayed as dot plots, with each dot representing a conjugate. Data are shown as mean ± SEM of two independent experiments (shCtrl = 40 cells; shSNX27 = 35 cells). Significance determined by unpaired *t-test* (*p < 0.05; **p < 0.01). **(D–F)** Representative confocal images of control of SNX27-silenced Jurkat T cells transfected with **(D, F)** a plasmid encoding mCherry-DGKζ WT (red) or with **(E)** a GFP-DGKζ ΔETAV (green) construct in basal conditions **(D, E)** or after incubation with TCD-CD86 (blue) **(F)**. A representative experiment out of three in **(D)** or two in **(E)** is shown. Pearson´s correlation coefficient in shCtrl cells = 0.648 in (**D**). **(G)** Quantitative image analysis of mCherry-DGKζ WT accumulated at IS compared with mCherry-DGKζ WT located in plasma membrane regions outside the IS. Data are shown as mean ± SEM from a representative experiment of two with similar results Significance was determined by unpaired *t-test* (*p < 0.05). Scale bar = 5 μm.

SNX27 Regulates MTOC Translocation to the IS

The formation of a stable DAG gradient upon T cell-APC engagement is required for the rapid docking of the MTOC at the IS in a process regulated by the dynein-dynactin motors (14–16). Noteworthy, the proteomic study in IS-forming Jurkat T cells revealed the presence of the p150^{Glued} dynactin complex subunit among the SNX27 interactors (44). Immunoprecipitation studies validated the reported association between p150^{Glued} and SNX27 (**Figure 3A**). Therefore, we explored the consequences of SNX27 silencing on p150^{Glued} dynamics upon T cell activation. We confirmed p150^{Glued} colocalization with SNX27 at the IS, and observed that its synaptic recruitment was lost when SNX27 was depleted **(Figures 3B, C).** Phosphorylated ζ-chain was stained as a marker for correct IS formation to discard the possibility of an ineffective T cell-APC engagement. These results corroborated the proteomic data and demonstrated that SNX27 contributes to the dynamic recruitment of p150^{Glued} to the IS upon APC engagement.

The observed failure of SNX27-silenced T cells to accumulate DAG and defective p150^{Glued} recruitment at the synaptic region

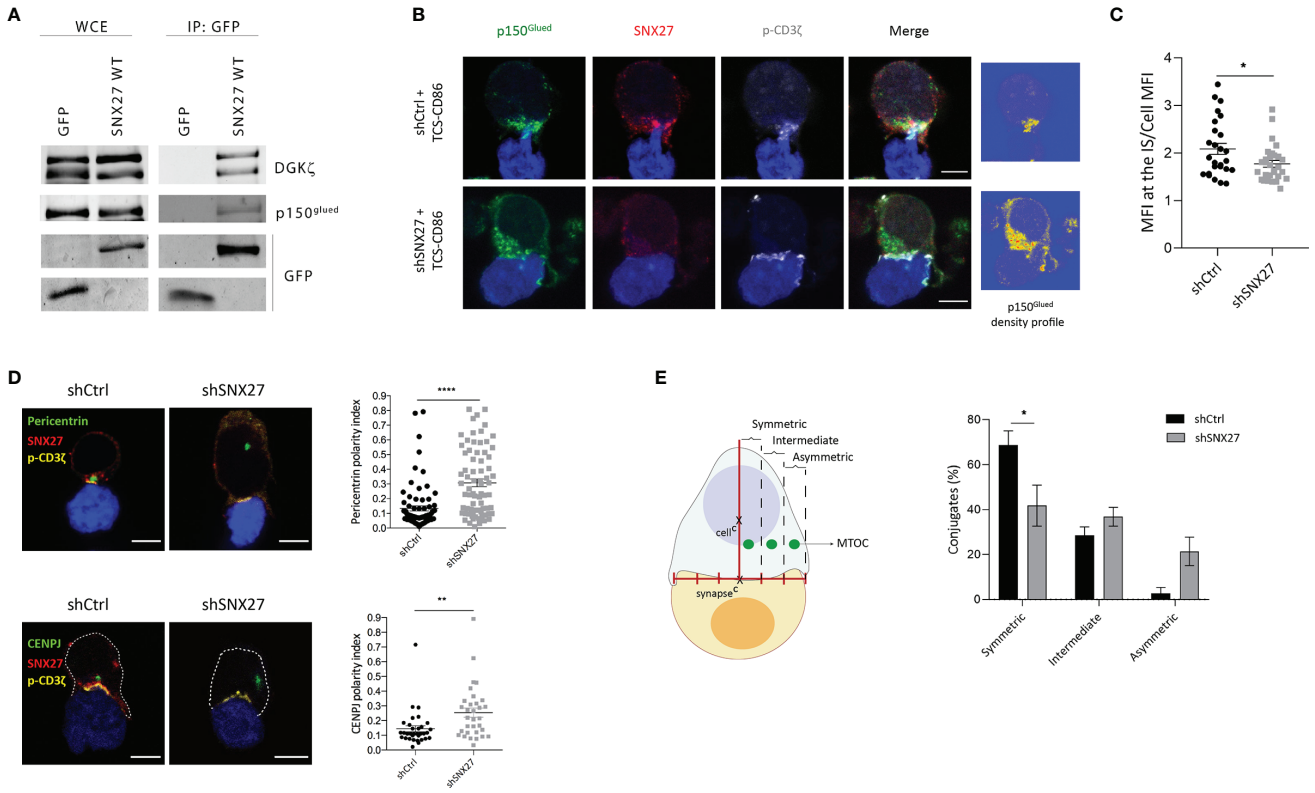

FIGURE 3 | SNX27 is necessary for MTOC translocation and its symmetry with the center of the IS in Jurkat T cells. **(A)** Western blot analysis of GFP immunoprecipitates confirmed interaction of p150^{glued} with GFP-SNX27 WT. DGKζ was used as a positive control. **(B)** Representative maximum intensity projection from confocal z-stacks of control and SNX27-silenced Jurkat T cells incubated with TCS-CD86 (blue). Cells were stained for the indicated proteins: dynactin-1/p150^{glued} (green), SNX27 (red) and phosphorylated CD3ζ (gray)Density profiles of dynactin-1 fluorescence obtained from the maximum intensity projections are shown in (**B**, right). Color scale goes from blue (zero) to yellow (intermediate) to red (maximal). **(C)** Quantification of p150^{glued} translocation measured as the ratio of signal intensity at the IS compared with total p150^{glued}. Ratio values are displayed as dot plots, with each dot representing a single cell. Data are shown as mean ± SEM of a representative experiment out of two run in duplicates (shCtrl = 26 cells; shSNX27 = 29 cells). Significance was determined by unpaired *t-test* (*p < 0.05; **p < 0.01, ****p < 0.0001). **(D)**, left] Representative confocal images of control and SNX27-silenced Jurkat T cells incubated with TCS-CD86 (blue). Cells were immunostained for pericentrin (MTOC, green) or CENPJ (green), SNX27 (red) and phosphorylated CD3ζ (yellow). Scale bar = 5 μm. [**(D)**, right] MTOC or CENPJ polarity index quantification calculated as the ratio between the distance from the MTOC or CENPJ to the IS and the distance from the IS to the distal pole of the cell. Polarity index values are displayed as dot plots, with each dot representing an individual cell. [**(E)**, left] Scheme depicting the strategy used to define MTOC symmetry (see methods section for detailed explanation). [**(E)**, right] Quantification of MTOC symmetry. Data in [**(D)**, right top; **(E)**] are mean ± SEM of three independent experiments in duplicates with shCtrl = 78 cells and shSNX27 = 74 cells, and in [**(D)**, left bottom] are mean ± SEM of a representative experiment out of three run in duplicates with shCtrl = 33 cells and shSNX27 = 32 cells. Significance was determined by unpaired *t* test in **(D)** and by two-way ANOVA with Bonferroni correction in **(E)**. (*p < 0.05; **p < 0.01; ****p < 0.0001).

strongly suggests a role for SNX27 in MTOC translocation. Immunofluorescence assessment of conjugates established between Jurkat T cells and TCS-CD86 demonstrated that pericentrin (MTOC protein) polarity index to the IS was statistically higher when SNX27 was depleted (**Figure 3D**, top). Our proteomic analysis in IS-forming Jurkat T cells had previously identified CENPJ as a PDZ-dependent cargo of SNX27 (44). CENPJ is a highly conserved centrosomal protein essential for centrosome biogenesis (48). In agreement with the defective pericentrin polarization, SNX27-silenced Jurkat T cells displayed impaired CENPJ reorientation upon engagement with TCS-CD86 stimulatory cells (**Figure 3D**, bottom).

Disrupted ability of T cells to sustain DAG at the IS prevents MTOC translocation, limiting the correct alignment of the protein trafficking machinery. We analyzed the impact of SNX27 silencing on the relative aligned position of the mass center of the MTOC and the center of the IS (**Figure 3E**, left). Distribution was categorized into symmetric, intermediate or asymmetric. SNX27 silencing led to a reduced percentage of cells with a symmetric MTOC position (**Figure 3E**, right). These results indicate that SNX27 facilitates the PDZ dependent transport of centrosomal proteins to the central region of the cell-cell contact area.

SNX27 Contributes to Peripheral, But Not Centrosomal, F-Actin Reorganization During T Cell Activation

F-actin depolymerization at the center of the IS has been described to play an important function in centrosome polarization in T cells

(49–53). Proteomic analysis in IS-forming T cells revealed a PDZ-independent interaction of SNX27 with the actin nucleators WASH complex, and Arp2/3 subunit ARPC5L (44). Using confocal microscopy, we evaluated the remodeling of F-actin at the IS in control and SNX27-silenced Jurkat T cells spread on anti-CD3 and ICAM-1-coated surfaces **(Figure 4A).** The establishment of pseudo-synapses on coverslips coated with stimulatory molecules facilitates the detailed analysis of molecule organization at the contact plane, and has been widely employed. F-actin organization patterns were classified in three phenotypes based on the F-actin pixel intensity plots across the synapse **(Figure 4A** lower panels): Ring, F-actin ring at the periphery with depletion of actin at the center; intermediate, uneven depletion of F-actin at the center of the synapse; accumulated, F-actin across the synapse. Although an F-actin ring was formed in both control and SNX27-silenced cells, we observed a modest defect in F-actin depletion across the center of the IS in SNX27-silenced cells, with a higher percentage of cells displaying an intermediate phenotype **(Figure 4B).** Besides, a significant reduction in F-actin MFI at the contact site was observed in the SNX27-silenced cells **(Figure 4C).** This suggests that failure in MTOC translocation could be prompted by a mild defect in F-actin depolymerization across the IS.

F-actin polymerization is also important around the centrosome to facilitate MTOC tethering to the nucleus in basal conditions (54–56). Studies in B cells have shown that F-actin nucleation around the centrosome is mediated by the nucleation-promoting factor WASH in combination with the Arp2/3 complex. Upon B lymphocyte activation, Arp2/3 translocates to the IS. This leads to F-actin depletion at the centrosomal area, favoring MTOC detachment and polarization to the cell-cell interface (54). The WASH complex associates to SNX27, so we wondered whether SNX27 deficiency would prevent centrosomal F-actin denucleation and MTOC detachment from the nucleus.

As reported by Farina et al. (55), F-actin filaments were found in the cortical region of Jurkat T cells, as well as in the vicinity of centrosomes **(Figure 5A).** Centrosomal F-actin and SNX27 exhibited a similar distribution. To determine the centrosomal F-actin area, we followed a procedure previously described by Obino et al. (56). Briefly, we carried out a radial line scan of F-actin fluorescence intensity from the centrosome of resting Jurkat T cells. Based on its gradual decrease, we defined the centrosomal actin area as a circumference of 1 μm of radius around the MTOC **(Figure 5B)**. Immunofluorescence analysis also confirmed the presence of a centrosomal F-actin pool in Jurkat T cells in synapse with TCS-CD86 **(Figure 5C).** Control and SNX27-silenced cells presented a similar percentage of centrosomal F-actin MFI in basal conditions, which was equally reduced upon synapse formation with TCS-CD86 **(Figure 5D).** In agreement, conjugate formation induced a mild physical separation of the MTOC from the nucleus. The shorter distance between the edges of these two organelles was measured in three dimensions, and no significant differences in MTOC-nucleus detachment were found between control and SNX27-silenced cells **(Figures 5E, F).** These results demonstrate that centrosomal F-actin nucleation and the derived MTOC detachment from the nucleus are SNX27-independent.

SNX27 Sustains Microtubule Organization at the IS

At the IS, microtubules growing from the MTOC radiate towards the periphery and anchor at the peripheral SMAC (pSMAC), characterized by dense LFA-1 clustering (57). In agreement, Jurkat T cells plated onto anti-CD3 and ICAM-1-coated coverslips showed a radially organized microtubule pattern, projecting to the periphery of the IS and with a visible translocated MTOC (defined as phenotype 1) **(Figure 6A**, top). SNX27-silenced Jurkat T cells more frequently displayed abnormal microtubule distribution that extended in filopodia-like shape unable to reach the periphery of the IS (defined as phenotype 2) (**Figure 6A**, bottom), as confirmed by image quantification (**Figure 6B**). Therefore, in addition to the mild defect in F-actin clearance at the IS and the failure to relocate the MTOC, SNX27-silenced Jurkat T cells present deficiencies in microtubule cytoskeleton organization at the IS. All in all, these results highlight a role for SNX27 in the control of cytoskeleton remodeling upon APC engagement.

SNX27 Facilitates Signaling Microclusters Organization at the IS

T cell interaction with an APC triggers the activation and recruitment of signaling and adaptor molecules that assemble into microclusters. The formation of supramolecular activation clusters in T cell synapses was first shown in the late 90s by Monks and colleagues using fluorescence microscopy (58). Although TCR signaling takes place at the IS, not all the molecules involved in this process are found at the plasma membrane, and regulated vesicular trafficking is crucial for their assembly and organization at the cell-cell interface. Signaling molecules described to be localized at vesicular compartments include TCR, LAT, and Lck (4, 59–64). Remarkably, the traffic of these molecules to the IS is not determined by the same routes, resulting in the spatial organization of signaling microclusters with distinct compositions. Of note, some of the molecules involved in TCR signaling, such as Lck, ZAP70, LAT, SLP76, PLCγ1, and the scaffolding protein ADAP have been reported to play a key role in MTOC translocation to the IS (16, 65, 66). Moreover, radial microtubules at the IS and dynein were shown to contribute to the centripetal transport of TCR and SLP microclusters, as well as to the p-LAT pattern at the IS (67, 68).

The finding that SNX27 silencing in Jurkat T cells affects cytoskeleton rearrangement, $p150^{Glued}$, and MTOC synaptic recruitment prompted us to evaluate the relationship between SNX27 and microclusters organization at the IS. In order to induce the formation of signaling microclusters, we set control or SNX27-silenced Jurkat T cells to spread over stimulation surfaces coated with anti-CD3 and ICAM-1. We fixed cells after 10 minutes and analyzed the density of Tyr 319 phosphorylated ZAP70 (p-ZAP70) and Tyr 220 phosphorylated LAT (p-LAT) by immunofluorescence. While the analysis of p-ZAP70 microclusters did not show major differences between control and SNX27-silenced cells **(Figures 7A, B),** we observed that the density of p-LAT microclusters was decreased in SNX27-silenced cells **(Figures 7C, D).** This revealed that presence of

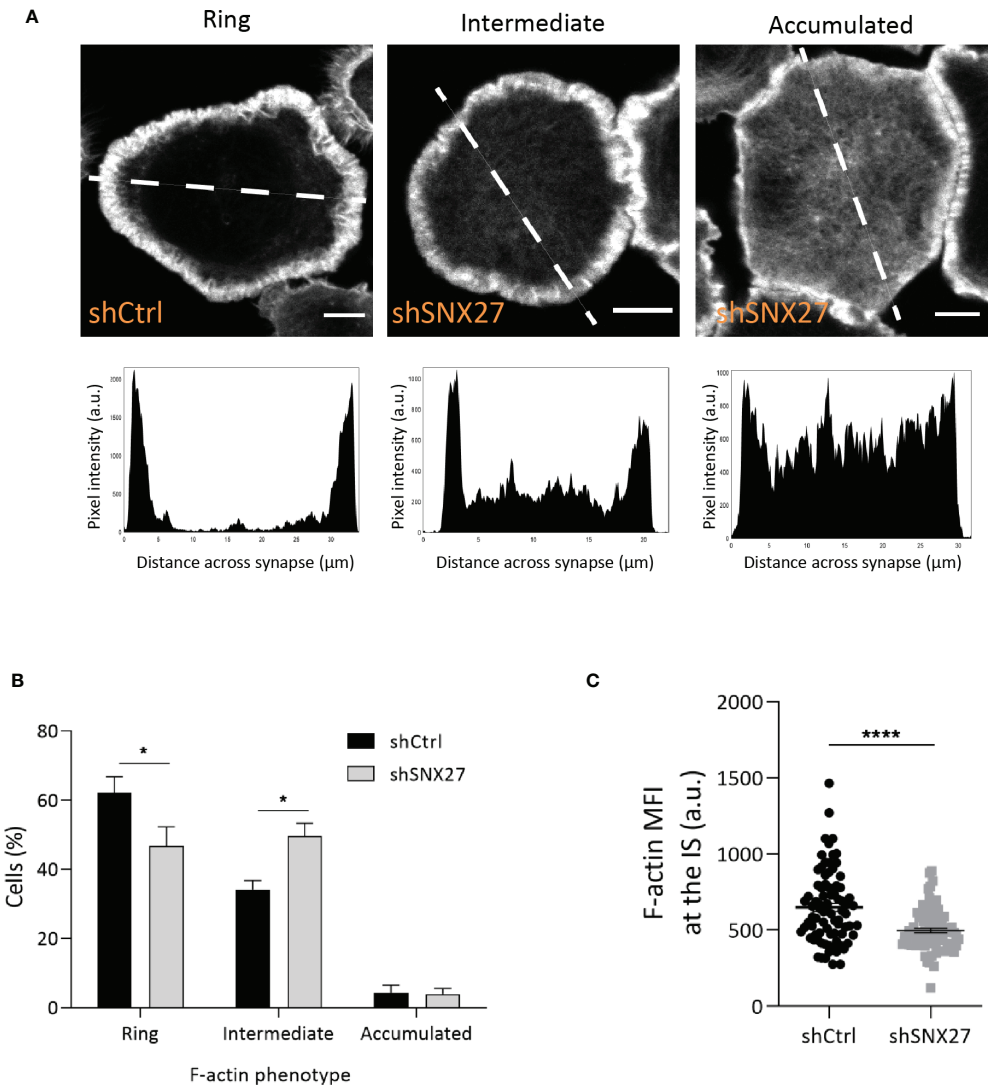

FIGURE 4 | SNX27 silencing in Jurkat T cells alters F-actin remodeling at the IS. Control and SNX27-silenced Jurkat T cells were stimulated on anti-CD3 and ICAM-1-coated coverslips and immunostained for phalloidin-A488 (F-actin). **(A)** Representative confocal section at the cell-coverslip interface. F-actin organization patterns were classified in three phenotypes based on the pixel intensity plots across the synapse (lower panels): ring: F-actin ring at the periphery with depletion of F-actin at the center; intermediate: uneven depletion of F-actin at the center of the synapse, low F-actin ring or clearance; accumulated: F-actin across the synapse. White line in the pictures represents the distance across the synapse plotted in graphs. Analyses were performed on a 1-µm-thick section at the cell-coverslips contact. Scale bar = 5 µm. **(B)** Quantification of F-actin phenotype at the IS. Data are shown as mean ± SEM of three experiments in duplicates (shCtrl= 306; shSNX27 = 330). Significance was determined by two-way ANOVA with Bonferroni correction (*$p < 0.05$). **(C)** Quantification of F-actin MFI carried out on control and SNX27-silenced cells on a 1-µm-thick section at the cell-coverslips contact, regardless of their F-actin pattern. Data are shown as mean ± SEM of a representative experiment out of three run in duplicates (shCtrl=82; shSNX27 = 83). Significance was determined by unpaired *t* -test (*$p < 0.05$; ****$p < 0.0001$).

SNX27 contributes to the correct arrangement of LAT signaling microclusters at the IS.

SNX27 Limits Transcriptional Activation, IL-2 Production and Secretion

Polarity regulators are crucial for T cell migration and cell remodeling upon encounter of an APC (69). Noteworthy, deficiency of some polarity proteins in T cells, such as ezrin, Dlg1 or adenomatous polyposis coli (Apc), lead to similar defects as the ones that we observe when silencing SNX27, such as impaired actin and microtubule reorganization at the IS or deficient MTOC translocation. These defects have been associated with altered T activation and effector function, such as hindered microclusters organization, decreased NFAT activation or IL-2 production (68, 70–72). In a previous study, we addressed in great detail the consequences of SNX27 silencing on T cell responses (33). Here we used the TPR Jurkat cell model engaged with TCS-CD86 to mimic the cell-cell contact between a

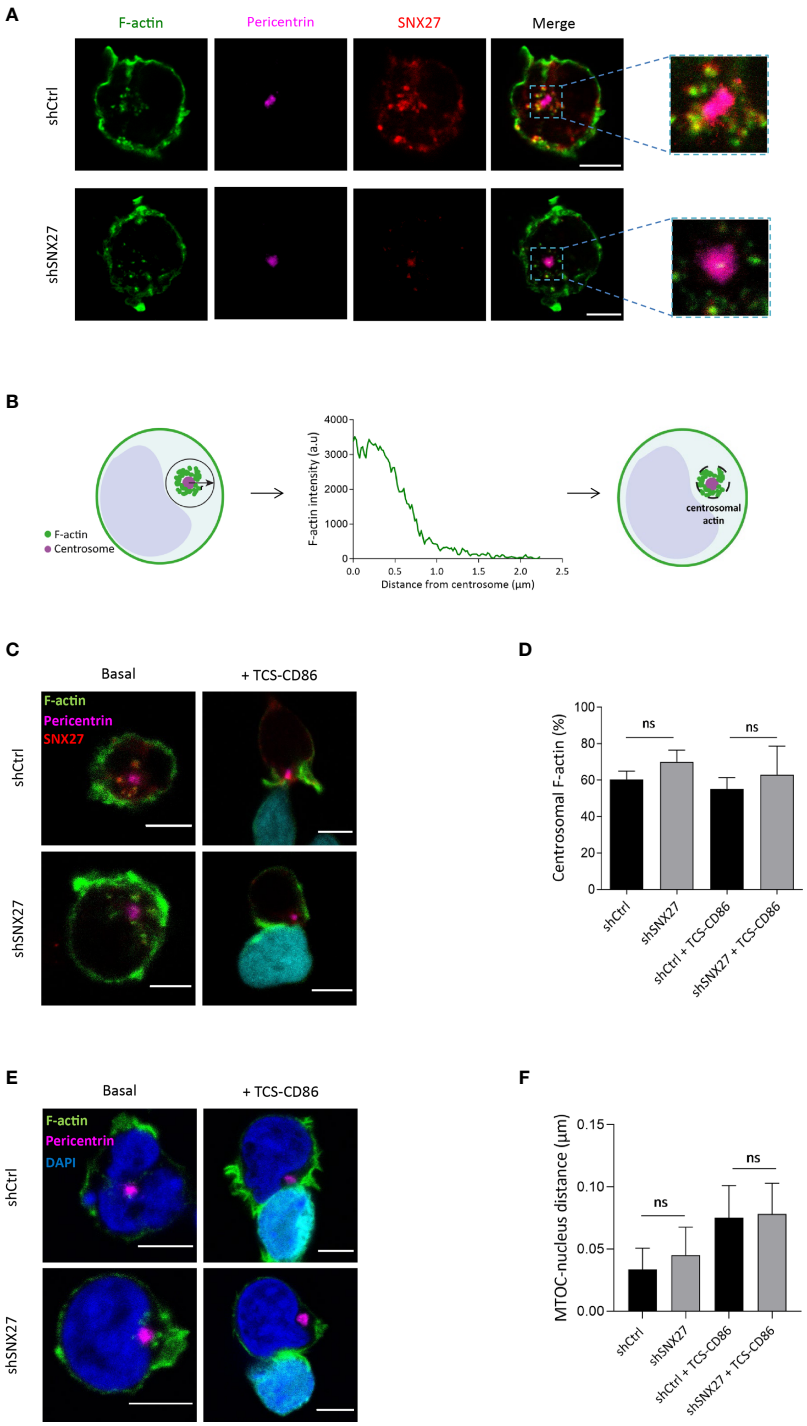

FIGURE 5 | Centrosomal F-actin nucleation and MTOC detachment from the nucleus in Jurkat T cells is not SNX27-dependent. **(A, C, E)** Representative confocal images of control and SNX27-silenced Jurkat T cells in basal conditions [**(A, C)**, left] or incubated with TCS-CD86 [**(C, E)**, right] labeled with CMAC in **(C)** and Bodipy in **(E)**. Cells were stained for the indicated proteins: phallo-A488 (F-actin, green), SNX27 (red), pericentrin (MTOC, pink) or DAPI (blue) to label the nuclei. Medial optical sections from a representative experiment out of three **(A)** or two **(C, E)** are shown. **(B)** Scheme depicting the strategy used to define the centrosome-associated F-actin region. **(D)** Quantification of the percentage of centrosomal F-actin from cells shown in **(C)**. Values correspond to the fraction of F-actin fluorescence in a 1 µm-wide area around the centrosome relative to the total fluorescence in the cell. **(F)** 3D Quantification of the shorter distance between the edge of the MTOC and the border of the nucleus from cells shown in **(E)**. Significance was determined by one-way ANOVA with Bonferroni correction (ns, not significant). Scales bars = 5 µm.

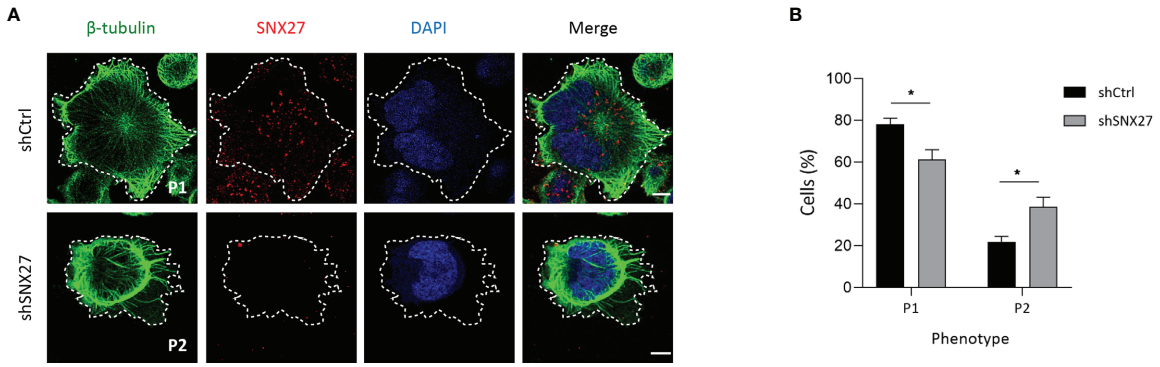

FIGURE 6 | SNX27 silencing in Jurkat T cells affects microtubule reorganization at the IS. **(A)** Representative confocal images of control and SNX27-silenced Jurkat T cells stimulated on anti-CD3 and ICAM-1-coated coverslips, and immunostained for SNX27 (red) together with anti-β-tubulin (green). Images were post-treated by deconvolution. Representative maximum intensity projections of 4 consecutive sections (0.8 µm) at the cell-coverslip contact are shown (n = 3). Dashed white line indicates cell contour, which was identified by thresholding β-tubulin fluorescence intensity signal. Scale bar = 5 µm. **(B)** Quantification of microtubule network organization patterns at the IS, categorized by observation of unlabeled images by three independent investigators in two classes: pattern 1 (P1), radial microtubules anchoring at the periphery of the IS, or pattern 2 (P2), non-radial microtubules unable to reach the periphery of the IS. Data shown as mean ± SEM of three independent experiments run in duplicates (shCtrl = 131 cells, shSNX27 = 141 cells). Significance was determined by two-way ANOVA with Bonferroni correction (*p <0.05).

T cell and an APC to further investigate the transcriptional control exerted by SNX27. TPR cells present response elements for NF-κB, NFAT, and AP-1 that drive the expression of the fluorescent proteins CFP, eGFP, and mCherry respectively, allowing assessment of these pathways by flow cytometry. (34). In agreement with previously reported data for DGKζ-silenced TPR cells (73), TCS-CD86 engagement of SNX27-silenced TPR cells promoted a more robust NF-κB and AP-1 induction but diminished that of NFAT compared to control cells (**Figure 8A**). The inhibitory effect of SNX27 silencing on NFAT activation resembles that described when silencing other polarity regulators, suggesting common mechanisms leading to it, such as defective microtubule organization (70).

The increased NF-κB and AP-1 activity correlated with an augmented IL-2 transcription in SNX27-silenced Jurkat T cells, as demonstrated by measuring the transcriptional activation of a luciferase-coupled IL-2 promoter in Jurkat T cells stimulated with TCS-CD86 for 24 h (**Figure 8B**). Determination of IL-2 on the supernatant revealed that TCR co-stimulation by TCS-CD86 resulted in increased IL-2 secretion in SNX27-silenced cells compared to control ones (**Figure 8C**). These results are in agreement with the enhanced IL-2 production and secretion reported in SNX27-silenced Jurkat T cells upon stimulation with soluble anti-CD3/CD28 (33). Altogether these data indicate an important contribution of SNX27 in the correct activation of T cell programs.

SNX27 Regulates Polarization of the Secretory Compartment

MTOC reorientation towards the IS facilitates polarized secretion of secretory granules and cytokines towards the cell-cell contact site (11, 74–76). It also mediates the polarization of MVB that fuse to the plasma membrane and release exosomes, favoring intercellular communication (12). Depletion of $p150^{Glued}$ in Jurkat T cells impaired clustering of vesicles around the MTOC although it did not prevent MTOC translocation (77). To evaluate the contribution of SNX27 in MVB polarization to the IS, we transfected Jurkat T cells with a plasmid encoding for GFP-fused CD63 and followed its localization upon stimulation with costimulatory TCS-CD86 cells. The tetraspanin CD63 is enriched on the intraluminal vesicles of late endosomes/MVB, which are secreted as exosomes. Besides, it is also abundant on lysosomes and a small pool is present at the cell surface (78). In control Jurkat T cells stimulated with TCS-CD86 cells, SNX27 appeared to colocalize with GFP-CD63, which congregated near the IS (**Figure 9A**, up). In contrast, GFP-CD63 in SNX27-silenced was found at distal locations from the cell-cell contact region (**Figure 9A**, bottom). Staining of phosphorylated CD3ζ at the IS was used to confirm cell activation. Polarity index of the MVB compartment was computed as the ratio between the distance from the center of mass of the MVB (MVB^C) to the IS ("a" distance) by the distance from the IS to the distal pole of the T cell ("b" distance) **(Figure 9B).** Calculation of MVB polarity indexes and percentage of conjugates with polarized MVB confirmed their impaired translocation in the absence of SNX27 **(Figure 9C).** Video-microscopy studies also corroborated the results observed in fixed conjugates (data not shown). This finding suggests that SNX27 is necessary for the efficient polarization of the exosome secretory machinery to the IS.

DISCUSSION

The polarization of the MTOC and the secretory machinery to the IS represent two mechanisms indispensable for correct T cell functions. SNX27 best characterized role is that of facilitating PDZ-mediated rapid recycling of its transmembrane cargoes from endosomes to the plasma membrane, avoiding their lysosomal degradation (8, 25, 28). Here we add a novel and

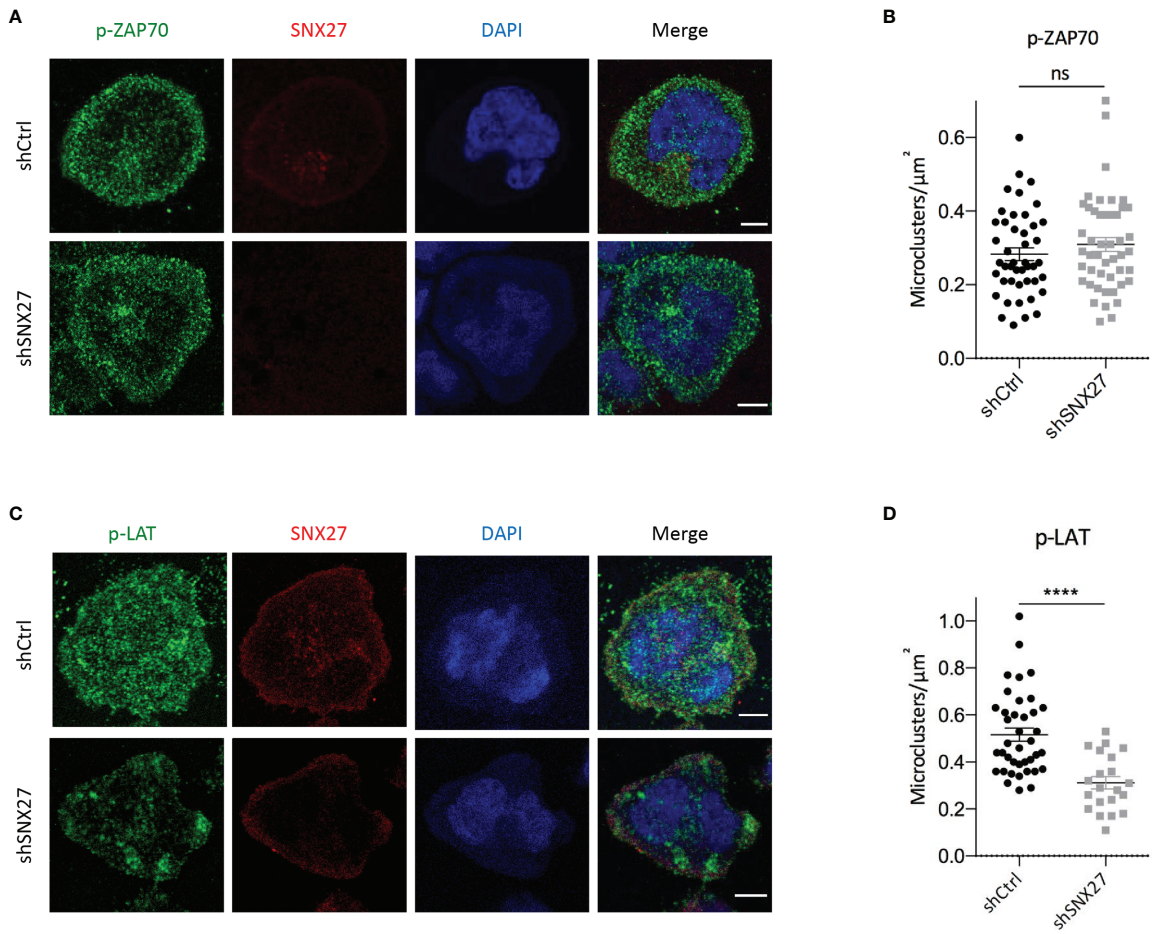

FIGURE 7 | SNX27 silencing affects the pattern of p-LAT but not p-ZAP70 microclusters at the IS. **(A, C)** Representative confocal images of control and SNX27-silenced Jurkat T cells at the contact surface of anti-CD3 and ICAM-1-coated coverslips, immunostained for SNX27 (red), p-ZAP70 (Tyr 319) or p-LAT (Tyr 220) (green). DAPI was used to label the nuclei. Scale bar = 5 µm. **(B, D)** Quantification, at the cell-coverslip optical section, of p-LAT and p-ZAP70 microclusters density. Plot in **(B)** shows mean ± SEM of a representative experiment of two independent ones with similar results (shCtrl = 45 cells, shSNX27 = 47 cells). Plot in **(D)** shows mean ± SEM of a representative experiment out of three (shCtrl = 39 cells, shSNX27 = 21 cells). Significance was determined by unpaired *t* test (ns, not significant; ****$p < 0.0001$).

important function for SNX27 by showing that it acts as a hub for adequate MTOC repositioning and polarization of secretory compartments in T lymphocytes upon APC engagement.

Despite being widely recognized as a critical event in lymphocyte function, the mechanisms driving MTOC translocation in T cells are not completely understood. Here we describe multiple, complementary mechanisms by which SNX27 translocation to the IS may be involved in this process. Firstly, we demonstrate that SNX27 is critical for the regulation of synaptic DAG accumulation, one of the reported triggers required for MTOC polarization. Secondly, we describe a mild defect in F-actin depletion across the synapse in SNX27-silenced cells. Thirdly, we report how SNX27 deficiency leads to randomly organized microtubules, unable to connect the MTOC to the cortex at the pSMAC.

Perturbation of the DAG gradient established during IS formation has been previously linked with impaired MTOC polarization (14–16). Reinforcing this notion, impaired DAG accumulation in SNX27-deficient cells correlates with defective MTOC orientation. The observed defects in DAG content at the IS following SNX27 silencing could be, at least partially, the consequence of abnormal localization of DGKζ. Several studies have reported substantial defects in the organization of the IS consequent to DGK deficiency. For instance, activated $CD4^+$ mouse T cells treated with DGK inhibitors or deficient for DGKα presented impaired DAG accumulation and MTOC recruitment to the IS (14, 16). Besides, DGKζ-deficient CTLs were unable to dock the MTOC to the IS (46), and DGKζ-deficient B cells presented impaired actin remodelling, force generation and MTOC translocation at the IS (79). Our studies show that not only the expression but also the correct spatial distribution of DGKζ are important for the regulation of DAG content in basal conditions and for the generation of DAG gradients upon antigen recognition. SNX27-dependent PDZ interaction allows retrograde DGKζ traffic to internal regions, that in turn facilitate its polarized recruitment to the IS. The high DAG amount in internal membranes derives to great extent from PA hydrolysis

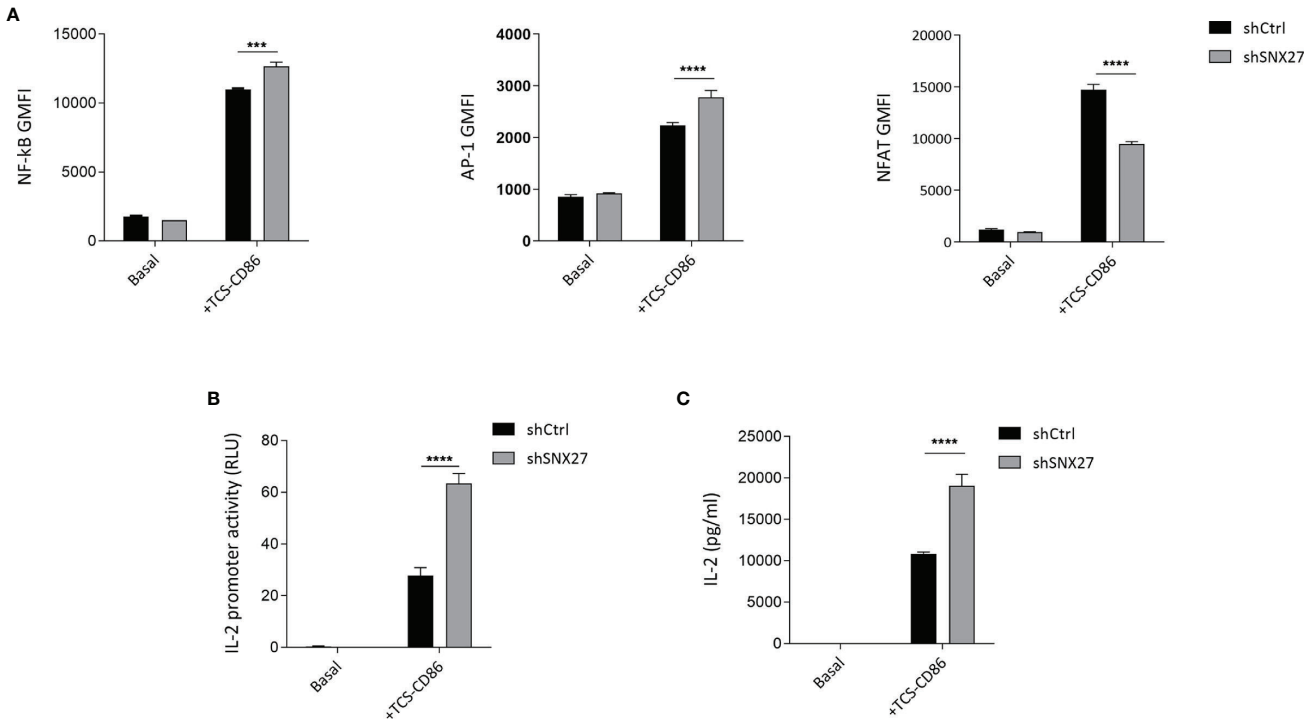

FIGURE 8 | SNX27 silencing alters NF-κB, AP-1 and NFAT transcription factor activity and enhances IL-2 production and secretion. **(A)** Control or SNX27-silenced cells were stimulated with TCS-CD86 for 24 h NF-κB (left), AP-1 (middle) and NFAT (right) geometric mean fluorescence intensity (GMFI) activity were analyzed. **(B)** Luciferase activity of an IL-2 reporter construct was evaluated in control or SNX27-silenced Jurkat T cells stimulated with TCS-CD86 for 24 h Luciferase activity was corrected employing an internal renilla luciferase control. **(C)** IL-2 secretion was determined by ELISA in the supernatants of control or SNX27-silenced Jurkat T cells stimulated with TCS-CD86 for 24 h Data are shown as mean ± SEM of a representative experiment of 3 with similar results. Significance was determined by two-way ANOVA with Bonferroni correction (***$p < 0.001$, ****$p < 0.0001$).

by PA phosphatases (39, 80). The failure of DGKζ to reach internal compartments as the results of SNX27 silencing could thus prevent an adequate supply of PA and ultimately lead to the shutdown of PA-dependent DAG generation.

The defect on MTOC translocation in the absence of SNX27 appears much stronger than the partial defect described in DGKζ-deficient CTLs and B cells, suggesting additional mechanisms governed by SNX27. As we show, SNX27-silenced cells display a mild defect in F-actin depletion across the IS that could contribute to the failure in MTOC polarization. Although studies in B cells and Jurkat T cells described that MTOC reorientation is independent of F-actin reorganization at the IS (74, 81, 82), other numerous investigations reported that it does play an important role in this mechanism (49–53). Recent studies have proposed that depletion of centrosomal F-actin by WASH-dependent mechanisms is required for MTOC translocation in Jurkat T cells upon IS triggering (54). However, in our hands, SNX27 silencing did not affect centrosomal F-actin reduction nor MTOC detachment from the nucleus upon engagement with TCS-CD86. Therefore, WASH functions at the IS and centrosomal area might be independent on SNX27 interaction.

Defects in microtubule reorganization during IS formation following SNX27 silencing correlates well with impaired $p150^{Glued}$ translocation to the cell-cell contact region following SNX27 silencing. Although the contribution of microtubule dynamics or stabilization to MTOC reorientation remains unresolved, inhibition of microtubule polymerization in human primary $CD4^+$ T cells and Jurkat T cells has been described to block MTOC translocation towards the APC (83, 84). Dynactin directly binds microtubules and cytoplasmic dynein, which stabilizes the association between dynein and its cargoes and facilitates their retrograde transport along the microtubule cytoskeleton (85–87; 88). In T cells, this complex is recruited to the IS upon TCR activation and has been described to be of great relevance for MTOC polarization (16, 65, 84, 89). Disruption of the dynein-dynactin complex at the IS by overexpression of p50-dynamitin-GFP impairs MTOC translocation. to the contact area between Jurkat and SEE-pulsed Raji cells (89). Localization of $p150^{Glued}$ at microtubules and the MTOC (77) correlates with our studies and identify SNX27 as essential for the correct localization of this protein. SNX27-retromer interaction with $p150^{Glued}$ would facilitate its transport to the IS, favoring the anchoring of this complex to the microtubules minus ends. In turn, this molecular motor would exert a pulling force on microtubules, dragging the attached MTOC to the IS. Further research on the relationship between

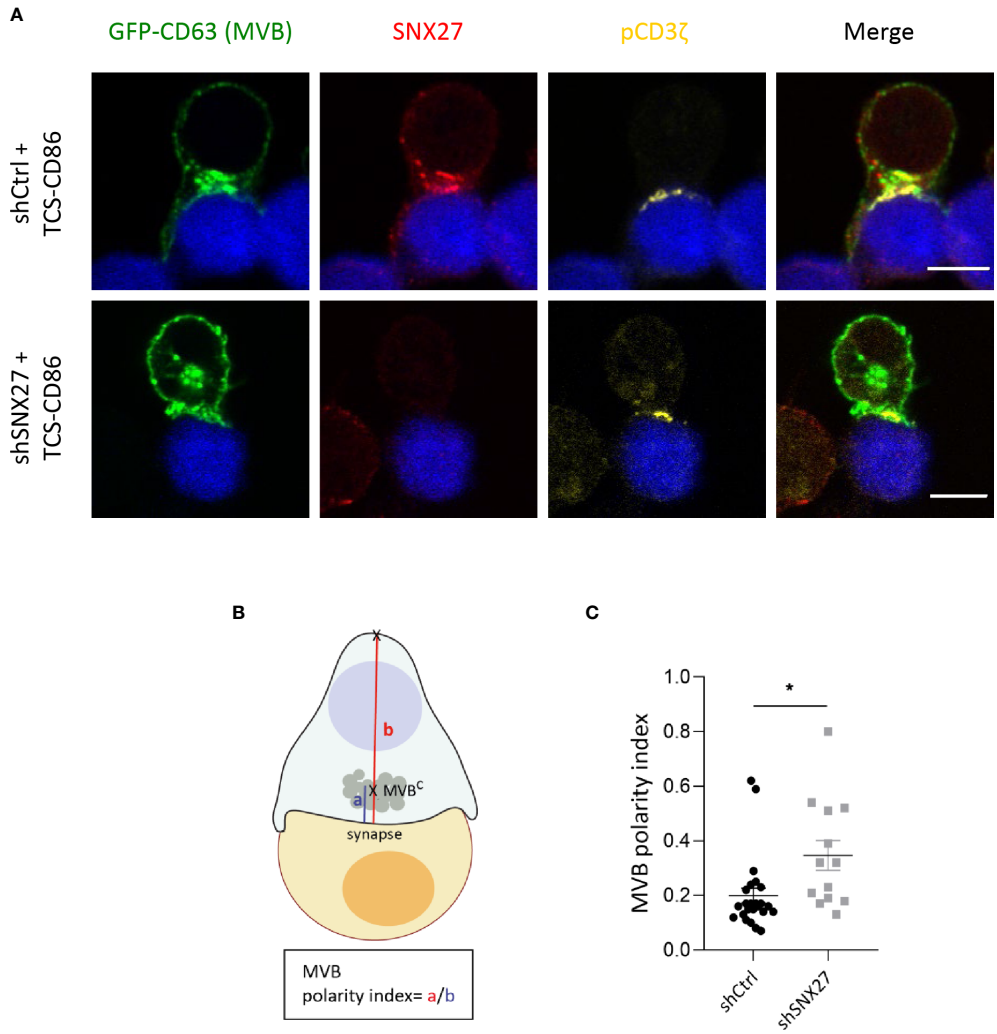

FIGURE 9 | MBV recruitment to the IS is impaired in SNX27-silenced Jurkat T cells. **(A)** Representative confocal images of SNX27-silenced and control Jurkat T cells transfected with a GFP-CD63 construct (MVB), and incubated with TCS-CD86 (blue). Intracellular SNX27 (red) and phosphorylated CD3ζ (yellow) were stained as control of silencing and correct IS formation, respectively. Single medial optical sections from a representative experiment are shown (n = 2). Scale bar = 5 μm. **(B)** Graphical representation of polarity index calculation, computed as the ratio between the distance from the center of mass of the MVB (MVB^C) to the IS ("a" distance) by the distance from the IS to the distal pole of the T cell ("b" distance). **(C)** MVB polarity index. Values are displayed as dot plots, with each dot representing an individual cell. Data shown as mean ± SEM of a representative experiment out of two (shCtrl = 24 cells, shSNX27 = 13 cells). Significance was determined by unpaired *t-test* (*p <0.05).

SNX27 and $p150^{Glued}$ will likely shed light on the exact mechanism linking SNX27 to the control of MTOC polarization.

SNX27 contribution to microtubule rearrangement has a direct impact in the correct organization of p-LAT microclusters. Phosphorylated LAT constitutes a docking site for multiple signaling and adaptor proteins such as the adaptor SLP76 and PLCγ1 (90; 91). PLCγ1 is responsible for initial generation of DAG at the cell-cell contact zone. Therefore, the defects observed in the organization of p-LAT microclusters in SNX27-silenced cells could translate into inappropriate PLCγ1 recruitment and activity. This would contribute to the impaired formation of a synaptic DAG gradient observed in these cells. These predicted outcomes are supported by reported data describing that defects in microtubule polymerization at the IS do not affect ZAP70 activation, but are associated with defective LAT activation and synaptic accumulation, as well as decreased PLCγ1 phosphorylation (92). Interestingly, silencing ezrin or its partner, the polarity regulator Dlg1, hinders microtubule anchoring to the cortical actin cytoskeleton, and its consequences are very much reminiscent of the alterations described here: defective MTOC polarization, microtubule network organization at the IS and p-LAT microcluster patterns. In addition, it is accompanied by defects in microcluster centripetal transport (68). Moreover, defects in the polarity regulator Apc, a partner of Dlg1, induces similar defects on microtubule organization patterns, actin clearance and cytotoxic granule localization and fusion at the IS (70, 71). Both Dlg1 and Apc are

components of cell polarity complexes interacting through PDZ/PDZbm domains (93). SNX27 in T cells could be contributing to regulate the coordinated action of cytoskeleton and vesicular traffic at the IS through the same mechanism, as it has been reported to interact with a partner of these cell polarity complexes termed β-PIX (44).

DGKζ-silenced Jurkat T cells enhanced activation of PKCθ downstream TCR/CD28 stimulation, which has been directly related to increased NF-κB-mediated transcription (94). Luciferase studies in SNX27-silenced Jurkat T cells confirmed an increased NF-κB activation that mirrored the one observed upon DGKζ silencing. Dual silencing of SNX27 and DGKζ had no additive effect, suggesting that SNX27 interaction with DGKζ sustained its function as a negative regulator of DAG metabolism (44). This is in accordance with our observation that SNX27 facilitates the control exerted by DGKζ on the correct formation of a synaptic DAG-gradient. In the current study, we further investigated the transcriptional regulation by SNX27 in IS-forming TPR cells. SNX27-silenced T cells stimulated with TCS-CD86 display increased AP-1 and NF-κB-dependent transcription, as well as augmented IL-2 secretion compared to control cells, an effect similar to that described for DGKζ-silenced TPR cells (73). The use of this model confirms previous luciferase studies in CD3/CD28-stimulated Jurkat T cells and demonstrates the strict regulation of NF-κB transcription by SNX27. Although IL-2 has been reported to focus at the IS closely associated with the MTOC, our data indicate that MTOC polarization is not required for the secretion of this cytokine. This finding is supported by previous studies showing enhanced IL-2 and IFN-γ secretion by T cells with impaired MTOC synaptic translocation (74, 95).

SNX27-silenced TPR cells display decreased NFAT-dependent activation upon TCS-CD86 engagement. Of interest, silencing of the polarity regulator Apc leads to deficiencies in microtubule organization in T cells, which in turn impair NFAT nuclear translocation and its mediated transcription (70, 71). In addition, other polarity proteins such as Dlg1 and ezrin control NFAT activation by alternative p38 activation (68, 72). In this study we show that SNX27 is involved in microtubule remodeling and synaptic organization of p-LAT microclusters. Therefore, we suggest that SNX27 silencing could be triggering a decreased NFAT activation through similar mechanisms as the described for the aforementioned polarity regulators. Further research will help to shed light to this issue.

In summary, our study reveals several meaningful details about the function of SNX27 to maintain a polarized intracellular organization, constituting an important regulator of cytoskeletal organization and T cell activation during IS formation. These results could also be of relevance in the analogous neuronal synapse. It is remarkable that some of the interactors identified in the Jurkat proteomic study are proteins with critical functions in centrosome orientation, whose defects are related to human and mice microcephaly due to impaired centrosomal localization during neurogenesis. This is the case of CENPJ where mutations are associated with microcephaly and Seckel syndrome (96, 97); citron kinase whose loss of activity leads to human microcephaly (98), and a malformative syndrome in mice (99); as well as β-PIX and GIT1 where mutations have been linked to intellectual disability and microcephaly (100–104). Additional research on SNX27-regulated functions will likely shed additional light on immune and neuronal synapse function and dysfunction.

DATA AVAILABILITY STATEMENT

The raw data supporting the conclusions of this article will be made available by the authors, without undue reservation.

AUTHOR CONTRIBUTIONS

NG-M: experimental procedures, data analysis, preparation of figures, original draft preparation. CR-R: experimental procedures, preparation of figures, original draft preparation. AA: conceptualization and coordination of the research, review. IM: conceptualization and coordination of the research, original draft preparation and review. All authors read and agreed to the published version of the manuscript.

FUNDING

NG-M received funding from the European Union Horizon 2020 research and innovation program under the Marie Sklodowska-Curie grant agreement 713673 and "La Caixa" Foundation (ID 100010434), with the fellowship code being LCF/BQ/DI17/11620027, as well as an EMBO short-term fellowship. CR-R held a predoctoral fellow of the Álvaro Entrecanales and Jérôme Lejeune Foundations. Research in IM's lab is funded by grants from the Spanish Association Against Cancer (AECC, CICPF18), Aplastic Anemia and MDS International Foundation (AAMDSIF, OPE01644), Spanish Ministry of Science and Innovation (PID2019-108357RB-100/AEI/10.13039/501100011033), and the Madrid regional government (IMMUNOTHERCAM Consortium S2010/BMD-2326) to IM. Research in AA's lab is funded by the French Ligue Nationale Contre le Cancer, Equipe Labellisée 2018).

ACKNOWLEDGMENTS

Editorial support was provided by Javier Arranz-Nicolás, PhD, in accordance with Good Publication Practice (GPP3) guidelines (Battisti, WP et al. Ann Intern Med. 2015). We thank Antonia Avila-Flores for critical reading of the manuscript.

SUPPLEMENTARY MATERIAL

The Supplementary Material for this article can be found online at: https://www.frontiersin.org/articles/10.3389/fimmu.2021.814570/full#supplementary-material

Supplementary Figure 1 | DAG generation at the plasma membrane of the IS precedes the full translocation of SNX27 and DAG-enriched compartments. Representative maximum intensity projections of control Jurkat T cells transfected with the C1 domain of PKCθ fused to GFP construct (GFP-C1bPKCθ, green) after incubation with TCS-CD86 (blue). Cells were immunostained for SNX27 (red). Arrowhead points DAG in intracellular compartments, while arrows show DAG generation at the plasma membrane of the IS. Scale bar = 5 μm.

REFERENCES

1. Krummel MF, Macara I. Maintenance and Modulation of T Cell Polarity. *Nat Immunol* (2006) 7(11):1143–9. doi: 10.1038/ni1404
2. Lasiecka ZM, Winckler B. Mechanisms of Polarized Membrane Trafficking in Neurons—Focusing in on Endosomes. *Mol Cell Neurosci* (2011) 48 (4):278–87. doi: 10.1016/j.mcn.2011.06.013
3. Sann S, Wang Z, Brown H, Jin Y. Roles of Endosomal Trafficking in Neurite Outgrowth and Guidance. *Trends Cell Biol* (2009) 19(7):317–24. doi: 10.1016/j.tcb.2009.05.001
4. Das V, Nal B, Dujeancourt A, Thoulouze M-I, Galli T, Roux P, et al. Activation-Induced Polarized Recycling Targets T Cell Antigen Receptors to the Immunological Synapse: Involvement of SNARE Complexes. *Immunity* (2004) 20(5):577–88. doi: 10.1016/S1074-7613(04)00106-2
5. Griffiths GM, Tsun A, Stinchcombe JC. The Immunological Synapse: A Focal Point for Endocytosis and Exocytosis. *J Cell Biol* (2010) 189(3):399–406. doi: 10.1083/jcb.201002027
6. Onnis A, Finetti F, Baldari CT. Vesicular Trafficking to the Immune Synapse: How to Assemble Receptor-Tailored Pathways From a Basic Building Set. *Front Immunol* (2016) 7. doi: 10.3389/fimmu.2016.00050
7. Soares H, Lasserre R, Alcover A. Orchestrating Cytoskeleton and Intracellular Vesicle Traffic to Build Functional Immunological Synapses. *Immunol Rev* (2013) 256(1):118–32. doi: 10.1111/imr.12110
8. Steinberg F, Gallon M, Winfield M, Thomas EC, Bell AJ, Heesom KJ, et al. A Global Analysis of SNX27–retromer Assembly and Cargo Specificity Reveals a Function in Glucose and Metal Ion Transport. *Nat Cell Biol* (2013) 15 (5):461–71. doi: 10.1038/ncb2721
9. Huse M, Lillemeier BF, Kuhns MS, Chen DS, Davis MM. T Cells Use Two Directionally Distinct Pathways for Cytokine Secretion. *Nat Immunol* (2006) 7(3):247–55. doi: 10.1038/ni1304
10. Huse M, Quann EJ, Davis MM. Shouts, Whispers and the Kiss of Death: Directional Secretion in T Cells. *Nat Immunol* (2008) 9(10):1105–11. doi: 10.1038/ni.f.215
11. Kupfer A, Mosmann TR, Kupfer H. Polarized Expression of Cytokines in Cell Conjugates of Helper T Cells and Splenic B Cells. *Proc Natl Acad Sci* (1991) 88(3):775–9. doi: 10.1073/pnas.88.3.775
12. Mittelbrunn M, Gutiérrez-Vázquez C, Villarroya-Beltri C, González S, Sánchez-Cabo F, González MÁ, et al. Unidirectional Transfer of microRNA-Loaded Exosomes From T Cells to Antigen-Presenting Cells. *Nat Commun* (2011) 2(1):282. doi: 10.1038/ncomms1285
13. Reichert P, Reinhardt RL, Ingulli E, Jenkins MK. Cutting Edge: In Vivo Identification of TCR Redistribution and Polarized IL-2 Production by Naive CD4 T Cells. *J Immunol* (2001) 166(7):4278–81. doi: 10.4049/jimmunol.166.7.4278
14. Chauveau A, Le Floc'h A, Bantilan NS, Koretzky GA, Huse M. Diacylglycerol Kinase α Establishes T Cell Polarity by Shaping Diacylglycerol Accumulation at the Immunological Synapse. *Sci Signaling* (2014) 7(340): ra82. doi: 10.1126/scisignal.2005287
15. Liu X, Kapoor TM, Chen JK, Huse M. Diacylglycerol Promotes Centrosome Polarization in T Cells via Reciprocal Localization of Dynein and Myosin II. *Proc Natl Acad Sci* (2013) 110(29):11976–81. doi: 10.1073/pnas.1306180110
16. Quann EJ, Merino E, Furuta T, Huse M. Localized Diacylglycerol Drives the Polarization of the Microtubule-Organizing Center in T Cells. *Nat Immunol* (2009) 10(6):627–35. doi: 10.1038/ni.1734
17. Quann EJ, Liu X, Altan-Bonnet G, Huse M. A Cascade of Protein Kinase C Isozymes Promotes Cytoskeletal Polarization in T Cells. *Nat Immunol* (2011) 12(7):647–54. doi: 10.1038/ni.2033
18. Gallon M, Clairfeuille T, Steinberg F, Mas C, Ghai R, Sessions RB, et al. A Unique PDZ Domain and Arrestin-Like Fold Interaction Reveals Mechanistic Details of Endocytic Recycling by SNX27-Retromer. *Proc Natl Acad Sci* (2014) 111(35):E3604–13. doi: 10.1073/pnas.1410552111
19. Horazdovsky BF, Davies BA, Seaman MN, McLaughlin SA, Yoon S, Emr SD. A Sorting Nexin-1 Homologue, Vps5p, Forms a Complex With Vps17p and Is Required for Recycling the Vacuolar Protein-Sorting Receptor. *Mol Biol Cell* (1997) 8(8):1529–41. doi: 10.1091/mbc.8.8.1529
20. Seaman MNJ, Michael McCaffery J, Emr SD. A Membrane Coat Complex Essential for Endosome-To-Golgi Retrograde Transport in Yeast. *J Cell Biol* (1998) 142(3):665–81. doi: 10.1083/jcb.142.3.665
21. Haft CR, Sierra M, de la L, Bafford R, Lesniak MA, Barr VA, et al. Human Orthologs of Yeast Vacuolar Protein Sorting Proteins Vps26, 29, and 35: Assembly Into Multimeric Complexes. *Mol Biol Cell* (2000) 11(12):4105–16. doi: 10.1091/mbc.11.12.4105
22. Hierro A, Rojas AL, Rojas R, Murthy N, Effantin G, Kajava AV, et al. Functional Architecture of the Retromer Cargo-Recognition Complex. *Nature* (2007) 449(7165):1063–7. doi: 10.1038/nature06216
23. Kerr MC, Bennetts JS, Simpson F, Thomas EC, Flegg C, Gleeson PA, et al. A Novel Mammalian Retromer Component, Vps26B: Novel Retromer Protein, Vps26B. *Traffic* (2005) 6(11):991–1001. doi: 10.1111/j.1600-0854.2005.00328.x
24. Attar N, Cullen PJ. The Retromer Complex. *Adv Enzyme Regul* (2010) 50 (1):216–36. doi: 10.1016/j.advenzreg.2009.10.002
25. Burd C, Cullen PJ. Retromer: A Master Conductor of Endosome Sorting. *Cold Spring Harbor Perspect Biol* (2014) 6(2):a016774–a016774. doi: 10.1101/cshperspect.a016774
26. Gallon M, Cullen PJ. Retromer and Sorting Nexins in Endosomal Sorting. *Biochem Soc Trans* (2015) 43(1):33–47. doi: 10.1042/BST20140290
27. Seaman MNJ. The Retromer Complex—Endosomal Protein Recycling and Beyond. *J Cell Sci* (2012) 125(20):4693–702. doi: 10.1242/jcs.103440
28. Temkin P, Lauffer B, Jäger S, Cimermancic P, Krogan NJ, von Zastrow M. SNX27 Mediates Retromer Tubule Entry and Endosome-to-Plasma Membrane Trafficking of Signalling Receptors. *Nat Cell Biol* (2011) 13 (6):715–21. doi: 10.1038/ncb2252
29. Wassmer T, Attar N, Harterink M, van Weering JRT, Traer CJ, Oakley J, et al. The Retromer Coat Complex Coordinates Endosomal Sorting and Dynein-Mediated Transport, With Carrier Recognition by the Trans-Golgi Network. *Dev Cell* (2009) 17(1):110–22. doi: 10.1016/j.devcel.2009.04.016
30. Loo LS, Tang N, Al-Haddawi M, Stewart Dawe G, Hong W. A Role for Sorting Nexin 27 in AMPA Receptor Trafficking. *Nat Commun* (2014) 5 (1):3176. doi: 10.1038/ncomms4176
31. Zimmerman SP, Hueschen CL, Malide D, Milgram SL, Playford MP. Sorting Nexin 27 (SNX27) Associates With Zonula Occludens-2 (ZO-2) and Modulates the Epithelial Tight Junction. *Biochem J* (2013) 455(1):95–106. doi: 10.1042/BJ20121755
32. Rincon E, de Guinoa JS, Gharbi SI, Sorzano COS, Carrasco YR, Merida I. Translocation Dynamics of Sorting Nexin 27 in Activated T Cells. *J Cell Sci* (2011) 124(5):776–88. doi: 10.1242/jcs.072447
33. Tello-Lafoz M, Rodríguez-Rodríguez C, Kinna G, Loo LS, Hong W, Collins BM, et al. SNX27 Links Dgkζ to the Control of Transcriptional and Metabolic Programs in T Lymphocytes. *Sci Rep* (2017) 7(1):16361. doi: 10.1038/s41598-017-16370-w
34. Jutz S, Leitner J, Schmetterer K, Doel-Perez I, Majdic O, Grabmeier-Pfistershammer K, et al. Assessment of Costimulation and Coinhibition in a Triple Parameter T Cell Reporter Line: Simultaneous Measurement of NF-κb, NFAT and AP-1. *J Immunol Methods* (2016) 430:10–20. doi: 10.1016/j.jim.2016.01.007
35. Leitner J, Kuschei W, Grabmeier-Pfistershammer K, Woitek R, Kriehuber E, Majdic O, et al. T Cell Stimulator Cells, an Efficient and Versatile Cellular System to Assess the Role of Costimulatory Ligands in the Activation of Human T Cells. *J Immunol Methods* (2010) 362(1–2):131–41. doi: 10.1016/j.jim.2010.09.020
36. Lauffer BEL, Melero C, Temkin P, Lei C, Hong W, Kortemme T, et al. SNX27 Mediates PDZ-Directed Sorting From Endosomes to the Plasma Membrane. *J Cell Biol* (2010) 190(4):565–74. doi: 10.1083/jcb.201004060

37. Rincón E, Santos T, Avila-Flores A, Albar JP, Lalioti V, Lei C, et al. Proteomics Identification of Sorting Nexin 27 as a Diacylglycerol Kinase Zeta-Associated Protein: New Diacylglycerol Kinase Roles in Endocytic Recycling. *Mol Cell Prot: MCP* (2007) 6(6):1073–87. doi: 10.1074/mcp.M700047-MCP200
38. Blott EJ, Griffiths GM. Secretory Lysosomes. *Nat Rev Mol Cell Biol* (2002) 3 (2):122–31. doi: 10.1038/nrm732
39. Carrasco S, Merida I. Diacylglycerol-Dependent Binding Recruits Pkcθ and RasGRP1 C1 Domains to Specific Subcellular Localizations in Living T Lymphocytes. *Mol Biol Cell* (2004) 15(6):2932–42. doi: 10.1091/mbc.e03-11-0844
40. Santos T, Carrasco S, Jones DR, Mérida I, Eguinoa A. Dynamics of Diacylglycerol Kinase ζ Translocation in Living T-Cells. *J Biol Chem* (2002) 277(33):30300–9. doi: 10.1074/jbc.M200999200
41. Carpier J-M, Zucchetti AE, Bataille L, Dogniaux S, Shafaq-Zadah M, Bardin S, et al. Rab6-Dependent Retrograde Traffic of LAT Controls Immune Synapse Formation and T Cell Activation. *J Exp Med* (2018) 215(4):1245–65. doi: 10.1084/jem.20162042
42. Schindelin J, Arganda-Carreras I, Frise E, Kaynig V, Longair M, Pietzsch T, et al. Fiji: An Open-Source Platform for Biological-Image Analysis. *Nat Methods* (2012) 9(7):676–82. doi: 10.1038/nmeth.2019
43. Bolte S, Cordelières FP. A Guided Tour Into Subcellular Colocalization Analysis in Light Microscopy. *J Microscopy* (2006) 224(Pt 3):213–32. doi: 10.1111/j.1365-2818.2006.01706.x
44. Tello-Lafoz M, Martínez-Martínez G, Rodríguez-Rodríguez C, Albar JP, Huse M, Gharbi S, et al. Sorting Nexin 27 Interactome in T-Lymphocytes Identifies Zona Occludens-2 Dynamic Redistribution at the Immune Synapse. *Traffic* (2017) 18(8):491–504. doi: 10.1111/tra.12492
45. Mao L, Liao C, Qin J, Gong Y, Zhou Y, Li S, et al. Phosphorylation of SNX27 by MAPK11/14 Links Cellular Stress–Signaling Pathways With Endocytic Recycling. *J Cell Biol* (2021) 220(4):e202010048. doi: 10.1083/jcb.202010048
46. Andrada E, Almena M, de Guinoa JS, Merino-Cortes SV, Liébana R, Arcos R, et al. Diacylglycerol Kinase ζ Limits the Polarized Recruitment of Diacylglycerol-Enriched Organelles to the Immune Synapse in T Cells. *Sci Signaling* (2016) 9(459):ra127–7. doi: 10.1126/scisignal.aaf7714
47. Clairfeuille T, Mas C, Chan ASM, Yang Z, Tello-Lafoz M, Chandra M, et al. A Molecular Code for Endosomal Recycling of Phosphorylated Cargos by the SNX27–retromer Complex. *Nat Struct Mol Biol* (2016) 23(10):921–32. doi: 10.1038/nsmb.3290
48. McIntyre RE, Chavali PL, Ismail O, Carragher DM, Sanchez-Andrade G, Forment JV, et al. Disruption of Mouse Cenpj, a Regulator of Centriole Biogenesis, Phenocopies Seckel Syndrome. *PloS Genet* (2012) 8(11): e1003022. doi: 10.1371/journal.pgen.1003022
49. Gawden-Bone CM, Frazer GL, Richard AC, Ma CY, Strege K, Griffiths GM. PIP5 Kinases Regulate Membrane Phosphoinositide and Actin Composition for Targeted Granule Secretion by Cytotoxic Lymphocytes. *Immunity* (2018) 49(3):427–437.e4. doi: 10.1016/j.immuni.2018.08.017
50. Randzavola LO, Strege K, Juzans M, Asano Y, Stinchcombe JC, Gawden-Bone CM, et al. Loss of ARPC1B Impairs Cytotoxic T Lymphocyte Maintenance and Cytolytic Activity. *J Clin Invest* (2019) 129(12):5600–14. doi: 10.1172/JCI129388
51. Ritter AT, Asano Y, Stinchcombe JC, Dieckmann NMG, Chen B-C, Gawden-Bone C, et al. Actin Depletion Initiates Events Leading to Granule Secretion at the Immunological Synapse. *Immunity* (2015) 42 (5):864–76. doi: 10.1016/j.immuni.2015.04.013
52. Sanchez E, Liu X, Huse M. Actin Clearance Promotes Polarized Dynein Accumulation at the Immunological Synapse. *PloS One* (2019) 14(7): e0210377. doi: 10.1371/journal.pone.0210377
53. Stinchcombe JC, Majorovits E, Bossi G, Fuller S, Griffiths GM. Centrosome Polarization Delivers Secretory Granules to the Immunological Synapse. *Nature* (2006) 443(7110):462–5. doi: 10.1038/nature05071
54. Bello-Gamboa A, Velasco M, Moreno S, Herranz G, Ilie R, Huetos S, et al. Actin Reorganization at the Centrosomal Area and the Immune Synapse Regulates Polarized Secretory Traffic of Multivesicular Bodies in T Lymphocytes. *J Extracell Vesicles* (2020) 9(1):1759926. doi: 10.1080/20013078.2020.1759926
55. Farina F, Gaillard J, Guérin C, Couté Y, Sillibourne J, Blanchoin L, et al. The Centrosome Is an Actin-Organizing Centre. *Nat Cell Biol* (2016) 18(1):65–75. doi: 10.1038/ncb3285
56. Obino D, Farina F, Malbec O, Sáez PJ, Maurin M, Gaillard J, et al. Actin Nucleation at the Centrosome Controls Lymphocyte Polarity. *Nat Commun* (2016) 7(1):10969. doi: 10.1038/ncomms10969
57. Kuhn JR, Poenie M. Dynamic Polarization of the Microtubule Cytoskeleton During CTL-Mediated Killing. *Immunity* (2002) 16(1):111–21. doi: 10.1016/S1074-7613(02)00262-5
58. Monks CRF, Freiberg BA, Kupfer H, Sciaky N, Kupfer A. Three-Dimensional Segregation of Supramolecular Activation Clusters in T Cells. *Nature* (1998) 395(6697):82–6. doi: 10.1038/25764
59. Bonello G. Dynamic Recruitment of the Adaptor Protein LAT: LAT Exists in Two Distinct Intracellular Pools and Controls Its Own Recruitment. *J Cell Sci* (2004) 117(7):1009–16. doi: 10.1242/jcs.00968
60. Bouchet J, del Río-Iñiguez I, Vázquez-Chávez E, Lasserre R, Agüera-González S, Cuche C, et al. Rab11-FIP3 Regulation of Lck Endosomal Traffic Controls TCR Signal Transduction. *J Immunol* (2017) 198(7):2967–78. doi: 10.4049/jimmunol.1600671
61. Ehrlich LIR, Ebert PJR, Krummel MF, Weiss A, Davis MM. Dynamics of P56lck Translocation to the T Cell Immunological Synapse Following Agonist and Antagonist Stimulation. *Immunity* (2002) 17(6):809–22. doi: 10.1016/S1074-7613(02)00481-8
62. Finetti F, Paccani SR, Riparbelli MG, Giacomello E, Perinetti G, Pazour GJ, et al. Intraflagellar Transport Is Required for Polarized Recycling of the TCR/CD3 Complex to the Immune Synapse. *Nat Cell Biol* (2009) 11 (11):1332–9. doi: 10.1038/ncb1977
63. Larghi P, Williamson DJ, Carpier J-M, Dogniaux S, Chemin K, Bohineust A, et al. VAMP7 Controls T Cell Activation by Regulating the Recruitment and Phosphorylation of Vesicular Lat at TCR-Activation Sites. *Nat Immunol* (2013) 14(7):723–31. doi: 10.1038/ni.2609
64. Soares H, Henriques R, Sachse M, Ventimiglia L, Alonso MA, Zimmer C, et al. Regulated Vesicle Fusion Generates Signaling Nanoterritories That Control T Cell Activation at the Immunological Synapse. *J Exp Med* (2013) 210(11):2415–33. doi: 10.1084/jem.20130150
65. Combs J, Kim SJ, Tan S, Ligon LA, Holzbaur ELF, Kuhn J, et al. Recruitment of Dynein to the Jurkat Immunological Synapse. *Proc Natl Acad Sci* (2006) 103(40):14883–8. doi: 10.1073/pnas.0600914103
66. Kuhné MR, Lin J, Yablonski D, Mollenauer MN, Ehrlich LIR, Huppa J, et al. Linker for Activation of T Cells, ζ-Associated Protein-70, and Src Homology 2 Domain-Containing Leukocyte Protein-76 Are Required for TCR-Induced Microtubule-Organizing Center Polarization. *J Immunol* (2003) 171(2):860–6. doi: 10.4049/jimmunol.171.2.860
67. Hashimoto-Tane A, Yokosuka T, Sakata-Sogawa K, Sakuma M, Ishihara C, Tokunaga M, et al. Dynein-Driven Transport of T Cell Receptor Microclusters Regulates Immune Synapse Formation and T Cell Activation. *Immunity* (2011) 34(6):919–31. doi: 10.1016/j.immuni.2011.05.012
68. Lasserre R, Charrin S, Cuche C, Danckaert A, Thoulouze M-I, de Chaumont F, et al. Ezrin Tunes T-Cell Activation by Controlling Dlg1 and Microtubule Positioning at the Immunological Synapse. *EMBO J* (2010) 29(14):2301–14. doi: 10.1038/emboj.2010.127
69. Ludford-Menting MJ, Oliaro J, Sacirbegovic F, Cheah ET-Y, Pedersen N, Thomas SJ, et al. A Network of PDZ-Containing Proteins Regulates T Cell Polarity and Morphology During Migration and Immunological Synapse Formation. *Immunity* (2005) 22(6):737–48. doi: 10.1016/j.immuni.2005.04.009
70. Agüera-González S, Burton OT, Vázquez-Chávez E, Cuche C, Herit F, Bouchet J, et al. Adenomatous Polyposis Coli Defines Treg Differentiation and Anti-Inflammatory Function Through Microtubule-Mediated NFAT Localization. *Cell Rep* (2017) 21(1):181–94. doi: 10.1016/j.celrep.2017.09.020
71. Juzans M, Cuche C, Rose T, Mastrogiovanni M, Bochet P, Di Bartolo V, et al. Adenomatous Polyposis Coli Modulates Actin and Microtubule Cytoskeleton at the Immunological Synapse to Tune CTL Functions. *ImmunoHorizons* (2020) 4 (6):363–81. doi: 10.4049/immunohorizons.2000044
72. Round JL, Humphries LA, Tomassian T, Mittelstadt P, Zhang M, Miceli MC. Scaffold Protein Dlgh1 Coordinates Alternative P38 Kinase Activation, Directing T Cell Receptor Signals Toward NFAT But Not NF-κb Transcription Factors. *Nat Immunol* (2007) 8(2):154–61. doi: 10.1038/ni1422
73. Arranz-Nicolás J, Martin-Salgado M, Rodríguez-Rodríguez C, Liébana R, Moreno-Ortiz MC, Leitner J, et al. Diacylglycerol Kinase ζ Limits IL-2-Dependent Control

of PD-1 Expression in Tumor-Infiltrating T Lymphocytes. *J Immunother Cancer* (2020) 8(2):e001521. doi: 10.1136/jitc-2020-001521
74. Chemin K, Bohineust A, Dogniaux S, Tourret M, Guégan S, Miro F, et al. Cytokine Secretion by CD4+ T Cells at the Immunological Synapse Requires Cdc42-Dependent Local Actin Remodeling But Not Microtubule Organizing Center Polarity. *J Immunol* (2012) 189(5):2159–68. doi: 10.4049/jimmunol.1200156
75. Kupfer H, Monks CR, Kupfer A. Small Splenic B Cells That Bind to Antigen-specific T Helper (Th) Cells and Face the Site of Cytokine Production in the Th Cells Selectively Proliferate: Immunofluorescence Microscopic Studies of Th-B Antigen-Presenting Cell Interactions. *J Exp Med* (2011) 179(5):1507–15. doi: 10.1084/jem.179.5.1507
76. Kupfer A, Dennert G, Singer SJ. Polarization of the Golgi Apparatus and the Microtubule-Organizing Center Within Cloned Natural Killer Cells Bound to Their Targets. *Proc Nat Acad Sci* (1983) 80(23):7224–8. doi: 10.1073/pnas.80.23.7224
77. Nath S, Christian L, Tan SY, Ki S, Ehrlich LI, Poenie M. Dynein Separately Partners With NDE1 and Dynactin to Orchestrate T Cell Focused Secretion. *J Immunol* (2016) 197(6):2090–101. doi: 10.4049/jimmunol.1600180
78. Pols MS, Klumperman J. Trafficking and Function of the Tetraspanin CD63. *Exp Cell Res* (2009) 315(9):1584–92. doi: 10.1016/j.yexcr.2008.09.020
79. Merino-Cortés SV, Gardeta SR, Roman-Garcia S, Martínez-Riaño A, Pineau J, Liebana R, et al. Diacylglycerol Kinase ζ Promotes Actin Cytoskeleton Remodeling and Mechanical Forces at the B Cell Immune Synapse. *Sci Signaling* (2020) 13(627). doi: 10.1126/scisignal.aaw8214
80. Baron CL, Malhotra V. Role of Diacylglycerol in PKD Recruitment to the TGN and Protein Transport to the Plasma Membrane. *Science* (2002) 295 (5553):325–8. doi: 10.1126/science.1066759
81. Gomez TS, Kumar K, Medeiros RB, Shimizu Y, Leibson PJ, Billadeau DD. Formins Regulate the Actin-Related Protein 2/3 Complex-Independent Polarization of the Centrosome to the Immunological Synapse. *Immunity* (2007) 26(2):177–90. doi: 10.1016/j.immuni.2007.01.008
82. Sedwick CE, Morgan MM, Jusino L, Cannon JL, Miller J, Burkhardt JK. TCR, LFA-1, and CD28 Play Unique and Complementary Roles in Signaling T Cell Cytoskeletal Reorganization. *J Immunol (Baltimore Md: 1950)* (1999) 162(3):1367–75.
83. Tourret M, Guégan S, Chemin K, Dogniaux S, Miro F, Bohineust A, et al. T Cell Polarity at the Immunological Synapse Is Required for CD154-Dependent IL-12 Secretion by Dendritic Cells. *J Immunol* (2010) 185 (11):6809–18. doi: 10.4049/jimmunol.1001501
84. Yi J, Wu X, Chung AH, Chen JK, Kapoor TM, Hammer JA. Centrosome Repositioning in T Cells Is Biphasic and Driven by Microtubule End-on Capture-Shrinkage. *J Cell Biol* (2013) 202(5):779–92. doi: 10.1083/jcb.201301004
85. Kardon JR, Vale RD. Regulators of the Cytoplasmic Dynein Motor. *Nat Rev Mol Cell Biol* (2009) 10(12):854–65. doi: 10.1038/nrm2804
86. McKenney RJ, Huynh W, Tanenbaum ME, Bhabha G, Vale RD. Activation of Cytoplasmic Dynein Motility by Dynactin-Cargo Adapter Complexes. *Science* (2014) 345(6194):337–41. doi: 10.1126/science.1254198
87. Schroer TA. Dynactin. *Annu Rev Cell Dev Biol* (2004) 20(1):759–79. doi: 10.1146/annurev.cellbio.20.012103.094623
88. Zhang K, Foster HE, Rondelet A, Lacey SE, Bahi-Buisson N, Bird AW, et al. Cryo-EM Reveals How Human Cytoplasmic Dynein Is Auto-Inhibited and Activated. *Cell* (2017) 169(7):1303–14.e18. doi: 10.1016/j.cell.2017.05.025
89. Martín-Cófreces NB, Robles-Valero J, Cabrero JR, Mittelbrunn M, Gordón-Alonso M, Sung C-H, et al. MTOC Translocation Modulates IS Formation and Controls Sustained T Cell Signaling. *J Cell Biol* (2008) 182(5):951–62. doi: 10.1083/jcb.200801014
90. Paz PE, Wang S, Clarke H, Lu X, Stokoe D, Abo A. Mapping the Zap-70 Phosphorylation Sites on LAT (Linker for Activation of T Cells) Required for Recruitment and Activation of Signalling Proteins in T Cells. *Biochem J* (2001) 356(Pt 2):461–71. doi: 10.1042/0264-6021:3560461
91. Zhang W, Irvin BJ, Trible RP, Abraham RT, Samelson LE. Functional Analysis of LAT in TCR-Mediated Signaling Pathways Using a LAT-Deficient Jurkat Cell Line. *Int Immunol* (1999) 11(6):943–50. doi: 10.1093/intimm/11.6.943
92. Martín-Cófreces NB, Baixauli F, López MJ, Gil D, Monjas A, Alarcón B, et al. End-Binding Protein 1 Controls Signal Propagation From the T Cell Receptor: EB1 Regulates TCR Signalling. *EMBO J* (2012) 31(21):4140–52. doi: 10.1038/emboj.2012.242
93. Mastrogiovanni M, Juzans M, Alcover A, Di Bartolo V. Coordinating Cytoskeleton and Molecular Traffic in T Cell Migration, Activation, and Effector Functions. *Front Cell Dev Biol* (2020) 8:591348. doi: 10.3389/fcell.2020.591348
94. Ávila-Flores A, Arranz-Nicolás J, Andrada E, Soutar D, Mérida I. Predominant Contribution of Dgkζ Over Dgkα in the Control of PKC/PDK-1-Regulated Functions in T Cells. *Immunol Cell Biol* (2017) 95(6):549–63. doi: 10.1038/icb.2017.7
95. Bustos-Morán E, Blas-Rus N, Martin-Cófreces NB, Sánchez-Madrid F. Microtubule-Associated Protein-4 Controls Nanovesicle Dynamics and T Cell Activation. *J Cell Sci* (2017) 130(7):1217–23. doi: 10.1242/jcs.199042
96. Al-Dosari MS, Shaheen R, Colak D, Alkuraya FS. Novel CENPJ Mutation Causes Seckel Syndrome. *J Med Genet* (2010) 47(6):411–4. doi: 10.1136/jmg.2009.076646
97. Bond J, Roberts E, Springell K, Lizarraga S, Scott S, Higgins J, et al. A Centrosomal Mechanism Involving CDK5RAP2 and CENPJ Controls Brain Size. *Nat Genet* (2005) 37(4):353–5. doi: 10.1038/ng1539
98. Li H, Bielas SL, Zaki MS, Ismail S, Farfara D, Um K, et al. Biallelic Mutations in Citron Kinase Link Mitotic Cytokinesis to Human Primary Microcephaly. *Am J Hum Genet* (2016) 99(2):501–10. doi: 10.1016/j.ajhg.2016.07.004
99. Di Cunto F, Imarisio S, Hirsch E, Broccoli V, Bulfone A, Migheli A, et al. Defective Neurogenesis in Citron Kinase Knockout Mice by Altered Cytokinesis and Massive Apoptosis. *Neuron* (2000) 28(1):115–27. doi: 10.1016/S0896-6273(00)00090-8
100. Hong S-T, Mah W. A Critical Role of GIT1 in Vertebrate and Invertebrate Brain Development. *Exp Neurobiol* (2015) 24(1):8–16. doi: 10.5607/en.2015.24.1.8
101. Menon P, Deane R, Sagare A, Lane SM, Zarcone TJ, O'Dell MR, et al. Impaired Spine Formation and Learning in GPCR Kinase 2 Interacting Protein-1 (GIT1) Knockout Mice. *Brain Res* (2010) 1317:218–26. doi: 10.1016/j.brainres.2009.11.084
102. Schmalzigaug R, Rodriguiz RM, Bonner PE, Davidson CE, Wetsel WC, Premont RT. Impaired Fear Response in Mice Lacking GIT1. *Neurosci Lett* (2009) 458(2):79–83. doi: 10.1016/j.neulet.2009.04.037
103. Walczak-Sztulpa J, Wisniewska M, Latos-Bielenska A, Linné M, Kelbova C, Belitz B, et al. Chromosome Deletions in 13q33–34: Report of Four Patients and Review of the Literature. *Am J Med Genet Part A* (2008) 146A(3):337–42. doi: 10.1002/ajmg.a.32127
104. Won H, Mah W, Kim E, Kim J-W, Hahm E-K, Kim M-H, et al. GIT1 Is Associated With ADHD in Humans and ADHD-Like Behaviors in Mice. *Nat Med* (2011) 17(5):566–72. doi: 10.1038/nm.2330

Conflict of Interest: The authors declare that the research was conducted in the absence of any commercial or financial relationships that could be construed as a potential conflict of interest.

Publisher's Note: All claims expressed in this article are solely those of the authors and do not necessarily represent those of their affiliated organizations, or those of the publisher, the editors and the reviewers. Any product that may be evaluated in this article, or claim that may be made by its manufacturer, is not guaranteed or endorsed by the publisher.

frontiers in Immunology

ORIGINAL RESEARCH
published: 26 January 2022
doi: 10.3389/fimmu.2021.792813

Examining the Effect of Kindlin-3 Binding Site Mutation on LFA-1-ICAM-1 Bonds by Force Measuring Optical Tweezers

Craig McDonald[1†], *Vicky L. Morrison*[2†], *David McGloin*[1,3‡] *and Susanna Carola Fagerholm*[2*†‡]

[1] SUPA, School of Science and Engineering, University of Dundee, Dundee, United Kingdom, [2] School of Medicine, University of Dundee, Dundee, United Kingdom, [3] School of Electrical and Data Engineering, University of Technology Sydney, Sydney, NSW, Australia

OPEN ACCESS

Edited by:
Jerome Delon,
INSERM U1016 Institut Cochin, France

Reviewed by:
Scott I. Simon,
University of California, Davis, United States
Philippe Robert,
Aix-Marseille Université, France

***Correspondence:**
Susanna Carola Fagerholm
susanna.fagerholm@helsinki.fi

[†]**Present address:**
Craig McDonald,
Rockend Limited, The Milner Therapeutics Institute, Jeffrey Cheah Biomedical Centre, Cambridge, United Kingdom
Vicky L. Morrison,
Institute of Infection, Immunity and Inflammation, University of Glasgow, Glasgow, United Kingdom
Susanna Carola Fagerholm,
Molecular and Integrative Biosciences Research Programme, Faculty of Biological and Environmental Sciences, University of Helsinki, Helsinki, Finland

[‡]These authors have contributed equally to this work

Specialty section:
This article was submitted to T Cell Biology, a section of the journal Frontiers in Immunology

Received: 11 October 2021
Accepted: 28 December 2021
Published: 26 January 2022

Citation:
McDonald C, Morrison VL, McGloin D and Fagerholm SC (2022) Examining the Effect of Kindlin-3 Binding Site Mutation on LFA-1-ICAM-1 Bonds by Force Measuring Optical Tweezers. Front. Immunol. 12:792813. doi: 10.3389/fimmu.2021.792813

Integrins in effector T cells are crucial for cell adhesion and play a central role in cell-mediated immunity. Leukocyte adhesion deficiency (LAD) type III, a genetic condition that can cause death in early childhood, highlights the importance of integrin/kindlin interactions for immune system function. A TTT/AAA mutation in the cytoplasmic domain of the β2 integrin significantly reduces kindlin-3 binding to the β2 tail, abolishes leukocyte adhesion to intercellular adhesion molecule 1 (ICAM-1), and decreases T cell trafficking *in vivo*. However, how kindlin-3 affects integrin function in T cells remains incompletely understood. We present an examination of LFA-1/ICAM-1 bonds in both wild-type effector T cells and those with a kindlin-3 binding site mutation. Adhesion assays show that effector T cells carrying the kindlin-3 binding site mutation display significantly reduced adhesion to the integrin ligand ICAM-1. Using optical trapping, combined with back focal plane interferometry, we measured a bond rupture force of 17.85 ±0.63 pN at a force loading rate of 30.21 ± 4.35 pN/s, for single integrins expressed on wild-type cells. Interestingly, a significant drop in rupture force of bonds was found for TTT/AAA-mutant cells, with a measured rupture force of 10.08 ± 0.88pN at the same pulling rate. Therefore, kindlin-3 binding to the cytoplasmic tail of the β2-tail directly affects catch bond formation and bond strength of integrin–ligand bonds. As a consequence of this reduced binding, CD8+ T cell activation *in vitro* is also significantly reduced.

Keywords: LFA-1, kindlin-3, T cell, bond strength, ICAM-1

1 INTRODUCTION

The ability of leukocytes to traffic into tissues and to make contact with other cells depends chiefly on β2 integrins, which are expressed exclusively on leukocytes (1). The $\alpha L\beta$2 integrin, commonly called leukocyte function-associated antigen 1 (LFA-1), is the most abundant and widespread in expression of the four members of the β2 family (1, 2). LFA-1 is expressed by all leukocytes and binds to members of the intercellular adhesion molecule (ICAM) family (1). This integrin mediates

the firm adhesion of leukocytes to the endothelial cells surrounding blood vessels and is necessary for leukocyte extravasation at the inflammatory site (3). The adhesion of murine effector T cells, generated *in vitro*, which play a central role in cell-mediated immunity, to ICAM-1 is completely dependent on β2 integrins (4).

The fundamental importance of β2 integrins is highlighted in the pathologies of several diseases and genetic syndromes, such as leukocyte adhesion deficiency (LAD) (1). LAD can be divided into three different subtypes, LAD-I–III, depending on the causative mutation (5), with types I and III being the most common. Patients who suffer from LAD-I have mutations that lead to a deficiency or absence of β2 integrin expression (1). Therefore, patients suffer from recurrent bacterial and fungal infections, delayed wound healing, and periodontitis (1). LAD-III, a variant of LAD-I, causes patients to present with similar symptoms to patients with LAD-I but with the added complications of a Glanzmann-type bleeding disorder and, in some cases, osteopetrosis (1). Mutations in the signalling protein kindlin-3 have been found to be the cause of LAD-III, thus preventing integrins from becoming fully activated, leading to deficiencies in T cell adhesion and homing (1, 6, 7).

Interaction of kindlin-3 with the β2 integrin in effector T cells is necessary for integrin-mediated adhesion to endothelial cells (6). Through mutating the TTT motif in the β2 integrin cytoplasmic domain, Morrison et al. generated a knock-in (KI) mouse where integrin binding to ICAM-1, T cell trafficking into lymph nodes and inflammatory sites, and T cell activation were severely diminished (7–9). The TTT/AAA mutation abolishes the interaction between integrin and kindlin-3 (7). However, the mechanism by which kindlin-3 affects integrin binding to ligand is still under debate, and it is currently unclear whether integrin/kindlin interactions affect integrin affinity, clustering, or other events involved in cellular adhesion (10–12).

In this paper, we directly assess the effect of mutation of the kindlin-3 binding site in LFA-1 on LFA-1/ICAM-1 bonds. We present an optical-tweezer-based approach for the quantification of the LFA-1–ICAM-1 bond rupture force. Primary murine effector T cells from wild-type and TTT/AAA-beta2-integrin KI mice were allowed to bind to ligand-coated silica beads, and the rupture force of LFA-1–ICAM-1 bonds at a specific pulling rate was measured. The results reveal that mutation of the kindlin-3 binding site in the β2-integrin results in a significantly lower rupture force of integrin–ligand bonds, indicating deficiency in integrin–ligand catch bond formation and resulting in lower bond strength. In addition, we show that this results in reduced cellular adhesion to coated ICAM-1 and in reduced CD8+ T cell activation *in vitro*. These findings thereby shed light on the role of kindlin-3 in regulation of LFA-1 function in T cells.

2 MATERIALS AND METHODS

2.1 Effector T Cell Generation

Effector T cells were generated as in Lek et al. (4). Briefly, splenocytes from either wild-type (WT) or TTT/AAA- β2 integrin knock-in (KI) mice were activated with 0.5 μ g/ml anti-CD3 (clone 2C11, R&D Systems, Minneapolis, MN, USA) together with 20 ng/ml IL-2 (R&D Systems). After 2 days, cells were washed free of activating agent and then maintained in 20 ng/ml IL-2 to be used for experimental purposes on days 6–8 of the culture. Throughout the culture, cells were passaged every 2 days, as well as the day before use in an experiment, to ˜1 x 10^6 cells per ml.

2.2 Static Adhesion Assay

Adhesion assays of effector T cells to coated ICAM-1 were performed as in Lek et al. (4).

2.3 T Cell Activation

CD8+ T cells were isolated using a MACS kit. Purified cells were suspended at 1 million cells/ml in medium and activated with 2.5 μg/ml soluble anti-CD3 antibody (clone 2C11, R&D systems) for the indicated times, followed by flow cytometry to detect the expression of activation markers or ELISA to detect the expression of cytokines, as previously (7).

2.4 ICAM-1 Bead Coating

Silica beads with a diameter of 2.56 μm were coated with 2 μg/ml ICAM-1 (R&D Systems). A large excess of ICAM-1 relative to beads was used to ensure full coating of the beads. Beads were washed twice in 1 ml PBS, by resuspending the beads in 1 ml PBS followed by centrifugation at 13,000 rpm for 1 min in an Eppendorf centrifuge and collecting the beads. After this, beads were resuspended in 500 μl of PBS with 2 μg/ml ICAM-1 and incubated, on rotation, at 4°C for at least 1 h. After incubation, beads were washed 3 times in PBS as above, to remove any excess ICAM-1 from solution.

2.5 Sample Preparation

Samples were prepared by mixing 15 μl of cells with 5 μl of silica beads. The mixture was placed between two microscope coverslips, separated by a 100-µm-thick vinyl spacer. Cells were left to settle for 15–30 min at room temperature before adhesion experiments. This allowed cells to settle on the coverslip, ensuring they were neither pushed away by the bead, nor attracted to the optical trap.

2.6 Experimental System

A force measuring optical tweezers (**Figure 1**) was constructed by expanding the beam from a 1.5-W (maximum output) 1,064-nm laser (Laser Quantum ventus 1064, Laser Quantum, Stockport, United Kingdom) to overfill the back aperture of a Nikon 1.25 NA 100x oil immersion objective (Spectra Services, Ontario, NY, USA). Samples were placed on a Thorlabs MAX302/M NanoMax piezoelectric stage (Thorlabs, Newton, NJ, USA), which was connected to a Thorlabs MDT630A 3-Axis piezo controller. The trap was imaged, *via* a Mitutoyo 0.55 NA 100x long working distance objective, onto a quadrant photodiode (QPD). The 2-mm-diameter InGaAs QPD (Hamamatsu, G6849, Hamamatsu Photonics, Hamamatsu, Japan) was used in back focal plane interferometry mode (13) and was connected to custom-built transimpedance amplifiers, which in turn were

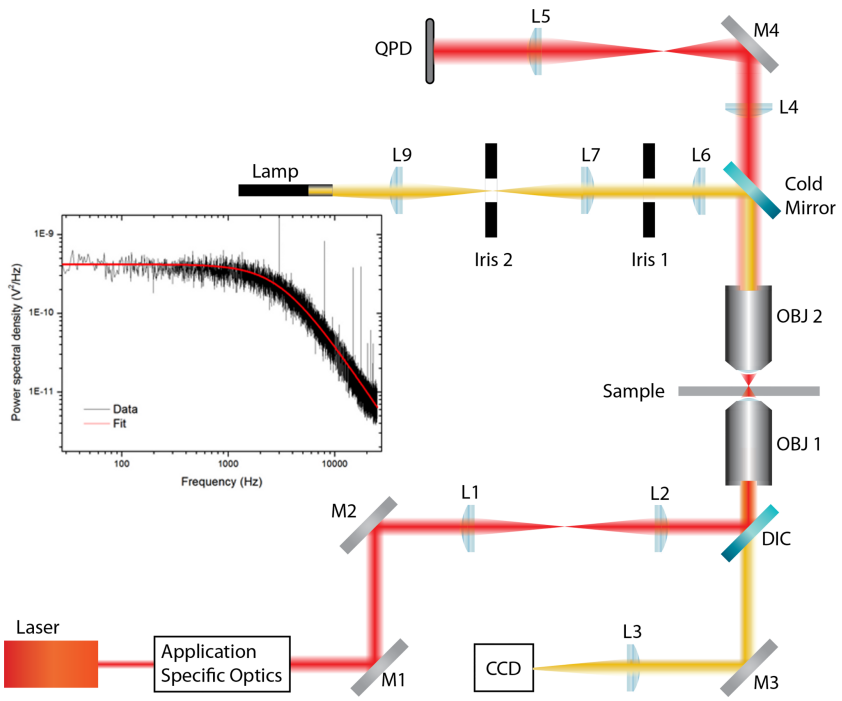

FIGURE 1 | Force measuring optical tweezer system used for static adhesion assays. OBJ 1, Nikon 1.25 NA 100x oil immersion objective; OBJ 2, Mitutoyo 0.55NA 100x long working distance objective. DIC, dichroic mirror; QPD, quadrant photodiode; L, lens; M, mirror. Application-specific optics refer to expansion and beam steering optics. The sample was placed on a Thorlabs MAX302/M NanoMax piezoelectric stage, which was connected to a Thorlabs MDT630A 3-Axis piezo controller.

connected to a National Instruments SCB-68A connector block (National Instruments, Austin, TX, USA). Signals were collected *via* a National Instruments PCI-6250 data acquisition card and analysed using an in-house LabVIEW program.

2.7 Adhesion Measuring Program

The binding between cell and bead was measured using a five-step process, illustrated in **Figures 2A–E**, *via* LabVIEW. Before executing the program, a bead was trapped with ˜200 mW and positioned ˜10 μm from a cell. Trap stiffness was determined by sampling the QPD at 100 kHz, in 4-s intervals for 20 s. Power spectra were calculated from the average signal of five intervals with the corner frequency, and hence trap stiffness, determined through a non-linear least square fitting of a Lorentzian function (14) (**Figure 1** inset). After determining trap stiffness, the cell and bead make contact, pushed together with ˜5 pN for 1 s, and then separated. While the data sampling rate from the QPD remained constant, the sample number was decreased to 8,000 samples per interval using the cell-bead approach, allowing for pseudo-real-time bead displacement monitoring. An integrin–ligand bond is broken when the bead jumps back into the centre of the trap, producing a similar QPD voltage trace to that of **Figure 2F**.

2.8 Single Bond Frequency

Three outcomes were possible when performing an adhesion measurement: the bead and cell did not stick; the bead and cell remained stuck together; or the bead would jump into the trap, breaking the bond with the cell. Successful adhesion events occurred with an average frequency of 25% for WT cells and 22% for KI cells. Due to Poisson distribution statistics (15, 16), this is indicative of a single LFA-1–ICAM bond probability for WT cells of 86.3%, while 12.4% will be double bonds and ˜1% will have 3 or more bonds (17). The slightly lower average binding frequency for KI cells gives bond probabilities of 88.7%, 10.5%, and ˜1% for, respectively, single, double, or three or more bonds.

3 RESULTS AND DISCUSSION

As we have previously shown (4), murine effector T cells display high spontaneous adhesion to coated ICAM-1 under static conditions, which could not be significantly upregulated with phorbol ester, anti-CD3, or Mg-treatment of the cells (**Figure 3**). Mutation of the kindlin-3 binding site in the integrin results in significantly reduced adhesion (**Figure 3**), as we have also previously shown with other immune cell types. However, how this mutation affects integrin–ligand bonds has remained unclear and has here been investigated utilizing optical trapping. The data presented in **Figure 4** show that LFA-1 on both WT and KI murine effector T cells can form spontaneous adhesive contacts to ICAM-1, its corresponding ligand, under force. An average integrin–ligand unbinding force of 17.85 ± 0.63 pN (mean ± std.

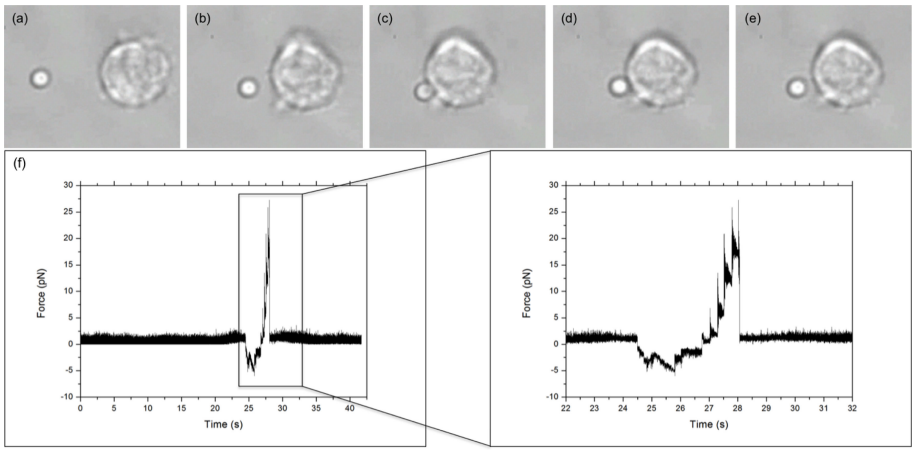

FIGURE 2 | LFA-1–ICAM-1 adhesion measurement. **(A–E)** show the five steps of an adhesion measurement: **(A)** trap stiffness; **(B)** approach; **(C)** stick; **(D)** pull; and **(E)** bond break. Arrow donates direction of stage/cell movement. **(F)** Typical force versus time graph obtained for an integrin–ligand unbinding event. The large peak, enlarged in the inset, represents the maximum unbinding force required to disrupt an integrin–ligand bond. The jagged profile of the peak is due to the piezo stage moving in "steps.".

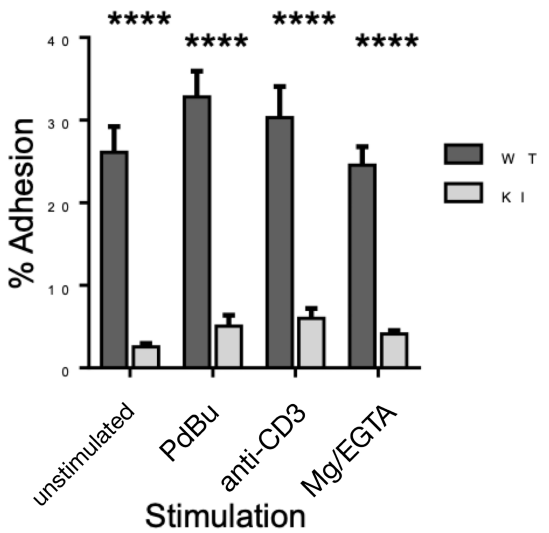

FIGURE 3 | Adhesion of WT and KI cells to coated ICAM-1, as measured by static adhesion assay. Pooled data from 3 independent experiments, each with 2 technical replicates. ****p < 0.0001.

error, N = 91) (most likely representing a single LFA-1-ICAM-1 bond) was measured for WT cells at an average force loading rate cell of 30.21 ± 4.35 pN/s. As expected, the unbinding force of the KI cells was significantly lower ($p << 0.01$, two tailed two-sample *t*-test), with an average unbinding force of 10.08 ± 0.88 pN (mean ± std. error, N = 49) at the same force loading rate. No bonds were measured as forming between uncoated silica beads.

The significant reduction of kindlin-3 binding to the integrin, achieved through the mutation of the TTT motif in the β2 integrin cytoplasmic domain, is mirrored in the reduction of rupture force of the integrin–ligand bonds when external force is applied. Integrins form so-called catch bonds, which are strengthened under force, until a limit is reached, breaking the bond. Under force, LFA-1 unbends from the closed conformation, allowing catch bond formation, as the applied force "pulls" the integrin open (18). The significantly lower rupture force of integrin–ligand bonds for the KI cells under force highlights the necessity of kindlin 3– β2 interaction for such catch bonds to form. Previous work by Morrison et al. showed that there was not a significant decrease in integrin expression of KI effector T cells (7); therefore, this is not a contributing factor for decreased integrin-mediated adhesion of these cells. However, Morrison et al. showed that, under shear flow (e.g., force), effector T cells with the TTT/AAA-mutated integrins were not able to form stable adhesion with ICAM-1 but were able to mediate cell rolling (7). Together with the results presented here, these results strongly indicate that the LFA-1–kindlin-3 interaction is necessary for LFA-1 catch bond formation.

Integrin-mediated ligand binding is important not only for recruitment of T cells from the blood stream but also for other T cell functions. For example, optimal T cell activation is known to require LFA-1. To investigate whether the integrin/kindlin interaction, and therefore strong integrin–ligand bonds, is required also for CD8+ T activation, we performed T cell activation studies *in vitro*. Purified CD8+ T cells were activated *in vitro* utilizing soluble anti-CD3 antibodies, a mode of activation which requires functional integrins (7). During activation with soluble anti-CD3 antibodies, the T cells form cell–cell aggregates involving LFA-1–ICAM-1 bonds, which is necessary for optimal T cell activation. We therefore employed this T cell activation assay, to correlate LFA-1 bond strength with a biological outcome. Indeed, as shown in **Figure 5**, when the integrin/kindlin interaction is disrupted, T cell activation *in vitro*

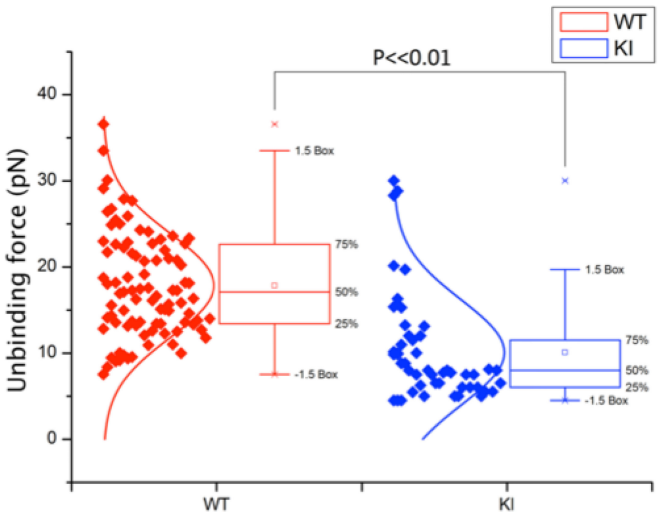

FIGURE 4 | Unbinding force of integrin–ligand pairs for both WT and KI cells, as measured by an optically trapped 2.56-μm bead, coated with 2 μg/ml ICAM-1, in contact with the cell for 1 s. WT unbinding force was measured as 17.85 ± 0.63 pN (N = 91), with KI unbinding force significantly lower at 10.08 ± 0.88 pN (N = 49) (mean ± std. error, p << 0.01) at an average force loading rate on the cell of 30.21 ± 4.35 pN/s.

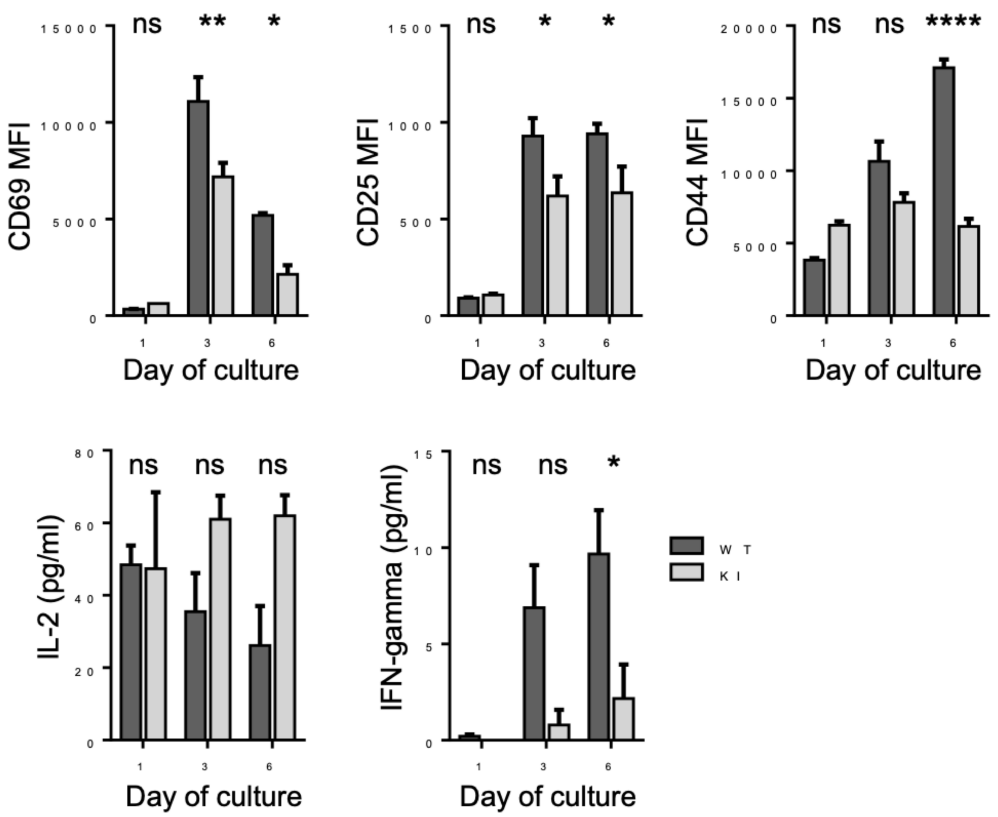

FIGURE 5 | Activation of WT and KI CD8+ T cells following stimulation with anti-CD3 stimulatory antibodies for 1-6 days *in vitro*. Pooled data from 2 independent experiments, each with 2 biological replicates (donor mice). *p < 0.05; **p < 0.01; ****p < 0.0001; ns, non significant.

(e.g., expression of activation markers CD69, CD25, and CD44, and production of the cytokine IFNgamma, but not IL-2) is significantly reduced.

In conclusion, we have shown that kindlin 3– β2 integrin interaction affects integrin–ligand catch bonds of effector T cells and that firm adhesion of WT integrin–ligand pairs relates to an unbinding force of 17.85±0.63 pN at an average force loading rate on the cell of 30.21 ± 4.35 pN/s. By reducing the kindlin 3–β2 interaction, integrin–ligand unbinding force fell significantly, to 10.08±0.88 pN. This confirms that there is still an integrin–ligand interaction without kindlin-3 binding but that kindlin-3 indeed is required for optimal integrin–ligand catch bond formation.

How might kindlin-3 affect LFA-1 catch bond formation? Integrin activation can be achieved by extracellular forces but, in addition to this, also by cytoskeletal forces (pulling on the integrin from the inside of the cell) (19). LFA-1 on the surface of effector T cells is not in an active conformation (20), but effector T cell adhesion to ICAM-1 under shear flow, e.g., catch bond formation, requires an intact actin cytoskeleton (4). Interestingly, the TTT/AAA mutation in the integrin tail disrupts the interaction of the integrin with the actin cytoskeleton (21). We therefore postulate that kindlin-3 affects LFA-1 catch bonds by indirectly mediating its connections with the actin cytoskeleton within the cell. These interactions would allow anchoring LFA-1 within the cell, and catch bond formation in the presence of ligand.

We note that there is still significant scope to expand the observed results in terms of exploring behaviour as a function of loading rate and also experiments with changes in ligand concentration to clarify the nature of the single and multiple bond response.

This study brings new information about the role of kindlin-3 in regulating LFA-1-mediated T cell adhesion events necessary for proper immune system function, through allowing for LFA-1 catch bond formation. In the future, it will be interesting to expand these studies to examine the exact mechanisms involved in kindlin-3-regulated LFA-1 binding to ICAM-1 in T cells, as well as in other cell types.

DATA AVAILABILITY STATEMENT

The original contributions presented in the study are included in the article/supplementary material. Further inquiries can be directed to the corresponding author.

ETHICS STATEMENT

The animal study was reviewed and approved by the University of Dundee ethics committee.

AUTHOR CONTRIBUTIONS

SF and DM designed the study, CM and VM performed experiments and analysed data, CM, VM, DM, and SF wrote the manuscript. All authors contributed to the article and approved the submitted version.

FUNDING

This study was funded by the Engineering and Physical Sciences Research Council (EPSRC) EP/J500392/1; Academy of Finland (to SF); and Ella and Georg Ehrnrooth Foundation (to VM).

ACKNOWLEDGMENTS

The authors wish to thank Dr. Hwee San Lek for the help with, and training in, culturing effector T cells.

REFERENCES

1. MacPherson M, Lek HS, Morrison VL, Fagerholm SC. Leukocyte Beta2-Integrins: Genes and Disease. *J Genet Syndr Gene Ther* (2013) 04:154–8. doi: 10.4172/2157-7412.1000154
2. Evans R, Patzak I, Svensson L, De Filippo K, Jones K, McDowall A, et al. Integrins in Immunity. *J Cell Sci* (2009) 122:215–25. doi: 10.1242/jcs.019117
3. Muller WA. Getting Leukocytes to the Site of Inflammation. *Vet Pathol* (2013) 50:7–22. doi: 10.1177/0300985812469883
4. Lek HS, Morrison VL, Conneely M, Campbell PA, McGloin D, Kliche S, et al. The Spontaneously Adhesive Leukocyte Function-Associated Antigen-1 (LFA-1) Integrin in Effector T Cells Mediates Rapid Actin- and Calmodulin-Dependent Adhesion Strengthening to Ligand Under Shear Flow. *J Biol Chem* (2013) 288:14698–708. doi: 10.1074/jbc.M112.430918
5. Etzioni A. Genetic Etiologies of Leukocyte Adhesion Defects. *Curr Opin Immunol* (2009) 21:481–6. doi: 10.1016/j.coi.2009.07.005
6. Moser M, Bauer M, Schmid S, Ruppert R, Schmidt S, Sixt M, et al. Kindlin-3 Is Required for Beta2 Integrin-Mediated Leukocyte Adhesion to Endothelial Cells. *Nat Med* (2009) 15:300–5. doi: 10.1038/nm.1921
7. Morrison VL, Macpherson M, Savinko T, Lek HS, Prescott A, Fagerholm SC. The Beta2 Integrin-Kindlin-3 Interaction is Essential for T Cell Homing But Dispensable for T Cell Activation *In Vivo*. *Blood* (2013) 122:1428–37. doi: 10.1182/blood-2013-02-484998
8. Morrison VL, Uotila LM, Llort Asens M, Savinko T, Fagerholm SC. Optimal T Cell Activation and B Cell Antibody Responses *In Vivo* Require the Interaction Between Leukocyte Function-Associated Antigen-1 and Kindlin-3. *J Immunol* (2015) 195:105–15. doi: 10.4049/jimmunol.1402741
9. Savinko T, Morrison V, Uotila L, Wolff H, Alenius H, Fagerholm SC. Functional Beta2-Integrins Restrict Skin Inflammation *In Vivo*. *J Invest Dermatol* (2015) 135:1–27. doi: 10.1038/jid.2015.164
10. Harburger DS, Bouaouina M, Calderwood DA. Kindlin-1 and -2 Directly Bind the C-Terminal Region of Integrin Cytoplasmic Tails and Exert Integrin-Specific Activation Effects. *J Biol Chem* (2009) 284:11485–97. doi: 10.1074/jbc.M809233200
11. Lefort CT, Rossaint J, Moser M, Petrich BG, Zarbock A, Monkley SJ, et al. Distinct Roles for Talin-1 and Kindlin-3 in LFA-1 Extension and Affinity Regulation. *Blood* (2012) 119:4275–82. doi: 10.1182/blood-2011-08-373118
12. Ye F, Petrich BG, Anekal P, Lefort CT, Kasirer-friede A, Sanford J, et al. The Mechanism of Kindlin-Mediated Activation of Integrin $\alpha IIb\beta 3$. *Curr Biol* (2013) 23:2288–95. doi: 10.1016/j.cub.2013.09.050
13. Neuman KC, Block SM. Optical Trapping. *Rev Sci Instrum* (2004) 75:2787–809. doi: 10.1063/1.1785844

14. Berg-Sørensen K, Flyvbjerg H. Power Spectrum Analysis for Optical Tweezers. *Rev Sci Instrum* (2004) 75:594. doi: 10.1063/1.1645654
15. Chesla SE, Selvaraj P, Zhu C. Measuring Two-Dimensional Receptor-Ligand Binding Kinetics by Micropipette. *Biophys J* (1998) 75:1553–72. doi: 10.1016/S0006-3495(98)74074-3
16. Merkel R, Nassoy P, Leung A, Ritchie K, Evans E. Energy Landscapes of Receptor-Ligand Bonds Explored With Dynamic Force Spectroscopy. *Nature* (1999) 397:50–3. doi: 10.1038/16219
17. Tees DF, Waugh RE, Hammer DA. A Microcantilever Device to Assess the Effect of Force on the Lifetime of Selectin-Carbohydrate Bonds. *Biophys J* (2001) 80:668–82. doi: 10.1016/S0006-3495(01)76047-X
18. Chen W, Lou J, Evans EA, Zhu C. Observing Force-Regulated Conformational Changes and Ligand Dissociation From a Single Integrin on Cells. *J Cell Biol* (2012) 199:497–512. doi: 10.1083/jcb.201201091
19. Nordenfelt P, Elliott NL, Springer TA. Coordinated Integrin Activation by Actin-Dependent Force During T-Cell Migration. *Nat Commun* (2016) 7:13119. doi: 10.1038/ncomms13119
20. Shulman Z, Cohen SJ, Roediger B, Kalchenko V, Jain R, Grabovsky V, et al. Transendothelial Migration of Lymphocytes Mediated by Intraendothelial Vesicle Stores Rather Than by Extracellular Chemokine Depots. *Nat Immunol* (2011) 13:67–76. doi: 10.1038/ni.2173
21. Morrison VL, James MJ, Grzes K, Cook P, Glass DG, Savinko T, et al. Loss of Beta2-Integrin-Mediated Cytoskeletal Linkage Reprogrammes Dendritic Cells to a Mature Migratory Phenotype. *Nat Commun* (2014) 5:5359. doi: 10.1038/ncomms6359

Conflict of Interest: The authors declare that the research was conducted in the absence of any commercial or financial relationships that could be construed as a potential conflict of interest.

Publisher's Note: All claims expressed in this article are solely those of the authors and do not necessarily represent those of their affiliated organizations, or those of the publisher, the editors and the reviewers. Any product that may be evaluated in this article, or claim that may be made by its manufacturer, is not guaranteed or endorsed by the publisher.

frontiers in Immunology

MINI REVIEW
published: 11 February 2022
doi: 10.3389/fimmu.2022.830835

Lymphocyte Polarization During Immune Synapse Assembly: Centrosomal Actin Joins the Game

Chiara Cassioli and Cosima T. Baldari**

Department of Life Sciences, University of Siena, Siena, Italy

Interactions among immune cells are essential for the development of adaptive immune responses. The immunological synapse (IS) provides a specialized platform for integration of signals and intercellular communication between T lymphocytes and antigen presenting cells (APCs). In the T cell the reorganization of surface molecules at the synaptic interface is initiated by T cell receptor binding to a cognate peptide-major histocompatibility complex on the APC surface and is accompanied by a polarized remodelling of the cytoskeleton and centrosome reorientation to a subsynaptic position. Although there is a general agreement on polarizing signals and mechanisms driving centrosome reorientation during IS assembly, the primary events that prepare for centrosome repositioning remain largely unexplored. It has been recently shown that in resting lymphocytes a local polymerization of filamentous actin (F-actin) at the centrosome contributes to anchoring this organelle to the nucleus. During early stages of IS formation centrosomal F-actin undergoes depletion, allowing for centrosome detachment from the nucleus and its polarization towards the synaptic membrane. We recently demonstrated that in $CD4^+$ T cells the reduction in centrosomal F-actin relies on the activity of a centrosome-associated proteasome and implicated the ciliopathy-related Bardet-Biedl syndrome 1 protein in the dynein-dependent recruitment of the proteasome 19S regulatory subunit to the centrosome. In this short review we will feature our recent findings that collectively provide a new function for BBS proteins and the proteasome in actin dynamics, centrosome polarization and T cell activation.

Keywords: immune synapse, centrosome polarization, F-actin clearance, T lymphocytes, B lymphocytes

OPEN ACCESS

Edited by:
Jerome Delon,
U1016 Institut Cochin (INSERM), France

Reviewed by:
Michael R. Gold,
University of British Columbia, Canada
Chang-Duk Jun,
Gwangju Institute of Science and Technology, South Korea
Clotilde Randriamampita,
U1016 Institut Cochin (INSERM), France

***Correspondence:**
Cosima T. Baldari
cosima.baldari@unisi.it
Chiara Cassioli
chiara.cassioli2@unisi.it

Specialty section:
This article was submitted to T Cell Biology, a section of the journal Frontiers in Immunology

Received: *07 December 2021*
Accepted: *20 January 2022*
Published: *11 February 2022*

Citation:
Cassioli C and Baldari CT (2022) Lymphocyte Polarization During Immune Synapse Assembly: Centrosomal Actin Joins the Game. Front. Immunol. 13:830835. doi: 10.3389/fimmu.2022.830835

INTRODUCTION

The immunological synapse (IS) is a specialized interface formed by T lymphocytes with antigen presenting cells (APCs) bearing a cognate peptide-major histocompatibility complex (pMHC) that allows for information exchange and execution of effector functions (1, 2). In its canonical configuration the IS is characterized by concentric Supra Molecular Activation Clusters (SMACs) differing in composition and function (3, 4). Ligand-bound antigen T cell receptors (TCRs) and associated signaling molecules occupy the central SMAC (cSMAC), which is surrounded by a peripheral SMAC (pSMAC) enriched in adhesion molecules, such as the integrin LFA-1, and an outer distal SMAC (dSMAC), where filamentous actin (F-actin) and CD45 are concentrated (4, 5).

Immune cell interactions rely on continuous cytoskeleton remodeling events, which not only shape the T cell-APC interface, but also asymmetrically distribute molecules and organelles within the lymphocyte, leading to the establishment of transient polarity (6, 7). Cytoskeleton remodeling is one of the earliest events induced by TCR signaling (8) and culminates in the formation of a synaptic F-actin ring, allowing the centrosome to polarize to the IS (9) together with the Golgi apparatus, endosomal and secretory compartments, multivesicular bodies (MBVs) and mitochondria (10–14). This polarized configuration is instrumental in the directional delivery of TCR^+ recycling endosomes to the synaptic membrane (15–17) that thus is refilled of signaling-competent receptors as exhausted TCRs are internalized to be sorted for recycling or lysosomal degradation (18, 19). Alternatively, post-endocytic TCRs are directed to MVBs and incorporated in intraluminal vesicles (ILVs), which are released into the synaptic cleft as exosomes and taken up by APCs (20). Mitochondria are also mobilized towards the APC contact site, where they contribute to IS formation and TCR signaling by providing a local source of ATP and modulating the concentration of intracellular calcium (13, 21, 22).

The rapid repositioning of the centrosome following F-actin depletion from the IS center highlights a spatiotemporal coordination between the actin and microtubule cytoskeletons during IS formation. Interestingly, recent studies have unveiled a new feature of the interplay between F-actin dynamics and centrosome repositioning during IS assembly, demonstrating that the balance between F-actin polymerization and depolymerization at the centrosome is crucial for its ability to untether from the nucleus and polarize to the IS. Here, we will summarize how actin dynamics at the synaptic and centrosomal areas regulate IS assembly. We will then describe the emerging role of the ubiquitin-proteasome system (UPS) in centrosomal F-actin remodeling, focusing on our recent findings that identify the ciliary protein Bardet-Biedl Syndrome 1 (BBS1) as a new regulator of T cell polarity during IS formation (23).

REGULATION OF CENTROSOME POLARIZATION BY THE ACTIN CYTOSKELETON

Synaptic F-Actin Controls Centrosome Repositioning to the IS and Microtubule-Driven Exocytosis

TCR engagement by cognate pMHC promotes profound cytoskeletal changes, achieved *via* the coordinated reorganization of the actin and microtubule cytoskeletons at the IS. Actin remodeling is triggered within seconds after TCR stimulation (8) and precedes centrosome translocation towards the IS (9). Imaging cortical actin at the T cell IS using super-resolution microscopy techniques has revealed the coexistence of distinct actin-based networks in the three concentric regions, or SMACs, featured by the IS: from the outer edge to the center, a lamellipodial branched actin network (dSMAC), the lamellar acto-myosin network (pSMAC), a network consisting of actin foci spread throughout the dSMAC and pSMAC, and an hypodense actin network at the center (cSMAC) [synaptic actin networks are extensively reviewed in (24, 25)]. Another category of actin-based structures, the microvilli, has been described at the T cell surface (26). Although these microvillar extensions are a feature of resting T cells, their study has been recently extended to activated cells based on the observation that TCRs cluster at microvillar tips (27). T cell microvilli had been initially considered as sensors during antigen survey on APCs. However, the discovery of T cell microvillar particles (TMP) deposited on the APC surface has suggested the possibility that they may act as "immunological synaptosomes" that deliver a new class of membrane vesicles as a means of intercellular communication (28, 29).

TCR signaling is the main extrinsic cue for centrosome reorientation to the IS (30), with the second messenger diacylglycerol (DAG), which forms a gradient centered at the cSMAC, acting as a polarity determinant (31, 32). Multiple signaling pathways initiated at the IS by the TCR, the integrin LFA-1 and the co-stimulatory receptor CD28 coordinate the activation of several actin-regulatory proteins that promote F-actin polymerization, feeding back for optimal TCR signaling, integrin activation and T cell spreading over the APC (33, 34). Interestingly, both disruption of synaptic actin networks and depletion of F-actin nucleators (e.g. the formins diaphanous 1 and formin-like-1) result not only in impaired centrosome mobilization but also in defective TCR signaling, suggesting an indirect role of actin in centrosome repositioning. The physical interaction between microtubule (+)ends and branched F-actin network at the IS periphery, which is mediated by molecular linkers that include the IQ domain-containing GTPase-activating protein, ezrin and Cdc42-interacting protein 4 (35–37), provides an additional function for actin in centrosome polarization by generating tension on microtubules.

Centrosome repositioning is considered a hallmark of T cell polarity during IS assembly. The reorientation of this organelle is accompanied by the polarization of other intracellular compartments, including secretory and recycling endosomes that require microtubule tracks for delivery to the IS and focalized exocytosis. Emerging evidence indicates an early participation of F-actin in polarized recycling. F-actin polymerizes at recycling endosomes through the assistance of the F-actin regulator Wiskott-Aldrich Syndrome protein and SCAR Homology (WASH) and its partner FAM21 to help membrane scission of nascent vesicles carrying recycling cargo, including the TCR, LFA-1, CD28 and the glucose transporter GLUT-1. These receptors exploit the recycling pathway to accumulate at the IS, where they participate in mature IS formation and maintenance, as well as in the metabolic reprogramming of activated T cells (38). The role of actin in the final steps of vesicle fusion and exocytosis at the IS is less clear-cut. Initially, cortical actin has been regarded as a barrier that prevents vesicle exocytosis. Consistent with this view, in T_H cells the focalized release of IFN-γ at the IS was found to be

impaired in Cdc42-silenced T cells due to their failure to form a synaptic actin ring (39). Moreover, lattice-light-sheet microscopy of CTL-target cell conjugates showed that at mature synapses F-actin is cleared from the cSMAC before lytic granule secretion, and that lytic granule release triggers F-actin recovery at the lytic synapse blocking further lytic granule exocytosis and serial killing (40, 41). However, a more in-depth analysis of actin dynamics at the lytic synapse using super-resolution microscopy has revealed that the cSMAC is not entirely free from F-actin, but rather occupied by a hypodense actin network (42–44). Upon cell activation, holes of a size compatible with the access of lytic granules to the plasma membrane for docking and fusion have been observed (42, 44). Hence actin plays a dual role during secretion depending on the maturation stage of the lytic synapse: at immature synapses a dense actin cortex blocks secretion, while in mature, actin-hypodense synapses nanoscale actin filament dynamics fine-tunes regulated lytic granule exocytosis (45).

A Centrosome-Associated F-Actin Pool Contributes to Lymphocyte Polarization

Although the centrosome is the major microtubule-organizing center, F-actin and microtubules coexist at the centrosomal area. Proteomic analyses have documented the presence of actin and actin-associated proteins at the centrosome (46–51) and different actin structures have been reported in association with the centrosome and the nucleus in different cell types (52–55). Recent studies carried out on B lymphocytes have revealed that the centrosome is surrounded by a local, cloud-like meshwork of F-actin. A central function of this F-actin pool is to anchor the centrosome to the nucleus *via* the Linker of Nucleoskeleton and Cytoskeleton (LINC) complex (51). Moreover, centrosome-associated F-actin can prevent microtubule growth from the centrosome, as supported by *in vitro* reconstitution assay on purified centrosomes (56), suggesting that synaptic F-actin clearance is not sufficient for centrosome polarization to the IS. Of note, the centrosome-associated F-actin network undergoes a dynamic turnover though repeated cycles of polymerization and depolymerization. Upstream centrosome polarization to the IS, the balance between F-actin assembly and disassembly is tilted towards the latter leading to a local depletion of centrosomal F-actin, which facilitates centrosome detachment from the nucleus and its subsequent translocation towards the IS. In B cells this occurs through a reduced recruitment of the actin nucleator Arp2/3 at the centrosome (**Figure 1**) in favor of its synaptic localization (51).

A more recent study on Jurkat T cell-APC conjugates has demonstrated that centrosome-associated F-actin remodeling is a mechanism controlling centrosome polarization also in T lymphocytes (57). A pathway involving protein kinase C-δ (PKCδ), which is activated downstream TCR engagement, has

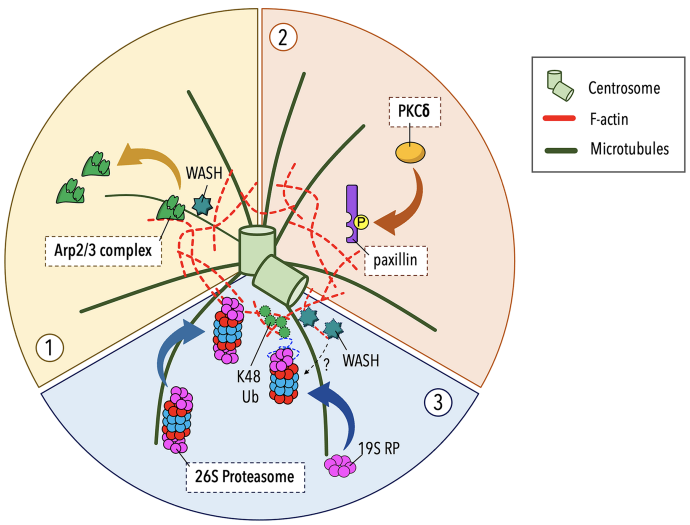

FIGURE 1 | Regulation of centrosomal F-actin clearance in lymphocytes. Recent studies carried out on B and T lymphocytes have implicated three discrete pathways in centrosomal F-actin clearance and centrosome polarization during early stages of IS assembly. (**1**) In B lymphocytes the recruitment of the branched F-actin nucleator Arp2/3 to the IS upon BCR activation leads to a local depletion of centrosome-associated Arp2/3 that results in reduced F-actin polymerization at the centrosome, allowing for centrosome untethering from the nucleus and its repositioning to the B cell IS (51). (**2**) In T lymphocytes protein kinase C-δ (PKCδ) has been identified as a novel regulator of centrosomal F-actin remodeling, beyond its role in cortical actin reorganization at the IS. Following TCR triggering, PKCδ phosphorylates the scaffold protein paxillin, which localizes at the centrosome where it contributes to centrosome translocation to the T cell IS by promoting a local F-actin clearance through an unknown mechanism (57). (**3**) An alternative pathway, based on the proteolytic activity of a centrosome-associated proteasome, controls F-actin clearance from the centrosome to enable its dissociation from the nucleus and polarization to the nascent IS. This pathway is exploited by both B and T lymphocytes with some cell type-dependent features. In B lymphocytes the intracellular distribution of the proteasome is regulated by the proteasome adapter and scaffold protein Ecm29 during B cell IS formation, allowing a sequential recruitment of the proteasome to the centrosome and then to the IS, which is crucial for F-actin reorganization at both locations (58, 59). In T lymphocytes proteasome-mediated degradation of unknown targets at early stages of IS assembly is dependent on the transport of the 19S regulatory particle (RP) to the centrosome, which is paralleled by an active degradation of K48-linked polyubiquitylated proteins (K48 Ub) (23). The contribution extent as well as the sequential implication of these pathways to the process remain to be elucidated.

been proposed to regulate centrosomal F-actin in T cells (**Figure 1**). The PKCδ-mediated phosphorylation of the cytoskeleton adaptor protein paxillin, which is associated with the centrosome under resting and stimulating conditions, has been related to F-actin clearance around the centrosome and its polarization to the IS (57), however the underlying mechanism remains to be elucidated. Since paxillin interacts with several signaling and cytoskeletal proteins (60, 61), it is likely that paxillin directly or indirectly binds to one or more actin regulators. Furthermore, paxillin associates with the microtubule cytoskeleton (62, 63), suggesting that it might play a role in the actin-microtubule interplay that drive centrosome repositioning to the IS. An interesting aspect in the model proposed by Bello-Gamboa et al. is that the reorganization of the actin cytoskeleton at the centrosome occurs in a coordinated fashion with synaptic F-actin remodeling. In fact, PKCδ was found to phosphorylate another substrate, the formin-like molecule FMNL1β, that is recruited to the IS (57), where membrane-bound formins generate bundles of linear actin filaments across the dSMAC (64, 65).

THE UBIQUITIN-PROTEASOME SYSTEM (UPS) AND BBS1 COOPERATE IN CENTROSOMAL F-ACTIN CLEARANCE IN T CELLS

In recent years new, unexpected players have been identified in the mechanisms that regulate centrosomal F-actin clearance and centrosome polarization during IS assembly. We and Ibañez-Vega et al. have implicated the ubiquitin-proteasome system (UPS) in this process (23, 58, 59) (**Figure 1**). The UPS is a major degradation pathway in eukaryotic cells and is responsible for proteolysis of cytosolic proteins regulating a variety of cellular processes. This system consists of ubiquitin ligases that target proteins for degradation by covalently adding ubiquitin to proteasome substrates, allowing for their recognition by the 26S proteasome. The 26S proteasome is a multisubunit complex, composed by the 19S regulatory particle (RP) and the 20S core particle (CP), which identifies, unfolds, and degrades ubiquitinated proteins in an ATP-dependent manner (66). Accumulating evidence suggests a role for the proteasome in centrosome proteostasis (67), and thus in centrosome-related functions, including cell polarity in neurons (68, 69), growth and signaling function of the primary cilium in ciliated cells (70–74), and differentiation and metabolic profile of $CD8^+$ T cells (75, 76).

Although the proteasome is largely cytosolic, a proteasomal pool is associated with the centrosome, as witnessed by a local accumulation of proteasome subunits and proteasomal substrates around the centrosome (67). Recently, it has been reported that in B cells proteasome relocalization from the centrosome to the IS is required for the spatiotemporal coordination of centrosomal and synaptic F-actin depolymerization (58, 59). In T lymphocytes a proteomic analysis of centrosomes purified from activated cells has revealed a local enrichment of proteasomal components (77). Consistent with this evidence, we observed that the centrosomal 19S RP pool increases early during IS formation, to progressively return to baseline with IS maturation (23). Additionally, we found that the centrosome failed to polarize to the IS in T cells pre-treated with proteasome inhibitors and that the mislocation of the centrosome in these cells is paralleled by F-actin accumulation at the centrosome, supporting a role for the centrosomal proteasome in IS formation. The mechanisms linking the centrosomal proteasome to the local F-actin pool remain unknown. While actin depletion is regulated by the balance in the depolymerization and *de novo* synthesis of actin filaments, proteasome-regulated and centrosome-associated actin nucleators, such as Arp2/3 and its activator WASH [assembly and activity of the WASH complex are extensively reviewed in (78)], which become depleted during IS assembly (23), may represent potential targets of the centrosomal proteasome. Particularly interesting candidates are the proteasome-regulated E3 ligase TRIM27, which activates WASH through K63 mono-ubiquitination (79), and the centriolar satellite protein PCM1 (80), which recruits Arp2/3 and WASH to the T cell centrosome (50). Whether these are actual targets of the centrosomal proteasome, and the relative contribution of degradation versus changes in subcellular localization to the centrosomal depletion of Arp2/3 and WASH as well as to the resulting local decrease in F-actin during IS formation, are important issues to be addressed.

An expected twist in the proteasome-dependent regulation of centrosomal F-actin was the identification of the ciliopathy-related protein BBS1 as a novel player in T cell IS assembly (23). The BBS complex, or BBSome, is an evolutionary conserved octameric complex that regulates cilia-based signaling pathways by acting as an adaptor between the Intraflagellar transport-B (IFT-B) complex and membrane proteins, of which activated G protein-coupled receptors (GPCRs) are the main group, for their ciliary exit (81, 82). Several ciliogenesis proteins and ciliary signaling pathways are important regulators of different steps in T cell IS assembly (83, 84) and the BBSome core component BBS1 is no exception. In our recent work we demonstrated that BBS1 controls a key event in IS formation, i.e. centrosome polarization, on which the synaptic recruitment of endosomal TCRs and accumulation of tyrosine phosphoproteins depend. Having ruled out an early TCR signaling defect as the cause of the inability of the centrosome to polarize to the IS in BBS1-depleted T cells, we hypothesized alternative explanations. Centrosomal F-actin clearance appeared an interesting possibility, since in BBS4-, BBS6- or BBS9-depleted cells ciliogenesis is compromised due to increased F-actin polymerization (85). Indeed, we found that F-actin failed to be cleared from the centrosome in the absence of BBS1 and that the persistence of a F-actin meshwork at the centrosome was paralleled by a local accumulation of WASH (23). Our results identify a novel cilium-independent function for BBS1 in the clearance of centrosomal F-actin, due at least in part to local depletion of WASH. This is expected to result in impaired F-actin nucleation that is not able to counterbalance the continuous depolymerization of pre-existing filaments,

eventually leading to centrosome disengagement from the nucleus and its polarization to the IS. A more in-depth investigation of the molecular mechanism by which BBS1 controls centrosomal F-actin dynamics in T cells revealed that, consistent with the BBSome function in dynein-dependent retrograde transport of ciliary cargo to the base of the cilium (82), BBS1 acts as a dynein adaptor coupling the 19S RP with dynein allowing for its transport to the centrosome. Consistent with this function, a lesser recruitment of 19S RP to the centrosome and an increased centrosomal accumulation of K48-polyubiquitylated proteins were observed in conjugates of BBS1-deficient T cells (23).

Taken together, our findings indicate that, similar to B cells, T cells exploit a proteasome-mediated pathway for centrosomal F-actin clearance, allowing for centrosome polarization to the IS. In this context, the ciliary protein BBS1 regulates the local activity of a centrosome-associated proteasome by coupling the 19S RP to dynein to allow for its retrograde transport to the centrosome (**Figure 2**).

CONCLUSIONS AND FUTURE DIRECTIONS

While cortical F-actin remodeling has been long considered sufficient for centrosome polarization (40), the existence of a F-actin meshwork around the centrosome, the clearance of which is required for centrosome polarization during IS assembly, has added a new level of complexity to the regulation of this process. Currently, three major pathways have been implicated in the depletion of the centrosome-associated F-actin pool and centrosome polarization in lymphocytes. Despite these recent advances, major questions remain to address. For example, whether at some point these pathways intersect converging on shared regulators, or whether they are distinct pathways that sequentially participate in centrosome repositioning to the IS. Imaging studies of the kinetics of centrosome polarization suggested that this process consists of two steps: a relative fast reorientation of the centrosome towards the IS, followed by a slower approach of

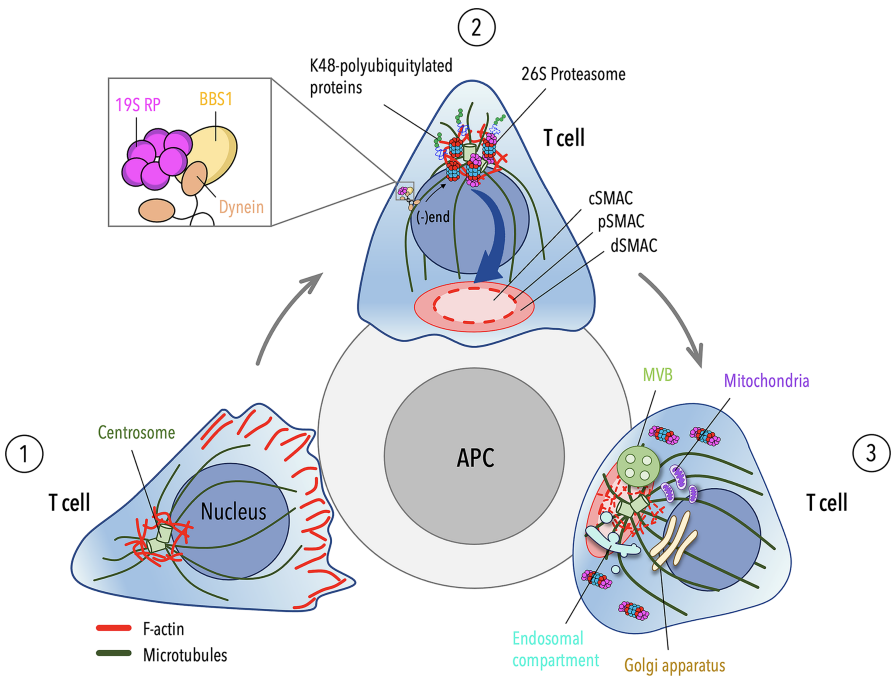

FIGURE 2 | Cytoskeleton-driven events leading to centrosome polarization during T cell IS assembly. (**1**) Migrating T cells exhibit an actin-rich leading-edge and a uropod protruding from the rear of the cell. The centrosome localizes at the trailing edge of the cell and is tethered to the nucleus by a F-actin pool associated with the centrosome. (**2**) Upon antigen presenting cell (APC) encounter, actin polymerizes and accumulates at the contact site to drive the spreading of the T cell across the APC. On the contrary, centrosomal F-actin undergoes depletion during IS formation to allow for centrosome detachment from the nucleus and its translocation to the nascent IS. Centrosome-associated proteasome, which is endowed of enhanced proteolytic activity within the first minute of IS assembly (23), plays a key role in this process by shifting the balance between polymerization and depolymerization of centrosomal F-actin towards the latter, thus leading to its clearance from the centrosome. The activity of the centrosome-associated proteasome is controlled by the ciliary protein BBS1, which regulates the traffic of the proteasome 19S regulatory particle (RP) to the centrosome by coupling 19S RP with the molecular motor dynein. (**3**) The centrosome moves from a site proximal to the IS close to the plasma membrane as cortical F-actin reorganizes into the distal SMAC (dSMAC), leaving a hypodense central SMAC (cSMAC) actin network at the mature IS. Microtubule tethering to the actin network (35–37, 86), capture of (+)ends by dynein at the synaptic membrane and microtubule dynamics (77, 87–90) contribute to the full polarization of the centrosome. In association with the centrosome, other organelles, such as the Golgi apparatus, the endosomal and recycling compartments, multivesicular bodies (MVBs) and mitochondria, converge to the IS to sustain TCR signaling and metabolic reprogramming leading to T cell activation.

the centrosome to the synaptic membrane (87). One possibility might be that the dynein- and -BBS1-mediated centrosomal recruitment of either the proteasome or its regulatory component occurs early during centrosome polarization promoting a partial centrosomal F-actin depletion, concomitant with centrosome mobilization to the IS. When the centrosome is in the correct orientation relative to the IS, the synaptic recruitment of the Arp2/3 complex or the PKCδ-dependent phosphorylation of paxillin might complete centrosomal F-actin clearance allowing a full polarization of the centrosome towards the synaptic membrane. Since centrosome polarization can be triggered both by TCR and non-TCR signals (91, 92), we can speculate that a rapid translocation of the centrosome to the IS is driven by TCR-independent signals or minimal TCR signals, while a slower movement of the centrosome towards the maturing IS is tightly controlled by the TCR signaling pathway.

Another major challenge due to the tight squeezing of organelles around the centrosome in the cytoplasm-poor lymphocyte is to image centrosomal F-actin in T cell-APC conjugates at a super-resolution level to confirm that the changes observed in the centrosomal F-actin meshwork are restricted to the centrosome without any involvement of membrane-bound organelles, such as the pericentrosomal endosomal compartment, which is also a site of active actin dynamics. Additionally, super-resolution live-cell imaging is expected to elucidate the interplay of centrosomal F-actin and microtubules during their coordinated reorganization. These considerations suggest novel, exciting directions to be explored in order to better characterize the role of F-actin in centrosome polarization and to identify new regulators of cell polarity during IS formation. Our implication of a BBSome component in IS assembly in the non-ciliated T cell, which further supports the homology of this structure with the primary cilium (83, 84) opens the possibility that other BBS proteins or ciliogenesis proteins functionally related to the BBSome may participate in these processes.

AUTHOR CONTRIBUTIONS

CC and CB wrote the manuscript and conceptualized the figures. CC prepared the figures. All authors substantially, directly, and intellectually contributed to the article and approved the submitted version.

FUNDING

The work discussed in this review was carried out with the support of AIRC (IG 2017- ID 20148), Ministero dell'Istruzione, dell'Università e della Ricerca (Grant PRIN bando 2017 – 2017FS5SHL), and ERC Synergy Grant 951329 to CB.

ACKNOWLEDGMENTS

The authors wish to thank members of Baldari, Dustin and Stepanek labs for productive discussions.

REFERENCES

1. Harwood NE, Batista FD. Early Events in B Cell Activation. *Annu Rev Immunol* (2010) 28:185–210. doi: 10.1146/annurev-immunol-030409-101216
2. Dustin ML, Chakraborty AK, Shaw AS. Understanding the Structure and Function of the Immunological Synapse. *Cold Spring Harb Perspect Biol* (2010) 2:a002311. doi: 10.1101/cshperspect.a002311
3. Monks CR, Freiberg BA, Kupfer H, Sciaky N, Kupfer A. Three-Dimensional Segregation of Supramolecular Activation Clusters in T Cells. *Nature* (1998) 395:82–6. doi: 10.1038/25764
4. Freiberg BA, Kupfer H, Maslanik W, Delli J, Kappler J, Zaller DM, et al. Staging and Resetting T Cell Activation in SMACs. *Nat Immunol* (2002) 3:911–7. doi: 10.1038/ni836
5. Stinchcombe JC, Bossi G, Booth S, Griffiths GM. The Immunological Synapse of CTL Contains a Secretory Domain and Membrane Bridges. *Immunity* (2001) 15:751–61. doi: 10.1016/s1074-7613(01)00234-5
6. Gomez TS, Billadeau DD. T Cell Activation and the Cytoskeleton: You Can't Have One Without the Other. *Adv Immunol* (2008) 97:1–64. doi: 10.1016/S0065-2776(08)00001-1
7. Huse M, Le Floc'h A, Liu X. From Lipid Second Messengers to Molecular Motors: Microtubule-Organizing Center Reorientation in T Cells. *Immunol Rev* (2013) 256:95–106. doi: 10.1111/imr.12116
8. Locard-Paulet M, Voisinne G, Froment C, Goncalves Menoita M, Ounoughene Y, Girard L, et al. LymphoAtlas: A Dynamic and Integrated Phosphoproteomic Resource of TCR Signaling in Primary T Cells Reveals ITSN2 as a Regulator of Effector Functions. *Mol Syst Biol* (2020) 16:e9524. doi: 10.15252/msb.20209524
9. Stinchcombe JC, Majorovits E, Bossi G, Fuller S, Griffiths GM. Centrosome Polarization Delivers Secretory Granules to the Immunological Synapse. *Nature* (2006) 443:462–5. doi: 10.1038/nature05071
10. Geiger B, Rosen D, Berke G. Spatial Relationships of Microtubule-Organizing Centers and the Contact Area of Cytotoxic T Lymphocytes and Target Cells. *J Cell Biol* (1982) 95:137–43. doi: 10.1083/jcb.95.1.137
11. Kupfer A, Swain SL, Singer SJ. The Specific Direct Interaction of Helper T Cells and Antigen-Presenting B Cells. II. Reorientation of the Microtubule Organizing Center and Reorganization of the Membrane-Associated Cytoskeleton Inside the Bound Helper T Cells. *J Exp Med* (1987) 165:1565–80. doi: 10.1084/jem.165.6.1565
12. Varma R, Campi G, Yokosuka T, Saito T, Dustin ML. T Cell Receptor-Proximal Signals Are Sustained in Peripheral Microclusters and Terminated in the Central Supramolecular Activation Cluster. *Immunity* (2006) 25:117–27. doi: 10.1016/j.immuni.2006.04.010
13. Quintana A, Schwindling C, Wenning AS, Becherer U, Rettig J, Schwarz EC, et al. T Cell Activation Requires Mitochondrial Translocation to the Immunological Synapse. *Proc Natl Acad Sci USA* (2007) 104:14418–23. doi: 10.1073/pnas.0703126104
14. Bustos-Morán E, Blas-Rus N, Martín-Cófreces NB, Sánchez-Madrid F. Orchestrating Lymphocyte Polarity in Cognate Immune Cell-Cell Interactions. *Int Rev Cell Mol Biol* (2016) 327:195–261. doi: 10.1016/bs.ircmb.2016.06.004
15. Soares H, Lasserre R, Alcover A. Orchestrating Cytoskeleton and Intracellular Vesicle Traffic to Build Functional Immunological Synapses. *Immunol Rev* (2013) 256:118–32. doi: 10.1111/imr.12110
16. Finetti F, Cassioli C, Baldari CT. Transcellular Communication at the Immunological Synapse: A Vesicular Traffic-Mediated Mutual Exchange. *F1000Research* (2017) 6:1880. doi: 10.12688/f1000research.11944.1
17. Onnis A, Baldari CT. Orchestration of Immunological Synapse Assembly by Vesicular Trafficking. *Front Cell Dev Biol* (2019) 7:110. doi: 10.3389/fcell.2019.00110
18. Vardhana S, Choudhuri K, Varma R, Dustin ML. Essential Role of Ubiquitin and TSG101 Protein in Formation and Function of the Central

Supramolecular Activation Cluster. *Immunity* (2010) 32:531–40. doi: 10.1016/j.immuni.2010.04.005
19. Alcover A, Alarcón B, Di Bartolo V. Cell Biology of T Cell Receptor Expression and Regulation. *Annu Rev Immunol* (2018) 36:103–25. doi: 10.1146/annurev-immunol-042617-053429
20. Choudhuri K, Llodrá J, Roth EW, Tsai J, Gordo S, Wucherpfennig KW, et al. Polarized Release of T-Cell-Receptor-Enriched Microvesicles at the Immunological Synapse. *Nature* (2014) 507:118–23. doi: 10.1038/nature12951
21. Quintana A, Kummerow C, Junker C, Becherer U, Hoth M. Morphological Changes of T Cells Following Formation of the Immunological Synapse Modulate Intracellular Calcium Signals. *Cell Calcium* (2009) 45:109–22. doi: 10.1016/j.ceca.2008.07.003
22. Baixauli F, Martín-Cófreces NB, Morlino G, Carrasco YR, Calabia-Linares C, Veiga E, et al. The Mitochondrial Fission Factor Dynamin-Related Protein 1 Modulates T-Cell Receptor Signalling at the Immune Synapse. *EMBO J* (2011) 30:1238–50. doi: 10.1038/emboj.2011.25
23. Cassioli C, Onnis A, Finetti F, Capitani N, Brunetti J, Compeer EB, et al. The Bardet-Biedl Syndrome Complex Component BBS1 Controls T Cell Polarity During Immune Synapse Assembly. *J Cell Sci* (2021) 134(16):jcs258462. doi: 10.1242/jcs.258462
24. Blumenthal D, Burkhardt JK. Multiple Actin Networks Coordinate Mechanotransduction at the Immunological Synapse. *J Cell Biol* (2020) 219 (2):e201911058. doi: 10.1083/jcb.201911058
25. Wang JC, Hammer JA. The Role of Actin and Myosin in Antigen Extraction by B Lymphocytes. *Semin Cell Dev Biol* (2020) 102:90–104. doi: 10.1016/j.semcdb.2019.10.017
26. Kim H-R, Jun C-D. T Cell Microvilli: Sensors or Senders? *Front Immunol* (2019) 10:1753. doi: 10.3389/fimmu.2019.01753
27. Jung Y, Riven I, Feigelson SW, Kartvelishvily E, Tohya K, Miyasaka M, et al. Three-Dimensional Localization of T-Cell Receptors in Relation to Microvilli Using a Combination of Superresolution Microscopies. *Proc Natl Acad Sci USA* (2016) 113:E5916–24. doi: 10.1073/pnas.1605399113
28. Cai E, Marchuk K, Beemiller P, Beppler C, Rubashkin MG, Weaver VM, et al. Visualizing Dynamic Microvillar Search and Stabilization During Ligand Detection by T Cells. *Science* (2017) 356(6338):eaal3118. doi: 10.1126/science.aal3118
29. Kim H-R, Mun Y, Lee K-S, Park Y-J, Park J-S, Park J-H, et al. T Cell Microvilli Constitute Immunological Synaptosomes That Carry Messages to Antigen-Presenting Cells. *Nat Commun* (2018) 9:3630. doi: 10.1038/s41467-018-06090-8
30. Sedwick CE, Morgan MM, Jusino L, Cannon JL, Miller J, Burkhardt JK. TCR, LFA-1, and CD28 Play Unique and Complementary Roles in Signaling T Cell Cytoskeletal Reorganization. *J Immunol Baltim Md 1950* (1999) 162:1367–75.
31. Spitaler M, Emslie E, Wood CD, Cantrell D. Diacylglycerol and Protein Kinase D Localization During T Lymphocyte Activation. *Immunity* (2006) 24:535–46. doi: 10.1016/j.immuni.2006.02.013
32. Quann EJ, Merino E, Furuta T, Huse M. Localized Diacylglycerol Drives the Polarization of the Microtubule-Organizing Center in T Cells. *Nat Immunol* (2009) 10:627–35. doi: 10.1038/ni.1734
33. Le Floc'h A, Huse M. Molecular Mechanisms and Functional Implications of Polarized Actin Remodeling at the T Cell Immunological Synapse. *Cell Mol Life Sci CMLS* (2015) 72:537–56. doi: 10.1007/s00018-014-1760-7
34. Comrie WA, Burkhardt JK. Action and Traction: Cytoskeletal Control of Receptor Triggering at the Immunological Synapse. *Front Immunol* (2016) 7:68. doi: 10.3389/fimmu.2016.00068
35. Gomez TS, Kumar K, Medeiros RB, Shimizu Y, Leibson PJ, Billadeau DD. Formins Regulate the Actin-Related Protein 2/3 Complex-Independent Polarization of the Centrosome to the Immunological Synapse. *Immunity* (2007) 26:177–90. doi: 10.1016/j.immuni.2007.01.008
36. Banerjee PP, Pandey R, Zheng R, Suhoski MM, Monaco-Shawver L, Orange JS. Cdc42-Interacting Protein-4 Functionally Links Actin and Microtubule Networks at the Cytolytic NK Cell Immunological Synapse. *J Exp Med* (2007) 204:2305–20. doi: 10.1084/jem.20061893
37. Lasserre R, Alcover A. Cytoskeletal Cross-Talk in the Control of T Cell Antigen Receptor Signaling. *FEBS Lett* (2010) 584:4845–50. doi: 10.1016/j.febslet.2010.09.001
38. Piotrowski JT, Gomez TS, Schoon RA, Mangalam AK, Billadeau DD. WASH Knockout T Cells Demonstrate Defective Receptor Trafficking, Proliferation, and Effector Function. *Mol Cell Biol* (2013) 33:958–73. doi: 10.1128/MCB.01288-12
39. Chemin K, Bohineust A, Dogniaux S, Tourret M, Guégan S, Miro F, et al. Cytokine Secretion by CD4+ T Cells at the Immunological Synapse Requires Cdc42-Dependent Local Actin Remodeling But Not Microtubule Organizing Center Polarity. *J Immunol Baltim Md 1950* (2012) 189:2159–68. doi: 10.4049/jimmunol.1200156
40. Ritter AT, Asano Y, Stinchcombe JC, Dieckmann NMG, Chen B-C, Gawden-Bone C, et al. Actin Depletion Initiates Events Leading to Granule Secretion at the Immunological Synapse. *Immunity* (2015) 42:864–76. doi: 10.1016/j.immuni.2015.04.013
41. Ritter AT, Kapnick SM, Murugesan S, Schwartzberg PL, Griffiths GM, Lippincott-Schwartz J. Cortical Actin Recovery at the Immunological Synapse Leads to Termination of Lytic Granule Secretion in Cytotoxic T Lymphocytes. *Proc Natl Acad Sci USA* (2017) 114:E6585–94. doi: 10.1073/pnas.1710751114
42. Rak GD, Mace EM, Banerjee PP, Svitkina T, Orange JS. Natural Killer Cell Lytic Granule Secretion Occurs Through a Pervasive Actin Network at the Immune Synapse. *PloS Biol* (2011) 9:e1001151. doi: 10.1371/journal.pbio.1001151
43. Brown ACN, Oddos S, Dobbie IM, Alakoskela J-M, Parton RM, Eissmann P, et al. Remodelling of Cortical Actin Where Lytic Granules Dock at Natural Killer Cell Immune Synapses Revealed by Super-Resolution Microscopy. *PloS Biol* (2011) 9:e1001152. doi: 10.1371/journal.pbio.1001152
44. Carisey AF, Mace EM, Saeed MB, Davis DM, Orange JS. Nanoscale Dynamism of Actin Enables Secretory Function in Cytolytic Cells. *Curr Biol CB* (2018) 28:489–502.e9. doi: 10.1016/j.cub.2017.12.044
45. Hammer JA. Immunology: Is Actin at the Lytic Synapse a Friend or a Foe? *Curr Biol CB* (2018) 28:R155–7. doi: 10.1016/j.cub.2018.01.013
46. Bornens M, Moudjou M. Studying the Composition and Function of Centrosomes in Vertebrates. *Methods Cell Biol* (1999) 61:13–34. doi: 10.1016/s0091-679x(08)61973-1
47. Andersen JS, Wilkinson CJ, Mayor T, Mortensen P, Nigg EA, Mann M. Proteomic Characterization of the Human Centrosome by Protein Correlation Profiling. *Nature* (2003) 426:570–4. doi: 10.1038/nature02166
48. Jakobsen L, Vanselow K, Skogs M, Toyoda Y, Lundberg E, Poser I, et al. Novel Asymmetrically Localizing Components of Human Centrosomes Identified by Complementary Proteomics Methods. *EMBO J* (2011) 30:1520–35. doi: 10.1038/emboj.2011.63
49. Firat-Karalar EN, Sante J, Elliott S, Stearns T. Proteomic Analysis of Mammalian Sperm Cells Identifies New Components of the Centrosome. *J Cell Sci* (2014) 127:4128–33. doi: 10.1242/jcs.157008
50. Farina F, Gaillard J, Guérin C, Couté Y, Sillibourne J, Blanchoin L, et al. The Centrosome Is an Actin-Organizing Centre. *Nat Cell Biol* (2016) 18:65–75. doi: 10.1038/ncb3285
51. Obino D, Farina F, Malbec O, Sáez PJ, Maurin M, Gaillard J, et al. Actin Nucleation at the Centrosome Controls Lymphocyte Polarity. *Nat Commun* (2016) 7:10969. doi: 10.1038/ncomms10969
52. Luxton GWG, Gomes ER, Folker ES, Vintinner E, Gundersen GG. Linear Arrays of Nuclear Envelope Proteins Harness Retrograde Actin Flow for Nuclear Movement. *Science* (2010) 329:956–9. doi: 10.1126/science.1189072
53. Kim D-H, Cho S, Wirtz D. Tight Coupling Between Nucleus and Cell Migration Through the Perinuclear Actin Cap. *J Cell Sci* (2014) 127:2528–41. doi: 10.1242/jcs.144345
54. Kutscheidt S, Zhu R, Antoku S, Luxton GWG, Stagljar I, Fackler OT, et al. FHOD1 Interaction With Nesprin-2G Mediates TAN Line Formation and Nuclear Movement. *Nat Cell Biol* (2014) 16:708–15. doi: 10.1038/ncb2981
55. Kwon M, Bagonis M, Danuser G, Pellman D. Direct Microtubule-Binding by Myosin-10 Orients Centrosomes Toward Retraction Fibers and Subcortical Actin Clouds. *Dev Cell* (2015) 34:323–37. doi: 10.1016/j.devcel.2015.06.013
56. Inoue D, Obino D, Pineau J, Farina F, Gaillard J, Guerin C, et al. Actin Filaments Regulate Microtubule Growth at the Centrosome. *EMBO J* (2019) 38(11):e99630. doi: 10.15252/embj.201899630
57. Bello-Gamboa A, Velasco M, Moreno S, Herranz G, Ilie R, Huetos S, et al. Actin Reorganization at the Centrosomal Area and the Immune Synapse Regulates Polarized Secretory Traffic of Multivesicular Bodies in T Lymphocytes. *J Extracell Vesicles* (2020) 9:1759926. doi: 10.1080/20013078.2020.1759926

58. Ibañez-Vega J, Del Valle Batalla F, Saez JJ, Soza A, Yuseff M-I. Proteasome Dependent Actin Remodeling Facilitates Antigen Extraction at the Immune Synapse of B Cells. *Front Immunol* (2019) 10:225. doi: 10.3389/fimmu.2019.00225
59. Ibañez-Vega J, Del Valle F, Sáez JJ, Guzman F, Diaz J, Soza A, et al. Ecm29-Dependent Proteasome Localization Regulates Cytoskeleton Remodeling at the Immune Synapse. *Front Cell Dev Biol* (2021) 9:650817. doi: 10.3389/fcell.2021.650817
60. Schaller MD. Paxillin: A Focal Adhesion-Associated Adaptor Protein. *Oncogene* (2001) 20:6459–72. doi: 10.1038/sj.onc.1204786
61. López-Colomé AM, Lee-Rivera I, Benavides-Hidalgo R, López E. Paxillin: A Crossroad in Pathological Cell Migration. *J Hematol OncolJ Hematol Oncol* (2017) 10:50. doi: 10.1186/s13045-017-0418-y
62. Herreros L, Rodríguez-Fernandez JL, Brown MC, Alonso-Lebrero JL, Cabañas C, Sánchez-Madrid F, et al. Paxillin Localizes to the Lymphocyte Microtubule Organizing Center and Associates With the Microtubule Cytoskeleton. *J Biol Chem* (2000) 275:26436–40. doi: 10.1074/jbc.M003970200
63. Robertson LK, Ostergaard HL. Paxillin Associates With the Microtubule Cytoskeleton and the Immunological Synapse of CTL Through Its Leucine-Aspartic Acid Domains and Contributes to Microtubule Organizing Center Reorientation. *J Immunol Baltim Md 1950* (2011) 187:5824–33. doi: 10.4049/jimmunol.1003690
64. Murugesan S, Hong J, Yi J, Li D, Beach JR, Shao L, et al. Formin-Generated Actomyosin Arcs Propel T Cell Receptor Microcluster Movement at the Immune Synapse. *J Cell Biol* (2016) 215:383–99. doi: 10.1083/jcb.201603080
65. Ramalingam N, Zhao H, Breitsprecher D, Lappalainen P, Faix J, Schleicher M. Phospholipids Regulate Localization and Activity of Mdia1 Formin. *Eur J Cell Biol* (2010) 89:723–32. doi: 10.1016/j.ejcb.2010.06.001
66. Baumeister W, Walz J, Zühl F, Seemüller E. The Proteasome: Paradigm of a Self-Compartmentalizing Protease. *Cell* (1998) 92:367–80. doi: 10.1016/s0092-8674(00)80929-0
67. Vora SM, Phillips BT. The Benefits of Local Depletion: The Centrosome as a Scaffold for Ubiquitin-Proteasome-Mediated Degradation. *Cell Cycle Georget Tex* (2016) 15:2124–34. doi: 10.1080/15384101.2016.1196306
68. Yan D, Guo L, Wang Y. Requirement of Dendritic Akt Degradation by the Ubiquitin-Proteasome System for Neuronal Polarity. *J Cell Biol* (2006) 174:415–24. doi: 10.1083/jcb.200511028
69. Hsu M-T, Guo C-L, Liou AY, Chang T-Y, Ng M-C, Florea BI, et al. Stage-Dependent Axon Transport of Proteasomes Contributes to Axon Development. *Dev Cell* (2015) 35:418–31. doi: 10.1016/j.devcel.2015.10.018
70. Spektor A, Tsang WY, Khoo D, Dynlacht BD. Cep97 and CP110 Suppress a Cilia Assembly Program. *Cell* (2007) 130:678–90. doi: 10.1016/j.cell.2007.06.027
71. Tuz K, Bachmann-Gagescu R, O'Day DR, Hua K, Isabella CR, Phelps IG, et al. Mutations in CSPP1 Cause Primary Cilia Abnormalities and Joubert Syndrome With or Without Jeune Asphyxiating Thoracic Dystrophy. *Am J Hum Genet* (2014) 94:62–72. doi: 10.1016/j.ajhg.2013.11.019
72. Kasahara K, Kawakami Y, Kiyono T, Yonemura S, Kawamura Y, Era S, et al. Ubiquitin-Proteasome System Controls Ciliogenesis at the Initial Step of Axoneme Extension. *Nat Commun* (2014) 5:5081. doi: 10.1038/ncomms6081
73. Liu YP, Tsai I-C, Morleo M, Oh EC, Leitch CC, Massa F, et al. Ciliopathy Proteins Regulate Paracrine Signaling by Modulating Proteasomal Degradation of Mediators. *J Clin Invest* (2014) 124:2059–70. doi: 10.1172/JCI71898
74. Gerhardt C, Leu T, Lier JM, Rüther U. The Cilia-Regulated Proteasome and its Role in the Development of Ciliopathies and Cancer. *Cilia* (2016) 5:14. doi: 10.1186/s13630-016-0035-3
75. Chang JT, Ciocca ML, Kinjyo I, Palanivel VR, McClurkin CE, Dejong CS, et al. Asymmetric Proteasome Segregation as a Mechanism for Unequal Partitioning of the Transcription Factor T-Bet During T Lymphocyte Division. *Immunity* (2011) 34:492–504. doi: 10.1016/j.immuni.2011.03.017
76. Widjaja CE, Olvera JG, Metz PJ, Phan AT, Savas JN, de Bruin G, et al. Proteasome Activity Regulates CD8+ T Lymphocyte Metabolism and Fate Specification. *J Clin Invest* (2017) 127:3609–23. doi: 10.1172/JCI90895
77. Martin-Cofreces NB, Chichon FJ, Calvo E, Torralba D, Bustos-Moran E, Dosil SG, et al. The Chaperonin CCT Controls T Cell Receptor-Driven 3D Configuration of Centrioles. *Sci Adv* (2020) 6(49):eabb7242. doi: 10.1126/sciadv.abb7242
78. Fokin AI, Gautreau AM. Assembly and Activity of the WASH Molecular Machine: Distinctive Features at the Crossroads of the Actin and Microtubule Cytoskeletons. *Front Cell Dev Biol* (2021) 9:658865. doi: 10.3389/fcell.2021.658865
79. Hao Y-H, Doyle JM, Ramanathan S, Gomez TS, Jia D, Xu M, et al. Regulation of WASH-Dependent Actin Polymerization and Protein Trafficking by Ubiquitination. *Cell* (2013) 152:1051–64. doi: 10.1016/j.cell.2013.01.051
80. Didier C, Merdes A, Gairin J-E, Jabrane-Ferrat N. Inhibition of Proteasome Activity Impairs Centrosome-Dependent Microtubule Nucleation and Organization. *Mol Biol Cell* (2008) 19:1220–9. doi: 10.1091/mbc.e06-12-1140
81. Nachury MV. The Molecular Machines That Traffic Signaling Receptors Into and Out of Cilia. *Curr Opin Cell Biol* (2018) 51:124–31. doi: 10.1016/j.ceb.2018.03.004
82. Nakayama K, Katoh Y. Ciliary Protein Trafficking Mediated by IFT and BBSome Complexes With the Aid of Kinesin-2 and Dynein-2 Motors. *J Biochem (Tokyo)* (2018) 163:155–64. doi: 10.1093/jb/mvx087
83. Cassioli C. Baldari CT. A Ciliary View of the Immunological Synapse. *Cells* (2019) 8(8):789. doi: 10.3390/cells8080789
84. Douanne T, Stinchcombe JC, Griffiths GM. Teasing Out Function From Morphology: Similarities Between Primary Cilia and Immune Synapses. *J Cell Biol* (2021) 220(6):e202102089. doi: 10.1083/jcb.202102089
85. Hernandez-Hernandez V, Pravincumar P, Diaz-Font A, May-Simera H, Jenkins D, Knight M, et al. Bardet-Biedl Syndrome Proteins Control the Cilia Length Through Regulation of Actin Polymerization. *Hum Mol Genet* (2013) 22:3858–68. doi: 10.1093/hmg/ddt241
86. Maskalenko N, Nath S, Ramakrishnan A, Anikeeva N, Sykulev Y, Poenie M. The DISC1-Girdin Complex - A Missing Link in Signaling to the T Cell Cytoskeleton. *J Cell Sci* (2020) 133(13):jcs242875. doi: 10.1242/jcs.242875
87. Yi J, Wu X, Chung AH, Chen JK, Kapoor TM, Hammer JA. Centrosome Repositioning in T Cells Is Biphasic and Driven by Microtubule End-on Capture-Shrinkage. *J Cell Biol* (2013) 202:779–92. doi: 10.1083/jcb.201301004
88. Combs J, Kim SJ, Tan S, Ligon LA, Holzbaur ELF, Kuhn J, et al. Recruitment of Dynein to the Jurkat Immunological Synapse. *Proc Natl Acad Sci USA* (2006) 103:14883–8. doi: 10.1073/pnas.0600914103
89. Martín-Cófreces NB, Robles-Valero J, Cabrero JR, Mittelbrunn M, Gordón-Alonso M, Sung C-H, et al. MTOC Translocation Modulates IS Formation and Controls Sustained T Cell Signaling. *J Cell Biol* (2008) 182:951–62. doi: 10.1083/jcb.200801014
90. Hooikaas PJ, Damstra HG, Gros OJ, van Riel WE, Martin M, Smits YT, et al. Kinesin-4 KIF21B Limits Microtubule Growth to Allow Rapid Centrosome Polarization in T Cells. *eLife* (2020) 9:e62876. doi: 10.7554/eLife.62876
91. Nejmeddine M, Negi VS, Mukherjee S, Tanaka Y, Orth K, Taylor GP, et al. HTLV-1-Tax and ICAM-1 Act on T-Cell Signal Pathways to Polarize the Microtubule-Organizing Center at the Virological Synapse. *Blood* (2009) 114:1016–25. doi: 10.1182/blood-2008-03-136770
92. Tsun A, Qureshi I, Stinchcombe JC, Jenkins MR, de la Roche M, Kleczkowska J, et al. Centrosome Docking at the Immunological Synapse is Controlled by Lck Signaling. *J Cell Biol* (2011) 192:663–74. doi: 10.1083/jcb.201008140

Conflict of Interest: The authors declare that the research was conducted in the absence of any commercial or financial relationships that could be construed as a potential conflict of interest.

frontiers in Immunology

MINI REVIEW
published: 25 February 2022
doi: 10.3389/fimmu.2022.845064

RhoG's Role in T Cell Activation and Function

Ana Masara Ahmad Mokhtar[1], Nor Hawani Salikin[1], Aminah Suhaila Haron[2], Syafinaz Amin-Nordin[3], Ilie Fadzilah Hashim[4], Muaz Mohd Zaini Makhtar[1,5], Siti Balqis Zulfigar[1] and Nurul Izza Ismail[6]*

[1] Bioprocess Technology Division, School of Industrial Technology, Universiti Sains Malaysia, Gelugor, Malaysia, [2] Faculty of Dentistry, AIMST University, Bedong, Malaysia, [3] Department of Medical Microbiology, Faculty of Medicine and Health Sciences, Universiti Putra Malaysia, Serdang, Malaysia, [4] Department of Clinical Medicine, Advanced Medical and Dental Institute, Universiti Sains Malaysia, Kepala Batas, Malaysia, [5] Fellow of Center for Global Sustainability Studies, Universiti Sains Malaysia, Gelugor, Malaysia, [6] School of Biological Sciences, Universiti Sains Malaysia, Gelugor, Malaysia

The role of RhoG in T cell development is redundant with other Racs subfamily members, and this redundancy may be attributed to redundant signal transduction pathways. However, the absence of RhoG increases TCR signalling and proliferation, implying that RhoG activity is critical during late T cell activation following antigen–receptor interaction. Moreover, RhoG is required to halt signal transduction and prevent hyper-activated T cells. Despite increase in TCR signalling, cell proliferation is inhibited, implying that RhoG induces T cell anergy by promoting the activities of transcription factors, including nuclear factor of activated T cell (NFAT)/AP-1. The role of NFAT plays in T cell anergy is inducing the transcription of anergy-associated genes, such as IL-2, IL-5, and IFN-γ. Although information about RhoG in T cell-related diseases is limited, mutant forms of RhoG, Ala151Ser and Glu171Lys have been observed in thymoma and hemophagocytic lymphohistiocytosis (HLH), respectively. Current information only focuses on these two diseases, and thus the role of RhoG in normal and pathological circumstances should be further investigated. This approach is necessary because RhoG and its associated proteins represent prospective targets for attack particularly in the therapy of cancer and immune-mediated illnesses.

Keywords: Small Rho GTPase, RhoG, T cell, cancer, hemophagocytic lymphohistiocytosis

OPEN ACCESS

Edited by:
Jerome Delon, U1016 Institut Cochin (INSERM), France

Reviewed by:
Fukun Guo, Cincinnati Children's Hospital Medical Center, United States
Henrik Hasseldam, University of Copenhagen, Denmark

****Correspondence:***
Ana Masara Ahmad Mokhtar
anamasara@usm.my

Specialty section:
This article was submitted to T Cell Biology, a section of the journal Frontiers in Immunology

Received: *29 December 2021*
Accepted: *08 February 2022*
Published: *25 February 2022*

Citation:
Ahmad Mokhtar AM, Salikin NH, Haron AS, Amin-Nordin S, Hashim IF, Mohd Zaini Makhtar M, Zulfigar SB and Ismail NI (2022) RhoG's Role in T Cell Activation and Function. Front. Immunol. 13:845064. doi: 10.3389/fimmu.2022.845064

1 INTRODUCTION

RhoG belongs to the Rho family of small GTPases, specifically the Rac subfamily. The Rho family is involved in actin–cytoskeletal rearrangements, intracellular membrane trafficking, cell cycle progression, and transcriptional activation (1, 2). According to their sequence similarity and biological roles, the Rho family can be divided into the Rho-, Rac-, Cdc42-, RhoU/RhoV-, Rnd-, RhoD/RhoF-, RhoBTB-, and RhoH subfamilies (3). Classical or typical small Rho GTPases are from the Rho-, Rac-, and Cdc42 subfamilies. The other small Rho GTPases are called non-classical or atypical small Rho GTPases because they cannot hydrolyze GTP in contrast to typical small Rho GTPases (4, 5).

Three Rac1, Rac2, Rac3 share 89% sequence similarity, except the C-terminal region (3, 6), whereas RhoG shares only 70%–72% sequence similarity with the other three Racs and may thus act differently within the subfamily. Typically, Rac-subfamily proteins stimulate the formation of membrane ruffles and lamellipodia by interacting with a panel of effector proteins, such as Wiskott–Aldrich syndrome protein (WASP) and p21-activated kinases (PAK) (7, 8). These interactions activate the Arp2/3 complex and subsequently induce actin polymerization (9–12).

The "on" and "off" states of RhoG are constrained to two flexible loop regions: switch 1 and switch 2, which acquire conformations in the GTP-bound state that enable downstream effector proteins to recognize and interact with small Rho GTPases (13). Additionally, the intrinsic GDP/GTP switching of RhoG is slow and requires three distinct types of regulatory proteins to function, namely, guanine nucleotide exchange factors (GEFs), GTPase-activating proteins (GAPs), and guanine nucleotide dissociation inhibitors (GDIs). GEFs enhance GDP dissociation and the binding of the more abundant GTP in the cytoplasm, allowing RhoG to become active and bind to its specific effectors and hence activating signalling pathways (14). By contrast, GAPs are responsible for terminating RhoG signalling by increasing the intrinsic GTPase activity of RhoG, thereby inducing GTP to GDP hydrolysis (15). Finally, GDIs are bifunctional negative regulators required to keep RhoG GDP-bound and physically sequester it from membranes by interacting with its geranyl–geranyl group (16).

2 FUNCTIONS OF RHOG IN T CELL HOMEOSTASIS

2.1 Role of RhoG in the Growth and Maturation of Thymocytes

The thymus is the site of T cell growth and maturation, which is critical to the sustenance of the peripheral immune system. The abnormal activities of small Rho GTPases, including RhoA (17), Rac1, Rac2 (18, 19), Cdc42 (20), and RhoH (3) are linked to thymocyte defects *in vitro* and *in vivo*. These deficiencies can be caused by defective RhoGEFs, such as Vav1, or missense mutations occurring within small Rho GTPases. For instance, loss of Vav1 in mice inhibits T cell positive and negative selection, and this process is affected by the activation status of its interacting proteins (21). Additionally, point mutations within the GEF interaction region of Rac2, such as Asp57Asn and Pro24His mutations, impair T cell development (22, 23). This finding supports the notion that proper small Rho GTPase activation is required for T cell development and maturation.

Either Rac1 or Rac2 deletion has no effect on thymocyte development, but simultaneous Rac1 and Rac2 deletions have a significant impact (18). Meanwhile, lack of RhoG has no effect on T cell formation, but it marginally increases T cell proliferation during antigen–receptor cross-linking. This finding suggests that the involvement of RhoG in T cell development is redundant compared with that of other Rac subfamily members (18), and this redundancy may be attributed to redundant signal transduction pathways (24). Both Racs and RhoG induce membrane ruffling despite their different subcellular localizations, indicating that they regulate similar signalling cascades. Nonetheless, enhanced T cell proliferation implies that RhoG has a negative impact on immune responses and its activity is crucial to the later phases of T cell activation upon antigen–receptor contact (25).

2.2 RhoG in Peripheral T Cell Activation

2.2.1 RhoG's Function in Proximal TCR Signalling

RhoG is involved in TCR internalization from the immunological synapse (IS) and is necessary to major histocompatibility complex (MHC) uptake in antigen-presenting cells (APCs). IS is a structured interface between a T cell and an APC, and TCR internalization at IS is required for successful T cell activation and long-term TCR engagement and signalling. However, the significance of IS in TCR activation regulation is controversial because TCR can be triggered prior to or in the absence of IS formation (26). Martínez-Martín et al. (2011) discovered that TCR endocytosis and signal extinction can occur at IS, indicating that not only IS is required to enhance TCR signalling in response to a small amount of peptide antigen-major histocompatibility complex (pMHC) ligand but also suppresses signalling by downregulating TCR in response to a high concentration of pMHC (27). The reason is that non-engaged TCRs continue to be internalized and recycled to the membrane through dynamin-dependent clathrin-mediated endocytosis (CME) in the absence of pMHC or stimulation. However, when TCRs are coupled with pMHC, their membrane expression is reduced because of enhanced TCR endocytosis, which can be regulated by CME and clathrin-independent endocytosis (28).

Martínez-Martín et al. found that RhoG enables TC21 (Rras2), a small GTPase-related to the R-RAS subfamily, to regulate TCR internalization through clathrin-independent endocytosis (26). This process may require both small G proteins to cycle between an active GTP-bound state and an inactive GDP-bound state because dominant inactive (Thr17Asn) and constitutively active (Gln61Leu) mutants cannot block TCR endocytosis. RhoG involvement in endocytosis is observed not only in T cells but also in macrophage (29) and caveolar endocytosis (30). Notably, RhoG and TC21 are associated with TCR-mediated peptide: MHC trogocytic absorption, which is needed for intercellular communication and immunological control (28). Trogocytosis is the exchange of intact membrane fragments across cells and is critical to T cell and APC activation modulation (31). Interestingly, Boccasavia et al. reported that when an antigen is introduced to naive CD4+ T cells by pMHC-II-dressed CD4+ T cells, the naive CD4+ T cells transform into pathogenic Th17 cells, and the process can be mediated by RhoG trogocytosis (32). This is because the loss of RhoG limits Th17 proinflammatory cell differentiation and promotes resistance to experimental autoimmune encephalitis development (32).

2.2.2 RhoG's Function in Distal TCR Signalling

Interestingly, immunoglobulin (Ig)G1 and IgG2b levels increase in RhoG^{-}deficient mice, indicating an increase in humoral immune response to antigens (24). This finding suggests that RhoG is required for signal transduction to terminate and for the prevention of T- or B cell hyperactivation and control of autoimmunity. However, given that its subfamily member Rac2 regulates Ca^{2+} influx in response to antigen stimulation (33), RhoG may regulate Ca^{2+} influx as well, which is required for T cell-dependent immune responses and rapid cytoskeleton remodelling (34). Nonetheless, only a slight drop in Ca^{2+} influx was observed in RhoG-deficient mice upon TCR stimulation, hinting that RhoG plays a role in Ca^{2+} influx regulation (24). Notably, nuclear factor of activated T cell (NFAT) activation is dependent on Ca^{2+} mobilization, specifically through calcium–calcineurin signalling. In this signalling pathway, Ca^{2+} influx *via* Ca^{2+} release-activated Ca^{2+} (CRAC) channels is required to activate calmodulin (CaM) and the serine/threonine phosphatase calcineurin. Calcineurin then dephosphorylates serine/threonine residues in the regulatory domain of NFAT, exposing nuclear localization signals and thus promoting NFAT nuclear localization. Surprisingly, the elevation of intracellular Ca^{2+} promotes T cell anergy, a state in which a TCR becomes uncoupled from its downstream signalling pathways. This result suggests that RhoG and NFAT play critical roles in T cell tolerance induction (27).

Vigorito et al. discovered that RhoG can enhance NFAT/AP-1-induced interleukin (IL)-2 or interferon-gamma (IFN-γ) transcription (35), and both cytokines are related to T cell anergy (36). Numerous studies have established a link between NFAT signalling and T cell unresponsiveness or reduced responsiveness to subsequent physiological outputs, such as T cell proliferation or differentiation. This T cell unresponsiveness can be induced by inducing the transcription of anergy-associated genes, such as IL-2, IL-5, and IFN-γ or disrupting the interaction between NFAT and AP-1 (36, 37) (**Figure 1**). The latter part is predicted because RhoG contains an NLS motif at Pro179 and Ile182 residues, implying that it might regulates the activities or interactions of transcription factors (35, 38). Apart from regulating NFAT activity, RhoG may also promote T cells in a quiescent state by regulating the activities of other transcription factors, including Stat3, as RhoG promotes the transcriptional activation of Stat3 in murine fibroblasts (38). Increased Stat3 activity limits T cell proliferation by up-regulating Class-O Forkhead transcription factors (FOXO) (39). The role of RhoG in T cell anergy is supported by Martínez-Martín et al., who discovered that T cell proliferation decreases as TCR proximal signalling increases in RhoG-deficient mice (26). However, Vigorito et al. demonstrated that RhoG deficiency enhances T cell proliferation (24). Difference in T cell proliferation rate is unexpected given that TCR signalling increases. Nevertheless, these data show that RhoG is required for successful TCR signalling activation. The contradictory results observed in both studies can be explained by the fact that the doses or affinity of peptide antigens used in each research varies (40).

Additionally, RhoG may impact TCR signalling and the NFAT nuclear translocation in a calcium–calcineurin-independent manner. This process can be induced by Jak3 kinase as NFAT2 nuclear translocation is dependent on Jak3 phosphorylation upon IL-7 activation. The process then leads to the nuclear translocation and activation of NFAT2 (27). Incidentally, JAK3 is necessary for optimal Rac1 activation (41), and given that RhoG and Rac1 are 70% identical (3), Jak3 may influence RhoG activation through Vav1 (42) and affect NFAT nuclear translocation (**Figure 1**). This finding is supported by Martínez-Martín et al., who found that RhoG must be capable of cycling between active and inactive states to regulate TCR internalization and activation (26). However, Puga et al. discovered that caspase 3 cleavage inactivates Vav1 in anergic T cells (43), indicating that the RhoG activation cycle is disrupted and it may exist primarily in an inactive GDP-bound state.

2.3 RhoG's Role in Controlling the Actin–Cytoskeleton and Migration of T Cells

Similar to other small Rho GTPases that are strongly associated with leukocyte transendothelial migration, RhoG is involved in the regulation of T cell migration, which requires a series of coordinated stages, complex modulation of integrin activation by chemokines, and cooperative action of adhesion molecules on endothelial cells and leukocytes (44). However, the involvement of RhoG in the control of actin–cytoskeleton complex is redundant. Nevertheless, it enhances NFAT-induced production of IFN-γ and promotes T cell recruitment to inflammatory sites (35). Additionally, the T cell production of IFN-γ is necessary for neutrophil chemotaxis to damage sites (45). Interestingly, the role of IFN-γ in the control of T cell or lymphocyte migration necessitates the modification of the expression of numerous integrins, including α4 (ITGA4), β7 (ITGβ7), and αvβ3 (35, 46, 47). For instance, upon IFN-γ stimulation, α4 and β7 expression increase, whereas αvβ3 expression decreases, and thus lymphocyte migration is promoted. These results show that RhoG has an indirect role in the control of integrin expression, as evidenced by its capacity to stimulate NFAT.

Upstream involvement of RhoG is necessary to the regulation of the activities of Cdc42 and Rac1, which are required for the production of membrane ruffles and filopodia (48). These characteristics are critical during cell migration and necessitate the participation of filamentous actin (F-actin). Reduced F-actin levels then influence the shapes of cells and the creation of force during cell migration and division. Interestingly, GTP-bound Rac1 regulates F-actin polymerization in lamellipodia (49), which may need the RhoG effector, ELMO, and the ELMO-binding protein Dock180 and Dock4, both of which are Rac1-specific GEFs (50). When RhoG is activated, the Dock-ELMO complex translocates to the plasma membrane, activating Rac1 and resulting in cell migration. This finding indicates that RhoG acts upstream to Rac1 and its activation is required for Rac1 activity, particularly cell motility. Interestingly, the absence of RhoG also inhibits RhoA activation, thereby decreasing the

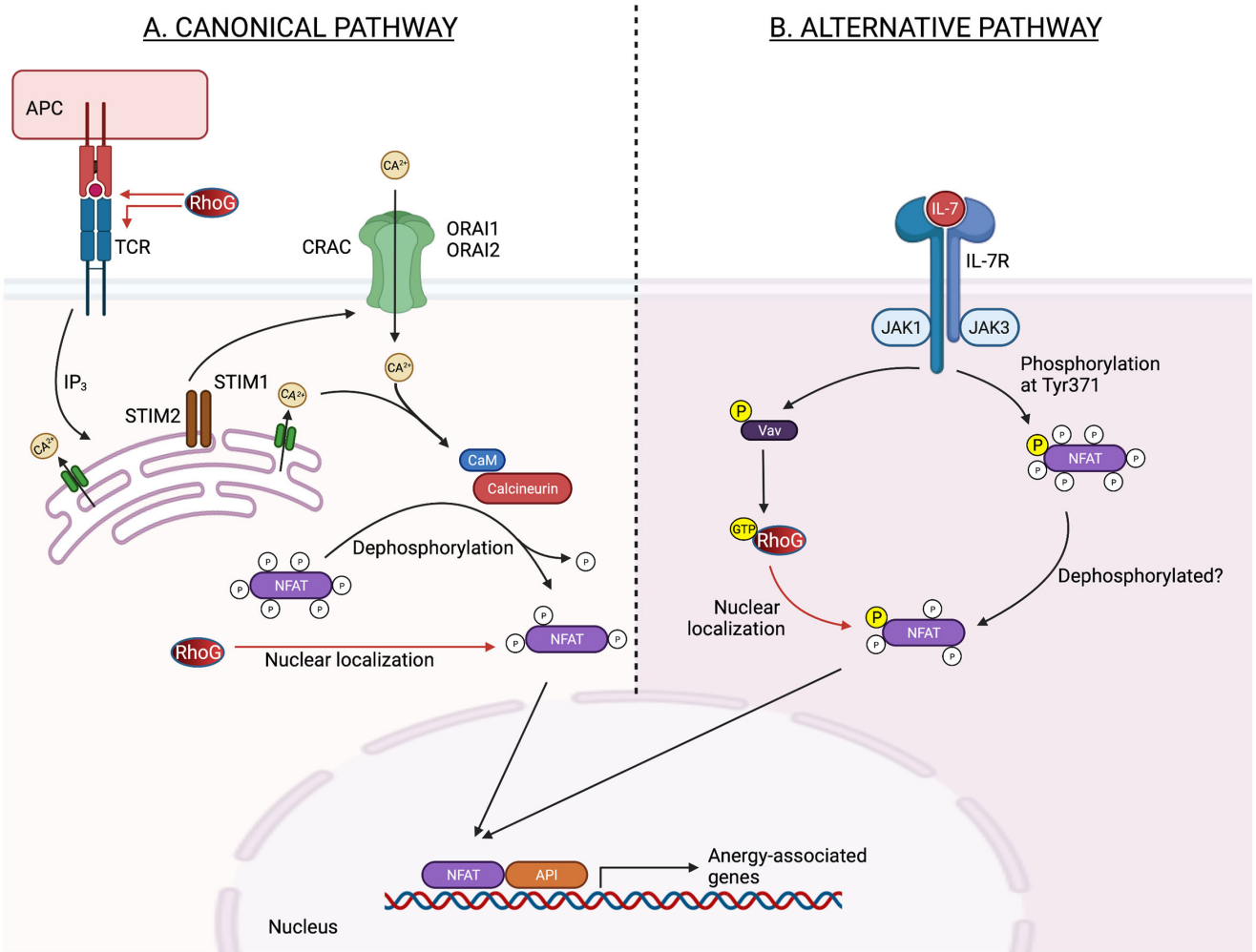

FIGURE 1 | Potential role of RhoG in the regulation of NFAT transcription activity in anergic T cell in canonical and alternative pathways. **(A)** In the classical pathway, antigen receptor stimulation causes the synthesis of inositol-1,4,5-triphosphate (IP_3), which opens IP_3 receptor channels in the ER. The drop in ER Ca^{2+} concentration activates STIM1 and STIM2, which are needed to bind to and open CRAC channels generated by ORAI1 and ORAI2 proteins in the plasma membrane. CaM and the serine/threonine phosphatase calcineurin are then activated by Ca^{2+} inflow *via* CRAC channels. Calcineurin dephosphorylates numerous serine/threonine residues in the regulatory domain of NFAT, causing a conformational shift, nuclear localization signal exposure, and NFAT nuclear import. Increased nuclear localization of NFAT may thereby potentiate the NFAT-induced-anergy-associated gene. **(B)** Meanwhile, in an alternate pathway, Jak3 phosphorylates a single tyrosine residue within the regulatory domain of NFAT, downstream of the IL-7 receptor, causing nuclear translocation and activation of NFAT in thymocytes independent of Ca2+ signals and calcineurin. Jak3 may activate RhoG *via* Vav, causing NFAT to be localized in the nucleus. ER, endoplasmic reticulum; NFAT, nuclear factor of activated T cells; STIM, stromal interaction molecule; CRAC, Ca2+ release-activated Ca 2+; CaM, calmodulin; Jak3, Janus kinase 3; IL-7, interleukin-7. Created with BioRender.com.

overall F-actin level (51). Altogether, these findings suggest the role of RhoG in T cell migration is regulating the activation of other small Rho GTPases.

3 RHOG ACTIVITY IS DYSREGULATED IN T CELL-RELATED DISORDERS

3.1 Thymoma

According to the cBioPortal and TCGA datasets (accessed December 2021), RhoG is frequently altered by amplification, deletion, or mutation, and aberrant RhoG gene expression has been observed in various malignancies, including thymoma. Thymoma is a relatively uncommon tumour of thymic epithelial cells. Various abnormalities have been described in thymomas and affect normal T cell development by distorting tumour architecture and inhibiting MHC class II expression, autoimmune regulator gene expression, and formation of regulatory T cells (52). RhoG has been implicated in thymoma in type AB thymoma (cBioPortal) caused by a RhoG mutation at Ala151Ser.

Interestingly, RhoH Ala151Val mutation produces a loss-of-function effect, implying that a RhoG mutation at the same

location may have the same effect. However, both RhoH and RhoG only share 40% sequence similarities (3), indicating that it may give a different effect. Most of the literature indicates that RhoG plays an active role in cancer progression by promoting cell migration, proliferation, and angiogenesis, and its absence is related to the reduction of cancer characteristics. Nonetheless, given the evidence of RhoG's involvement in thymoma and lack of its function in the regulation of thymocyte development, RhoG Ala151Ser mutation may affect the activities of other small Rho GTPases, such as Rac1 and Cdc42, leading to impaired thymocytes development.

3.2 Hemophagocytic Lymphohistiocytosis

Hemophagocytic lymphohistiocytosis (HLH) is a potentially fatal disease characterized by a generalized inflammatory response caused by abnormal immune activation. The estimated prevalence of HLH cases in different regions worldwide varies from 1 to 10 in 1,000,000 of people. However, the reported data might have been underestimated because of scarce documentation (53–56). In general, HLH can be distinguished into primary (or familial) that is inheritable, whereas secondary HLH (predominantly endured by adult individuals) are mostly triggered by three main factors: infections, autoimmune diseases, and neoplasms (56, 57). Secondary HLH particularly induced by infection is almost similar to sepsis according to abnormal inflammatory syndrome as a consequence of infection and leads to organ dysfunction resulting from a "cytokine storm." Given that HLH syndrome can be nearly identical to sepsis, it may unintentionally lead to the death of individuals who were misdiagnosed with sepsis (58). Mechanistically, this immunological disorder is characterized by systemic inflammation produced by the defective exocytosis of cytotoxic granules (CG), required for lymphocytes to eliminate infected or malignant cells (51).

Recently, a missense mutation, Glu171Lys in RhoG has been found to impair cytotoxic T lymphocyte (CTL) and natural killer (NK) cell exocytosis, resulting in the development of a severe HLH (51). RhoG knockout promotes deleterious effects on human NK and CD8+ T cell exocytosis as manifested by impaired cytoskeletal and cell morphology and abnormal migratory capacity (51). The data hence suggest the critical role of RhoG in CG docking to the membrane of cytotoxic lymphocytes.

4 CONCLUSIONS AND FUTURE PERSPECTIVES

RhoG is a critical component of T cell signalling and may be used or targeted therapeutically in cancer and immune-related diseases. However, existing understanding is insufficient and requires additional comprehensive experimental validation. Besides, inquiry into various illnesses and biological functions is also needed to enhance the knowledge of the therapeutic utility of targeting RhoG signalling axes.

The role of RhoG in thymocyte development is redundant compared with the roles of other members in the subfamily. Nonetheless, RhoG may be crucial to the control of T cell anergy through NFAT transcriptional activity or TCR endocytosis from the IS. Thus, further research into the role of RhoG in the control of T cell anergy may aid the development of therapeutic targets for the rescue of anergic T cells in human diseases, such as cancer, autoimmune disease, and viral infection. However, targeting a signalling node protein required for normal physiology is difficult, justifying the need for substantial research before identifying and designing the most effective attack points for treating RhoG-associated diseases.

AUTHOR CONTRIBUTIONS

All authors listed have made a substantial, direct, and intellectual contribution to the work, and approved it for publication.

FUNDING

The work has been funded by the Universiti Sains Malaysia (Short-term Research Grant) No. 304/PTEKIND/6315523 granted to AMAM.

REFERENCES

1. Ridley AJ, Hall A. The Small GTP-Binding Protein Rho Regulates the Assembly of Focal Adhesions and Actin Stress Fibers in Response to Growth Factors. *Cell* (1992) 70:389–99. doi: 10.1016/0092-8674(92)90163-7
2. Sulciner DJ, Irani K, Yu ZX, Ferrans VJ, Goldschmidt-Clermont P, Finkel T. Rac1 Regulates a Cytokine-Stimulated, Redox-Dependent Pathway Necessary for NF-Kappab Activation. *Mol Cell Biol* (1996) 16:7115 LP – 7121. doi: 10.1128/MCB.16.12.7115
3. Ahmad Mokhtar AM, Hashim IF, Mohd Zaini Makhtar M, Salikin NH, Amin-Nordin S. The Role of Rhoh in TCR Signalling and Its Involvement in Diseases. *Cells* (2021) 10:950. doi: 10.3390/cells10040950
4. Wennerberg K, Der CJ. Rho-Family Gtpases: It's Not Only Rac and Rho (and I Like it). *J Cell Sci* (2004) 117:1301–12. doi: 10.1242/jcs.01118
5. Citalán-Madrid AF, García-Ponce A, Vargas-Robles H, Betanzos A, Schnoor M. Small Gtpases of the Ras Superfamily Regulate Intestinal Epithelial Homeostasis and Barrier Function *via* Common and Unique Mechanisms. *Tissue Barriers* (2013) 1:e26938. doi: 10.4161/tisb.26938
6. Haataja L, Groffen J, Heisterkamp N. Characterization of RAC3, a Novel Member of the Rho Family. *J Biol Chem* (1997) 272:20384–8. doi: 10.1074/jbc.272.33.20384
7. Ridley AJ, Paterson HF, Johnston CL, Diekmann D, Hall A. The Small GTP-Binding Protein rho Regulates the Assembly of Focal Adhesions and Actin Stress Fibers in Response to Growth Factors. *Cell* (1992) 70:401–10. doi: 10.1016/0092-8674(92)90163-7
8. Nobes CD, Hall A. Rho, Rac, and Cdc42 Gtpases Regulate the Assembly of Multimolecular Focal Complexes Associated With Actin Stress Fibers, Lamellipodia, and Filopodia. *Cell* (1995) 81:53–62. doi: 10.1016/0092-8674(95)90370-4
9. Aspenström P, Lindberg U, Hall A. Two Gtpases, Cdc42 and Rac, Bind Directly to a Protein Implicated in the Immunodeficiency Disorder Wiskott–Aldrich Syndrome. *Curr Biol* (1996) 6:70–5. doi: 10.1016/S0960-9822(02)00423-2

10. Machesky LM, Insall RH. Scar1 and the Related Wiskott–Aldrich Syndrome Protein, WASP, Regulate the Actin Cytoskeleton Through the Arp2/3 Complex. *Curr Biol* (1998) 8:1347–56. doi: 10.1016/S0960-9822(98)00015-3
11. Eden S, Rohatgi R, Podtelejnikov A, Mann M, Kirschner MW. Mechanism of Regulation of WAVE1-Induced Actin Nucleation by Rac1 and Nck. *Nature* (2002) 418:790–3. doi: 10.1038/nature00859
12. ten Klooster JP, Jaffer ZM, Chernoff J, Hordijk PL. Targeting and Activation of Rac1 are Mediated by the Exchange Factor β-Pix. *J Cell Biol* (2006) 172:759–69. doi: 10.1083/jcb.200509096
13. Milburn M, Tong L, DeVos AM, Brunger A, Yamaizumi Z, Nishimura S, et al. Molecular Switch for Signal Transduction: Structural Differences Between Active and Inactive Forms of Protooncogenic Ras Proteins. *Sci (New York N.Y.)* (1990) 247:939–45. doi: 10.1126/science.2406906
14. Cherfils J, Zeghouf M. Regulation of Small Gtpases by Gefs, Gaps, and Gdis. *Physiol Rev* (2013) 93:269–309. doi: 10.1152/physrev.00003.2012
15. Bos JLJ, Rehmann H, Wittinghofer A. Gefs and Gaps: Critical Elements in the Control of Small G Proteins. *Cell* (2007) 129:865–77. doi: 10.1016/j.cell.2007.05.018
16. Ahmad Mokhtar AM, Ahmed SBM, Darling NJ, Harris M, Mott HR, Owen D. A Complete Survey of Rhogdi Targets Reveals Novel Interactions With Atypical Small Gtpases. *Biochemistry* (2021) 60:1533–51. doi: 10.1021/acs.biochem.1c00120acs.biochem.1c00120
17. Manresa-Arraut A, Johansen FF, Brakebusch C, Issazadeh-Navikas S, Hasseldam H. Rhoa Drives T-Cell Activation and Encephalitogenic Potential in an Animal Model of Multiple Sclerosis. (2018) 9:1235. doi: 10.3389/fimmu.2018.01235
18. Guo F, Cancelas JA, Hildeman D, Williams DA, Zheng Y. Rac Gtpase Isoforms Rac1 and Rac2 Play a Redundant and Crucial Role in T-Cell Development. *Blood* (2008) 112:1767–75. doi: 10.1182/blood-2008-01-132068
19. Dumont C, Corsoni-Tadrzak A, Ruf S, de Boer J, Williams A, Turner M, et al. Rac Gtpases Play Critical Roles in Early T-Cell Development. *Blood* (2009) 113:3990–8. doi: 10.1182/blood-2008-09-181180
20. Smits K, Iannucci V, Stove V, van Hauwe P, Naessens E, Meuwissen PJ, et al. Rho Gtpase Cdc42 Is Essential for Human T-Cell Development. *Haematologica* (2010) 95:367–75. doi: 10.3324/haematol.2009.006890
21. Saoudi A, Kassem S, Dejean A, Gaud G. Rho-Gtpases as Key Regulators of T Lymphocyte Biology. *Small GTPases* (2014) 5:e28208. doi: 10.4161/sgtp.28208
22. Accetta D, Syverson G, Bonacci B, Reddy S, Bengtson C, Surfus J, et al. Human Phagocyte Defect Caused by a Rac2 Mutation Detected by Means of Neonatal Screening for T-Cell Lymphopenia. *J Allergy Clin Immunol* (2011) 127:535–538.e2. doi: 10.1016/j.jaci.2010.10.013
23. Lougaris V, Chou J, Beano A, Wallace JG, Baronio M, Gazzurelli L, et al. A Monoallelic Activating Mutation in RAC2 Resulting in a Combined Immunodeficiency. *J Allergy Clin Immunol* (2019) 143:1649–1653.e3. doi: 10.1016/j.jaci.2019.01.001
24. Prieto-Sánchez RM, Bustelo XR. Structural Basis for the Signaling Specificity of Rhog and Rac1 Gtpases. *J Biol Chem* (2003) 278:37916–25. doi: 10.1074/jbc.M301437200
25. Vigorito E, Bell S, Hebeis BJ, Reynolds H, McAdam S, Emson PC, et al. Immunological Function in Mice Lacking the Rac-Related Gtpase Rhog. *Mol Cell Biol* (2004) 24:719–29. doi: 10.1128/MCB.24.2.719-729.2004
26. Martínez-Martín N, Fernández-Arenas E, Cemerski S, Delgado P, Turner M, Heuser J, et al. T Cell Receptor Internalization From the Immunological Synapse Is Mediated by TC21 and Rhog Gtpase-Dependent Phagocytosis. *Immunity* (2011) 35:208–22. doi: 10.1016/j.immuni.2011.06.003
27. Vaeth M, Feske S. NFAT Control of Immune Function: New Frontiers for an Abiding Trooper. *F1000Research* (2018) 7:260. doi: 10.12688/f1000research.13426.1
28. Charpentier JC, King PD. Mechanisms and Functions of Endocytosis in T Cells. *Cell Communication Signaling* (2021) 19:92. doi: 10.1186/s12964-021-00766-3
29. Nakaya M, Tanaka M, Okabe Y, Hanayama R, Nagata S. Opposite Effects of Rho Family Gtpases on Engulfment of Apoptotic Cells by Macrophages *. *J Biol Chem* (2006) 281:8836–42. doi: 10.1074/jbc.M510972200
30. Prieto-Sánchez RM, Berenjeno IM, Bustelo XR. Involvement of the Rho/Rac Family Member Rhog in Caveolar Endocytosis. *Oncogene* (2006) 25:2961–73. doi: 10.1038/sj.onc.1209333
31. Nakayama M, Hori A, Toyoura S, Yamaguchi S-I. Shaping of T Cell Functions by Trogocytosis. *Cells* (2021) 10:1155. doi: 10.3390/cells10051155
32. Boccasavia VL, Bovolenta ER, Villanueva A, Borroto A, Oeste CL, van Santen HM, et al. : Antigen Presentation Between T Cells Drives Th17 Polarization Under Conditions of Limiting Antigen. *Cell Rep* (2021) 34:108861. doi: 10.1016/j.celrep.2021.108861
33. Baier A, Ndoh VNE, Lacy P, Eitzen G. Rac1 and Rac2 Control Distinct Events During Antigen-Stimulated Mast Cell Exocytosis. *J Leukocyte Biol* (2014) 95:763–74. doi: 10.1189/jlb.0513281
34. Joseph N, Reicher B, Barda-Saad M. The Calcium Feedback Loop and T Cell Activation: How Cytoskeleton Networks Control Intracellular Calcium Flux. *Biochim Biophys Acta (BBA) - Biomembranes* (2014) 1838:557–68. doi: 10.1016/j.bbamem.2013.07.009
35. Vigorito E, Billadeu DD, Savoy D, McAdam S, Doody G, Fort P, et al. Rhog Regulates Gene Expression and the Actin Cytoskeleton in Lymphocytes. *Oncogene* (2003) 22:330–42. doi: 10.1038/sj.onc.1206116
36. Macián F, García-Cózar F, Im S-H, Horton HF, Byrne MC, Rao A. Transcriptional Mechanisms Underlying Lymphocyte Tolerance. *Cell* (2002) 109:719–31. doi: 10.1016/S0092-8674(02)00767-5
37. Hogan PG. Calcium-NFAT Transcriptional Signalling in T Cell Activation and T Cell Exhaustion. *Cell calcium* (2017) 63:66–9. doi: 10.1016/j.ceca.2017.01.014
38. de León-Bautista MP, Cardenas-Aguayo MDC, Casique-Aguirre D, Almaraz-Salinas M, Parraguirre-Martinez S, Olivo-Diaz A, et al. Immunological and Functional Characterization of Rhogdi3 and Its Molecular Targets Rhog and Rhob in Human Pancreatic Cancerous and Normal Cells. *PloS One* (2016) 11:e0166370. doi: 10.1371/journal.pone.0166370
39. Oh H-M, Yu C-R, Golestaneh N, Amadi-Obi A, Lee YS, Eseonu A, et al. STAT3 Protein Promotes T-Cell Survival and Inhibits Interleukin-2 Production Through Up-Regulation of Class O Forkhead Transcription Factors *. *J Biol Chem* (2011) 286:30888–97. doi: 10.1074/jbc.M111.253500
40. Conley JM, Gallagher MP, Berg LJ. T Cells and Gene Regulation: The Switching on and Turning Up of Genes After T Cell Receptor Stimulation in CD8 T Cells. *Front Immunol* (2016) 7:76. doi: 10.3389/fimmu.2016.00076
41. Ambriz-Peña X, García-Zepeda EA, Meza I, Soldevila G. Jak3 Enables Chemokine-Dependent Actin Cytoskeleton Reorganization by Regulating Cofilin and Rac/Rhoa Gtpases Activation. *PloS One* (2014) 9:e88014–4. doi: 10.1371/journal.pone.0088014
42. Montresor A, Bolomini-Vittori M, Toffali L, Rossi B, Constantin G, Laudanna C. JAK Tyrosine Kinases Promote Hierarchical Activation of Rho and Rap Modules of Integrin Activation. *J Cell Biol* (2013) 203:1003–19. doi: 10.1083/jcb.201303067
43. Puga I, Rao A, Macian F. Targeted Cleavage of Signaling Proteins by Caspase 3 Inhibits T Cell Receptor Signaling in Anergic T Cells. *Immunity* (2008) 29:193–204. doi: 10.1016/j.immuni.2008.06.010
44. Hashim IF, Mokhtar A. Small Rho Gtpases and Their Associated Rhogefs Mutations Promote Immunological Defects in Primary Immunodeficiencies. *Int J Biochem Cell Biol* (2021) 137:106034. doi: 10.1016/j.biocel.2021.106034. A.M.
45. Borges WG, Augustine NH, Hill HR. Defective Interleukin-12/Interferon-γ Pathway in Patients With Hyperimmunoglobulinemia E Syndrome. *J Pediatr* (2000) 136:176–80. doi: 10.1016/S0022-3476(00)70098-9
46. Russo E, Salzano M, Postiglione L, Guerra A, Marotta V, Vitale M. Interferon-γ Inhibits Integrin-Mediated Extracellular Signal-Regulated Kinase Activation Stimulated by Fibronectin Binding in Thyroid Cells. *J Endocrinol Invest* (2013) 36:375–8. doi: 10.3275/8649
47. Ellison MA, Gearheart CM, Porter CC, Ambruso DR. Ifn-γ Alters the Expression of Diverse Immunity Related Genes in a Cell Culture Model Designed to Represent Maturing Neutrophils. *PloS One* (2017) 12:e0185956. doi: 10.1371/journal.pone.0185956
48. Gauthier-Rouvière C, Vignal E, Mériane M, Roux P, Montcourier P, Fort P. Rhog Gtpase Controls a Pathway That Independently Activates Rac1 and Cdc42Hs. *Mol Biol Cell* (1998) 9:1379–94. doi: 10.1091/mbc.9.6.1379
49. Derivery E, Gautreau A. Generation of Branched Actin Networks: Assembly and Regulation of the N-WASP and WAVE Molecular Machines. *BioEssays* (2010) 32:119–31. doi: 10.1002/bies.200900123
50. Katoh H, Hiramoto K, Negishi M. Activation of Rac1 by Rhog Regulates Cell Migration. *J Cell Sci* (2006) 119:56 LP – 65. doi: 10.1242/jcs.02720
51. Kalinichenko A, Perinetti Casoni G, Dupré L, Trotta L, Huemer J, Galgano D, et al. Rhog Deficiency Abrogates Cytotoxicity of Human Lymphocytes and

Causes Hemophagocytic Lymphohistiocytosis. *Blood* (2021) 137:2033–45. doi: 10.1182/blood.2020008738
52. Weksler B, Lu B. Alterations of the Immune System in Thymic Malignancies. *J Thorac Oncol* (2014) 9:S137–42. doi: 10.1097/JTO.0000000000000299
53. Aricò M, Danesino C, Pende D, Moretta L. Pathogenesis of Haemophagocytic Lymphohistiocytosis. *Br J Haematol* (2001) 114:761–9. doi: 10.1046/j.1365-2141.2001.02936.x
54. Machaczka M, Vaktnäs J, Klimkowska M, Hägglund H. Malignancy-Associated Hemophagocytic Lymphohistiocytosis in Adults: A Retrospective Population-Based Analysis From a Single Center. *Leukemia lymphoma* (2011) 52:613–9. doi: 10.3109/10428194.2010.551153
55. Henter J-I, Aricò M, Elinder G, Imashuku S, Janka G. Familial Hemophagocytic Lymphohistiocytosis: Primary Hemophagocytic Lymphohistiocytosis. *Hematol/Oncol Clinics North America* (1998) 12:417–33. doi: 10.1016/S0889-8588(05)70520-7
56. Bursa D, Bednarska A, Pihowicz A, Paciorek M, Horban A. Analysis of the Occurrence of Hemophagocytic Lymphohistiocytosis (HLH) Features in Patients With Sepsis: A Prospective Study. *Sci Rep* (2021) 11:1–10. doi: 10.1038/s41598-021-90046-4
57. Ramos-Casals M, Brito-Zerón P, López-Guillermo A, Khamashta MA, Bosch X. Adult Haemophagocytic Syndrome. *Lancet* (2014) 383:1503–16. doi: 10.1016/S0140-6736(13)61048-X
58. Machowicz R, Janka G, Wiktor-Jedrzejczak W. Similar But Not the Same: Differential Diagnosis of HLH and Sepsis. *Crit Rev Oncol/Hematol* (2017) 114:1–12. doi: 10.1016/j.critrevonc.2017.03.023

Conflict of Interest: The authors declare that the research was conducted in the absence of any commercial or financial relationships that could be construed as a potential conflict of interest.

frontiers | Frontiers in Immunology

REVIEW
published: 26 May 2022
doi: 10.3389/fimmu.2022.886328

Mechanosurveillance: Tiptoeing T Cells

Janett Göhring[1,2]*, *Lukas Schrangl*[2], *Gerhard J. Schütz*[2] *and Johannes B. Huppa*[1]

[1] *Institute for Hygiene and Applied Immunology, Center for Pathophysiology, Infectiology and Immunology, Medical University of Vienna, Vienna, Austria,* [2] *Institute of Applied Physics, TU Wien, Vienna, Austria*

Efficient scanning of tissue that T cells encounter during their migratory life is pivotal to protective adaptive immunity. In fact, T cells can detect even a single antigenic peptide/MHC complex (pMHC) among thousands of structurally similar yet non-stimulatory endogenous pMHCs on the surface of antigen-presenting cells (APCs) or target cells. Of note, the glycocalyx of target cells, being composed of proteoglycans and bulky proteins, is bound to affect and even modulate antigen recognition by posing as a physical barrier. T cell-resident microvilli are actin-rich membrane protrusions that puncture through such barriers and thereby actively place the considerably smaller T-cell antigen receptors (TCRs) in close enough proximity to APC-presented pMHCs so that productive interactions may occur efficiently yet under force. We here review our current understanding of how the plasticity of T-cell microvilli and physicochemical properties of the glycocalyx may affect early events in T-cell activation. We assess insights gained from studies on T-cell plasma membrane ultrastructure and provide an update on current efforts to integrate biophysical aspects such as the amplitude and directionality of TCR-imposed mechanical forces and the distribution and lateral mobility of plasma membrane-resident signaling molecules into a more comprehensive view on sensitized T-cell antigen recognition.

Keywords: immune surveillance, mechanical force, T-cell antigen recognition, glycocalyx, physical barriers, microvilli, membrane ultrastructure

OPEN ACCESS

Edited by:
Jerome Delon, INSERM U1016 Institut Cochin, France

Reviewed by:
Claire Hivroz, Maria Sklodowska-Curie National Research Institute of Oncology, Poland
Janis K. Burkhardt, University of Pennsylvania, United States
Kheya Sengupta, Centre Interdisciplinaire de Nanoscience de Marseille (CINaM)/CNRS, France

***Correspondence:**
Janett Göhring
janett.goehring@meduniwien.ac.at

Specialty section:
This article was submitted to T Cell Biology, a section of the journal Frontiers in Immunology

Received: *28 February 2022*
Accepted: *19 April 2022*
Published: *26 May 2022*

Citation:
Göhring J, Schrangl L, Schütz GJ and Huppa JB (2022) Mechanosurveillance: Tiptoeing T Cells. Front. Immunol. 13:886328. doi: 10.3389/fimmu.2022.886328

INTRODUCTION

The adaptive immune response is an extraordinarily complex process involving a multitude of different cell types, transmitters, and effector molecules performing their intended function in diverse tissue environments, some of which are altered by disease and infection. Slight deviations within the involved mechanisms can lead to severe medical complications, namely, allergies, autoimmune diseases, hypo- or hyper-reactions to invading pathogens, and the development of cancer. The degree of fine-tuning required for immune protection becomes apparent at multiple regulatory levels controlling T-cell activation. The pivotal event preceding many of the ensuing cellular interactions concerns the specific molecular recognition of processed pathogenic peptides displayed in the context of the major histocompatibility complex (MHC and peptide-presenting MHC; pMHC) by T cells *via* their clonotypic and genetically recombined T-cell antigen receptors (TCRs).

Interactions between stimulatory pMHCs and TCRs are highly specific and confer exquisite T-cell antigen sensitivity, a *sine qua non* considering the consequences of recognition failure. It is, however, not yet clear how such a level of specificity and sensitivity is maintained, since measured biochemical affinities between TCRs and pMHCs are astonishingly low. A number of models have been conceived and tested in the last two decades. Experimental efforts focused on revealing the molecular machinery involved in antigen recognition events and led to the formulation of concepts implicating kinetic segregation, kinetic proof-reading, co-receptor involvement, ligation-triggered conformational changes, serial engagement, and the contribution of mechanical forces in early recognition events [reviewed in (1)]. These models have their merits, and the ground truth will very likely be a combination of their aspects.

The complex interaction of naïve antigen-inexperienced T cells with antigen-presenting cells such as dendritic and B cells can be described on different spatial and temporal scales (see **Figure 1** for an illustration of these processes). Highly dynamic cellular interactions involving massive cytoskeletal rearrangements transpire during the entirety of the cell–cell contact. Before antigen recognition, pre-existing membrane protrusions such as microvilli scan the surface of the target cell in search of their cognate antigen (2–5). As a result, physical barriers such as the glycocalyx of the target cell are overcome by the surveilling microvilli. During scanning, surface receptors at the tip of the microvilli are subject to a large range of mechanical forces such as tensile, compressive, and shear stresses (6). Once a specific recognition event is established, the T cell receives a movement arrest signal and the two interacting cells start reorganizing their conjugation plane, which involves massive membrane undulations and the formation of other membrane projections such as invadosome-like structures (2, 7–9). Proteins within the entire conjugation plane become spatially reorganized, forming the immunological synapse with a central and peripheral domain (10).

The unique two- and three-dimensional properties of immune synapses are likely to influence the dynamics of intrinsic receptor–ligand interactions (11). For example, massive membrane rearrangements ensue after initial contact and produce spatial constraints that eventually result in the molecular segregation of membrane receptors and ligands based on the size of their extracellular domains (12). Signal-maintaining microclusters are formed, containing ligated TCRs, which are subsequently dragged by the cytoskeleton toward the center of the synapse (13–17). This active process creates drag on other constituents, causing membrane undulations due to elastic deformation and relaxation (18). In this fashion, measurable

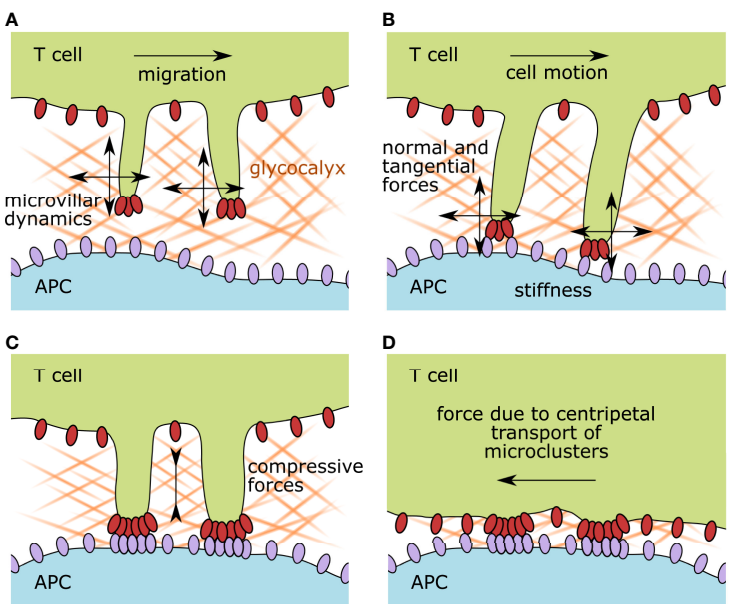

FIGURE 1 | Illustration of the membrane organization of scanning and activated T cells and the accompanying possible mechanical forces affecting surface receptors. **(A)** During immune surveillance, T cells scan target cells via microvillar protrusions. The first physical barrier they encounter is the glycocalyx of the target cell. Antigen scanning speed is impacted by the glycocalyx physicochemical properties such as stiffness, density, and matrix composition, but also by the migrational speed of the T cell itself and its microvillar dynamics. **(B)** As soon as surface receptors on the microvillar tips interact with their ligands on the opposing membrane, the formed bonds experience a force vector with normal and tangential components. The surface stiffness of the target cell and the microvillar elasticity also influence the interacting receptor–ligand pairs. **(C)** Upon recognition of a cognate antigen, T-cell activation starts. Surface receptor molecules build signaling platforms while the two participating plasma membranes approach each other, compressing the remaining glycocalyx components. **(D)** After the initiation of TCR signaling, the zonal organization of the immunological synapse is established and signaling foci, called microclusters, are pulled by the actin cytoskeleton toward the center of the cell. This dragging motion is also causing mechanical strain on the involved receptor–ligand pairs. APC, antigen-presenting cell.

pulling forces are exerted by the regulated, centripetal flow of the cortical actin cytoskeleton (19).

Considering the temporal flow of events, one must consider that signaling events during T-cell activation are divided into early recognition events, which eventually lead to motility arrest, and signal-maintaining events. Early recognition events fulfill the purpose of fast and efficient antigen screening (20, 21), whereas later events are needed to maintain a steady T-cell response at a continuous antigenic stimulus (14, 17, 22, 23).

In this review, we highlight the cell biological and biophysical features of T-cell microvilli, which act as antigen-sensing units and, in turn, reevaluate the impact of physical barriers and mechanical forces on immune surveillance.

ANTIGEN SCANNING ENTITIES: MICROVILLI OF T CELLS

T cells are exceptionally motile as they roam a multitude of different environments during their life cycle (24, 25). After differentiation and selection in the thymus, naïve T cells move into the blood and lymphatic system to reach secondary lymphoid systems. In doing so, T cells are exposed to strong shear forces caused, for example, by the dynamics of the blood flow. To leave the blood stream, T cells perform a complex maneuver along the endothelial wall, comprising a selectin-mediated rolling and adhesion cycle that eventually leads to diapedesis. After entering a lymph node or tissue of interest, T cells start migrating through dense three-dimensional extracellular matrices while continuously screening antigen-presenting cells (APCs) or target cells, which they continuously encounter for cognate antigen. Upon stimulation, T cells switch their migration mode and form cell–cell interfaces, which, depending on tissue properties, are termed immunological kinapses or synapses. Subsequently, they start proliferating, and eventually start their surveilling migration anew throughout the body. Further triggering of an antigen-experienced T cell leads to the fulfillment of its effector function according to the subtype of the T cell.

During immune surveillance, the membrane ultrastructure of scanning T cells is especially dynamic in order to guarantee adaptation to different physical environments and functions. Prominent structures are the actin-rich membrane protrusions called microvilli, which play a central role in antigen surveillance.

Physical Barriers in Immune Surveillance

An interesting aspect of T-cell interactions concerns the biophysical environment T cells experience while they are scanning their surroundings. T cells are actively probing for pathogen-derived or otherwise atypical or non-endogenous peptides presented on the surface of cells that they encounter in their migratory life. However, cells are protected by the glycocalyx, a dense and wide coat of extracellular polysaccharides and proteins, which creates a physical barrier, preventing the close apposition of the cellular membranes and, consequently, any intercellular ligand–receptor interaction (26–28). To deal with this, T cells feature membrane protrusions that can puncture through the cell-resident glycocalyx to efficiently scan large portions of a large variety of cells and drive TCR-specific signaling (2, 4, 7, 29). The glycocalyx is a naturally occurring physical barrier made of extracellular branched carbohydrates, glycolipids, glycoproteins, and proteoglycans that covers the plasma membrane of cells (30). The involved carbohydrates (i) can be directly linked to their respective anchor molecules *via* N- or O-glycosidic bonds or are independent entities within the matrix, (ii) are continuously remodeled by cellular enzymes, (iii) are primarily negatively charged, and (iv) play an important role in cellular processes such as signal amplification, adhesion, migration, and cell death (31). The complexity and height of this dense, gel-like coating can vary from 250 to >500 nm (32) and it is filled with ions, growth factors, chemo- and cytokines.

The exact composition of the glycocalyx has been characterized in detail for endothelial cells: prominent membrane-anchored proteoglycan groups are syndecans and glypicans, whereas other proteoglycans such as mimecan, perlecan, and biglycan are actively secreted into the extracellular space and blood stream (33). These proteoglycans form a dense network by associating with glycosaminoglycans (GAGs) such as heparan sulfate, dermatan sulfate, chondroitin sulfate, and hyaluronic acid, to name a few ubiquitous GAGs. Apart from these components, a large variety of glycoproteins such as selectins, integrins, and immunoglobulin-like proteins also participate in forming a dense extracellular network (33). It is beyond the scope of this review to discuss all the participating glycocalyx players, but it is important to note the existence of a complex, multi-layered, and highly dynamic layer beyond the plasma membrane that impacts any cell–cell interaction.

The glycocalyx of the T cell consists mainly of a few prominent surface proteins with large extracellular domains, namely CD43 and CD44, and the protein tyrosine phosphatases CD45 and CD148. These proteins' extracellular domains are 3–4 fold larger in length than the physiological intermembrane distance, allowing for a pMHC–TCR bond (~15 nm) (26, 34), and resemble stiff rod-like structures that are unlikely to bend in response to external tensile forces (35). Similarly, CD148 and CD45 also carry large extracellular domains but fulfill additional signaling functions in the wake of TCR triggering. During the immune synapse formation, these proteins and integrin LFA-1 binding to ICAM-1 are positioned in distinct zones creating varying intermembrane distances. This zonal reorganization after TCR triggering leads to steep membrane curvatures accompanied by dynamic membrane tension profiles in the contacting APC and T cell membranes [reviewed in (34)]. Not much is yet known with regard to the presence of typical membrane-anchored and secreted proteoglycans and glycoproteins in the glycocalyx of T cells, yet one study investigated the upregulation of Mucin-1 (a very large glycocalyx-building proteoglycan) after mitogenic stimulus in activated T cells (36) and another study detected hyaluronan (a prominent GAG) on the surface of T cells in certain conditions (37). However, given their migratory lifestyle and the necessity to visit and scan a large variety of tissues, the presence of a bulky

glycocalyx network seems disadvantageous and may only be upregulated in certain scenarios such as trafficking and homing. Also, T cells exhibit a stiffness modulus of only ~85 Pa, which is very soft in comparison to other cell systems (38). This has implications for cell–cell interactions, as the cell with the lower rigidity spreads at the interface. Recent rheological measurements of the viscoelastic properties of T cells during activation show a 2–3 fold increase in stiffness after stimulation with an activating microbead (39). The authors also performed AFM experiments with T cell–APC conjugates and concluded that mechanical changes occur within seconds of initial contact (39).

The glycocalic layers of professional APCs have so far been investigated to a much lesser extent, and given the migratory life of these cells, it is unclear if the glycocalyx layers are up or downregulated in their immature/mature states or the varying lymphoid environments they reside in. One study showed the presence of Mucin-1 on dendritic cells *in vivo* (40). Also, a recent publication investigated the contribution of hyaluronan (HA) to the glycocalyx layer of migratory DCs and discovered a 400–500 nm thick glycocalyx layer anchored and regulated by the HA-receptor CD44 (41). The study also showed that the HA content within the glycocalyx was upregulated for mature DCs compared to immature DCs, and consequently, that the presence of HA glycocalyx is necessary for trafficking over the lymphatic endothelium and allowing crawling along the endothelia (41, 42). This aspect becomes crucial considering that long-lived MHC-dependent T cell–DC interactions occur on the luminal side of afferent lymphatic capillaries (43, 44).

An interesting mechanism was recently uncovered in the work of Imbert et al., characterizing the immune-modulatory impact of the glycocalyx on the target cell during phagocytosis in *in vitro* and *in vivo* settings (45). The elegant experiments showed that the presence of a repulsive glycocalyx on target cells prevents phagocytosis, leading to effective immune evasion, and that, similarly the upregulation of glycocalyx layers on the phagocyte itself led to the same inhibition of phagocytosis. The study clearly showed that glycocalyx layers can actively prevent immune recognition and the triggering of surface receptors by restricting their accessibility. Along this line of thought, cancerous cells have been shown to alter their glycocalyx composition (46, 47), in that they vary its height and other biophysical parameters, thereby promoting their immune evasion capabilities (48, 49).

Biophysical parameters of the glycocalyx have been measured using AFM nano-indentation (50), resulting in an elastic modulus of around 0.39 kPa. The plasma membrane lacking a glycocalyx has been found to be less flexible with an elastic modulus of about 3 kPa. The corresponding stiffness of cells has been experimentally determined to be in the range of 10 Pa to 10 kPa, the variability resulting from different cell types and confounding parameters like intracellular pressure and actin–myosin contractility of the underlying cytoskeleton and differences in methodology (51). Interestingly, spread mesenchymal stem cells exhibit a larger stiffness modulus than rounded ones, with 3.2 and 2.5 kPa, respectively (52). The stiffness of monocyte-derived dendritic cells has been reported to be in the range of 0.5 kPa, with their stiffness changing upon inflammation (38), whereas another study reports a 2–3 fold increase in stiffness for maturing DCs (within the range of 2 to 8 kPa) (53).

All these aspects become relevant when considering the sensitivity of the T cell toward different substrate stiffnesses. The stiffness and porosity of the glycocalyx of both T cell and APC may hence be critical for antigen accessibility, whereas the APC cortex stiffness may be critical for antigen sensitivity and subsequent signaling (54). It has been comprehensively shown that the stiffness of the ligand-presenting surface impacts T cell signaling, proliferation, and differentiation (54–59). Some of these studies report a positive correlation between the substrate stiffness and T-cell activation (55–57), while others show an inverse correlation (54, 58). The investigated stiffness ranged from a few Pa to MPa, while most studies report a maximum cellular response at a substrate stiffness of 100 kPa. In a more physiological setting, Blumenthal et al. investigated the impact of the cortical stiffness of dendritic cells on the T-cell response (53): by varying the stiffness of stimulatory hydrogels in the physiological range of immature and mature DCs (2 to 8 kPa, respectively), the authors showed an increase in $CD4^+$ T-cell antigen sensitivity and responses under stiffness conditions reflecting that of mature DCs. Strikingly and in contrast, $CD8^+$ T cells only showed modest sensitivity toward stiffness. By substituting pMHC as a stimulatory ligand for activating antibodies, the authors revealed a dependence of the stiffness response on the type of TCR–ligand engagement. Within the measured physiological stiffness range (2–8 kPa), this limitation dramatically affected T-cell responsiveness, as only treatment with pMHCs but not with antibodies triggered T-cell activation under these conditions, except for very high ligand densities (53). Considering the effect of substrate stiffness on T-cell effector function, recent studies reporting on the vulnerability of cancer cells to T-cell cytolytic activity showed a positive correlation between immune response and cellular rigidity (60). As a consequence, cancer cells may actively evade antitumor immune responses by softening their cortical actin cytoskeleton.

Microvilli Dimensions and Localization

In the mid-1970s to 1980s, efforts were made to morphologically characterize lymphocytes using the then newly developed technique of scanning electron microscopy, and consequently, microvillar protrusions were discovered covering the surface of lymphocytes (61–63). These membrane structures were described as being dynamic and dependent on the cell cycle, temperature, inter-cell contact, and even antigenic stimulus (64). Twenty-five years later, it was possible to detect the presence of membrane protrusions on the surface of circulating T cells (65), and prior to engagement with antigen-presenting cells (2, 4, 66) and within lymph nodes (3). These studies demonstrated the existence of such membrane protrusions during initial contact formation. Cai et al. quantified the occurrence of microvillar protrusions *via* Lattice Light Sheet Microscopy: the cell membrane is densely packed with highly dynamic microvillar protrusions that cover 98% of the cellular surface over a time

period of 1 min (2). After the formation of the immunological synapse, the membrane structure ultimately becomes more planar, creating wider close-contact zones between the participating cell membranes (66, 67). Leukocyte microvillar protrusions, used for initial tethering to and rolling along the endothelia within the high shear force conditions of the blood stream (9, 68, 69), will not be the focus of this review in view of their largely different functions and surface receptor composition.

Electron-microscopic snapshots of T cells interacting with antigen-presenting cells allow the characterization of the morphology of membrane protrusions on resting, scanning, and activating T cells. The protrusions are 300–400 nm long (median, up to 4 μm has been reported) and 70–350 nm in diameter with a density of 3–4 protrusions per μm^2 on a resting T cell (3, 5, 7, 65, 70). So far, we are not aware of any comparative study quantifying the abundance of microvilli on circulating and scanning T cells. Interestingly, the dimensions of microvillar protrusions are similar when comparing murine and human blood-isolated lymphocytes, even though human lymphocytes are in general twice as large in cell diameter (65). This conserved feature size of the microvilli indicates the existence of a common physical parameter T cells must overcome during their life time, e.g., the thickness of the glycocalyx during immune surveillance or similar shear forces during rolling tethering in the blood stream. Upon contact formation with a professional antigen-presenting cell, the protrusion tips form close contacts with the opposing cellular membrane in an antigen-independent manner, i.e., the interaction frequency and protrusion density remain unchanged during surveillance and immune synapse formation (2). Upon TCR ligation, however, the ensuing antigen-specific interactions appear to lead to a longer dwell time of the microvilli tip in the synaptic area (2) and may even deform the target cell membrane, forming invadosome-like structures (4). It still remains to be investigated whether microvilli and invadosome-like structures are in fact morphologically and functionally similar protrusions. Recent studies from the Husson as well as the Hivroz group (71–73) have revealed the formation of large membrane protrusions after synapse formation, the physiological role of which remains unknown, but may not be confused with microvillar protrusions during diapedesis and immune surveillance.

Microvilli were described as continuously forming under the leading edge of the lamellipodium of migrating T cells. Upon antigen encounter and synapse formation, membrane protrusions can be preferentially observed forming at the synaptic periphery of the T cell–APC interface (4). Importantly, the transient interactions scanning microvilli form with their target surface do not cease after antigen-dependent triggering of the T cell (2), much in line with the findings that synapse maintenance depends on continuous recruitment of new TCR–pMHC interactions (14, 17, 74, 75).

Monitoring and characterizing of T cell microvilli during antigen scanning remains a big challenge within the otherwise extensively researched field of T-cell activation. Previous investigations are confounded by varying cell types, T-cell receptors, and presented ligands, but ultimately by the applied techniques and stimulation platforms. Studies were especially hindered by the lack of methods to investigate three-dimensional and highly dynamic nanostructures on living cells (7). A few research groups applied indirect observation methods to prove the existence of membrane protrusions within the immunological synapse, such as confocal microscopy (4), total internal reflection microscopy (TIRF) (5, 70, 76), and super-resolution techniques (3, 77). Other techniques like lattice light-sheet microscopy and synaptic contact mapping allow a more direct assessment of the membrane structure of activating T cells (2).

Distribution of Signaling Molecules on Microvillar Protrusions

As extensively reviewed by Orbach and Su (78), microvilli are well-equipped for antigen recognition, and recent studies show that microvillar protrusions are indeed the antigen-sensing entities driving immune surveillance (79–81). In short, TCRs and CD4 coreceptors, CD2 adhesion molecules and essential proteins for T-cell activation, such as Lck and LAT, have been found enriched in microvilli (80). Jung et al. investigated the impact of membrane ultrastructure on TCR distribution on T cells and observed TCR pre-clustering on resting T cells (3). Interestingly, no TCR clusters were observed when T cells were allowed to flatten out on non-activating surfaces (82). Recently, the Ley group observed CD45 exclusion from microvilli tips before antigen recognition (83), whereas Razvag et al. observed an exclusion of CD45 shortly after contact formation (77). Considering the kinetic segregation model, which postulates that T-cell activation is induced by the spatial separation of phosphatases such as CD45 from the phosphorylation sites of TCRs, this implies a high sensitivity of tip-resident TCRs toward antigenic pMHC. Indeed, contacts between microvilli and stimulating surfaces were found to be sufficient for T-cell activation (76, 84). What drives the organization of signaling molecules in microvilli has so far remained elusive, but it is speculated that the extreme membrane curvature and the lipid composition, in particular cholesterol content, may play a role (78). Furthermore, it is generally accepted that microvillar protrusions contain parallel bundles of actin filaments (2, 65) and may colocalize often, but not necessarily always, with TCR molecules [(2) and reviewed in (78)].

In summary, it is evident that microvilli form a restricted reaction volume harboring the necessary molecules for T-cell activation. An exciting observation was recently made by Klotzsch and colleagues, who demonstrated the ability of the T cell to reach into narrowly confined spaces and who showcased the very dynamic nature of their microvillar protrusions and their ability to scan for occluded antigens (85). Interestingly, when T cells reached into micropits below 200 nm in diameter, a slight yet quantifiable antigen-independent cytokine upregulation started. This observation indicates that the signaling molecules within the limited reaction volume of microvilli may be sufficient for cell-body independent signal amplification or, alternatively, that T cells may reach an even higher degree of antigen sensitivity when the dimensions of their microvilli are severely restricted. Effective T-cell activation may hence be aided by enforcing the spatial proximity of signaling molecules downstream of the TCR.

Microvilli Scanning Speed on Artificial and Natural APCs

The fractal arrangement of microvilli enables T cells to efficiently scan the surfaces of antigen-presenting cells (2). Scanning human $CD4^+$ T cells move with a mean velocity of ~3 μm/min over cell surfaces (4). T cells perform immune surveillance in lymph nodes in the presence of antigen with a scanning speed of 2.6 to 5.4 μm/min in a random walk fashion (86, 87), and a dendritic cell typically interacts for ~3 min with individual T cells (88). In resting murine OT-1 TCR-transgenic T cells, microvilli were found to move at an average speed of 5.2 ± 0.4 μm/min, resulting in a 98% coverage of the T cell surface within 1 min. Similarly, the leading edge of the lamellipodium of migrating fibroblasts moves at a velocity of 6.3 μm/min (89). Note that comparable migration velocities have been observed for TCR microclusters in Jurkat T cells (8.4 ± 0.36 μm/min) (90). The mean velocity of actin retrograde flow in Jurkat T cells stimulated with a strong agonist has been recorded to be ~4.8–5.4 μm/min (91, 92), with faster velocities observed for weaker agonists (92).

Motion of any biological membrane in a perpendicular direction to the plane of the receptor–ligand interaction occurs at high frequencies and in the range of tens of nanometers due to thermal fluctuations or stochastic membrane displacement (reviewed in (34)). Perpendicular fluctuations of microvilli tips of about 67 nm were observed within 1 second-long observation windows (70). The lateral movement of microvilli within this experimental setup across a non-activating surface was however minimal, and only rarely spurts of tenths of a micrometer could be observed (70). These results indicate that microvilli move perpendicularly toward a cell surface and retract without much lateral movement to reappear at a different position to continue probing the APC surface. This observation of dynamic microvilli behavior is intriguing, considering that T cells must overcome the glycocalyx in order to probe for surface receptors. Lateral movement through the dense surface layer may be energetically disadvantageous. Also, the geometry of the antigen-presenting surface is likely to influence scanning membrane protrusions (4, 93).

In 2012, Sage et al. performed a series of experiments aimed at determining the depth and width of "invadosome-like" podosomes (ILPs). Although the depth of these structures was found to be stimulus-independent, the width showed a significant decrease in the presence of a specific antigen (4). The authors also showed that calcium flux is initiated ~25 s after the first appearance of an ILP. Interestingly, the presence of antigen caused a substantial stabilization of the ILP lifetime (4), i.e., the transient nature of the scanning ILP ceased to exist after contact with cognate antigen. Cai et al. observed rapid scanning of the opposing surface by microvillar structures and their subsequent arrest or stabilization upon encountering cognate antigen (2). This process seemed, however, to be independent of downstream signaling. A theoretical model has been proposed, attributing the microvilli contact stabilization to the formation of catch bonds (non-covalent bonds whose lifetime increases under force) between TCR and MHC loaded with stimulatory peptide (21), implying a critical role of mechanical forces exerted *via* microvilli in antigen discrimination. The suggested mechanism is in agreement with the finding that microvilli stabilization is independent of actin (2). Further theoretical work indicated that the antigen-dependent arrest of microvilli may indeed be essential for ligand discrimination (94): Within their framework, which was based on kinetic segregation, Fernandes and coworkers found specific TCR triggering if (i) close contact areas between T cells and APCs persisted for at least two seconds and (ii) the radius of the area was smaller than 220 nm.

Considering the mobility of pMHCs on APCs as an additional parameter for T-cell recognition, the field has not yet reached a consensus on to what extent the laterally immobile or the mobile fraction of pMHCs lead to efficient triggering *in vivo* (95–97). Several studies have identified the velocity and quantified the mobile fraction within the membranes of APC (98–100), but to our knowledge, none has shown the functional connection to T cell activation of either fraction. From our own experiments using activating adhesion-competent gel-phase and fluid-phase glass-supported lipid bilayers, we do know that T cells scan and activate efficiently on both surfaces (101), but we could observe a slight delay in response on laterally immobile surfaces, most likely due to a stalled microcluster formation. These results were corroborated by other studies (102, 103). A faster moving pMHC molecule would increase the likelihood of encountering the microvilli tips, which becomes important when contemplating scenarios with very low densities of cognate antigens (21). On the other hand, slower moving or immobilized pMHCs may facilitate rebinding events if microvilli tips stay in close proximity (21), which could influence antigen recognition thresholds (104).

Force Profile of Membrane Protrusions

As motile entities, T cells experience considerable strain. T-cell protrusions share many properties with filopodia, which are actively used by other motile cells when they screen the surroundings for biochemical and mechanical cues through environment-sensing receptors residing on their tips (105). Filopodia generation requires 5–30 pN (piconewton) of protrusion force (106). Once formed and anchored to cortical actin, they can exert extensive pulling forces on their own (79, 107). Podosome protrusion force was quantified using monocyte-derived cells spreading on a deformable artificial membrane: an average of 29 to 155 nN pushing force was measured, which was positively correlated with substrate rigidity (108). Interestingly, podosomes could adjust their core elasticity toward the substrate rigidity, maintaining a constant indentation depth. Similar results were obtained for podosomes of fibroblasts pushing against SLBs (109). The latter study quantified the molecular tension exerted by individual integrin molecules using DNA-based tension-gauge tethers, hence confirming the tendency of podosomes to predominantly exert perpendicular forces.

Via 3D traction force microscopy employing beads bound to an elastic hydrogel, forces of up to several hundred piconewtons exerted by single microvilli were observed (79). Force application *via* membrane protrusions was found to be crucial for the cytotoxic activity of $CD8^+$ T cells (110): Knocking out the

cytoskeletal regulator WASP not only led to diminished forces and deformation of target cells, but also to a 50% reduction in killing efficiency at low antigen levels.

MECHANICAL FORCES IN T-CELL ANTIGEN RECOGNITION

For decades, scientists have attempted to tackle the mystery surrounding the high sensitivity and specificity of T cells for their cognate antigen and have naturally created a multitude of T-cell activation models, each with their own merits and weaknesses. These early models mainly investigated biochemical aspects of the TCR–pMHC interaction, such as the multimeric state of the ligands, the required ligand density for activation, or the influence of co-receptor binding on triggering potency. However, it quickly became apparent that all these models could not sufficiently explain the high sensitivity and specificity of the TCR–pMHC interaction. Eventually, a new parameter entered the field. In 2001, the Dustin group observed that different experimental methods led to marked differences in the measured kinetic parameters of the TCR–pMHC interaction. Consequently, it was hypothesized that the k_{off} may increase due to mechanical force in a 2D setting, where settling T cells interact with immobilized ligands on a surface (111). The intuitive explanation for this phenomenon was the involvement of dynamic cellular processes in destabilizing the TCR–pMHC interaction. Indeed, ten years later, Huppa et al. observed a significant difference in 2D and 3D binding kinetics and, additionally, a pronounced increase in TCR–pMHC interaction lifetime upon the destabilization of the cortical cytoskeleton, indicating that mechanical forces impact T-cell antigen recognition and triggering (112).

The advancement of new techniques followed, with the purpose of identifying the impact of mechanical forces on/during T-cell activation (see **Figure 2** for an overview of the most prominent methods). For this review, we will discriminate between the effects of externally applied mechanical forces and forces exerted through the TCR itself.

Impact of Externally Applied Mechanical Forces on T-Cell Activation

In a multitude of studies, mechanical forces were applied to the TCR–pMHC bond to characterize the TCR as a mechanosensor. Different approaches were devised to stretch the bond in a defined manner (see overview in **Table 1**):

One of the first experimental strategies was to confront T cells with a bead coated with a defined number of TCR–ligands, followed by targeted force application and simultaneous recording of TCR-downstream signaling. A force of as little as 50 pN applied to the pMHC-coated bead in a tangential but not normal orientation with regard to the T cell surface turned out to be sufficient to activate T cells (113). A subsequent study

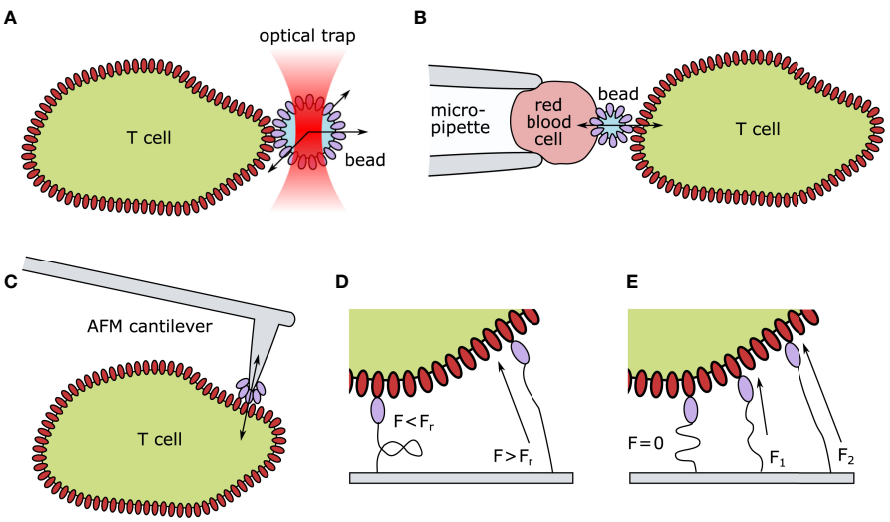

FIGURE 2 | Technical approaches for quantifying mechanical forces exerted on TCR–pMHC pairs. **(A)** Optical tweezer setup: ligand-coated beads are spatially fixed by an optical trap. Upon TCR engagement, the bead is moved out of the laser focus. The deflection indicates the TCR-imposed mechanical force. **(B)** Biomembrane Force Probes: A T cell and a red blood cell are aspirated and held in place *via* a micropipette setup. A ligand-coated bead is attached to the surface of the red blood cells. Upon T-cell contact, altered thermal fluctuation of the bead indicates TCR–ligand engagement. Forces can be exerted by retracting the micropipette. **(C)** Atomic Force Microscopy: A ligand-coated cantilever tip is brought into close proximity of the T cell surface. Upon TCR engagement, the deflection of the cantilever indicates force generation. **(D)** Digital Molecular Force Sensors (MFS): A ligand is attached to a fluorescently labeled MFS unit. In their folded state, the fluorescence is entirely quenched. Such sensors can withstand a certain threshold of strain before (F_r) unfolding. Upon TCR engagement and force generation, the digital MFS unfolds, reducing the quencher efficiency and leading to a quantifiable increase in fluorescence. **(E)** Analog MFS: A ligand is attached to a fluorescently labeled spring unit framed with a FRET (Förster resonance energy transfer) pair. In its coiled state (F=0) the fluorophores are in close proximity and the FRET efficiency is high. Upon TCR engagement and force generation (F_1<F_2) the spring unit uncoils continuously decreasing the FRET efficiency between the two fluorophores. AFM, Atomic Force Microscopy; F, Force; F_r, hairpin rupture force.

TABLE 1 | Overview of published articles investigating the impact of mechanical forces on T-cell activation.

Forces Activate T cells	Force Amplitude & Direction	# Ligands	Triggered Cells, Stimulus	Ref.
Optical Tweezers	Shear force (50 pN) activates T cells	~10/bead	T cells (murine), pMHCI	(113)
Flow Chamber/Micropipette	Shear/Pulling forces activate T cells	n.d. (cell surface)	T cells (murine), αCD3 on aAPCs	(114)
Atomic Force Microscopy	~20 +/−10 pN/bond sensitivity ~10 pN	1/interface	$CD8^+$ T cells (murine), pMHCI	(115)
Micropipette Assay	Applied forces activate T cells	15–30/μm^2	$CD8^+$ T cells (murine), pMHCI	(116)
Biomembrane Force Probe	Up to ~10 pN/bond enhances lifetime (catch)	1/interface	$CD8^+$ T cells (murine), pMHCI	(117)
Optical Tweezer	Up to ~15 pN/bond enhances lifetime (catch)	1/interface	$CD8^+$ T cells (murine), pMHCI	(118)
Biomembrane Force Probe	Up to ~10 pN/bond enhances lifetime (catch)	1/interface	$CD4^+$ T cells (murine), pMHCII	(119)
Biomembrane Force Probe	Up to ~10 pN/bond enhances lifetime (catch)	1/interface	Pre-pMHC/TCR (murine), pMHCI	(120)
Biomembrane Force Probe	Up to ~10 pN/bond enhances lifetime (catch)	1/interface	$CD8^+$ Native/Recombinant TCR	(121)
Optical Tweezer	10–20 pN/bond (in shear & normal direction); Shear forces activate T cells more efficiently	1/interface to 200/interface (20,000 in experiments without force)	$CD8^+$ T cells (murine), pMHCI	(122)
Biomembrane Force Probe	Up to ~15 pN/bond enhances lifetime (catch)	1/interface	$CD4^+$ T cells (human), pMHCII	(123)

pN, picoNewton; αCD3, antibody against CD3; aAPC, artificial antigen-presenting cell; n.d., not determined; Ref., reference number.

determined the effect of applied shear and pulling forces on the TCR–pMHC bond using artificial APCs and demonstrated that mechanical forces can activate T cells as well in a cell–cell conjugate (114). Forces of as little as 10 pN were found sufficient to induce signaling when imposed through pMHCs or TCR/CD3-specific antibodies (122). Combined, these studies are consistent with the notion that triggering thresholds are not only defined by the intrinsic biochemical properties of TCRs and pMHC but also by force load and directionality. Interestingly, the latter study revealed that forces applied to no more than 1 molecule at the bead–cell interface could not trigger a robust T-cell response, whereas forces applied over 2 bonds resulted in T-cell activation. Given that the physiological concentration of presented antigen *via* pMHCI is estimated to be around 10–100 per interface (124), and as few as 3–10 bonds are sufficient to trigger cytotoxicity (125), these insights let mechanical forces in the context of scanning microvilli tips shine in a new light.

Adding to the multitude of unique insights, the study by Feng et al. provided the first clear evidence that forces applied over multiple bonds at the bead–cell interface are being distributed (122). A prerequisite to load distribution would be the physical coupling of the involved surface area. Along this line of reasoning, the biophysical parameters of membrane curvature and tension recently emerged as a possible mechanism influencing T-cell motility, protrusion, and immune synapse formation (reviewed in (126)). The decisive physical parameter in this model is the modulation of membrane tension and tension decay at the triggering point, which could even be used to explain certain aspects of ligand discrimination (127) and synapse breaking (128).

By measuring TCR–pMHC dissociation kinetics under load with the use of a biomembrane force probe (BFP), Zhu and colleagues found a correlation between the bond lifetime and stimulatory potency (116, 117, 119, 129). BFP probes were used to apply mechanical forces to $CD8^+$ (117) and $CD4^+$ T cells (119, 123), and showed that for agonistic antigens, forces up to 10 pN prolong the interaction lifetime, forming 'catch bonds,' while non-stimulatory pMHCs give rise to much reduced lifetimes under load ('slip bonds'). By using an optical tweezer setup (118), catch-bond characteristics of stimulatory TCR–pMHC interactions were also observed by others. Furthermore, the directionality of externally applied forces probing the TCR–pMHC interaction impacts the antigen sensitivity of the T cell (122). Therefore, one prevalent model in the field describing antigen discrimination concerns the mechanical probing of each TCR–pMHC interaction. The TCR-imposed molecular forces exerted by the structural dynamics of the cellular membrane help in probing the ligand–receptor interaction, and only strong agonists allow the necessary resistance (life-time) to trigger activation (117, 122). It seems, therefore, plausible that linking forces to synaptic lifetime and the stimulatory potency of a given TCR–pMHC pair manifests as a major principle underlying antigen discrimination in the physiological context of T-cell antigen recognition. However, this has been contested by the recent observation that even agonist pMHCs coated on beads and interacting with a TCR-coated surface exhibited a clear slip bond behaviour behavior under defined flow-generated force in an *in vitro* experiment without cells (130).

Force Amplitude of TCR-Imposed Mechanical Forces

Adhesion-related forces of about 1–2 nN have been reported within cell–cell contacts. However, measured values varied significantly depending on the cell line under investigation (131, 132). Moreover, net adhesion forces recorded between the conjugated cells correlated with the stimulatory potency of the pMHC (132). Several attempts have since been made to assess forces imposed on a truly molecular level (see **Table 2**).

Husson et al. (71) adapted the BFP technology with single-molecule detection to visualize the temporal response of single T cells to glass beads functionalized with anti-CD3 and covalently

attached to the surface of a red blood cell. Force generation was monitored by the elongation of the red blood cell. In this fashion, distinct pulling and pushing phases could be observed in receptor-engaged T cells.

Traction force microscopy (TFM) has been applied to assess forces related to T-cell adhesion and activation. This methodology involves tracking the force-induced displacement of fluorescent beads embedded in a matrix of defined stiffness resulting from cells crawling or spreading thereon. From such studies, it was concluded that T cells adapt their signaling response according to substrate stiffness. TFM provided the net amplitude and directionality of averaged cellular mechanical forces. With the use of elastic pillars coated with pMHC or activating antibodies, Bashour et al. visualized and quantified TCR-imposed forces (133): T cells deflected pillars with approximately 200 pN per pillar in an antigen-dependent manner. However, the exact number of participating molecular bonds could not be determined. A similar TFM experiment conducted with Jurkat T cells revealed that activating surface conditions (anti-CD3 antibodies) produce higher deforming forces than non-activating conditions (56).

Atomic force microscopy (AFM) using pMHC-coated cantilevers confronting the T cell surface showed distinct pushing and pulling phases without further application of external force (19). The net pulling forces of activating T cells were stronger for high affinity antibodies than for pMHC and absent for control antibodies. Similarly, T cells immobilized on AFM cantilevers exhibited both pushing and pulling forces when contacting activating supported lipid bilayers (76).

Intra- and extracellular molecular force sensors (MFSs) are recent technological additions to the field of nano-mechanosensors and can either have an analog (for peptide/PEG-based sensors) or digital readout (for DNA-based sensors). By defining the mechanical force necessary to unzip a DNA hairpin spanned between a fluorescent dye and a quenching gold particle, Salaita and colleagues successfully measured the range of forces exerted by a defined number of TCR. $CD8^+$ T cells were shown to unzip pMHC-carrying hairpins of 12 pN but not of 19 pN resistance, and $CD4^+$ T cells unzipped hairpins of 4.7 pN resistance (134, 135). In this follow-up study by the same group, force probe-decorated gold particles were anchored to a fluid lipid bilayer (135). Although this system can be considered mobile, the force probe itself was still immobilized on a rigid surface, resulting in a high counter force. Furthermore, the same technique was applied to gain insights into the mechanical sampling of antigenic peptides of varying potency. The authors reported a correlation between tension, potency, and successful TCR triggering (136).

The shortcomings of digital MFSs can be mitigated by using peptide-based analog MFSs. These contain a flexible peptide whose extension is a continuous function of the applied force. Like a macroscopic spring, the higher the pulling force is exerted, the larger the end-to-end distance of the peptide becomes, allowing for direct measurement of the force. This approach has been showcased by the quantification of forces exerted by single integrins by Morimatsu et al. in 2013 (137). Reasonable estimates of single integrin forces were between 2 and 40 pN (AFM rupture forces), and maximal transmitted forces were measured by a digital DNA-based force sensor to be 20–30 pN. However, peptide-based analog force sensors reported only 1–5 pN (extrapolated from bulk measurements) (137) and 1–3 pN (determined by single-molecule FRET measurements) (138) for individual integrins. There is a considerable difference between the results of these studies depending on the acquisition method. Given the more direct

TABLE 2 | Overview of published articles investigating mechanical forces exerted by T cells.

T cells Generate Forces	Exerted Force	Triggered Cells	Ref.
Biomembrane Force Probe	Contact force ~5 pN, ~25 pN (pushing), ~ 2 pN/s loading rate (pulling) [stiffness: 50 pN/µm; sensitivity ~10 pN]	$CD4^+$ T cells (murine), αCD3	(71)
Micropillars (TFM)	~200 pN/pillar	$CD4^+$ T cells (murine)	(133)
Atomic Force Microscopy	~500 pN/cell (push) & ~800 pN/cell (pull)	CD4+ T cells (murine)	(19)
Digital Molecular Force Sensor	12–19 pN/bond [results given in F1/2 values]	$CD8^+$ T cells (murine), pMHCI	(134)
Digital Molecular Force Sensor	>4.7 pN/bond [results given in F1/2 values]	$CD4^+$ T cells (murine), αCD3	(135)
Digital Molecular Force Sensor	>4.7 pN/bond [results given in F1/2 values]	$CD8^+$ T cells (murine), OT-1, pMHCI, αCD3, anti-PD1	(136)
Analog Molecular Force Sensor (single-molecule resolution)	2–6 pN/bond (activating & scanning conditions) [1.5 pN/s loading rate] 2 pN/bond (scanning conditions)	$CD4^+$ T cells (murine), αTCR $CD4^+$ T cells (murine), pMHCII	(101)
AFM	Up to 1 nN/cell pushing, 2 nN/cell pulling	$CD4^+$ T cells (murine), OT-II TCR, pMHC and αCD3 on AFM cantilevers	(19)
AFM	Up to 2.5 nN/cell	$CD4^+$ T cells (murine), 5c.c7 TCR, pMHC on lipid bilayer	(76)
Micropipette Force Probe	Up to 0.5 nN/cell	$CD4^+$ T cells (human), αCD3, αCD28	(72)

pN, picoNewton; αCD3, antibody against CD3; αTCR, antibody against TCRβ; Ref., reference number.

method of data acquisition with single-molecule resolution, the latter studies likely approach the ground truth.

Using an analog peptide-based MFS, we recently quantified the mechanical forces exerted by single TCRs and found a striking difference between activating and scanning conditions (101). We developed a quantitative FRET-based force sensor for application within the immunological synapse, which operates at the single-molecule level (101). As a spring element, we employed a peptide derived from the flagelliform spider silk protein with known elastic properties (139, 140). The biotinylated spring peptide was conjugated to either (i) a stimulating single-chain antibody fragment derived from the TCRβ-reactive H57 monoclonal antibody or (ii) the natural ligand, an MCC-presenting MHC protein. The sensor fits well within the immunological synapse, as it only spans 8 nm in its collapsed configuration (2, 141). We observed 5 to 8 pN force-peaks per TCR for T cells engaging gel-phase and ~2 pN for fluid-phase glass-supported lipid bilayers using the H57-derived MFS, and T cells stimulated with the natural ligand exerted an average force of ~2 pN on gel-phase surfaces. The functional consequences of mechanical forces along the bond axis remain to be investigated, but this study suggests that perpendicular endogenous forces seem negligible. Additionally, temporal single-molecule force profiles revealed a strong molecular force peak of 7.5 pN in early contact situations while T cells scan for antigen and a late arising force peak of 5.6 pN after T-cell activation (101). These results clearly show that force profiles experienced by individual TCR–ligand pairs differ during antigen surveillance and synapse formation. The analog MFS further enabled us to record the time course of force application. We observed linearly increasing forces at a rate of 1.5 pN/s for 2–3 s, followed by a sudden drop to zero, which we speculate is due to TCRs losing their frictional coupling to the actin cytoskeleton.

Force Orientation During TCR Triggering

The impact of the orientation of the force vector on mechanotransduction is another hotly debated topic in the immune surveillance and T-cell triggering fields. The aforementioned experiments using optical tweezers to pull a bead tangentially or perpendicularly with respect to the T cell surface (113) yielded the first insights into a differential response toward the directionality of externally applied forces. Here, non-agonistic antibodies binding to the CD3εγ subunit of the TCR could be used for triggering if pulled tangentially, but not normally with respect to the cell surface. A recent study by the Salaita group yielded the latest insights into the force vector directionality for triggering of TCRs by applying a newly developed technique named SIM-MFM, in which polarization-modulated structured illumination is combined with DNA-based membrane force sensor technology (142). Using an activating antibody against CD3ε, they found no preferred direction of TCR-imposed forces. Although these results do not answer the question of force orientation during immune surveillance, the reported method provides a first step toward resolving the force direction required for TCR triggering.

Impact of Mechanical Forces After Immunological Synapse Formation

Investigating mechanical forces during T-cell activation lays bare numerous differences in the mechanisms employed by various T cell lineages and subtypes. Adhesion cascades, cytoskeletal rearrangement, and, consequently, synapse shape and dynamics are very much dependent on the encountered cellular target. LFA-1 conformation and function clearly depend on the retrograde flow of the actin cytoskeleton and impacts T-cell activation *via* co-stimulation (143, 144). Naïve T cells scanning DCs within the lymphoid tissue experience a rapid LFA-1 maturation cascade in view of the ligand rigidification on the DC membrane (53, 98). The latter study showed that for a DC subset, MHC mobility remained unchanged upon DC cell differentiation (98). Whether MHC molecules also experience mobility changes during or as a result of certain signaling events or synapse formation remains to be addressed (143). Another prominent example of how mechanical forces act during T-cell activation concerns target cell killing by $CD8^+$ T cells. As shown by Huse and colleagues, antigen-experienced cytolytic T cells massively strain and deform the target cell membrane surface and promote in this fashion perforin function (145).

CONCLUDING REMARKS

T cells feature specialized membrane protrusions in varying environmental contexts. In the last few years, membrane protrusions have received much attention for their active role during immune surveillance. Microvilli provide the platform for exerting forces based on their cytoskeletal core and their dynamic nature. So far, the community has gained the following insights into the topic:

(i) Microvilli are important for fast and efficient antigen scanning and sampling.

(ii) Microvilli carry all molecules necessary for adhesion and initiating TCR-proximal signaling.

(iii) Microvilli form limited reaction volumes, which may sensitize T cells for antigen.

(iv) Microvilli may not only be involved in the biochemical probing of the environment but may also be necessary for testing the biomechanical properties of the target cells and tissues.

(v) Glycocalyx and cellular stiffness parameters affect TCR triggering.

Considering the dynamic cellular processes surrounding mechanosurveillance, a precise temporal control of the triggering event is a *sine qua non* for further insights in the field, and based on the aforementioned studies, a number of conclusions can already be drawn:

(i) Tensile forces do affect early T cell activation.

(ii) Force transduction is TCR- and peptide-dependent.

(iii) Shear forces or torque affect T cell activation more strongly than normal forces.

(iv) Generated tensile forces are invariably tied to physiological T cell recognition and precede T cell activation.

(v) Individual molecules at protrusion tips are subject to pulling and pushing forces in the pN range.

(vi) Tensile forces are generated internally by rearrangements of the actin cytoskeleton and do not involve the action of acto-myosin motor proteins.

(vii) Immune synapse formation generates mechanical forces that activate ligand-bound integrins.

(viii) T cell-imposed forces deform target cells and promote their killing.

OPEN QUESTIONS

(i) Are there any lateral movements of antigen-bound microvilli tips? What resistance does the glycocalyx pose to the lateral movement of microvilli? Can the microvillar scanning process be imagined more like a "dragging through the waves" or more like a repeated "poking through the barrier"?

(ii) There is conflicting evidence for increased microvilli life- or dwell times upon antigen encounter. Does antigen binding lead to an arrest of microvilli dynamics? Are such arrests only happening for triggering interactions or also for probing events?

(iii) Is the glycocalyx posing a resistance to microvilli penetration?

(iv) At what point is the force vector reversed from pushing to pulling? How are adhesive interactions influencing this process? Is this process used for ligand discrimination by mechanical probing?

(v) What is the fate of microvillar protrusions after TCR triggering? Are the protein platforms at the microvillar tips evolving to microclusters? What is the impact of LFA-1 maturation on signaling within microvillar protrusions?

(vi) Is the mobility of the pMHCs decisive for the interaction probability and/or rebinding in the context of microvillar scanning? Are target cells mechanically altering their presenting surfaces to allow or inhibit efficient scanning of the surface?

(vii) How are microvilli recognition events coupled to the movement of the entire cell body? How are these signals communicated within the T cell?

AUTHOR CONTRIBUTIONS

JG conceived and drafted the manuscript. JG and LS conducted literature review and wrote the manuscript. LS designed the figures. JG, LS, GS, and JH revised the manuscript. All authors listed have made a substantial, direct, and intellectual contribution to the work and approved it for publication.

FUNDING

This work was supported by the Austrian Science Fund (FWF) project P32307-B (JG, LS, and GS), and I5056-B (LS and GS), and by the Vienna Science and Technology Fund (WWTF) project LS13-030 (JG, LS, JH, and GS).

REFERENCES

1. Malissen B, Bongrand P. Early T Cell Activation: Integrating Biochemical, Structural, and Biophysical Cues. *Annu Rev Immunol* (2015) 33(1):539–61. doi: 10.1146/annurev-immunol-032414-112158
2. Cai E, Marchuk K, Beemiller P, Beppler C, Rubashkin MG, Weaver VM, et al. Visualizing Dynamic Microvillar Search and Stabilization During Ligand Detection by T Cells. *Science* (2017) 356(6338):eaal3118. doi: 10.1126/science.aal3118
3. Jung Y, Riven I, Feigelson SW, Kartvelishvily E, Tohya K, Miyasaka M, et al. Three-Dimensional Localization of T-cell Receptors in Relation to Microvilli Using a Combination of Superresolution Microscopies. *Proc Natl Acad Sci USA* (2016) 113(40):E5916–24. doi: 10.1073/pnas.1605399113
4. Sage PT, Varghese LM, Martinelli R, Sciuto TE, Kamei M, Dvorak AM, et al. Antigen Recognition is Facilitated by Invadosome-like Protrusions Formed by Memory/Effector T Cells. *J Immunol* (2012) 188(8):3686–99. doi: 10.4049/jimmunol.1102594
5. Brodovitch A, Bongrand P, Pierres A. T Lymphocytes Sense Antigens Within Seconds and Make a Decision Within One Minute. *J Immunol* (2013) 191(5):2064–71. doi: 10.4049/jimmunol.1300523
6. Ji L, Lim J, Danuser G. Fluctuations of Intracellular Forces During Cell Protrusion. *Nat Cell Biol* (2008) 10(12):1393–400. doi: 10.1038/ncb1797
7. Pettmann J, Santos AM, Dushek O, Davis SJ. Membrane Ultrastructure and T Cell Activation. *Front Immunol* (2018) 9:2152. doi: 10.3389/fimmu.2018.02152
8. Stinchcombe JC, Bossi G, Booth S, Griffiths GM. The Immunological Synapse of CTL Contains a Secretory Domain and Membrane Bridges. *Immunity* (2001) 15(5):751–61. doi: 10.1016/S1074-7613(01)00234-5
9. Carman CV, Sage PT, Sciuto TE, de la Fuente MA, Geha RS, Ochs HD, et al. Transcellular Diapedesis Is Initiated by Invasive Podosomes. *Immunity* (2007) 26(6):784–97. doi: 10.1016/j.immuni.2007.04.015
10. Dustin ML, Chakraborty AK, Shaw AS. Understanding the Structure and Function of the Immunological Synapse. *Cold Spring Harb Perspect Biol* (2010) 2(10):a002311. doi: 10.1101/cshperspect.a002311
11. Ma Z, Janmey PA, Finkel TH. The Receptor Deformation Model of TCR Triggering. *FASEB J* (2008) 22(4):1002–8. doi: 10.1096/fj.07-9331hyp
12. Davis SJ, Merwe PA. The Kinetic-Segregation Model: TCR Triggering and Beyond. *Nat Immunol* (2006) 7(8):803–9. doi: 10.1038/ni1369
13. Bunnell SC, Hong DI, Kardon JR, Yamazaki T, McGlade CJ, Barr VA, et al. T Cell Receptor Ligation Induces the Formation of Dynamically Regulated Signaling Assemblies. *J Cell Biol* (2002) 158(7):1263–75. doi: 10.1083/jcb.200203043
14. Campi G, Varma R, Dustin ML. Actin and Agonist MHC-peptide Complex-Dependent T Cell Receptor Microclusters as Scaffolds for Signaling. *J Exp Med* (2005) 202(8):1031–6. doi: 10.1084/jem.20051182
15. Yi J, Wu XS, Crites T, Hammer JA. Actin Retrograde Flow and Actomyosin II Arc Contraction Drive Receptor Cluster Dynamics at the Immunological Synapse in Jurkat T Cells. *Mol Biol Cell* (2012) 23(5):834–52. doi: 10.1091/mbc.e11-08-0731
16. Lee K-H, Holdorf AD, Dustin ML, Chan AC, Allen PM, Shaw AS. T Cell Receptor Signaling Precedes Immunological Synapse Formation. *Science* (2002) 295(5559):1539–42. doi: 10.1126/science.1067710
17. Yokosuka T, Sakata-Sogawa K, Kobayashi W, Hiroshima M, Hashimoto-Tane A, Tokunaga M, et al. Newly Generated T Cell Receptor Microclusters Initiate and Sustain T Cell Activation by Recruitment of Zap70 and SLP-76. *Nat Immunol* (2005) 6(12):1253–62. doi: 10.1038/ni1272

18. Hivroz C, Saitakis M. Biophysical Aspects of T Lymphocyte Activation at the Immune Synapse. *Front Immunol* (2016) 7:46. doi: 10.3389/fimmu.2016.00046
19. Hu KH, Butte MJ. T Cell Activation Requires Force Generation. *J Cell Biol* (2016) 213(5):535–42. doi: 10.1083/jcb.201511053
20. Pielak RM, O'Donoghue GP, Lin JJ, Alfieri KN, Fay NC, Low-Nam ST, et al. Early T Cell Receptor Signals Globally Modulate Ligand:Receptor Affinities During Antigen Discrimination. *Proc Natl Acad Sci USA* (2017) 114 (46):12190–5. doi: 10.1073/pnas.1613140114
21. Pullen RH, Abel SM. Mechanical Feedback Enables Catch Bonds to Selectively Stabilize Scanning Microvilli at T-Cell Surfaces. *Mol Biol Cell* (2019) 30(16):2087–95. doi: 10.1091/mbc.E19-01-0048
22. Huppa JB, Gleimer M, Sumen C, Davis MM. Continuous T Cell Receptor Signaling Required for Synapse Maintenance and Full Effector Potential. *Nat Immunol* (2003) 4(8):749–55. doi: 10.1038/ni951
23. Kuhns MS, Davis MM. Tcr Signaling Emerges From the Sum of Many Parts. *Front Immunol* (2012) 3:159. doi: 10.3389/fimmu.2012.00159
24. Moreau JM, Gouirand V, Rosenblum MD. T-Cell Adhesion in Healthy and Inflamed Skin. *JID Innov* (2021) 1(2):100014. doi: 10.1016/j.xjidi.2021.100014
25. Hor JL, Whitney PG, Zaid A, Brooks AG, Heath WR, Mueller SN. Spatiotemporally Distinct Interactions With Dendritic Cell Subsets Facilitates CD4+ and CD8+ T Cell Activation to Localized Viral Infection. *Immunity* (2015) 43(3):554–65. doi: 10.1016/j.immuni.2015.07.020
26. Springer TA. Adhesion Receptors of the Immune System. *Nature* (1990) 346 (6283):425–34. doi: 10.1038/346425a0
27. Bell GI, Dembo M, Bongrand P. Cell Adhesion. Competition Between Nonspecific Repulsion and Specific Bonding. *Biophys J* (1984) 45(6):1051–64. doi: 10.1016/S0006-3495(84)84252-6
28. Ardman B, Sikorski MA, Staunton DE. CD43 Interferes With T-lymphocyte Adhesion. *Proc Natl Acad Sci USA*. (1992) 89(11):5001–5. doi: 10.1073/pnas.89.11.5001
29. Zhao Y, Chien S, Weinbaum S. Dynamic Contact Forces on Leukocyte Microvilli and Their Penetration of the Endothelial Glycocalyx. *Biophys J* (2001) 80(3):1124–40. doi: 10.1016/S0006-3495(01)76090-0
30. Tarbell JM, Pahakis MY. Mechanotransduction and the Glycocalyx. *J Internal Med* (2006) 259(4):339–50. doi: 10.1111/j.1365-2796.2006.01620.x
31. Bi S, Baum LG. Sialic Acids in T Cell Development and Function. *Biochim Biophys Acta (BBA) - Gen Subjects* (2009) 1790(12):1599–610. doi: 10.1016/j.bbagen.2009.07.027
32. Weinbaum S, Tarbell JM, Damiano ER. The Structure and Function of the Endothelial Glycocalyx Layer. *Annu Rev BioMed Eng* (2007) 9:121–67. doi: 10.1146/annurev.bioeng.9.060906.151959
33. Reitsma S, Slaaf DW, Vink H, van Zandvoort MAMJ, oude Egbrink MGA. The Endothelial Glycocalyx: Composition, Functions, and Visualization. *Pflugers Arch* (2007) 454(3):345–59. doi: 10.1007/s00424-007-0212-8
34. Al-Aghbar MA, Jainarayanan AK, Dustin ML, Roffler SR. The Interplay Between Membrane Topology and Mechanical Forces in Regulating T Cell Receptor Activity. *Commun Biol* (2022) 5(1):1–16. doi: 10.1038/s42003-021-02995-1
35. Chang VT, Fernandes RA, Ganzinger KA, Lee SF, Siebold C, McColl J, et al. Initiation of T Cell Signaling by CD45 Segregation at 'Close Contacts'. *Nat Immunol* (2016) 17(5):574–82. doi: 10.1038/ni.3392
36. Agrawal B, Krantz MJ, Parker J, Longenecker BM. Expression of MUC1 Mucin on Activated Human T Cells: Implications for a Role of MUC1 in Normal Immune Regulation. *Cancer Res* (1998) 58(18):4079–81.
37. Mummert ME, Mummert D, Edelbaum D, Hui F, Matsue H, Takashima A. Synthesis and Surface Expression of Hyaluronan by Dendritic Cells and Its Potential Role in Antigen Presentation. *J Immunol* (2002) 169(8):4322–31. doi: 10.4049/jimmunol.169.8.4322
38. Bufi N, Saitakis M, Dogniaux S, Buschinger O, Bohineust A, Richert A, et al. Human Primary Immune Cells Exhibit Distinct Mechanical Properties That Are Modified by Inflammation. *Biophys J* (2015) 108(9):2181–90. doi: 10.1016/j.bpj.2015.03.047
39. Zak A, Merino-Cortés SV, Sadoun A, Mustapha F, Babataheri A, Dogniaux S, et al. Rapid Viscoelastic Changes Are a Hallmark of Early Leukocyte Activation. *Biophys J* (2021) 120(9):1692–704. doi: 10.1016/j.bpj.2021.02.042
40. Cloosen S, Thio M, Vanclée A, van Leeuwen EBM, Senden-Gijsbers BLMG, Oving EBH, et al. Mucin-1 Is Expressed on Dendritic Cells, Both *In Vitro* and *In Vivo*. *Int Immunol* (2004) 16(11):1561–71. doi: 10.1093/intimm/dxh157
41. Johnson LA, Banerji S, Lagerholm BC, Jackson DG. Dendritic Cell Entry to Lymphatic Capillaries Is Orchestrated by CD44 and the Hyaluronan Glycocalyx. *Life Sci Alliance* (2021) 4(5):e202000908. doi: 10.26508/lsa.202000908
42. Teijeira A, Hunter MC, Russo E, Proulx ST, Frei T, Debes GF, et al. T Cell Migration From Inflamed Skin to Draining Lymph Nodes Requires Intralymphatic Crawling Supported by ICAM-1/LFA-1 Interactions. *Cell Rep* (2017) 18(4):857–65. doi: 10.1016/j.celrep.2016.12.078
43. Hunter MC, Teijeira A, Montecchi R, Russo E, Runge P, Kiefer F, et al. Dendritic Cells and T Cells Interact Within Murine Afferent Lymphatic Capillaries. *Front Immunol* (2019) 10:520. doi: 10.3389/fimmu.2019.00520
44. Arasa J, Collado-Diaz V, Halin C. Structure and Immune Function of Afferent Lymphatics and Their Mechanistic Contribution to Dendritic Cell and T Cell Trafficking. *Cells* (2021) 10(5):1269. doi: 10.3390/cells10051269
45. Imbert PRC, Saric A, Pedram K, Bertozzi CR, Grinstein S, Freeman SA. An Acquired and Endogenous Glycocalyx Forms a Bidirectional "Don't Eat" and "Don't Eat Me" Barrier to Phagocytosis. *Curr Biol* (2021) 31(1):77–89. doi: 10.1016/j.cub.2020.09.082
46. Paszek MJ, DuFort CC, Rossier O, Bainer R, Mouw JK, Godula K, et al. The Cancer Glycocalyx Mechanically Primes Integrin-Mediated Growth and Survival. *Nature* (2014) 511(7509):319–25. doi: 10.1038/nature13535
47. Ghasempour S, Freeman SA. The Glycocalyx and Immune Evasion in Cancer. *FEBS J* (2022). doi: 10.1111/febs.16236
48. Möckl L, Pedram K, Roy AR, Krishnan V, Gustavsson A-K, Dorigo O, et al. Quantitative Super-Resolution Microscopy of the Mammalian Glycocalyx. *Dev Cell* (2019) 50(1):57–72.e6. doi: 10.1016/j.devcel.2019.04.035
49. Möckl L. The Emerging Role of the Mammalian Glycocalyx in Functional Membrane Organization and Immune System Regulation. *Front Cell Dev Biol* (2020) 8:253/full. doi: 10.3389/fcell.2020.00253/full
50. Bai K, Wang W. Spatio-Temporal Development of the Endothelial Glycocalyx Layer and Its Mechanical Property *In Vitro*. *J R Soc Interface* (2012) 9(74):2290–8. doi: 10.1098/rsif.2011.0901
51. Bao G, Suresh S. Cell and Molecular Mechanics of Biological Materials. *Nat Mater* (2003) 2(11):715–25. doi: 10.1038/nmat1001
52. Guimarães CF, Gasperini L, Marques AP, Reis RL. The Stiffness of Living Tissues and Its Implications for Tissue Engineering. *Nat Rev Mater* (2020) 5 (5):351–70. doi: 10.1038/s41578-019-0169-1
53. Blumenthal D, Chandra V, Avery L, Burkhardt JK. Mouse T Cell Priming is Enhanced by Maturation-Dependent Stiffening of the Dendritic Cell Cortex. *eLife* (2020) 9:e55995. Akhmanova A, Dustin ML, Hivroz C, Huse M. doi: 10.7554/eLife.55995
54. O'Connor RS, Hao X, Shen K, Bashour K, Akimova T, Hancock WW, et al. Substrate Rigidity Regulates Human T Cell Activation and Proliferation. *J Immunol* (2012) 189(3):1330–9. doi: 10.4049/jimmunol.1102757
55. Judokusumo E, Tabdanov E, Kumari S, Dustin ML, Kam LC. Mechanosensing in T Lymphocyte Activation. *Biophys J* (2012) 102(2): L5–7. doi: 10.1016/j.bpj.2011.12.011
56. Hui KL, Balagopalan L, Samelson LE, Upadhyaya A. Cytoskeletal Forces During Signaling Activation in Jurkat T-Cells. *Mol Biol Cell* (2015) 26 (4):685–95. doi: 10.1091/mbc.E14-03-0830
57. Saitakis M, Dogniaux S, Goudot C, Bufi N, Asnacios S, Maurin M, et al. Different TCR-Induced T Lymphocyte Responses Are Potentiated by Stiffness With Variable Sensitivity. *eLife* (2017) 6:e23190. Dustin ML, editor. doi: 10.7554/eLife.23190
58. Nataraj NM, Dang AP, Kam LC, Lee JH. *Ex Vivo* Induction of Regulatory T Cells From Conventional CD4+ T Cells Is Sensitive to Substrate Rigidity. *J Biomed Materials Res Part A*. (2018) 106(12):3001–8. doi: 10.1002/jbm.a.36489
59. Alatoom A, Sapudom J, Soni P, Mohamed WKE, Garcia-Sabaté A, Teo J. Artificial Biosystem for Modulation of Interactions Between Antigen-Presenting Cells and T Cells. *Adv Biosyst* (2020) 4(7):e2000039. doi: 10.1002/adbi.202000039
60. Tello-Lafoz M, Srpan K, Sanchez EE, Hu J, Remsik J, Romin Y, et al. Cytotoxic Lymphocytes Target Characteristic Biophysical Vulnerabilities in Cancer. *Immunity* (2021) 54(5):1037–1054.e7. doi: 10.1016/j.immuni.2021.02.020

61. van Ewijk W. Immunoelectron-Microscopic Characterization of Lymphoid Microenvironments in the Lymph Node and Thymus. *Ciba Found Symp* (1980) 71:21–37. doi: 10.1002/9780470720547.ch3
62. Polliack A, Lampen N, Clarkson BD, de Harven E, Bentwich Z, Siegal FP, et al. Identification of Human B and T Lymphocytes by Scanning Electron Microscopy. *J Exp Med* (1973) 138(3):607–24. doi: 10.1084/jem.138.3.607
63. Sanderson CJ, Glauert AM. The Mechanism of T-cell Mediated Cytotoxicity. VI. T-Cell Projections and Their Role in Target Cell Killing. *Immunology* (1979) 36(1):119–29.
64. Polliack A. The Contribution of Scanning Electron Microscopy in Haematology: Its Role in Defining Leucocyte and Erythrocyte Disorders. *J Microscopy* (1981) 123(2):177–87. doi: 10.1111/j.1365-2818.1981.tb01293.x
65. Majstoravich S, Zhang J, Nicholson-Dykstra S, Linder S, Friedrich W, Siminovitch KA, et al. Lymphocyte Microvilli Are Dynamic, Actin-Dependent Structures That Do Not Require Wiskott-Aldrich Syndrome Protein (Wasp) for Their Morphology. *Blood* (2004) 104(5):1396–403. doi: 10.1182/blood-2004-02-0437
66. Brossard C, Feuillet V, Schmitt A, Randriamampita C, Romao M, Raposo G, et al. Multifocal Structure of the T Cell - Dendritic Cell Synapse. *Eur J Immunol* (2005) 35(6):1741–53. doi: 10.1002/eji.200425857
67. Ueda H, Zhou J, Xie J, Davis MM. Distinct Roles of Cytoskeletal Components in Immunological Synapse Formation and Directed Secretion. *J Immunol* (2015) 195(9):4117–25. doi: 10.4049/jimmunol.1402175
68. Robert P, Touchard D, Bongrand P, Pierres A. Biophysical Description of Multiple Events Contributing Blood Leukocyte Arrest on Endothelium. *Front Immunol* (2013) 4:108. doi: 10.3389/fimmu.2013.00108
69. Abadier M, Pramod AB, McArdle S, Marki A, Fan Z, Gutierrez E, et al. Effector and Regulatory T Cells Roll at High Shear Stress by Inducible Tether and Sling Formation. *Cell Rep* (2017) 21(13):3885–99. doi: 10.1016/j.celrep.2017.11.099
70. Brodovitch A, Limozin L, Bongrand P, Pierres A. Use of TIRF to Monitor T-Lymphocyte Membrane Dynamics With Submicrometer and Subsecond Resolution. *Cell Mol Bioeng* (2015) 8(1):178–86. doi: 10.1007/s12195-014-0361-8
71. Husson J, Chemin K, Bohineust A, Hivroz C, Henry N. Force Generation Upon T Cell Receptor Engagement. *PloS One* (2011) 6(5):e19680. doi: 10.1371/journal.pone.0019680
72. Sawicka A, Babataheri A, Dogniaux S, Barakat AI, Gonzalez-Rodriguez D, Hivroz C, et al. Micropipette Force Probe to Quantify Single-Cell Force Generation: Application to T-cell Activation. *MBoC* (2017) 28(23):3229–39. Théry M, editor. doi: 10.1091/mbc.e17-06-0385
73. Zucchetti AE, Paillon N, Markova O, Dogniaux S, Hivroz C, Husson J. Influence of External Forces on Actin-Dependent T Cell Protrusions During Immune Synapse Formation. *Biol Cell* (2021) 113(5):250–63. doi: 10.1111/boc.202000133
74. DeMond AL, Mossman KD, Starr T, Dustin ML, Groves JT. T Cell Receptor Microcluster Transport Through Molecular Mazes Reveals Mechanism of Translocation. *Biophys J* (2008) 94(8):3286–92. doi: 10.1529/biophysj.107.119099
75. Varma R, Campi G, Yokosuka T, Saito T, Dustin ML. T Cell Receptor-Proximal Signals Are Sustained in Peripheral Microclusters and Terminated in the Central Supramolecular Activation Cluster. *Immunity* (2006) 25 (1):117–27. doi: 10.1016/j.immuni.2006.04.010
76. Fölser M, Motsch V, Platzer R, Huppa JB, Schütz GJ. A Multimodal Platform for Simultaneous T-Cell Imaging, Defined Activation, and Mechanobiological Characterization. *Cells* (2021) 10(2):235. doi: 10.3390/cells10020235
77. Razvag Y, Neve-Oz Y, Sajman J, Reches M, Sherman E. Nanoscale Kinetic Segregation of TCR and CD45 in Engaged Microvilli Facilitates Early T Cell Activation. *Nat Commun* (2018) 9(1):732. doi: 10.1038/s41467-018-03127-w
78. Orbach R, Su X. Surfing on Membrane Waves: Microvilli, Curved Membranes, and Immune Signaling. *Front Immunol* (2020) 11:2187/full. doi: 10.3389/fimmu.2020.02187/full
79. Aramesh M, Mergenthal S, Issler M, Plochberger B, Weber F, Qin X-H, et al. Functionalized Bead Assay to Measure Three-Dimensional Traction Forces During T-cell Activation. *Nano Lett* (2021) 21(1):507–14. doi: 10.1021/acs.nanolett.0c03964
80. Ghosh S, Di Bartolo V, Tubul L, Shimoni E, Kartvelishvily E, Dadosh T, et al. Erm-Dependent Assembly of T Cell Receptor Signaling and Co-stimulatory Molecules on Microvilli Prior to Activation. *Cell Rep* (2020) 30(10):3434–3447.e6. doi: 10.1016/j.celrep.2020.02.069
81. Farrell MV, Webster S, Gaus K, Goyette J. T Cell Membrane Heterogeneity Aids Antigen Recognition and T Cell Activation. *Front Cell Dev Biol* (2020) 8:609. doi: 10.3389/fcell.2020.00609
82. Rossboth B, Arnold AM, Ta H, Platzer R, Kellner F, Huppa JB, et al. Tcrs Are Randomly Distributed on the Plasma Membrane of Resting Antigen-Experienced T Cells. *Nat Immunol* (2018) 19(8):821–7. doi: 10.1038/s41590-018-0162-7
83. Jung Y, Wen L, Altman A, Ley K. CD45 Pre-Exclusion From the Tips of T Cell Microvilli Prior to Antigen Recognition. *Nat Commun* (2021) 12 (1):3872. doi: 10.1038/s41467-021-23792-8
84. Razvag Y, Neve-Oz Y, Sajman J, Yakovian O, Reches M, Sherman E. T Cell Activation Through Isolated Tight Contacts. *Cell Rep* (2019) 29(11):3506–3521.e6. doi: 10.1016/j.celrep.2019.11.022
85. Aramesh M, Stoycheva D, Sandu I, Ihle SJ, Zünd T, Shiu J-Y, et al. Nanoconfinement of Microvilli Alters Gene Expression and Boosts T Cell Activation. *Proc Natl Acad Sci USA* (2021) 118(40):e2107535118. doi: 10.1073/pnas.2107535118
86. Miller MJ, Safrina O, Parker I, Cahalan MD. Imaging the Single Cell Dynamics of CD4+ T Cell Activation by Dendritic Cells in Lymph Nodes. *J Exp Med* (2004) 200(7):847–56. doi: 10.1084/jem.20041236
87. Mempel TR, Henrickson SE, Von Andrian UH. T-Cell Priming by Dendritic Cells in Lymph Nodes Occurs in Three Distinct Phases. *Nature* (2004) 427 (6970):154–9. doi: 10.1038/nature02238
88. Miller MJ, Hejazi AS, Wei SH, Cahalan MD, Parker I. T Cell Repertoire Scanning Is Promoted by Dynamic Dendritic Cell Behavior and Random T Cell Motility in the Lymph Node. *Proc Natl Acad Sci USA* (2004) 101 (4):998–1003. doi: 10.1073/pnas.0306407101
89. Giannone G, Dubin-Thaler BJ, Döbereiner H-G, Kieffer N, Bresnick AR, Sheetz MP. Periodic Lamellipodial Contractions Correlate With Rearward Actin Waves. *Cell* (2004) 116(3):431–43. doi: 10.1016/S0092-8674(04)00058-3
90. Kaizuka Y, Douglass AD, Varma R, Dustin ML, Vale RD. Mechanisms for Segregating T Cell Receptor and Adhesion Molecules During Immunological Synapse Formation in Jurkat T Cells. *PNAS* (2007) 104 (51):20296–301. doi: 10.1073/pnas.0710258105
91. Murugesan S, Hong J, Yi J, Li D, Beach JR, Shao L, et al. Formin-Generated Actomyosin Arcs Propel T Cell Receptor Microcluster Movement at the Immune Synapse. *J Cell Biol* (2016) 215(3):383–99. doi: 10.1083/jcb.201603080
92. Colin-York H, Javanmardi Y, Skamrahl M, Kumari S, Chang VT, Khuon S, et al. Cytoskeletal Control of Antigen-Dependent T Cell Activation. *Cell Rep* (2019) 26(12):3369–79. doi: 10.1016/j.celrep.2019.02.074
93. Ueda H, Morphew MK, McIntosh JR, Davis MM. Cd4+ T-cell Synapses Involve Multiple Distinct Stages. *Proc Natl Acad Sci USA* (2011) 108 (41):17099–104. doi: 10.1073/pnas.1113703108
94. Fernandes RA, Ganzinger KA, Tzou JC, Jönsson P, Lee SF, Palayret M, et al. A Cell Topography-Based Mechanism for Ligand Discrimination by the T Cell Receptor. *PNAS* (2019) 116(28):14002–10. doi: 10.1073/pnas.1817255116
95. Aleksic M, Dushek O, Zhang H, Shenderov E, Chen J-L, Cerundolo V, et al. Dependence of T Cell Antigen Recognition on T Cell Receptor-Peptide Mhc Confinement Time. *Immunity* (2010) 32(2):163–74. doi: 10.1016/j.immuni.2009.11.013
96. Luxembourg AT, Brunmark A, Kong Y, Jackson MR, Peterson PA, Sprent J, et al. Requirements for Stimulating Naive Cd8+ T Cells *Via* Signal 1 Alone. *J Immunol* (1998) 161(10):5226–35.
97. Segura J-M, Guillaume P, Mark S, Dojcinovic D, Johannsen A, Bosshard G, et al. Increased Mobility of Major Histocompatibility Complex I-Peptide Complexes Decreases the Sensitivity of Antigen Recognition. *J Biol Chem* (2008) 283(35):24254–63. doi: 10.1074/jbc.M803549200
98. Comrie WA, Li S, Boyle S, Burkhardt JK. The Dendritic Cell Cytoskeleton Promotes T Cell Adhesion and Activation by Constraining ICAM-1 Mobility. *J Cell Biol* (2015) 208(4):457–73. doi: 10.1083/jcb.201406120
99. Mecheri S, Edidin M, Dannecker G, Mittler RS, Hoffmann MK. Immunogenic Ia-binding Peptides Immobilize the Ia Molecule and Facilitate Its Aggregation on the B Cell Membrane. Control by the M1s-1 Gene. *J Immunol* (1990) 144(4):1361–8.

100. Treanor B, Harwood NE, Batista FD. Microsignalosomes: Spatially Resolved Receptor Signalling. *Biochem Soc Trans* (2009) 37(5):1014–8. doi: 10.1042/BST0371014
101. Göhring J, Kellner F, Schrangl L, Platzer R, Klotzsch E, Stockinger H, et al. Temporal Analysis of T-Cell Receptor-Imposed Forces *Via* Quantitative Single Molecule Fret Measurements. *Nat Commun* (2021) 12(1):2502. doi: 10.1038/s41467-021-22775-z.
102. Hsu C-J, Hsieh W-T, Waldman A, Clarke F, Huseby ES, Burkhardt JK, et al. Ligand Mobility Modulates Immunological Synapse Formation and T Cell Activation. *PloS One* (2012) 7(2):e32398. doi: 10.1371/journal.pone.0032398
103. Dillard P, Varma R, Sengupta K, Limozin L. Ligand-Mediated Friction Determines Morphodynamics of Spreading T Cells. *Biophys J* (2014) 107 (11):2629–38. doi: 10.1016/j.bpj.2014.10.044
104. Hellmeier JP, Platzer R, Karner A, Motsch V, Bamieh V, Preiner J, et al. Spatial Requirements for T-Cell Receptor Triggering Probed Via Functionalized Dna Origami Platforms. *Biophys J* (2020) 118(3):245a. doi: 10.1016/j.bpj.2019.11.1437
105. Mattila PK, Lappalainen P. Filopodia: Molecular Architecture and Cellular Functions. *Nat Rev Mol Cell Biol* (2008) 9(6):446–54. doi: 10.1038/nrm2406
106. Dai J, Sheetz MP. Mechanical Properties of Neuronal Growth Cone Membranes Studied by Tether Formation With Laser Optical Tweezers. *Biophys J* (1995) 68(3):988–96. doi: 10.1016/S0006-3495(95)80274-2
107. Schwarz US, Gardel ML. United We Stand: Integrating the Actin Cytoskeleton and Cell-Matrix Adhesions in Cellular Mechanotransduction. *J Cell Sci* (2012) 125(Pt 13):3051–60. doi: 10.1242/jcs.093716
108. Labernadie A, Bouissou A, Delobelle P, Balor S, Voituriez R, Proag A, et al. Protrusion Force Microscopy Reveals Oscillatory Force Generation and Mechanosensing Activity of Human Macrophage Podosomes. *Nat Commun* (2014) 5(1):5343. doi: 10.1038/ncomms6343
109. Glazier R, Salaita K. Supported Lipid Bilayer Platforms to Probe Cell Mechanobiology. *Biochim Biophys Acta* (2017) 1859(9 Pt A):1465–82. doi: 10.1016/j.bbamem.2017.05.005
110. Tamzalit F, Wang MS, Jin W, Tello-Lafoz M, Boyko V, Heddleston JM, et al. Interfacial Actin Protrusions Mechanically Enhance Killing by Cytotoxic T Cells. *Sci Immunol* (2019) 4(33):22. doi: 10.1126/sciimmunol.aav5445
111. Dustin ML, Bromley SK, Davis MM, Zhu C. Identification of Self Through Two-Dimensional Chemistry and Synapses. *Annu Rev Cell Dev Biol* (2001) 17:133–57. doi: 10.1146/annurev.cellbio.17.1.133
112. Huppa JB, Axmann M, Mörtelmaier MA, Lillemeier BF, Newell EW, Brameshuber M, et al. Tcr-peptide-MHC Interactions *In Situ* Show Accelerated Kinetics and Increased Affinity. *Nature* (2010) 463(7283):963–7. doi: 10.1038/nature08746
113. Kim ST, Takeuchi K, Sun Z-YJ, Touma M, Castro CE, Fahmy A, et al. The αβ T Cell Receptor Is an Anisotropic Mechanosensor. *J Biol Chem* (2009) 284 (45):31028–37. doi: 10.1074/jbc.M109.052712
114. Li Y-C, Chen B-M, Wu P-C, Cheng T-L, Kao L-S, Tao M-H, et al. Cutting Edge: Mechanical Forces Acting on T Cells Immobilized *Via* the TCR Complex Can Trigger TCR Signaling. *J Immunol* (2010) 184(11):5959–63. doi: 10.4049/jimmunol.0900775
115. Puech P-H, Nevoltris D, Robert P, Limozin L, Boyer C, Bongrand P. Force Measurements of TCR/pMHC Recognition at T Cell Surface. *PloS One* (2011) 6(7):e22344. doi: 10.1371/journal.pone.0022344
116. Pryshchep S, Zarnitsyna VI, Hong J, Evavold BD, Zhu C. Accumulation of Serial Forces on TCR and CD8 Frequently Applied by Agonist Antigenic Peptides Embedded in MHC Molecules Triggers Calcium in T Cells. *J Immunol* (2014) 193(1):68–76. doi: 10.4049/jimmunol.1303436
117. Liu B, Chen W, Evavold BD, Zhu C. Accumulation of Dynamic Catch Bonds Between TCR and Agonist Peptide-MHC Triggers T Cell Signaling. *Cell* (2014) 157(2):357–68. doi: 10.1016/j.cell.2014.02.053
118. Das DK, Feng Y, Mallis RJ, Li X, Keskin DB, Hussey RE, et al. Force-Dependent Transition in the T-Cell Receptor β-Subunit Allosterically Regulates Peptide Discrimination and pMHC Bond Lifetime. *Proc Natl Acad Sci USA* (2015) 112(5):1517–22. doi: 10.1073/pnas.1424829112
119. Hong J, Persaud SP, Horvath S, Allen PM, Evavold BD, Zhu C. Force-Regulated *In Situ* TCR-Peptide-Bound Mhc Class Ii Kinetics Determine Functions of CD4+ T Cells. *J Immunol* (2015) 195(8):3557–64. doi: 10.4049/jimmunol.1501407
120. Mallis RJ, Bai K, Arthanari H, Hussey RE, Handley M, Li Z, et al. Pre-TCR Ligand Binding Impacts Thymocyte Development Before αβtcr Expression. *Proc Natl Acad Sci USA* (2015) 112(27):8373–8. doi: 10.1073/pnas.1504971112
121. Liu B, Chen W, Natarajan K, Li Z, Margulies DH, Zhu C. The Cellular Environment Regulates *In Situ* Kinetics of T-cell Receptor Interaction With Peptide Major Histocompatibility Complex. *Eur J Immunol* (2015) 45 (7):2099–110. doi: 10.1002/eji.201445358
122. Feng Y, Brazin KN, Kobayashi E, Mallis RJ, Reinherz EL, Lang MJ. Mechanosensing Drives Acuity of $\alpha\beta$ T-cell Recognition. *Proc Natl Acad Sci USA* (2017) 114(39):E8204–13. doi: 10.1073/pnas.1703559114
123. Sibener LV, Fernandes RA, Kolawole EM, Carbone CB, Liu F, McAffee D, et al. Isolation of a Structural Mechanism for Uncoupling T Cell Receptor Signaling From Peptide-MHC Binding. *Cell* (2018) 174(3):672–687.e27. doi: 10.1016/j.cell.2018.06.017
124. Bernardeau K, Gouard S, David G, Ruellan A-L, Devys A, Barbet J, et al. Assessment of CD8 Involvement in T Cell Clone Avidity by Direct Measurement of HLA-A2/Mage3 Complex Density Using a High-Affinity TCR Like Monoclonal Antibody. *Eur J Immunol* (2005) 35(10):2864–75. doi: 10.1002/eji.200526307
125. Purbhoo MA, Irvine DJ, Huppa JB, Davis MM. T Cell Killing Does Not Require the Formation of a Stable Mature Immunological Synapse. *Nat Immunol* (2004) 5(5):524–30. doi: 10.1038/ni1058
126. Chabaud M, Paillon N, Gaus K, Hivroz C. Mechanobiology of Antigen-Induced T Cell Arrest. *Biol Cell* (2020) 112(7):196–212. doi: 10.1111/boc.201900093
127. Allard JF, Dushek O, Coombs D, van der Merwe PA. Mechanical Modulation of Receptor-Ligand Interactions at Cell-Cell Interfaces. *Biophys J* (2012) 102 (6):1265–73. doi: 10.1016/j.bpj.2012.02.006
128. Kumari S, Mak M, Poh Y, Tohme M, Watson N, Melo M, et al. Cytoskeletal Tension Actively Sustains the Migratory T-Cell Synaptic Contact. *EMBO J* (2020) 39(5):e102783. doi: 10.15252/embj.2019102783
129. Zhu C, Chen Y, Ju LA. Dynamic Bonds and Their Roles in Mechanosensing. *Curr Opin Chem Biol* (2019) 53:88–97. doi: 10.1016/j.cbpa.2019.08.005
130. Limozin L, Bridge M, Bongrand P, Dushek O, van der Merwe PA, Robert P. Tcr–pMHC Kinetics Under Force in a Cell-Free System Show No Intrinsic Catch Bond, But a Minimal Encounter Duration Before Binding. *Proc Natl Acad Sci USA* (2019) 116(34):16943–8. doi: 10.1073/pnas.1902141116
131. Hosseini BH, Louban I, Djandji D, Wabnitz GH, Deeg J, Bulbuc N, et al. Immune Synapse Formation Determines Interaction Forces Between T Cells and Antigen-Presenting Cells Measured by Atomic Force Microscopy. *Proc Natl Acad Sci USA* 106(42):17852–7. doi: 10.1073/pnas.0905384106
132. Lim TS, Mortellaro A, Lim CT, Hämmerling GJ, Ricciardi-Castagnoli P. Mechanical Interactions Between Dendritic Cells and T Cells Correlate With T Cell Responsiveness. *J Immunol* (2011) 187(1):258–65. doi: 10.4049/jimmunol.1100267
133. Bashour KT, Gondarenko A, Chen H, Shen K, Liu X, Huse M, et al. CD28 and CD3 Have Complementary Roles in T-Cell Traction Forces. *PNAS* (2014) 111(6):2241–6. doi: 10.1073/pnas.1315606111
134. Liu Y, Blanchfield L, Ma VP-Y, Andargachew R, Galior K, Liu Z, et al. DNA-Based Nanoparticle Tension Sensors Reveal That T-cell Receptors Transmit Defined Pn Forces to Their Antigens for Enhanced Fidelity. *PNAS* (2016) 113 (20):5610–5. doi: 10.1073/pnas.1600163113
135. Ma VP-Y, Liu Y, Blanchfield L, Su H, Evavold BD, Salaita K. Ratiometric Tension Probes for Mapping Receptor Forces and Clustering at Intermembrane Junctions. *Nano Lett* (2016) 16(7):4552–9. doi: 10.1021/acs.nanolett.6b01817
136. Ma R, Kellner AV, Ma VP-Y, Su H, Deal BR, Brockman JM, et al. DNA Probes That Store Mechanical Information Reveal Transient Piconewton Forces Applied by T Cells. *Proc Natl Acad Sci USA* (2019) 116(34):16949–54. doi: 10.1073/pnas.1904034116
137. Morimatsu M, Mekhdjian AH, Adhikari AS, Dunn AR. Molecular Tension Sensors Report Forces Generated by Single Integrin Molecules in Living Cells. *Nano Lett* (2013) 13(9):3985–9. doi: 10.1021/nl4005145
138. Chang AC, Mekhdjian AH, Morimatsu M, Denisin AK, Pruitt BL, Dunn AR. Single Molecule Force Measurements in Living Cells Reveal a Minimally Tensioned Integrin State. *ACS Nano* (2016) 10(12):10745–52. doi: 10.1021/acsnano.6b03314

139. Becker N, Oroudjev E, Mutz SJ, Cleveland JP, Hansma PK, Hayashi CY, et al. Molecular Nanosprings in Spider Capture-Silk Threads. *Nat Materials* (2003) 2(4):278–83. doi: 10.1038/nmat858
140. Brenner MD, Zhou R, Conway DE, Lanzano L, Gratton E, Schwartz MA, et al. Spider Silk Peptide Is a Compact, Linear Nanospring Ideal for Intracellular Tension Sensing. *Nano Lett* (2016) 16(3):2096–102. doi: 10.1021/acs.nanolett.6b00305
141. Choudhuri K, Wiseman D, Brown MH, Gould K, van der Merwe PA. T-Cell Receptor Triggering Is Critically Dependent on the Dimensions of Its peptide-MHC Ligand. *Nature* (2005) 436(7050):578–82. doi: 10.1038/nature03843
142. Blanchard A, Combs JD, Brockman JM, Kellner AV, Glazier R, Su H, et al. Turn-Key Mapping of Cell Receptor Force Orientation and Magnitude Using a Commercial Structured Illumination Microscope. *Nat Commun* (2021) 12:4693. doi: 10.1038/s41467-021-24602-x
143. Basu R, Huse M. Mechanical Communication at the Immunological Synapse. *Trends Cell Biol* (2017) 27(4):241–54. doi: 10.1016/j.tcb.2016.10.005
144. Comrie WA, Burkhardt JK. Action and Traction: Cytoskeletal Control of Receptor Triggering at the Immunological Synapse. *Front Immunol* (2016) 7:68. doi: 10.3389/fimmu.2016.00068
145. Basu R, Whitlock BM, Husson J, Le Floc'h A, Jin W, Oyler-Yaniv A, et al. Cytotoxic T Cells Use Mechanical Force to Potentiate Target Cell Killing. *Cell* (2016) 165(1):100–10. doi: 10.1016/j.cell.2016.01.021

Conflict of Interest: The authors declare that the research was conducted in the absence of any commercial or financial relationships that could be construed as a potential conflict of interest.

Publisher's Note: All claims expressed in this article are solely those of the authors and do not necessarily represent those of their affiliated organizations, or those of the publisher, the editors and the reviewers. Any product that may be evaluated in this article, or claim that may be made by its manufacturer, is not guaranteed or endorsed by the publisher.

frontiers | Frontiers in Immunology

ORIGINAL RESEARCH
published: 09 June 2022
doi: 10.3389/fimmu.2022.856977

Ena/VASP Protein-Mediated Actin Polymerization Contributes to Naïve CD8$^+$ T Cell Activation and Expansion by Promoting T Cell–APC Interactions *In Vivo*

Monique M. Waldman[1,2], *Jeremy T. Rahkola*[3], *Ashton L. Sigler*[1,2], *Jeffrey W. Chung*[1,2], *Benjamin A. S. Willett*[1], *Ross M. Kedl*[1], *Rachel S. Friedman*[1,2] *and Jordan Jacobelli*[1,2,4*]

[1] *Department of Immunology and Microbiology, University of Colorado Anschutz Medical Campus, Aurora, CO, United States,* [2] *Barbara Davis Research Center, University of Colorado Anschutz Medical Campus, Aurora, CO, United States,* [3] *Rocky Mountain Regional Veterans Affairs (VA) Medical Center, Department of Medicine, University of Colorado Anschutz Medical Campus, Aurora, CO, United States,* [4] *Department of Immunology and Genomic Medicine, National Jewish Health, Denver, CO, United States*

OPEN ACCESS

Edited by:
Jerome Delon, INSERM U1016 Institut Cochin, France

Reviewed by:
Tomoya Katakai, Niigata University, Japan
Hélène D. Moreau, INSERM U932 Immunité et Cancer, France
Federica Benvenuti, International Centre for Genetic Engineering and Biotechnology, Italy

***Correspondence:**
Jordan Jacobelli
Jordan.Jacobelli@cuanschutz.edu

Specialty section:
This article was submitted to T Cell Biology, a section of the journal Frontiers in Immunology

Received: *18 January 2022*
Accepted: *28 April 2022*
Published: *09 June 2022*

Citation:
Waldman MM, Rahkola JT, Sigler AL, Chung JW, Willett BAS, Kedl RM, Friedman RS and Jacobelli J (2022) Ena/VASP Protein-Mediated Actin Polymerization Contributes to Naïve CD8$^+$ T Cell Activation and Expansion by Promoting T Cell–APC Interactions In Vivo. Front. Immunol. 13:856977. doi: 10.3389/fimmu.2022.856977

Naïve T cell activation in secondary lymphoid organs such as lymph nodes (LNs) occurs upon recognition of cognate antigen presented by antigen presenting cells (APCs). T cell activation requires cytoskeleton rearrangement and sustained interactions with APCs. Enabled/vasodilator-stimulated phosphoprotein (Ena/VASP) proteins are a family of cytoskeletal effector proteins responsible for actin polymerization and are frequently found at the leading edge of motile cells. Ena/VASP proteins have been implicated in motility and adhesion in various cell types, but their role in primary T cell interstitial motility and activation has not been explored. Our goal was to determine the contribution of Ena/VASP proteins to T cell–APC interactions, T cell activation, and T cell expansion *in vivo*. Our results showed that naïve T cells from Ena/VASP-deficient mice have a significant reduction in antigen-specific T cell accumulation following *Listeria monocytogenes* infection. The kinetics of T cell expansion impairment were further confirmed in Ena/VASP-deficient T cells stimulated *via* dendritic cell immunization. To investigate the cause of this T cell expansion defect, we analyzed T cell–APC interactions *in vivo* by two-photon microscopy and observed fewer Ena/VASP-deficient naïve T cells interacting with APCs in LNs during priming. We also determined that Ena/VASP-deficient T cells formed conjugates with significantly less actin polymerization at the T cell–APC synapse, and

that these conjugates were less stable than their WT counterparts. Finally, we found that Ena/VASP-deficient T cells have less LFA-1 polarized to the T cell–APC synapse. Thus, we conclude that Ena/VASP proteins contribute to T cell actin remodeling during T cell–APC interactions, which promotes the initiation of stable T cell conjugates during APC scanning. Therefore, Ena/VASP proteins are required for efficient activation and expansion of T cells *in vivo*.

Keywords: T cell, cytoskeleton, VASP, T cell activation, T cell motility, two-photon microscopy, immunological synapse, EVL

INTRODUCTION

T cells patrol the body for signs of infection and cancer by recirculating through the blood and lymph and homing to secondary lymphoid organs (SLOs) such as lymph nodes (LNs). While patrolling, T cells scan antigen presenting cells (APCs) for the presence of their cognate peptide antigens bound to proteins encoded in the major histocompatibility complex (MHC). To scan for antigen within the LN, migrating T cells utilize the fibroblastic reticular cell (FRC) network and the associated network of lymphoid resident dendritic cells (DCs) as guiding structures for otherwise stochastic exploration (1–3). Naïve T cell motility is driven by chemokine receptor signaling, which stimulates actin polymerization. This actin polymerization is then translated into forward movement by the frictional interface mediated by low affinity integrin adhesion (4) and through interactions with the local environmental topography (5). T cells undergo rapid, amoeboid movement within LNs, and significant alterations in T cell speed and directionality can skew APC scanning and lead to defects in T cell priming (6, 7). Indeed, actin retrograde flow promoted by CCL19 enhances the crawling/scanning behavior of naive T cells and optimizes interactions with APCs, leading to a higher frequency of T cell encounters with rare cognate antigen *in vitro* (8).

Upon encounter with cognate antigen-bearing APCs, T cells receive "stop signals" by which the T cell decelerates and eventually arrests as actin polymerization is translated towards the development of a stable interaction between the T cell and APC instead of into forward motility (9, 10). This can occur gradually and sequentially as T cells accumulate activation signals over multiple short serial interactions with APCs (11, 12). These serial interactions function to initiate the process of T cell activation, accumulating signals that lead to changes within the T cell necessary to override the pull of chemokine mediated motility. For example, T cell receptor (TCR) signaling leads to the downregulation of CCR7 and the conversion of LFA-1 into a high affinity conformation (13). This decreases chemokine mediated motility and increases adhesion between T cells and APCs, facilitating the transition into long-lasting and stable interactions.

To maintain sustained T cell–APC interactions, T cells undergo extensive actin reorganization and form an immunological synapse (IS). The IS is comprised of distinct zones of filamentous actin (F-actin) composition, which also structurally facilitates the organization, movement, and internalization of TCRs and co-receptors (14–16). Within these synapses, microclusters of TCRs, co-stimulatory molecules, and adhesion receptors engage their ligands on the APC surface to trigger downstream signaling, resulting in T cell activation and proliferation (17). Actin cytoskeletal effectors, such as formins and WASP, have been shown to contribute to the formation of actin structures important for TCR centralization and to actin retrograde flow important for regulating integrin function and T cell–APC interactions (18–23). The classic, TCR monofocal configuration of the IS is typically observed in artificial synapses created with supported lipid bilayers or in synapses with APC cell lines (24, 25). However, physiological interactions between T cells and DCs often lead to multifocal synapses, in which there are multiple local ensembles of TCR, co-receptors, and adhesion molecules (26). While there have been many effector molecules identified as essential for these processes in *in vitro* systems, there is still more to uncover in detailing the specific proteins responsible for actin rearrangement throughout T cell activation. In particular, the function of specific cytoskeletal effectors of actin remodeling in primary T cell activation *in vivo* is still mostly unknown.

The spatial and temporal organization of the actin cytoskeleton is regulated at many levels: cells rely on effectors of actin polymerization to efficiently nucleate and elongate actin filaments, actin filament capping proteins to stop polymerization, and severing proteins to break filaments (27, 28). Branched actin networks are initiated through the actin-related protein 2/3 (Arp2/3) complex, which binds to pre-existing actin filaments to nucleate new filaments at an angle of 70 degrees. In T cells, linear actin polymerization is conducted by two major families of effector proteins: the formin family and the enabled/vasodilator-stimulated phosphoprotein (Ena/VASP) family. The formin family, which can both nucleate new linear actin filament production and elongate actin filaments, has been implicated in T cell activation, egress from the thymus, and activated T cell trafficking to inflamed tissues (29–32). Ena/VASP proteins enhance barbed-end elongation and prevent capping proteins from binding. Although Ena/VASP proteins are not actin polymerization nucleators, they participate in forming branched actin networks by linearly elongating filaments nucleated by Arp2/3, and in linear actin networks by elongating formin-initiated filaments (33, 34). The Ena/VASP family is composed of three members—Mena (mammalian Ena), Ena/VASP-like (EVL), and VASP—though only EVL and VASP are expressed in hematopoietic cells (35). EVL and VASP share

significant structural homology including an N-terminal EVH1 domain, which regulates cellular localization, and a C-terminal EVH2 domain, which mediates interactions with actin (36). EVL and VASP localize to lamellipodia, filopodia tips, and adhesive sites such as fibroblast focal adhesions (36–43). Fibroblasts lacking Ena/VASP produce shorter filopodia and a slower moving lamellipodium, which paradoxically leads to enhanced fibroblast motility (44). In other cell types, however, loss of Ena/VASP impairs the generation of traction forces as well as integrin-mediated adhesion and can impair motility (45). Further, metastatic cancers express higher levels of EVL, and small-molecule inhibitors of the EVH1 domain impair invasion and extravasation of breast cancer cells (46, 47).

While the roles of the Ena/VASP protein family in the motility, adhesion, and sensory capacity of many cell types are well defined, they have not been studied extensively in T cells. Data from experiments using Jurkat cells *in vitro* suggests that EVL plays a role in actin remodeling downstream of TCR signaling (40, 48), but this has not been confirmed in primary cells or *in vivo*. Previous work from our lab indicates that EVL and VASP play a role in the expression and function of the integrin alpha-4 subunit (CD49d), and are therefore required for activated T cell transendothelial migration and trafficking, but are not necessary for naïve T cell trafficking to LNs and spleen (49). This previous work also showed that EVL and VASP can compensate for each other since only EVL/VASP doubly deficient T cells show a trafficking defect (49).

Given the roles of the Ena/VASP protein family in other cell types, coupled with the understanding that actin remodeling has key effects on T cell activation, we sought to explore the role of the Ena/VASP protein family in the cytoskeletal rearrangements necessary for T cell navigation in LNs, finding and engaging APCs, and activation *in vivo*. In this paper, we demonstrate that EVL/VASP proteins contribute to the accumulation of T cells during an immune response. Further, we find a novel role for the Ena/VASP protein family in facilitating the initiation and stability of T cell–APC interactions, and in mediating actin polymerization at the IS.

RESULTS

Ena/VASP Deficiency Reduces T Cell Expansion in Response to *Listeria monocytogenes* Challenge

Since EVL/VASP proteins can promote actin polymerization in response to CD3 stimulation in Jurkat T cells (48) and effector T cell trafficking and integrin function are modulated by Ena/VASP proteins (49), we investigated the role of Ena/VASP proteins in T cell responses and differentiation *in vivo*. We thus analyzed the effect of EVL/VASP deletion in naïve $CD8^+$ T cell expansion following *Listeria monocytogenes* (LM) infection. To assess T cell intrinsic effects, we adoptively co-transferred low numbers (to approximate physiological conditions) of naïve WT and EVL/VASP double knockout (dKO) Ovalbumin (OVA)-specific $CD8^+$ OT-I T cells into WT recipient mice (**Figures 1A, B**). First, we established that under homeostatic conditions naïve WT and EVL/VASP dKO OT-I T cells had similar homing and persistence in the spleen (**Figure 1C**). Next, we infected recipient mice with LM expressing OVA (LM-OVA). On day 6 after the infection, we found that the number of EVL/VASP dKO OT-I T cells in the spleen was significantly reduced compared to their WT counterparts (2.6-fold average reduction compared to WT) (**Figure 1D**). We next analyzed T cell proliferation on day 3 post-LM infection by proliferation dye dilution. Our data showed a significantly reduced number of divided T cells in the EVL/VASP dKO population (**Figure 1E**). These data suggest that EVL/VASP proteins play an important role in $CD8^+$ T cell expansion and accumulation in response to LM infection. Additionally, in the EVL/VASP dKO population there was a small but significant reduction in the number and percentage of short-lived effector cells (SLECs), characterized by $KLRG1^{hi}$ $CD127^{lo}$ expression (**Figure 1F**).

EVL/VASP dKO T Cells Defects Are not Due to Thymic Priming Differences

We previously showed that T cell subset development is largely normal in the EVL/VASP dKO mice (49). However, since EVL/VASP dKO mice are germline double knockouts, their thymic epithelial cells and DCs are also deficient in EVL/VASP, which may alter T cell signaling and priming during thymocyte development. Thus, to ensure that phenotypic differences observed in EVL/VASP dKO T cells were T cell-intrinsic and not due to T cell development in an EVL/VASP-deficient thymic environment, we created bone marrow chimeras. We transferred bone marrow from WT or EVL/VASP dKO OT-I mice into separate WT recipients, such that both control and EVL/VASP dKO T cells matured within WT thymuses. After ≥8 weeks, we isolated peripheral EVL/VASP dKO and WT OT-I T cells from the LNs and spleen of bone marrow chimeras and adoptively co-transferred them into WT recipient mice for LM-OVA infection (**Supplementary Figure 1A**). We then compared T cell numbers in the spleens 6 days after LM-OVA infection as described above. Regardless of whether T cells matured in bone marrow chimeras or endogenously in intact mice, EVL/VASP dKO T cell responses were similarly impaired compared to WT T cells (**Supplementary Figure 1B**). These results indicate that EVL/VASP dKO T cell expansion defects are T-cell intrinsic, and not due to differences in the thymic environment in which they develop.

Ena/VASP Deficiency Reduces T Cell Expansion Following Immunization With Dendritic Cells

To investigate the cause of the T cell expansion defect, we next established an *in vivo* system in which we could activate T cells while also being able to visualize the interaction of T cells with APCs in the physiological environment of a LN. For this purpose, we used antigen-pulsed bone marrow-derived dendritic cells (BMDCs) as a stimulus (**Figure 2A**). First, similar to the LM infection experiments, we confirmed that

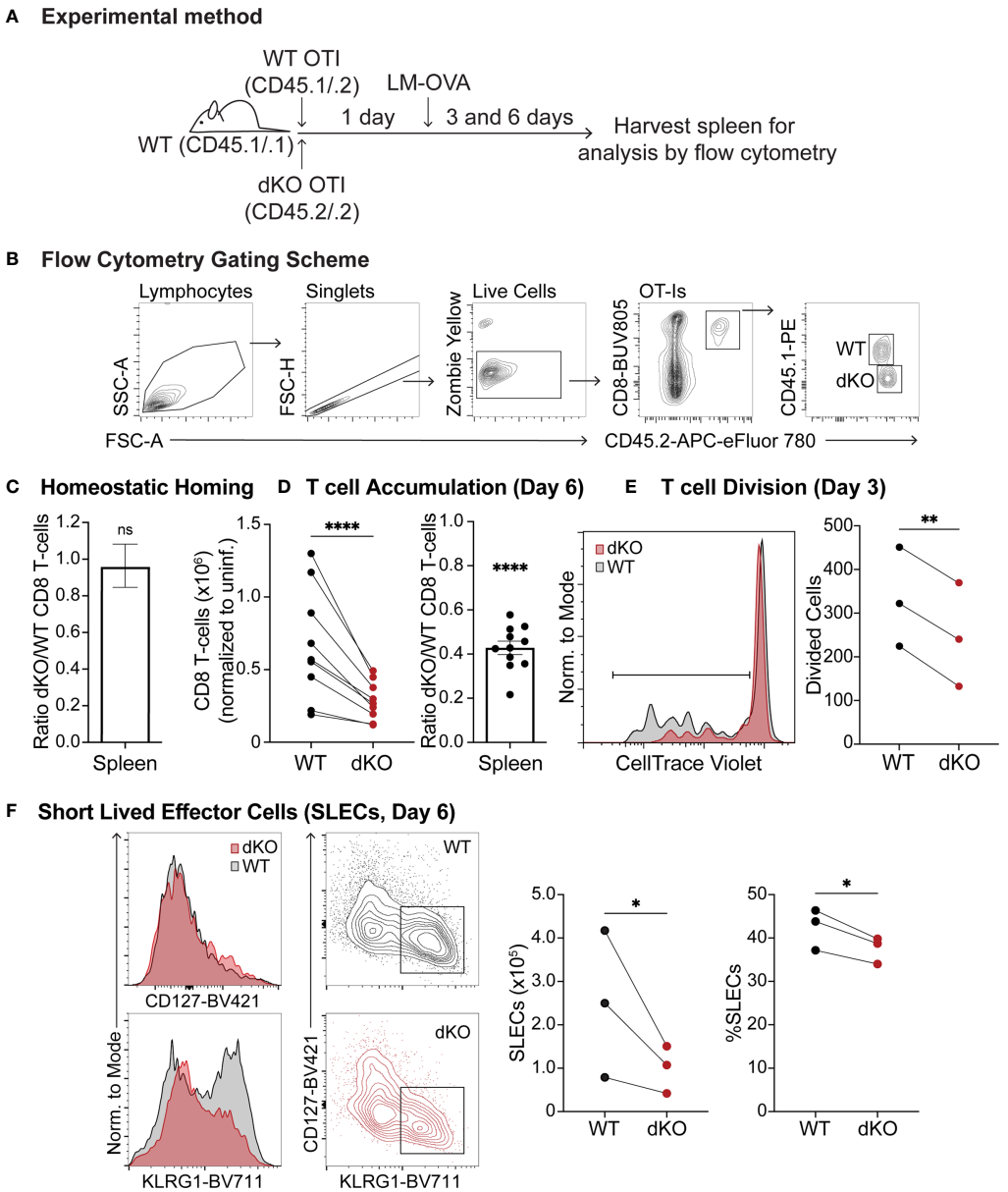

FIGURE 1 | Ena/VASP deficiency reduces T cell accumulation in response to Listeria Monocytogenes challenge. Congenically distinct naïve WT CD45$^{.1/.2}$ OT-I and EVL/VASP dKO CD45$^{.2/.2}$ OT-I T cells were isolated from donor mice and transferred at a 1:1 ratio I.V. into WT CD45$^{.1/.1}$ recipient mice. **(A)** Graphical schematic of the experimental method. **(B)** Representative flow cytometry gating scheme used to detect transferred T cells. **(C)** WT and EVL/VASP dKO naïve T cells have similar persistence *in vivo*. 1×10^6 WT and EVL/VASP dKO naïve OT-I CD8$^+$ T cells, were co-transferred I.V. into uninfected WT CD45$^{.1/.1}$ recipient mice and spleens were harvested 6 days later to determine a persistence baseline. **(D–F)** EVL/VASP dKO T cells have reduced proliferation and accumulation in response to LM challenge. 10,000 of each naïve WT CD45$^{.1/.2}$ OT-I and EVL/VASP dKO CD45$^{.2/.2}$ OT-I T cells were co-transferred I.V. into WT CD45$^{.1/.1}$ recipient mice one day before infection with LM-OVA (2×10^3 PFUs). Spleens from recipient mice were then harvested 3 or 6 days later for analysis by flow cytometry. **(D)** T cell numbers recovered from the spleen at day 6 post LM infection (left) and ratios of EVL/VASP dKO/WT CD8$^+$ T cells (right). EVL/VASP dKO T cell numbers were normalized to the ratio of EVL/VASP dKO/WT T cells recovered from spleens of uninfected recipient mice at day 6 from the same experiment [i.e., homing ratio in **(C)**]. **(E)** Example CTV proliferation dye dilution curves and quantification of the average number of divided cells, determined by CTV dilution, from spleens on day 3 post LM-OVA infection. **(F)** Representative histograms of KLRG1 and CD127 expression, and flow cytometry contour plots showing the gates used to identify SLECs (KLRG1^{hi} CD127^{lo}). The number (normalized to uninfected mice) and percent of WT and EVL/VASP dKO SLEC T cells are plotted. Data are from ≥9 experiments each with ≥2 mice per group/experiment, except for **(E)**, **(F)**, which are from 3 independent experiments with ≥2 mice per group/experiment. Significance was defined by paired t tests (for T cell numbers) and one sample t tests compared to a hypothetical value of 1.0 (for the EVL/VASP dKO/WT ratios); ns is not significant, * is $p < 0.05$, ** is $p < 0.01$, and **** is $p < 0.0001$.

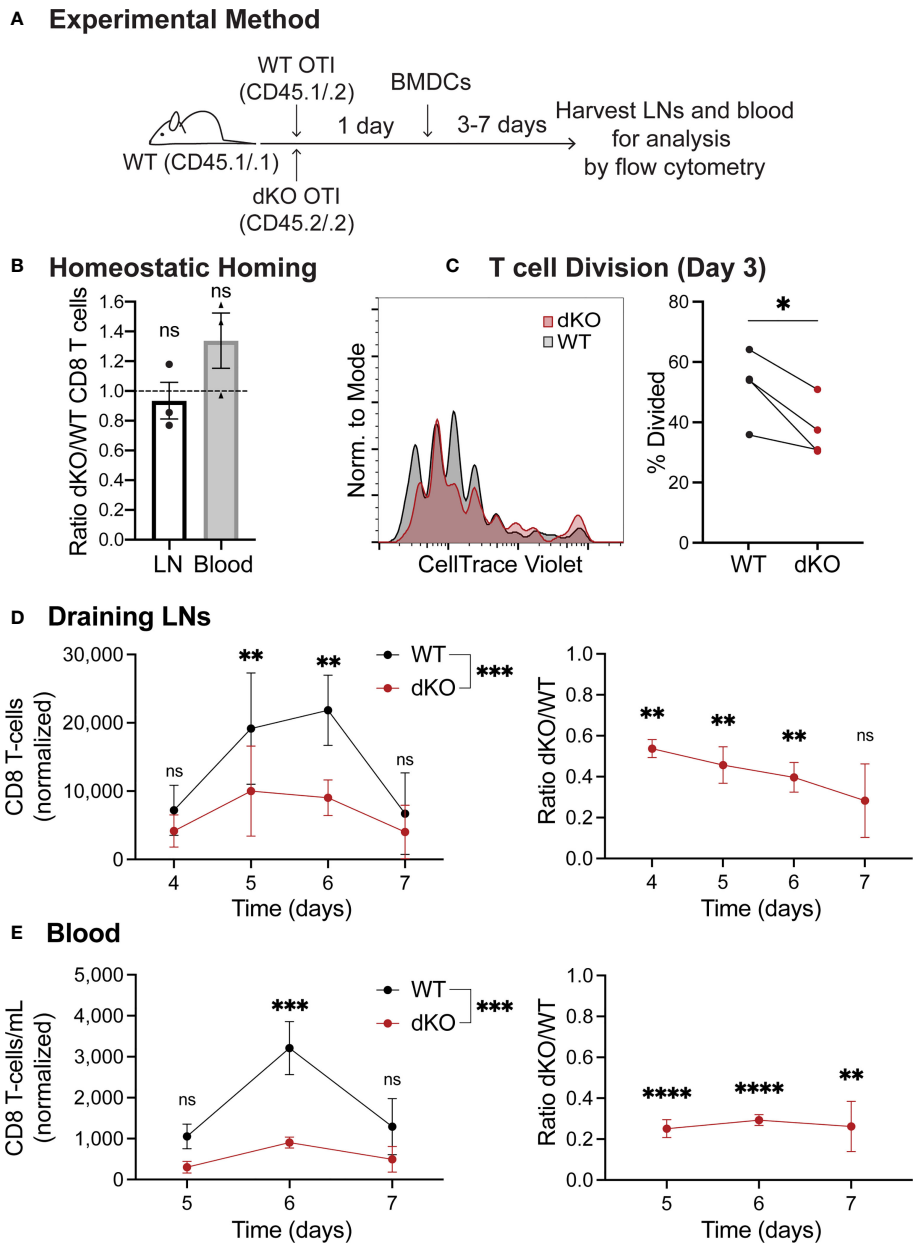

FIGURE 2 | Ena/VASP deficiency reduces T cell expansion in response to stimulation with bone marrow-derived dendritic cells *in vivo*. Congenically distinct naïve WT CD45$^{.1/.2}$ OT-I and EVL/VASP dKO CD45$^{.2/.2}$ OT-I T cells were isolated from donor mice and co-transferred I.V. into WT CD45$^{.1/.1}$ recipient mice. **(A)** Graphical schematic of the experimental method. **(B)** WT and EVL/VASP dKO T cells have similar homing to LNs and persistence in the blood. 1×10^6 WT and EVL/VASP dKO naïve OT-I CD8$^+$ T cells, were co-transferred I.V. into unimmunized WT CD45$^{.1/.1}$ recipient mice and LNs and blood were harvested 24 hours later to determine a homing and persistence baseline. **(C–E)** EVL/VASP dKO T cells have reduced proliferation and expansion in response to BMDC stimulation. 10,000 of each naïve WT CD45$^{.1/.2}$ OT-I and EVL/VASP dKO CD45$^{.2/.2}$ OT-I T cells were co-transferred I.V. into WT CD45$^{.1/.1}$ recipient mice. 24 hours later, 2.5×10^5 mature, LPS-activated OVA-pulsed BMDCs were injected subcutaneously into both hind footpads of recipient mice. At the indicated time-points, mice were euthanized and the draining popliteal LNs and blood were collected for analysis by flow cytometry. **(C)** Reduced proliferation of EVL/VASP dKO T cells. Example CTV proliferation dye dilution curves and quantification of the average percent of T cells divided, 3 days post BMDC immunization. **(D, E)** Reduced expansion of EVL/VASP dKO T cells. T cell numbers in draining popliteal LNs and blood measured at days 4–7 after stimulation with BMDCs (left) and ratios of EVL/VASP dKO/WT T cells (right). EVL/VASP dKO T cell numbers were normalized to the ratio of EVL/VASP dKO/WT T cells recovered from the equivalent tissue of unimmunized recipient mice from the same experiment. Data shown are means ± SEM from ≥3 experiments with ≥2 mice per group. Significance was assessed by 2-way ANOVA (for T cell numbers) and one sample t test compared to a hypothetical value of 1.0 (for the EVL/VASP dKO/WT ratio); ns is not significant, * is $p < 0.05$, ** is $p < 0.01$, *** is $p < 0.001$, and **** is $p < 0.0001$.

WT and EVL/VASP dKO T cells had comparable homing to LNs under homeostatic conditions in the absence of antigen stimulation (**Figure 2B**). We then analyzed T cell responses by subcutaneously injecting mature, LPS-activated, SIINFEKL peptide-pulsed BMDCs into mice bearing co-adoptively transferred WT and EVL/VASP dKO OT-I T cells (**Figure 2A**). We analyzed T cell proliferation 3 days post BMDC immunization and found a significant reduction in the percentage of divided EVL/VASP dKO T cells (**Figure 2C**). We also performed a time-course analysis and determined that this experimental system confirmed the T cell expansion defect seen with LM challenge. Specifically, upon BMDC immunization we detected significantly fewer EVL/VASP dKO T cells at the peak of the T cell effector response in draining LNs (Day 4–7: 1.9–3.5-fold less) as well as in the blood (Day 5–7: 3.4–4.0-fold less) once the activated T cells began exiting the LNs (**Figures 2D, E**). These differences in EVL/VASP dKO T cell numbers were also similar in highly vascularized organs such as the spleen, liver, and lungs (data not shown).

EVL/VASP dKO Naïve T Cells Navigate the LN Normally Under Homeostatic Conditions

We then inquired if the T cell expansion defect was in part due to reduced ability of naïve EVL/VASP dKO T cells to migrate within lymph nodes and thus encounter APCs and be activated. Therefore, we compared EVL/VASP dKO and WT naïve T cell motility in the LN under homeostatic conditions in the absence of cognate antigen. Analysis of T cell motility in lymph nodes showed no significant differences in the speed, displacement, straightness, or arrest coefficient between WT and EVL/VASP dKO naïve T cells (**Supplementary Figure 2**, **Supplementary Movie 1**). This suggests that an inherent motility defect is not the cause of impaired T cell expansion of the EVL/VASP dKO naïve T cells.

EVL/VASP dKO T Cells Have Impaired APC Interactions *In Vivo*

We next sought to assess whether EVL/VASP dKO T cell expansion defects originate during the T cell priming phase *in vivo*. For these experiments, we used fluorescent BMDCs to stimulate adoptively transferred differentially dye-labeled WT and EVL/VASP dKO OT-I T cells along with polyclonal T cell controls (experimental setup similar to that depicted in **Figure 2A**). While imaging experiments typically rely on high numbers ($\geq 2\times10^6$) of transferred T cells (1–3, 11, 12, 50–54), we maintained the more physiological low T cell numbers (2×10^4) established in our *in vivo* T cell activation experiments. This required collecting a large amount of time-lapse data from multiple recipient mice in order to acquire a sufficient number of T cells for analysis, given the low precursor frequency of antigen-specific T cells used. We visualized T cell–APC interactions during the early stages of T cell activation *in vivo* by two-photon microscopy 13-19 hours post BMDC transfer (**Figure 3A** and **Supplementary Movies 2**, **3**). Previous work suggests that depending on the time-point and T cells analyzed, a variety of both transient and sustained interactions with DCs can be visualized (11, 12, 55). However, since data from *in vivo* imaging with physiologically low numbers of antigen-specific T cells is lacking, it was unknown what kind of T cell–APC interaction dynamics should be expected.

Quantification of T cell motility parameters in the presence of antigen-pulsed BMDCs indicated that EVL/VASP dKO OT-I T cells had higher average motility rates, greater displacement, and reduced arrest compared to WT OT-I T cells (**Figures 3B–E**), displaying an intermediate phenotype in-between WT antigen-specific and non-antigen-specific polyclonal T cells. These motility data also showed that EVL/VASP dKO cells decelerated less than WT cells, suggesting reduced frequency and/or duration of interactions with APCs. Indeed, in examining the frequency distribution of T cell speeds, we found that a subset of dKO cells had higher speeds, more similar to the polyclonal T cells, and this higher speed subset was practically absent from the antigen-specific WT T cell population (**Figure 3C**). The higher variability in the displacement of the EVL/VASP dKO population (**Figure 3D**) further suggests that these data likely represent a mixed population of dKO T cells—some interact with APCs while others do not. Thus, a subset of EVL/VASP dKO T cells exhibited motility patterns similar to the WT OT-I T cells while other EVL/VASP dKO T cells exhibited motility similar to the polyclonal T cell population. We next directly analyzed T cell–APC interactions in LNs. Our data showed that a greater percentage of WT OT-I T cells interacted for at least 2 minutes with BMDCs compared to EVL/VASP dKO OT-I T cells (**Figure 3F**). Additionally, significantly more WT OT-I T cells formed contacts with BMDCs that lasted for at least 10 minutes; however, the frequency of T cell–APC interactions longer than 30 minutes was similar for EVL/VASP dKO T cells (**Figure 3G**). Finally, we also found that of the T cells that did contact BMDCs, a greater percentage of T cell–APC interactions were non-productive (lasting less than 2 min) amongst EVL/VASP dKO T cells compared to their WT counterparts (**Figure 3H**). Together this suggests a defect in the ability of a subset of EVL/VASP dKO T cells to shift from an initial contact to a stable T cell–APC interaction. Overall, these motility and T cell–APC interaction data support that a driving factor leading to the difference between WT and EVL/VASP dKO OT-I T cell interactions with BMDCs is in their ability to stop migrating and form a stable interaction *in vivo*.

We next sought to gain a readout of the potential functional consequence of the impaired *in vivo* APC interactions of EVL/VASP dKO T cells during this early priming phase. Thus, immediately following two-photon microscopy, the imaged LNs were digested, and T cells were analyzed by flow cytometry to assess their activation status. Expression of the early T cell activation marker CD69 was significantly reduced in the EVL/VASP dKO T cells, consistent with the observed reduction in T cell–APC interactions (**Figure 3I**).

EVL/VASP dKO T Cell Signaling and Proliferation *In Vitro* Are Normal

Having determined that EVL/VASP-deficient T cells have an expansion defect following *in vivo* pathogen challenge and reduced ability to form conjugates with APCs *in vivo*, we asked

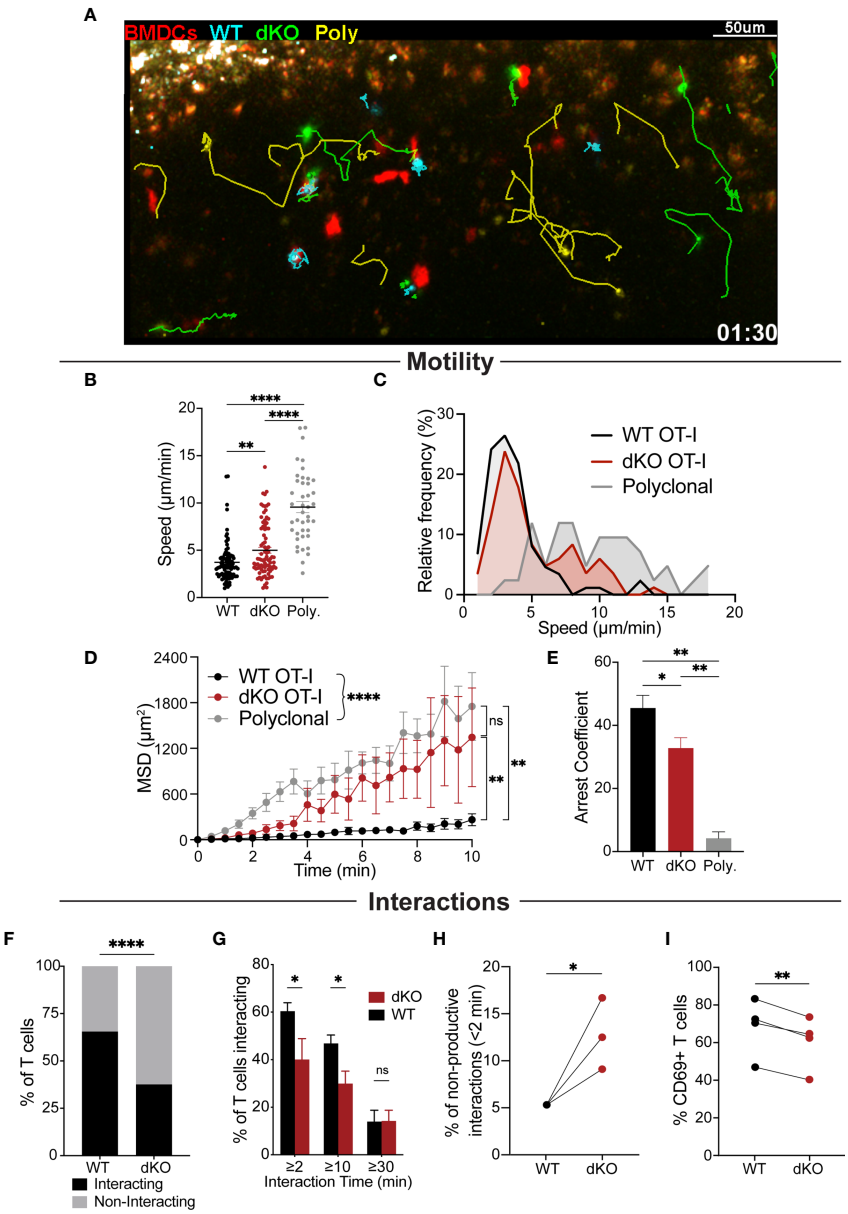

FIGURE 3 | EVL/VASP dKO T cells have impaired APC interactions *in vivo*. Naïve WT OT-I and EVL/VASP dKO OT-I T cells were isolated from donor mice, differentially dye labeled with CTV or CTFR, and 20,000 of each were co-transferred into WT recipient mice. In a subset of experiments, 200,000 polyclonal WT T cells dye labelled with CFSE were also co-transferred with the OT-I T cells. 24 hours later, OVA-pulsed tdTomato-BMDCs were injected subcutaneously into recipient mice. After 13–19 hours, mice were euthanized and the draining popliteal LNs were harvested and analyzed by time-lapse two-photon microscopy. T cells were tracked and their interactions with BMDCs were also quantified. **(A)** Representative snapshot from a movie depicting the movement of EVL/VASP dKO OT-I T cells (green), WT OT-I T cells (cyan), polyclonal control T cells (yellow), and BMDCs (red). Track lines show the path of T cell movement imaged over 30 minutes. Scale bar, 50 μm. **(B)** Mean velocities of WT OT-I, EVL/VASP dKO OT-I, and polyclonal control T cells in the presence of antigen-pulsed BMDCs. Each dot represents a single T cell. **(C)** Frequency distribution of T cell speed. **(D)** Mean square displacement (MSD, +/-SEM) over time of WT OT-I, EVL/VASP dKO OT-I, and polyclonal control T cells. **(E)** Average arrest coefficient (percentage of time that a T cell's instantaneous velocity <2 μm/min) of WT OT-I, EVL/VASP dKO OT-I, and polyclonal control T cells. Mean +/- SEM. **(F)** Total number of WT and EVL/VASP dKO OT-I T cells interacting (for at least 2 minutes) and non-interacting with APCs. n=130 WT cells and 128 EVL/VASP dKO cells. **(G)** Distribution of T cell–APC interaction times shown by graphing percent of WT and EVL/VASP dKO OT-I T cells interacting with BMDCs for given durations. **(H)** Quantification of non-productive T cell–APC interactions: graph of percent of interactions that occurred in which T cells disengaged from APCs within 2 minutes. **(I)** Quantification of CD69 expression in T cells from the LNs of the imaging experiments. Immediately following two-photon microscopy, imaged LNs were digested and analyzed by flow cytometry. Data in **(B–G)** are from ≥5 experiments each with ≥2 mice per group, data in **(H)** are from 3 experiments, as experiments with <20 cells were excluded, and data in **(I)** are from 4 experiments. Significance was assessed by 1-way ANOVA **(B, E)**, 2-way ANOVA **(D, G)**, paired t test **(H, I)**, and Fisher's exact test **(F)**; ns is not significant, * is $p < 0.05$, ** is $p < 0.01$, and **** is $p < 0.0001$.

whether EVL/VASP dKO T cells have generalized impaired signaling and/or ability to proliferate. To assess whether the Ena/VASP family plays a role in the signaling required for T cell activation, we stimulated WT and EVL/VASP dKO OT-I T cells with WT splenocytes as APCs pulsed with varying concentrations of SIINFEKL peptide *in vitro*, and spun APCs and T cells together to enforce T cell–APC encounters. Then, to evaluate TCR signaling, nuclei from the T cell–APC conjugates were isolated and analyzed by flow cytometry to quantify translocation into the nucleus of transcription factors associated with T cell activation, NFAT1 and NFκB, as previously described (56) (**Figure 4A**). For both transcription factors, there was no difference in nucleus translocation between WT and EVL/VASP dKO T cells at various antigen concentrations (**Figure 4B**). To evaluate proliferation capacity, WT and EVL/VASP dKO OT-I T cells were stimulated *in vitro* with antigen-pulsed splenocytes and cultured for 3 days, and cell division was quantified by dilution of CellTrace Violet (CTV) proliferation dye. No difference between WT and EVL/VASP dKO T cell proliferation was detected in this setting (**Figure 4C**). Taken together, these results demonstrate that EVL/VASP dKO T cells do not have an inherent/intrinsic proliferation defect. Furthermore, in these *in vitro* conditions, EVL/VASP dKO T cell stimulation is also normal, indicating that Ena/VASP proteins are not required for TCR-mediated signaling leading to NFAT1 and NFκB translocation or proliferation.

EVL/VASP dKO T Cells Have Impaired F-Actin Polarization at the Immune Synapse and Form Conjugates With APCs That Are Less Stable

Our *in vivo* imaging data supports that EVL/VASP-deficient T cells have an impairment in establishing stable interactions with APCs. First, we tested whether there were any differences in the ability of EVL/VASP dKO T cells to form conjugates with APCs *in vitro* when the cells were spun together to facilitate contacts (**Figure 5A** left panel). At all concentrations of antigen tested, EVL/VASP dKO and WT OT-I T cells had similar conjugation efficiency *in vitro* (**Figure 5B**). Given that Ena/VASP proteins participate in actin network remodeling, we asked if EVL/VASP dKO T cells were impaired in actin polymerization upon encountering antigen-bearing APCs. Using the same *in vitro* setup for conjugate formation, we stimulated WT and EVL/VASP dKO OT-I T cells with splenocytes pulsed with varying concentrations of SIINFEKL peptide *in vitro*, and quantified actin polymerization in the T cell–APC conjugates. Using phalloidin to stain for F-actin we found a strong impairment in actin polymerization in the EVL/VASP dKO T cell–APC conjugates by flow cytometry (**Figures 5A, C**). To explore whether this impaired actin polymerization correlated with differences in stability of T cell–APC conjugates, we repeated the conjugate formation experiment, but disrupted the conjugates by vortexing to dissociate those with weak interactions before fixation. Indeed, the EVL/VASP dKO T cells lost slightly, but significantly, more conjugates after disruption than WT T cells, implying that the EVL/VASP dKO conjugates are less stable (**Figure 5D**).

Furthermore, using the ImageStream platform for high throughput imaging of T cell–APC conjugates, we analyzed F-actin specifically at the immune synapse of WT and EVL/VASP dKO OT-I T cells. Our data show a reduction in the level of actin polymerization at the T cell–APC interface formed by EVL/VASP dKO T cells compared to their WT counterparts (**Figure 6**). This observation suggests that EVL/VASP proteins play a role in actin polymerization at the IS during T cell–APC interactions. To garner further insight into how T cell–APC conjugate stability may be modulated by Ena/VASP proteins, we analyzed the accumulation of the TCR complex and LFA-1 integrin at the IS in WT and EVL/VASP dKO OT-I T cells (**Figures 7A, B**). While our data showed equivalent CD3 accumulation at the synapse, we found a small but significant reduction in the amount of LFA-1 that polarized to the T cell–APC interface (**Figure 7C**). Overall, these data suggest that Ena/VASP proteins promote conjugate stability through actin polymerization and integrin recruitment at the immunological synapse.

EVL has been implicated in actin polymerization downstream of TCR stimulation in Jurkat cells (40), but this had not previously been assessed for VASP or in primary T cells. VASP activation is modulated by phosphorylation at multiple sites and the Serine 153 (S153) site has been shown to control subcellular localization of VASP to the cell membrane (43). Thus, to assess whether TCR engagement can activate VASP and trigger recruitment of VASP to the synapse, we next stimulated polyclonal T cells using anti-CD3/CD28 conjugated beads, and quantified VASP phosphorylation at the S153 site. Indeed, VASP S153 phosphorylation was significantly elevated after CD3/CD28 stimulation (**Figure 8**), suggesting that TCR engagement by APCs can recruit VASP to the T cell membrane for actin remodeling.

DISCUSSION

The goal of this work was to determine whether actin polymerization mediated by the Ena/VASP protein family plays a role in T cell priming and expansion *in vivo*. Using T cells from EVL/VASP double-knockout mice, we demonstrate that Ena/VASP proteins play an important role in the accumulation of T cells over the course of an immune response following either *L. monocytogenes* infection or subcutaneous immunization with BMDCs. We also found that the Ena/VASP family promotes efficient T cell scanning and interactions with APCs *in vivo*, resulting in fewer activated EVL/VASP dKO T cells, supporting a role for Ena/VASP proteins in optimizing T cell priming. Investigating the potential mechanisms through which EVL and VASP regulate T cell–APC interactions, we determined that T cells deficient in Ena/VASP proteins form T cell–APC conjugates with less F-actin and that are less stable than WT conjugates. Importantly, the stability and duration of T cell–APC conjugates can affect the ensuing T cell response (51, 57, 58). We thus conclude that Ena/VASP family-mediated actin polymerization downstream of TCR signaling plays an important role in the initiation and stabilization of T cell–APC conjugates, which likely drives the impaired Ena/VASP-deficient T cell accumulation phenotype.

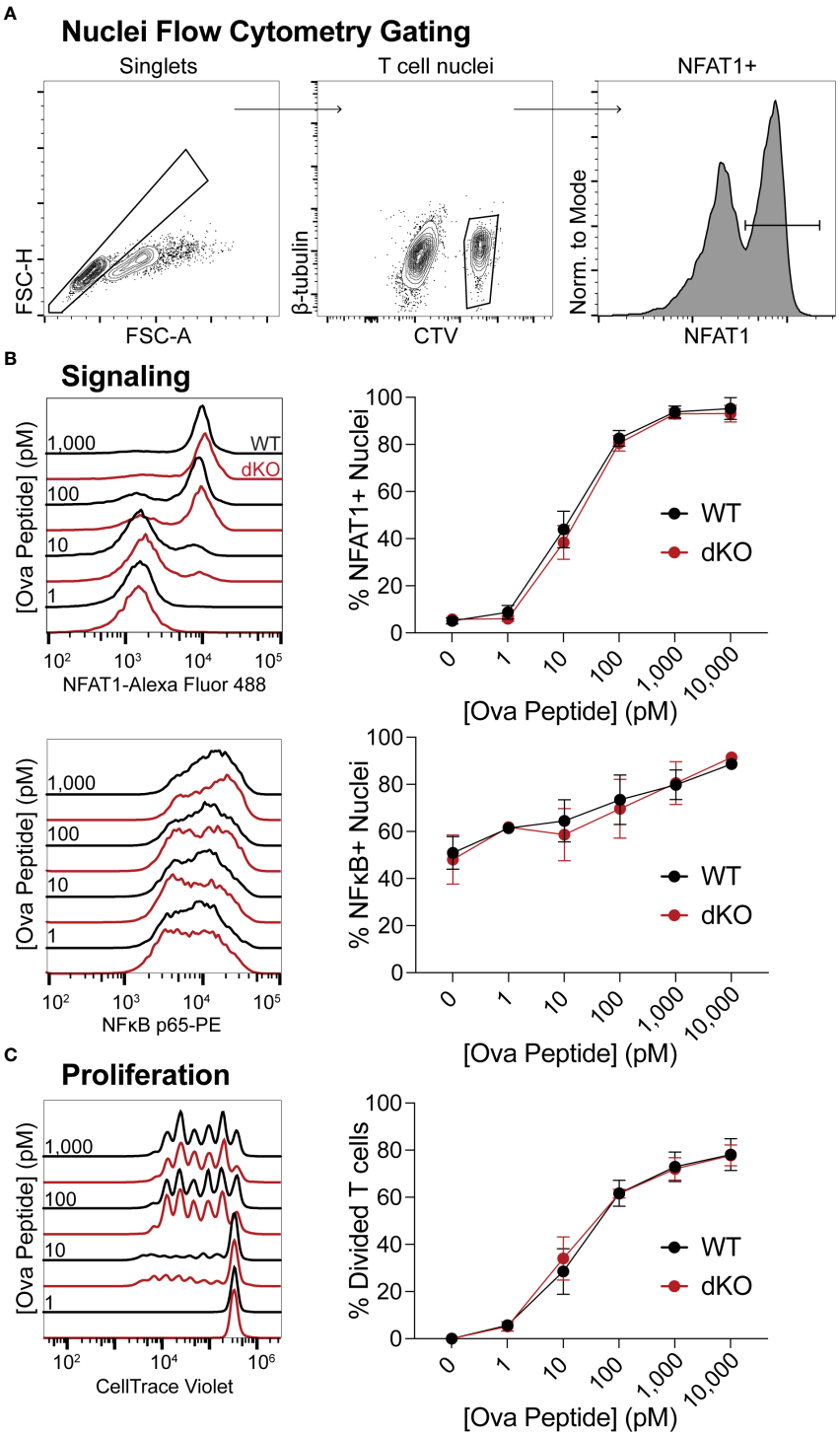

FIGURE 4 | EVL/VASP-deficient T cell signaling and proliferation *in vitro* are normal. Naïve WT and EVL/VASP dKO OT-I T cells were CTV dye-labeled, mixed with antigen-pulsed WT splenocytes, centrifuged, and cocultured. **(A)** Representative flow cytometry gating scheme used to identify isolated T cell nuclei in **(B)**. **(B)** T cells were incubated with splenocytes for 45 minutes, and nuclei were isolated for analysis of nuclear translocation of transcription factors by flow cytometry. Left: Representative histograms of NFAT1 (top) or NFκB (bottom) fluorescence in WT and EVL/VASP dKO T cell nuclei. Right: Dose response plots of the percentage of NFAT1+ (top) or NFκB+ (bottom) T cell nuclei. **(C)** T cells were cocultured with SIINFEKL-pulsed splenocytes for 3 days, and proliferation was assessed by CTV dye dilution. Left: representative histograms of CTV dilution; right: dose response plot shows quantification of % of T cells divided. Data shown are means ± SEM; averaged from ≥3 experiments each with ≥3 replicates per group. There was no significant difference between WT and EVL/VASP dKO T cells, as assessed by two-way ANOVA interaction effects.

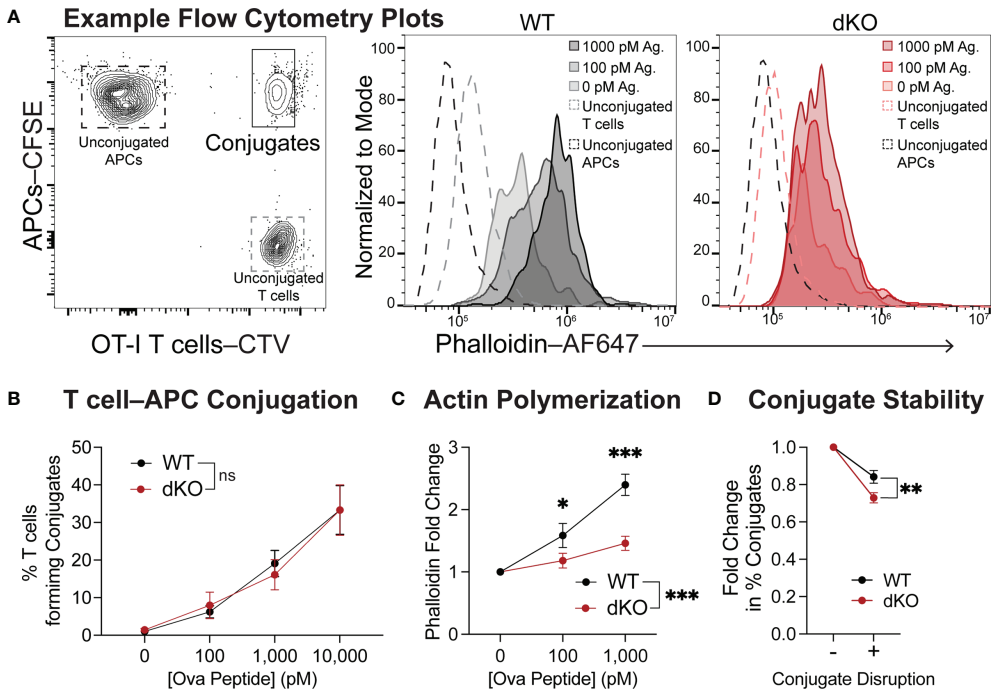

FIGURE 5 | EVL/VASP-deficient T cells have impaired actin polymerization during conjugation with APCs and form fewer stable conjugates. Naïve WT and EVL/VASP dKO OT-I T cells were dye-labeled with CTV and mixed with CFSE-labeled WT splenocytes pulsed with SIINFEKL peptide. T cells and APCs were centrifuged together, cocultured for 2 minutes, and stained for F-actin with phalloidin. **(A)** Left; gating used to identify T cell–APC conjugates. Right; example histograms of phalloidin staining in the conjugates formed by WT and EVL/VASP dKO T cells. **(B)** Quantification of the % of naïve WT and EVL/VASP dKO OT-I T cells that formed conjugates with APCs. No significant difference (ns) determined by 2-way ANOVA. **(C)** F-actin polymerization in T cell–APC conjugates. Graph depicts the fold change in phalloidin (GMFI) in WT and EVL/VASP dKO T cell conjugates compared to conjugates that formed in the absence of antigen (0 pM). Data are from 3 experiments each with ≥2 replicates per group. Significance was assessed by 2-way ANOVA; * is $p < 0.05$, *** is $p < 0.001$. **(D)** T cell conjugate stability was quantified by comparing T cell–APC conjugates (using 1000 pM OVA peptide) fixed immediately after 2-minute incubation (- Conjugate Disruption) or disturbed by briefly vortexing tubes before fixation (+ Conjugate Disruption). Graph depicts fold change in % of conjugates from the undisrupted control. Data are from 3 experiments with 3 replicates per group. Significance was assessed by paired t test; ** is $p < 0.01$.

The microenvironment of the LN is relatively permissive for migration, but an environment characterized by large numbers of tightly packed motile cells constantly exposes T cells seeking interactions with APCs to mechanical stresses. Not unlike navigating through a dense crowd with a partner at a concert, where staying still and together can be difficult, the motion of all proximal cells in a LN is interdependent and maintaining adhesive cell-cell interactions with APCs can be mechanically challenging. Furthermore, the chemokine milieu in LNs is favorable for rapid T cell motility. In fact, CCR7 signals have been demonstrated to override 'stop signals' from peptide-MHC *in vitro* (59). However, CCR7 chemokines can also promote transient tethering of T cells to neighboring chemokine-coated cells, which then favors subsequent interaction with antigen-bearing APCs (60). Thus, sustained interactions with APCs must be able to overcome motility signals as well as be strong enough to withstand the physical and mechanical forces of the surrounding environment. Throughout the early phases of priming, T cells engage in both transient and sustained interactions with APCs (11, 12, 51, 55). Additionally, T cells engage in motile interactions, termed kinapses, in which T cells continue migrating over the surface of an APC (61, 62). Eventually, activation signals from TCR and costimulatory receptors accumulate over time and serve as 'stop signals' by inducing cellular changes (13), mediated primarily by actin rearrangement, necessary to establish tight binding and sustained T cell–APC interactions. For example, actin polymerization mediated by PKCθ inhibition and WASp activation favors stable IS formation over migration (63, 64). High-affinity antigen signals induce actin-related protein 2/3 complex (Arp2/3) activity, which has also been shown to promote arrest *in vitro* (65). Furthermore, formin-mediated actin flow sweeps the integrin LFA-1 towards the center of the immune synapse, activating and stabilizing its high affinity conformation to enable tight binding to ICAM-1 on APCs, which controls the stability and duration of T cell–APC contacts (21, 22, 66–68).

Based on our observations, EVL/VASP-deficient T cells interact less effectively with APCs *in vivo* during initial phases of T cell priming. Given that homeostatic intranodal motility is normal in naïve EVL/VASP dKO T cells, this defect does not stem from the inability to cover sufficient ground in

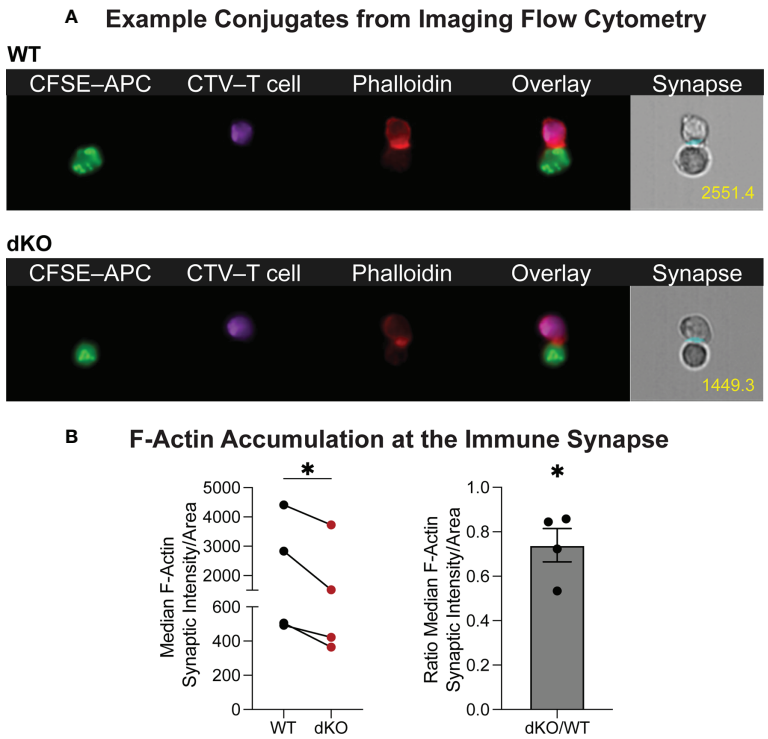

FIGURE 6 | Ena/VASP proteins contribute to actin rearrangement at the immunological synapse. CTV-labeled WT or EVL/VASP dKO naïve OT-I T cells were conjugated with antigen-loaded CFSE-labeled APCs and stained for F-actin. **(A)** Representative ImageStream images of WT and EVL/VASP dKO T cell–APC conjugates stained for phalloidin. Number in yellow indicates phalloidin GMFI measured at the immune synapse. **(B)** Left; quantification of median phalloidin intensity at the immunological synapse divided by the synapse area. Right; quantification of the EVL/VASP dKO/WT fluorescence intensity ratio at the synapse. Data represent averages from 4 independent experiments with ~1000–7000 conjugates analyzed per sample. Statistics were performed using one-tailed paired t test and one sample t test compared to a hypothetical value of 1.0; * is $p < 0.05$.

the LN, but instead is likely an impairment in a T cell's ability to stop and to form or maintain interactions with cognate APCs. Studies in Natural Killer (NK) cells identified a role for EVL in the generation of F-actin at the cytotoxic synapse impacting NK cell–target cell adhesion *in vitro* (69). In T cells, multiple molecules that have been implicated in maintaining the stability of T cell–APC interactions, including the actin bundling protein L-Plastin and ADAP, ultimately play roles in the organization, localization, and stability of LFA-1 (67, 68, 70). We have previously demonstrated a role for Ena/VASP proteins in the expression and function of the α_4 integrin (CD49d) in T cells (49). Additionally, VASP has been associated with integrin activation in other cell types, including $\alpha_{IIb}\beta_3$ activation in platelets (71). Thus, we assessed F-actin and LFA-1 enrichment at the immunological synapse in EVL/VASP dKO T cells. We show that EVL/VASP dKO T cells exhibit impaired actin polymerization and a small but significant reduction of LFA-1 localization at the IS. This suggests that EVL/VASP proteins promote conjugate stability through actin polymerization and integrin recruitment. Nevertheless, future studies should more closely explore the role of EVL/VASP proteins in LFA-1 clustering and stability at the IS.

During the first few hours of T cell interactions with antigen-bearing DCs *in vivo*, T cells progressively receive activation signals that can lead to CD69 upregulation (11, 12). We observed fewer EVL/VASP dKO T cells expressing CD69 after initial priming, which supports our observation that the EVL/VASP dKO T cells interact less effectively with APCs. Furthermore, it has been demonstrated that biasing towards transient interactions and signaling, as opposed to prolonged contacts, can lead to abortive T cell activation (58, 72). Our quantification of non-productive T cell–APC contacts (lasting less than 2 min) showed that EVL/VASP dKO T cells have an increased rate of aborted T cell interactions. It is possible that over time, most EVL/VASP dKO T cells will form enough interactions with APCs to trigger the start of activation, but having a higher frequency of non-productive interactions with APCs, their activation signals may not be sufficient for a robust proliferative response *in vivo*. Our *in vitro* proliferation data suggest that EVL/VASP-deficient T cells can proliferate normally. Thus, the reduced number of EVL/VASP dKO T cells is not related to intrinsic defects in cell division, but likely compounds from reduced T cell accumulation over time in the *in vivo* setting due to inefficient stimulation. Given that Ena/VASP-deficient T cell proliferation is already impaired by 72

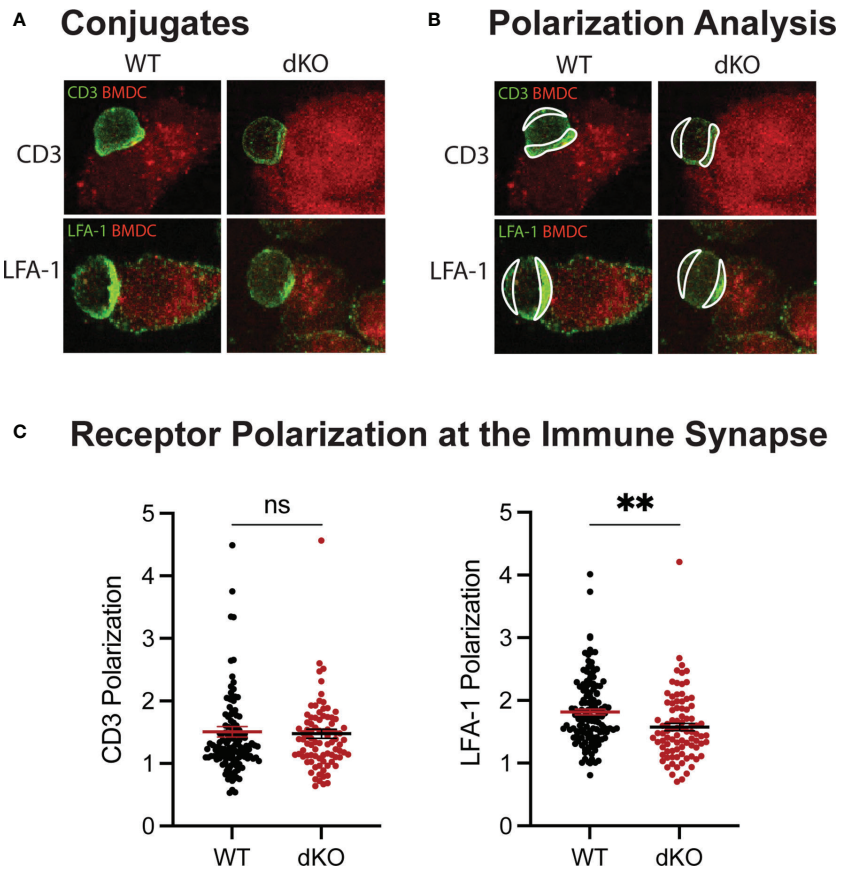

FIGURE 7 | EVL/VASP dKO T cells polarize less LFA-1 at the immunological synapse. Mature, LPS-activated, OVA-pulsed tdTomato-BMDCs were adhered to chamber slides. Naïve WT and EVL/VASP dKO OT-I T cells were added to the chamber slides to form conjugates. Conjugates were then fixed and stained for CD3 and LFA-1. **(A)** Example images of conjugates stained for CD3 (top) or LFA-1 (bottom). **(B)** Examples of regions drawn to assess polarization of receptors at the immunological synapse. **(C)** Quantification of receptor polarization at the immune synapse. The mean fluorescence intensity (MFI) of the contact region at the synapse was divided by the MFI of the region defined at the back of the cell. Each dot represents an individual T cell–APC conjugate, data are pooled from 3 independent experiments. Significance was assessed by unpaired t test; ns is not significant, and ** is $p < 0.01$.

hours after stimulation, these deficits can intensify over time and contribute to the significant reduction of EVL/VASP dKO T cells by the peak of the immune response. It will be interesting for future studies to explore the strength of activation signals in EVL/VASP dKO T cells under physiological *in vivo* conditions.

The experiments we conducted *in vitro* were used to assess whether Ena/VASP deficiency plays a role in T cell activation signals and the maintenance of interactions. In these experiments, T cell–APC contact was enforced by spinning them down together. Because previous experiments have demonstrated that T cells need approximately 2–3 minutes to "decide" whether to initiate conjugation (73), we assessed actin polymerization after 2 minutes of coculture with cognate APCs. We found clear differences in actin polymerization in EVL/VASP dKO T cells, indicating that EVL and VASP mediate actin rearrangement during T cell–APC interactions. However, the formation of conjugates, downstream signaling, and proliferation were unimpacted in these *in vitro* conditions. These data support that when T cell–APC interactions are forced by centrifugation or by high cell numbers and proximity *in vitro*, Ena/VASP proteins are dispensable for T cell activation. Thus, we posit that these *in vitro* systems lack the necessary physiological microenvironment to identify the requirement for EVL/VASP function in T cell activation. In particular, *in vitro* models are insufficient at encompassing the processes of T cell–APC scanning and interactions within tissues. However, in physiological *in vivo* conditions, we find that T cell stopping and conjugate formation with APCs is impaired by Ena/VASP deficiency. Thus, we conclude that a key function of Ena/VASP proteins in naïve T cell activation is in the establishment of T cell–APC interactions *in vivo*. Our data demonstrating that VASP is activated by CD3+CD28 stimulation and that Ena/VASP protein deficient T cell–APC conjugates are less stable than their WT counterparts further support that reduced actin polymerization and LFA-1 accumulation contribute to the EVL/VASP dKO T cell's impaired ability to form conjugates with APCs *in vivo*.

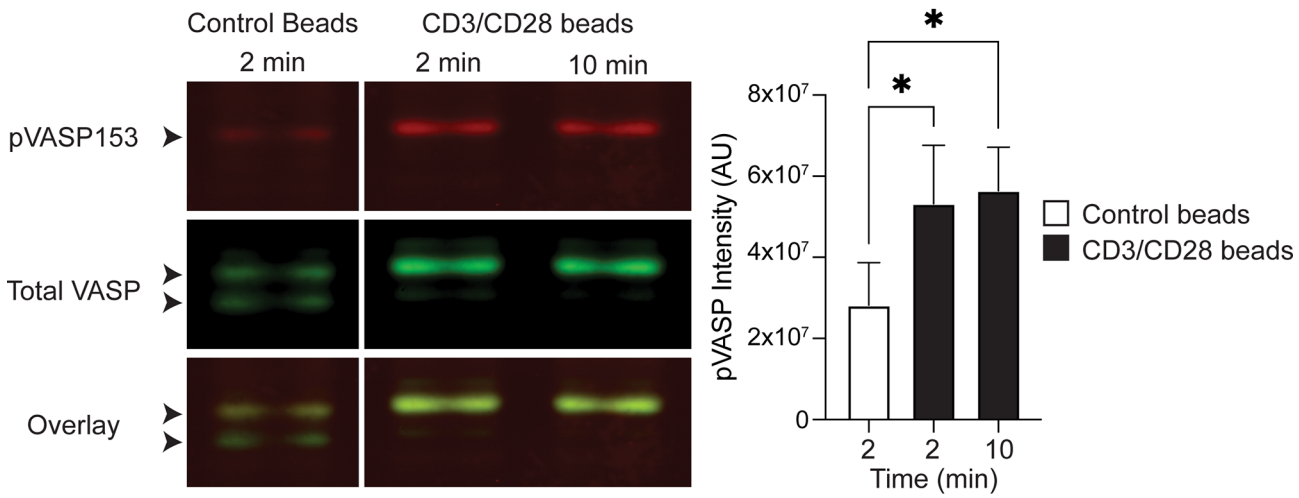

FIGURE 8 | VASP is activated downstream of CD3/CD28 stimulation in T cells. *In vitro* activated T cells were stimulated with control or anti-CD3/CD28 beads and VASP phosphorylation at S153 was determined by western blotting. Left; example western blot showing detection of total VASP and pVASP-S153. Arrowheads point to the VASP protein doublet: the bottom band is the non-phosphorylated isoform, and the top band is phosphorylated. Right; quantification of pVASP signal intensity, normalized to GAPDH intensity. Data is from a total of 3 independent experiments. Statistics were performed using a one-way repeated measures ANOVA; * is $p < 0.05$.

There are still open questions regarding the specific location and contribution of Ena/VASP proteins in T cell–APC interactions and IS formation and organization. In subsequent studies, these parameters should be assessed under physiological *in vivo* conditions, and thus standard *in vitro* methods for visualizing the IS may not be appropriate. Furthermore, while this work clearly demonstrates a role for Ena/VASP proteins in mediating naïve T cell–APC interactions and activation, productive T cell–APC contacts are also essential for activated T cell functions. Thus, future studies could explore the functional implications for EVL/VASP dKO T cells in downstream effector functions and protective immunity. For example, it would be interesting to assess whether EVL/VASP dKO T cells exhibit defects in cytokine production, pathogen clearance, and memory formation.

While Ena/VASP proteins have been described to play varying roles in enhancing or suppressing motility in different cell types (35, 42, 44–46), our work is the first to explore Ena/VASP proteins in naïve T cell motility. We demonstrate that Ena/VASP proteins are dispensable for homeostatic naïve T cell intranodal migration. Ena/VASP proteins have also been implicated in regulating adhesion in other cell types (37, 40, 45), but our work uncovers a previously unidentified role for Ena/VASP proteins in stabilizing initial T cell interactions with APCs. Additionally, while EVL was suggested to play a role in actin polymerization downstream of CD3 engagement in Jurkat cells (48) and in Natural Killer cell cytotoxicity (69), our work identifies a role for Ena/VASP proteins in actin polymerization in response to antigen-bearing APCs in primary T cells. Finally, we also demonstrate a novel role for Ena/VASP proteins in promoting T cell activation and accumulation *in vivo*.

METHODS

Mice

EVL KO mice were generated by Kwiatkowski et al. (74) and VASP KO mice were generated by Aszodi et al. (75). EVL/VASP dKO mice (originally on a 129/C57BL/6 mixed background) were a gift from Dr. Frank Gertler (MIT). The EVL/VASP dKO mice were backcrossed to C57BL/6 at least 8 times and then crossed with OT-I TCR transgenic mice (also on the C57BL/6 background). CD45.1 congenically-marked C57BL/6 recipient mice were purchased from Charles River (Strain #564). WT OT-I T cells were isolated from transgenic OT-I $CD45^{.1/.2}$ C57BL/6 mice, and EVL/VASP-deficient OT-I T cells were isolated from transgenic $EVL^{-/-}$ $VASP^{-/-}$ OT-I $CD45^{.2/.2}$ C57BL/6 mice, unless otherwise specified. This study and mouse protocol were reviewed and approved by the Institutional Animal Care and Use Committees at the University of Colorado Anschutz Medical Campus and at National Jewish Health, and all efforts were made to minimize mouse suffering.

Bone Marrow Chimeras

Bone marrow chimeras were generated by γ-irradiating $CD45^{.1/.1}$ congenically-marked C57BL/6 recipient mice at 500 Rads twice, four hours apart. Immediately following the second irradiation treatment, mice were reconstituted by I.V. injection of at least 1×10^6 cells from bone marrow isolated from either transgenic OT-I $CD45^{.1/.2}$ C57BL/6 mice or transgenic $EVL^{-/-}$ $VASP^{-/-}$ OT-I $CD45^{.2/.2}$ C57BL/6 mice. Bone marrow chimeras were given at least 8 weeks to mature before use in experiments. Both WT and EVL/VASP dKO OT-I T cells reconstituted recipient mice

Target	Fluorophore	Brand/catalog number
CD8α	BUV-805	BD Biosciences/612898
CD45.1	PE	Biolegend/110707
CD45.2	APC-efluor780	eBioscience/47-04540-82
KLRG1	BV-711	Biolegend/138427
CD127	BV-421	Biolegend/135023
Vα2	Alexa Fluor 647	Biolegend/127812
CD69	PE-Cy7	ThermoFisher/25-0691-82
Dead cells	Zombie Yellow	Biolegend/423104
NFATc2 (NFAT1)	Alexa Fluor 488	CST/14324S
NFκB	PE	CST/9460S
β-tubulin	Alexa Fluor 647	CST/3624S
CellTrace Violet	–	ThermoFisher/C34557
CellTrace Far Red	–	ThermoFisher/C34572
CellTrace CFSE	–	ThermoFisher/C34554
Phalloidin	Alexa Fluor 647	ThermoFisher/A22287

equivalently and averaged at least 90% reconstitution by the donor cells based on congenic marker expression.

Flow Cytometry

Activation and expansion of T cells was assessed *via* Flow Cytometry on a Fortessa flow cytometer (Beckton Dickinson) or an Aurora spectral flow cytometer (Cytek). T cell numbers were determined using CountBright Absolute Counting beads (Invitrogen, Cat. C36950) and proliferation was assessed by Cell Trace Violet (CTV, Thermo Fisher Scientific) dilution. The following antibodies/dyes were used throughout this project:

Infection and Immunization

Congenically distinct WT ($CD45^{.1/.2}$) and EVL/VASP dKO ($CD45^{.2/.2}$) OT-I T cells were isolated using negative selection with an EasySep Mouse $CD8^+$ T cell isolation kit (STEMCELL Technologies, Cat. 19853) from either endogenously matured or bone marrow chimera matured mice and co-transferred into $CD45^{.1/.1}$ WT recipient mice (10,000 T cells of each for day 6 LM-OVA and BMDC time course experiments; 20,000 T cells of each for two-photon imaging experiments and day 3 harvests). To assess proliferation on day 3 in both LM-OVA and BMDC time course experiments, prior to transfer T cells were first dye-labeled with 2.5 μM CellTrace Violet in PBS for 20 minutes. 24 hours post T cell transfer, recipient mice were immunized or infected.

For infection experiments, mice were injected with 2×10^3 CFUs recombinant *L. monocytogenes* expressing full-length OVA (LM-OVA) and an erythromycin (Erm) resistance (ErmR) marker through the lateral tail vein (76). LM-OVA was grown and titrated as previously described (77): 1×10^8 mouse-passaged LM-OVA aliquots were frozen at −80°C, thawed, and used to inoculate 10 mL of fresh Brain Heart Infusion (BHI) broth with Erm, grown at 37°C in a shaker overnight, then split into fresh BHI broth without Erm and grown for 2–3 hours to log phase. Titer estimates were determined by OD_{600} values, and 2×10^3 CFU injections were prepared in PBS. Spleens were harvested 3 or 6 days after immunization for analysis by flow cytometry. T cell numbers were determined by flow cytometry, and total T cell numbers for a given tissue were calculated using CountBright Absolute Counting beads (Invitrogen, Cat. C36950). To account for potential differences in the actual T cell injection ratio and/or homing and survival of WT vs. EVL/VASP dKO T cells *in vivo*, we normalized the T cell numbers for each organ (i.e. spleen or LN) from immunized mice to the ratio of dKO/WT T cells in the equivalent organ and timepoint from non-immunized mice. Specifically, to normalize, we divided the EVL/VASP dKO numbers in the immunized organ by the dKO/WT ratio in the respective unimmunized organ.

For footpad immunizations, tdTomato-BMDCs were generated by culturing bone marrow from 3.5–8 week old B6.Cg-Gt(ROSA) 26Sortm14(CAG-tdTomato)Hze/J (Rosa-Red mice) mice (Jackson Strain #007914) (in which the stop cassette was floxed-out in the germline) for 7–9 days in the presence of GMCSF. IL-4 was added to cultures to mature DCs 48 hours prior to use. Purity was typically more than 95%. BMDCs were pulsed and activated with 2 ng/mL $OVA_{257–264}$ peptide and 1 mg/mL LPS for 1 hour and washed 3x before subcutaneous (s.c.) injection. Mice were anesthetized with isoflurane, and 2.5×10^5 mature, antigen-pulsed activated BMDCs in a total volume of 25 μL PBS were administered s.c. in the hind footpads of mice. T cell numbers in each organ were measured and analyzed as described above for the LM experiments. $OVA_{257–264}$ peptide (SIINFEKL) was purchased from Chi Scientific or Genscript and LPS was purchased from Invitrogen (Cat. 00-4976-93). GMCSF and IL-4 were made in house using G6 and I3L6 cell lines respectively (a gift of Dr. Matthew Krummel, UCSF).

Isolation of Cells

For isolation of T cells from draining LNs or spleens at timepoints 72 hours or less after immunization, footpad immunized and LM-OVA infected mice were first euthanized by CO_2 at the indicated time points, and the draining popliteal LNs and spleens were then removed and minced in 500 μL HBSS (Life Technologies) +10% FBS containing 1 mg/mL Collagenase D (Roche) and 50 μg/mL DNase I (Worthington Biochemical) per LN to break up T cell–APC conjugates. After a 30 minute incubation at 37°C, one volume of 0.1 M EDTA was added, and cells were incubated 5 additional minutes. Dissociated cells were then washed with HBSS containing 5 mM EDTA and forced through 70 μm strainers to generate single cell suspensions. After digestion, T cells from LM-OVA infected spleens at day 3 were enriched by negative selection using the following antibodies (see table below) and streptavidin beads (Biolegend, Cat. 480016). Finally, the remaining splenocytes were stained for flow cytometry analysis as above.

For isolation of T cells from the spleen and LNs of immunized and infected mice at later time points, organs were harvested dissociated and forced through 70 μm strainers to generate single

Target	Brand/catalog number
Biotin anti-mouse CD4	Biolegend/100404
Biotin anti-mouse B220	Biolegend/103204
Biotin anti-mouse CD19	Tonbo/30-0193-U500
Biotin anti-mouse Ter119	Tonbo/30-5921-U500

cell suspensions. For collection of T cells in the blood, ~1 mL of blood was collected by cardiac puncture immediately after euthanasia and RBCs were lysed in 175 mM NH_4Cl.

In Vitro Activation and Proliferation

Spleens from C57BL/6 mice were harvested and red blood cells lysed for 2.5 minutes in 175 mM NH_4Cl. Splenocytes were pulsed with various concentrations of SIINFEKL for 30 minutes, and washed 3 times. WT and EVL/VASP dKO OT-I T cells were isolated from lymphocytes *via* negative selection with a $CD8^+$ EasySep kit. OT-I T cells were dye-labeled with CTV (1.67 μM in PBS) for 20 minutes, quenched with FBS for 5 minutes and washed 2 times. WT and EVL/VASP dKO OT-I T cells were plated in separate wells with peptide-pulsed splenocytes at a 1:3 ratio in 100 μL in a round bottom 96 well plate. Cells were fed at 48 hours by adding to each well 1 volume of fresh media and 10 U/mL IL-2 (obtained through the AIDS Research and Reference Reagent Program, Division of AIDS, NIAID, NIH from Dr. Maurice Gately, Hoffmann - La Roche Inc.). On day 3, cells were analyzed by flow cytometry. FlowJo's (Beckton Dickinson) proliferation tool was used to analyze CTV dilution and quantify % of cells divided.

Nucleus Flow Cytometry

Nuclei isolation and flow cytometry staining of OT-I T cells stimulated in cocultures were performed as previously described (78). Briefly, WT and EVL/VASP dKO OT-I $CD8^+$ T cells were negatively enriched from LNs and spleens (using $CD8^+$ EasySep kits) and labeled with 2.5 μM CTV dye for 15 minutes prior to mixing with peptide-pulsed splenocytes at a 3:1 ratio of APCs to T cells. Cells were briefly/gently spun together in FACS tubes (214 g for 1 minute) and cocultured for 45 minutes at 37°C with 10% CO_2. For nuclei isolation, cells were treated and washed with sucrose and detergent buffers (78). The nuclei were fixed in 4% paraformaldehyde, and then intranuclear staining was performed with a 0.3% Triton-X 100 detergent PBS buffer.

In Vivo Two-Photon Microscopy

$CD8^+$ T cells were isolated from WT OT-I or EVL/VASP dKO OT-I mice (using $CD8^+$ EasySep kits), labelled for 15–25 minutes at 37°C with 2.5 μM CTV or 0.2 μM CellTrace Far Red (CTFR, Thermo Fisher) and 20×10^3 of each WT and EVL/VASP dKO OT-I T cells were transferred into WT recipient mice by injection into the tail vein. Fluorescent dyes were swapped between WT and EVL/VASP dKO T cells between experimental repeats to control for potential effects from the dyes. In a subset of experiments, 200×10^3 polyclonal WT T cells dye-labelled with Carboxyfluorescein succinimidyl ester (CFSE) were also co-transferred with the OT-I T cells as a negative control. The following day, tdTomato-BMDCs were pulsed with 2 ng/mL $OVA_{257-264}$ and activated with 1 μg/mL LPS. 2.5×10^5 BMDCs in 25 μL PBS were injected into the hind footpads of recipient mice. Between 13–19 hours following immunization, mice were euthanized and their draining popliteal LNs were surgically removed for imaging [similar to (79)]. Explanted LNs were immobilized on coverslips with the efferent lymphatics adhered to the coverslip with Vetbond (3M). Mounted LNs were positioned on a heated flow chamber from Warner instruments (PH-1). During imaging, LNs were maintained at 35–37°C in a flow chamber perfused with RPMI medium without phenol red (Gibco) saturated with 95% O_2/5% CO_2. Two-photon imaging was done using a Leica SP8 DIVE upright two-photon microscope with a SpectraPhysics InsightX3 dual line (tunable 680–1300 nm and 1045 nm) IR laser with pre-chirp compensation, 4 tunable non-descanned detectors, galvanometer confocal scanner and high-speed resonant confocal scanner. Time-lapse image acquisition was done by repeated imaging of XY planes of 512x512 pixels at 1.16 μm/pixel and Z-steps of 3 μm with XYZ stacks acquired every 30–60 sec for 30–60 min.

Two-Photon Image Analysis

Image analysis was performed using Imaris (Bitplane) and MATLAB (MathWorks). Images were linearly unmixed for possible bleed-over between channels, as previously described (80). Cells in lymph nodes that could be tracked for ≥10 minutes were used to obtain mean square displacement (MSD), speed, and arrest coefficient (time spent migrating at <2 μm/min). The Imaris 'surface' function was used to create a volume rendering of the T cells and BMDCs. T cell and BMDC motility was then tracked and T cell–APC interaction frequency and duration were calculated with a custom MATLAB script using a maximum distance between cells of 1 pixel (1.16 μm), with a minimum interaction of two minutes to be defined as an interaction.

Conjugate Assays and Actin Polymerization

$CD8^+$ T cells were negatively enriched from OT-I spleens (using $CD8^+$ EasySep kits) and labeled with 2.5 μM CTV in PBS for 15 min. For APCs, spleens were harvested from $CD45^{.1/.1}$ WT mice, RBCs lysed for 2.5 minutes in 175 mM NH_4Cl, and the splenocytes dye-labeled with 1 μM CFSE in PBS for 15 minutes. Splenocytes were pulsed with various concentrations of OVA peptide for 30 minutes, washed, and mixed with T cells at a 3:1 ratio of APCs to T cells (600,000:200,000 in 100 μL). Cells were briefly spun together in FACS tubes (214 g for 1 minute) and cocultured at 37°C with 10% CO_2. After 2 minutes, cells were fixed with 2% (w/v) paraformaldehyde (Electron Microscopy Sciences) in PBS for 10 minutes. The percentage of T cells that formed conjugates with APCs was then measured by flow cytometry. For actin polymerization analysis, cells were subsequently permeabilized with 0.5% (w/v) saponin (Millipore-Sigma) and stained with phalloidin-Alexa647 (ThermoFisher, Cat. A22287). Actin polymerization was assessed by flow cytometry and ImageStream (see next section). Fold change in phalloidin staining for both WT and EVL/VASP dKO T cell conjugates was calculated by normalizing phalloidin GMFI to respective conjugates that formed in the absence of antigen ("0 pM"). For conjugate stability experiments, splenocytes were pulsed with 1000 pM OVA peptide, and after a 2 minute incubation, T cell–APC co-cultures were vortexed (at a speed of 7/10 on a Vortex-Genie2 by Scientific Industries) for 1 second before adding PFA (2%) to fix conjugates. The change in frequency of T cell–APC conjugates was then measured by flow cytometry.

ImageStream Analysis

Cells from the same samples analyzed by flow cytometry in the conjugate assays and actin polymerization section were analyzed by imaging flow cytometry. Data was acquired and analyzed similarly to (81). In brief, images were collected on an ImageStream X cytometer for brightfield (BF), side scatter (SSC), CTV, CFSE, and Phalloidin-AlexaFluor-647 fluorescence. The gating strategy for analysis involved first selecting focused cells, *via* the 'gradient RMS' of the BF image, then an aspect ratio to include only doublet events. To refine the selection further, we then gated on CFSE and CTV double-positive doublets. Doublet-only T cell–APC conjugates were successfully identified using this strategy. Single color controls were used to create a compensation matrix that was applied to all sample files. T cells and APCs were defined using 'object' masks and identified based on fluorescence of the CFSE label (APCs) and the CTV label (T cells). After defining these objects, the interface feature was used to generate the masked region of overlap between the T cell and APC, considered the "synapse", in which phalloidin intensity was measured as intensity at the synapse/area of the synapse.

VASP Phosphorylation

Polyclonal WT T cells were harvested from C57BL/6 mice and activated with plate-bound anti-CD3 (2C11) and soluble anti-CD28 (PV-1) (BioXCell, Cat. BE0001-1 and BE0015) with autologous splenocytes for two days. Cells were then removed and re-plated with 10U/mL recombinant human IL-2, with media replacement every 2 days post-activation. On day 4 post-activation, dead cells were removed from the culture using a Histopaque-1119 (Sigma) density gradient. To measure VASP phosphorylation, day 7 polyclonal activated T cells were resuspended at 10×10^6 cells/mL in serum-free RPMI supplemented with 2% BSA (Sigma) and HEPES buffer (Corning). Control non-stimulating beads were prepared using latex beads (Invitrogen, Cat. S37227) coated with 4 μg/mL polyclonal Armenian hamster IgG (BioXCell, Cat. BE0091). DynaBeads Mouse T-Activator CD3/CD28 (ThermoFisher, Cat. 11452D) were used as directed by the manufacturer for stimulations. 1×10^6 cells were stimulated per sample by adding prewarmed beads to chilled cells, then briefly spun for 30 s at 6000 g to bring the cells and beads into contact. The samples were then placed on a 37°C heat block for 2 minutes or 10 minutes. Stimulation was quenched with cold PBS, and samples were vortexed, pelleted, and then lysed in a 1% Triton-X100 (Sigma, Cat. T9284) buffer containing Halt Protease and Phosphatase Inhibitors (Thermo Scientific, Cat. 78440). Lysates were stored at -80°C before processing. Lysates were run on SDS-PAGE with reducing buffer, then proteins were transferred to a nitrocellulose membrane. Total VASP was detected using a monoclonal rabbit antibody (Sigma; HPA005724) and pVASP-S153 (equivalent to human pVASP-S157) was detected using a monoclonal mouse antibody (Santa Cruz, Cat. sc-365564). As a loading control, GAPDH was detected using a monoclonal mouse antibody (Santa Cruz, Cat. sc-365062). For secondary antibodies, we used fluorophore conjugated donkey anti-mouse (Licor, Cat. 926-68072) and donkey anti-rabbit antibodies (Licor, Cat. 926-32213) and imaged and quantified the membranes using the Azure Biosystems Sapphire Imager and associated software.

Conjugate Immunofluorescence

tdTomato-BMDCs were differentiated, matured, and activated as described in the "Immunization and infection" Methods section above. On day 9 of culture, BMDCs were pulsed and activated with 2ng/mL $OVA_{257–264}$ peptide and 1 mg/mL LPS for 1 hour and washed. Nunc Lab-Tek II Chambered Coverglass (ThermoFisher, Cat. 155409) were coated with Poly-L-Lysine for 1 hour before 100,000 antigen-pulsed and activated BMDCs were plated and incubated at 37°C to enable adherence. After 1 hour, 150,000 $CD8^+$ T cells isolated from WT OT-I or EVL/VASP dKO OT-I mice (using $CD8^+$ EasySep kits) were gently added to chamber slides and incubated for 45 minutes to form conjugates. Cells were then fixed with 0.5% PFA for 10 minutes and stained using anti-mouse CD11a antibody (Biolegend, Cat. 101117) followed by anti-rat FITC or A647 (Jackson Immuno) and anti-mouse CD3ε A647 or FITC (Biolegend). Images were acquired on a Zeiss LSM800 scanning confocal with a 63X oil immersion objective. Image analysis was performed in ImageJ (version 2.1.0/1.53c; NIH) on unadjusted images. Receptor polarization was analyzed by defining the mean fluorescence intensity (MFI) of the contact region at the synapse divided by the MFI of a similar sized region at the back of the cell.

Statistical Analyses

Graphs of data and statistical analyses were done using Prism software (versions 7–9, GraphPad). The individual statistical tests used to analyze each experiment and the experimental repeats and sample sizes are reported in the figure legends.

DATA AVAILABILITY STATEMENT

The original contributions presented in the study are included in the article/**Supplementary Material**. Further inquiries can be directed to the corresponding author.

ETHICS STATEMENT

The animal study was reviewed and approved by Institutional Animal Care and Use Committee at the University of Colorado Anschutz Medical Campus and Institutional Animal Care and Use Committee at National Jewish Health.

AUTHOR CONTRIBUTIONS

MW designed research, performed experiments, analyzed the data, and wrote the manuscript. JR ran ImageStream and analyzed the respective data. AS helped with MATLAB script analysis and performed the experiments analyzing VASP phosphorylation. BW helped with listeria infections. JC helped with BMDC and bone marrow chimera generation. RK provided

guidance and lab space for listeria experiments. RF provided experimental design guidance and feedback on the manuscript. JJ designed and supervised the research, acquired funding, participated in data analysis, and wrote the manuscript. All authors contributed to the article and approved the submitted version.

FUNDING

This work was supported in part by grants from: NIAID R01AI125553 (JJ) and NIDDK R01DK111733 (RSF). MW and AS were supported in part by NIH Training Grant T32AI007405. This work was also supported in part by the University of Colorado Diabetes Research Center (DRC) grant P30DK116073; the spectral flow cytometer and the two-photon microscope employed for imaging are part of the Cell and Tissue Analysis Core of the University of Colorado Diabetes Research Center. The content of this work is solely the responsibility of the authors and does not necessarily represent the official views of the NIH.

ACKNOWLEDGMENTS

We would like to thank J. Olivas-Corral, B. Basta, J. Phares, E. Rodriguez, and O. Castro-Villasano for technical help with mouse colony maintenance and genotyping; S. Beard for technical assistance with flow cytometer maintenance; P. Beemiller, B. Levitt and J. Kleponis for assistance with coding MATLAB analysis scripts; J. Conley for guidance with nuclei isolation and staining. We would also like to thank the University of Colorado OLAR personnel for animal husbandry and technical assistance.

SUPPLEMENTARY MATERIAL

The Supplementary Material for this article can be found online at: https://www.frontiersin.org/articles/10.3389/fimmu.2022.856977/full#supplementary-material

Supplementary Figure 1 | EVL/VASP dKO T cells from bone marrow chimeras are functionally the same as those isolated directly from EVL/VASP dKO mice. Bone marrow chimeras were generated by reconstituting WT CD45$^{.1/.1}$ mice with EVL/VASP dKO OT-I CD45$^{.2/.2}$ or WT OT-I CD45$^{.1/.2}$ bone marrow. CD8$^+$ T cells were isolated from chimeric mice ≥8 weeks after reconstitution and 10,000 of each were transferred into WT CD45$^{.1/.1}$ recipient mice. Recipient mice were then infected I.V. with LM-OVA (2×10^3 PFUs) the following day and analyzed for Ag-specific CD8$^+$ T cell responses 6 days later. Endogenously matured CD8$^+$ T cells were harvested directly from EVL/VASP dKO OT-I CD45$^{.2/.2}$ or WT OT-I CD45$^{.1/.2}$ mice and transferred into WT CD45$^{.1/.1}$ recipient mice and infected in the same way. T cell numbers were normalized to the ratio of transferred EVL/VASP dKO/WT T cells recovered from spleens of uninfected recipient mice at the same timepoint. **(A)** Graphical schematic of the experimental method for obtaining donor T cells. **(B)** T cell numbers in the spleen of recipient mice at day 6 post LM infection. Recipient mice were transferred with endogenously matured T cells (left) or with bone marrow chimera matured T cells (middle). Ratios of EVL/VASP dKO/WT OT-I T cells for the two kinds of donor T cells (right panel). Each dot represents an average from a single experiment with ≥2 mice per group, from ≥4 experiments. Significance was assessed by paired t tests or for the EVL/VASP dKO/WT ratio one sample t tests compared to a hypothetical value of 1.0; ns is not significant, ** is $p < 0.01$, *** is $p < 0.001$, and **** is $p < 0.0001$.

Supplementary Figure 2 | EVL/VASP dKO T cells navigate the LN normally under homeostatic conditions. WT OT-I and EVL/VASP dKO OT-I T cells were isolated from donor mice and differentially dye-labeled with CTV or CTFR, and 5×10^5-1×10^6 of each were co-transferred at a 1:1 ratio into WT recipient mice. 24 hours later, popliteal LNs were harvested and analyzed by time-lapse two-photon microscopy. **(A)** Representative snapshot from a movie depicting the movement of EVL/VASP dKO OT-I T cells (cyan) and WT OT-I T cells (red) in the absence of cognate antigen. Track lines show the path of T cell movement imaged over 10 minutes. Time in min:sec; scale bar, depicted under the time-stamp, is 20 μm. **(B)** Mean square displacement (MSD ± SEM) over time of WT and EVL/VASP dKO OT-I T cells during homeostatic conditions in the absence of cognate antigen. **(C)** Analysis of T cell motility parameters. Quantification of WT and EVL/VASP dKO OT-I T cell average mean track speed, track straightness, and arrest coefficient (percentage of each track in which instantaneous velocity <2 μm/min) during homeostatic conditions. Data represents averages from a total of 3 experiments. There was no significant difference (ns), as assessed by two-way ANOVA interaction effects **(B)** and paired T tests **(C)**.

Supplementary Movie 1 | Polyclonal WT and EVL/VASP dKO T cells were isolated, differentially dye-labeled with CTV or CTFR, and co-transferred at a 1:1 ratio into WT recipient mice. 24 hours later, popliteal LNs were harvested and analyzed by time-lapse two-photon microscopy. Individual EVL/VASP dKO T cells (cyan) and WT T cells (red) were tracked in the absence of cognate antigen over 30 minutes. Track lines show the path of T cell movement imaged over the last 10 minutes. Scale bar, 20 μm.

Supplementary Movie 2 | WT OT-I, EVL/VASP dKO OT-I, and polyclonal WT T cells were isolated, differentially dye-labeled, and co-transferred into WT recipient mice. 24 hours later, 2.5×10^5 mature, LPS-activated OVA-pulsed tdTomato-BMDCs were injected subcutaneously into both hind footpads of recipient mice. After 13 hours, mice were euthanized and the draining popliteal LNs were harvested and analyzed by time-lapse two-photon microscopy. Individual T cells were tracked and their interactions with BMDCs were also quantified. This example movie depicts the movement of EVL/VASP dKO OT-I T cells (green), WT OT-I T cells (cyan), polyclonal control T cells (yellow), and pulsed BMDCs (red). Track lines show the path of T cell movement imaged over 33 minutes. Scale bar, 50 μm; time in min:sec.

Supplementary Movie 3 | WT OT-I, EVL/VASP dKO OT-I, and polyclonal WT T cells were isolated, differentially dye-labeled, and co-transferred into WT recipient mice. 24 hours later, 2.5×10^5 mature, LPS-activated OVA-pulsed tdTomato-BMDCs were injected subcutaneously into both hind footpads of recipient mice. After 13 hours, mice were euthanized and the draining popliteal LNs were harvested and analyzed by time-lapse two-photon microscopy. Individual T cells were tracked and their interactions with BMDCs were also quantified. This example movie depicts the movement of EVL/VASP dKO OT-I T cells (green), WT OT-I T cells (cyan), polyclonal control T cells (yellow), and pulsed BMDCs (red). Track lines show the path of T cell movement imaged over 30 minutes. Scale bar, 30 μm; time in min:sec.

REFERENCES

1. Katakai T, Habiro K, Kinashi T. Dendritic Cells Regulate High-Speed Interstitial T Cell Migration in the Lymph Node *via* LFA-1/ICAM-1. *J Immunol (Baltimore Md 1950).* (2013) 191(3):1188–99. doi: 10.4049/jimmunol.1300739
2. Bajénoff M, Egen JG, Koo LY, Laugier JP, Brau F, Glaichenhaus N, et al. Stromal Cell Networks Regulate Lymphocyte Entry, Migration, and Territoriality in Lymph Nodes. *Immunity* (2006) 25(6):989–1001. doi: 10.1016/j.immuni.2006.10.011
3. Miller MJ, Hejazi AS, Wei SH, Cahalan MD, Parker I. T Cell Repertoire Scanning Is Promoted by Dynamic Dendritic Cell Behavior and Random T

Cell Motility in the Lymph Node. *Proc Natl Acad Sci USA* (2004) 101(4):998–1003. doi: 10.1073/pnas.0306407101
4. Hons M, Kopf A, Hauschild R, Leithner A, Gaertner F, Abe J, et al. Chemokines and Integrins Independently Tune Actin Flow and Substrate Friction During Intranodal Migration of T Cells. *Nat Immunol* (2018) 19 (6):606–16. doi: 10.1038/s41590-018-0109-z
5. Reversat A, Gaertner F, Merrin J, Stopp J, Tasciyan S, Aguilera J, et al. Cellular Locomotion Using Environmental Topography. *Nature* (2020) 582 (7813):582–5. doi: 10.1038/s41586-020-2283-z
6. Krummel MF, Bartumeus F, Gerard A. T Cell Migration, Search Strategies and Mechanisms. *Nat Rev Immunol* (2016) 16(3):193–201. doi: 10.1038/nri.2015.16
7. Gerard A, Patino-Lopez G, Beemiller P, Nambiar R, Ben-Aissa K, Liu Y, et al. Detection of Rare Antigen-Presenting Cells Through T Cell-Intrinsic Meandering Motility, Mediated by Myo1g. *Cell* (2014) 158(3):492–505. doi: 10.1016/j.cell.2014.05.044
8. Kaiser A, Donnadieu E, Abastado JP, Trautmann A, Nardin A. CC Chemokine Ligand 19 Secreted by Mature Dendritic Cells Increases Naive T Cell Scanning Behavior and Their Response to Rare Cognate Antigen. *J Immunol (Baltimore Md 1950).* (2005) 175(4):2349–56. doi: 10.4049/jimmunol.175.4.2349
9. Wülfing C, Davis MM. A Receptor/cytoskeletal Movement Triggered by Costimulation During T Cell Activation. *Sci (New York NY).* (1998) 282 (5397):2266–9. doi: 10.1126/science.282.5397.2266
10. Skokos D, Shakhar G, Varma R, Waite JC, Cameron TO, Lindquist RL, et al. Peptide-MHC Potency Governs Dynamic Interactions Between T Cells and Dendritic Cells in Lymph Nodes. *Nat Immunol* (2007) 8(8):835–44. doi: 10.1038/ni1490
11. Mempel TR, Henrickson SE, Von Andrian UH. T-Cell Priming by Dendritic Cells in Lymph Nodes Occurs in Three Distinct Phases. *Nature* (2004) 427 (6970):154–9. doi: 10.1038/nature02238
12. Miller MJ, Safrina O, Parker I, Cahalan MD. Imaging the Single Cell Dynamics of CD4+ T Cell Activation by Dendritic Cells in Lymph Nodes. *J Exp Med* (2004) 200(7):847–56. doi: 10.1084/jem.20041236
13. Dustin ML, Bromley SK, Kan Z, Peterson DA, Unanue ER. Antigen Receptor Engagement Delivers a Stop Signal to Migrating T Lymphocytes. *Proc Natl Acad Sci USA* (1997) 94(8):3909–13. doi: 10.1073/pnas.94.8.3909
14. Yi J, Wu XS, Crites T, Hammer JA 3rd. Actin Retrograde Flow and Actomyosin II Arc Contraction Drive Receptor Cluster Dynamics at the Immunological Synapse in Jurkat T Cells. *Mol Biol Cell* (2012) 23(5):834–52. doi: 10.1091/mbc.e11-08-0731
15. Friedman RS, Beemiller P, Sorensen CM, Jacobelli J, Krummel MF. Real-Time Analysis of T Cell Receptors in Naive Cells *In Vitro* and *In Vivo* Reveals Flexibility in Synapse and Signaling Dynamics. *J Exp Med* (2010) 207 (12):2733–49. doi: 10.1084/jem.20091201
16. Babich A, Li S, O'Connor RS, Milone MC, Freedman BD, Burkhardt JK. F-Actin Polymerization and Retrograde Flow Drive Sustained Plcγ1 Signaling During T Cell Activation. *J Cell Biol* (2012) 197(6):775–87. doi: 10.1083/jcb.201201018
17. Campi G, Varma R, Dustin ML. Actin and Agonist MHC-Peptide Complex-Dependent T Cell Receptor Microclusters as Scaffolds for Signaling. *J Exp Med* (2005) 202(8):1031–6. doi: 10.1084/jem.20051182
18. Varma R, Campi G, Yokosuka T, Saito T, Dustin ML. T Cell Receptor-Proximal Signals Are Sustained in Peripheral Microclusters and Terminated in the Central Supramolecular Activation Cluster. *Immunity* (2006) 25 (1):117–27. doi: 10.1016/j.immuni.2006.04.010
19. Das V, Nal B, Dujeancourt A, Thoulouze MI, Galli T, Roux P, et al. Activation-Induced Polarized Recycling Targets T Cell Antigen Receptors to the Immunological Synapse; Involvement of SNARE Complexes. *Immunity* (2004) 20(5):577–88. doi: 10.1016/S1074-7613(04)00106-2
20. Comrie WA, Babich A, Burkhardt JK. F-Actin Flow Drives Affinity Maturation and Spatial Organization of LFA-1 at the Immunological Synapse. *J Cell Biol* (2015) 208(4):475–91. doi: 10.1083/jcb.201406121
21. Murugesan S, Hong J, Yi J, Li D, Beach JR, Shao L, et al. Formin-Generated Actomyosin Arcs Propel T Cell Receptor Microcluster Movement at the Immune Synapse. *J Cell Biol* (2016) 215(3):383–99. doi: 10.1083/jcb.201603080
22. Lafouresse F, Cotta-de-Almeida V, Malet-Engra G, Galy A, Valitutti S, Dupre L. Wiskott-Aldrich Syndrome Protein Controls Antigen-Presenting Cell-Driven CD4+ T-Cell Motility by Regulating Adhesion to Intercellular Adhesion Molecule-1. *Immunology* (2012) 137(2):183–96. doi: 10.1111/j.1365-2567.2012.03620.x
23. Bouma G, Mendoza-Naranjo A, Blundell MP, de Falco E, Parsley KL, Burns SO, et al. Cytoskeletal Remodeling Mediated by WASp in Dendritic Cells Is Necessary for Normal Immune Synapse Formation and T-Cell Priming. *Blood* (2011) 118(9):2492–501. doi: 10.1182/blood-2011-03-340265
24. Grakoui A, Bromley SK, Sumen C, Davis MM, Shaw AS, Allen PM, et al. The Immunological Synapse: A Molecular Machine Controlling T Cell Activation. *Sci (New York NY).* (1999) 285(5425):221–7. doi: 10.1126/science.285.5425.221
25. Monks CRF, Freiberg BA, Kupfer H, Sciaky N, Kupfer A. Three-Dimensional Segregation of Supramolecular Activation Clusters in T Cells. *Nature* (1998) 395(6697):82–6. doi: 10.1038/25764
26. Brossard C, Feuillet V, Schmitt A, Randriamampita C, Romao M, Raposo G, et al. Multifocal Structure of the T Cell – Dendritic Cell Synapse. *Eur J Immunol* (2005) 35(6):1741–53. doi: 10.1002/eji.200425857
27. Thompson SB, Waldman MM, Jacobelli J. Polymerization Power: Effectors of Actin Polymerization as Regulators of T Lymphocyte Migration Through Complex Environments. *FEBS J* (2021). doi: 10.1111/febs.16130
28. Chesarone MA, Goode BL. Actin Nucleation and Elongation Factors: Mechanisms and Interplay. *Curr Opin Cell Biol* (2009) 21(1):28–37. doi: 10.1016/j.ceb.2008.12.001
29. Gomez TS, Kumar K, Medeiros RB, Shimizu Y, Leibson PJ, Billadeau DD. Formins Regulate the Actin-Related Protein 2/3 Complex-Independent Polarization of the Centrosome to the Immunological Synapse. *Immunity* (2007) 26(2):177–90. doi: 10.1016/j.immuni.2007.01.008
30. Sakata D, Taniguchi H, Yasuda S, Adachi-Morishima A, Hamazaki Y, Nakayama R, et al. Impaired T Lymphocyte Trafficking in Mice Deficient in an Actin-Nucleating Protein, Mdia1. *J Exp Med* (2007) 204(9):2031–8. doi: 10.1084/jem.20062647
31. Eisenmann KM, West RA, Hildebrand D, Kitchen SM, Peng J, Sigler R, et al. T Cell Responses in Mammalian Diaphanous-Related Formin Mdia1 Knock-Out Mice. *J Biol Chem* (2007) 282(34):25152–8. doi: 10.1074/jbc.M703243200
32. Thompson SB, Sandor AM, Lui V, Chung JW, Waldman MM, Long RA, et al. Formin-Like 1 Mediates Effector T Cell Trafficking to Inflammatory Sites to Enable T Cell-Mediated Autoimmunity. *eLife* (2020) 9. doi: 10.7554/eLife.58046
33. Breitsprecher D, Kiesewetter AK, Linkner J, Urbanke C, Resch GP, Small JV, et al. Clustering of VASP Actively Drives Processive, WH2 Domain-Mediated Actin Filament Elongation. *EMBO J* (2008) 27(22):2943–54. doi: 10.1038/emboj.2008.211
34. Chen XJ, Squarr AJ, Stephan R, Chen B, Higgins TE, Barry DJ, et al. Ena/VASP Proteins Cooperate With the WAVE Complex to Regulate the Actin Cytoskeleton. *Dev Cell* (2014) 30(5):569–84. doi: 10.1016/j.devcel.2014.08.001
35. Krause M, Dent EW, Bear JE, Loureiro JJ, Gertler FB. Ena/VASP Proteins: Regulators of the Actin Cytoskeleton and Cell Migration. *Annu Rev Cell Dev Biol* (2003) 19:541–64. doi: 10.1146/annurev.cellbio.19.050103.103356
36. Ferron F, Rebowski G, Lee SH, Dominguez R. Structural Basis for the Recruitment of Profilin-Actin Complexes During Filament Elongation by Ena/VASP. *EMBO J* (2007) 26(21):4597–606. doi: 10.1038/sj.emboj.7601874
37. Reinhard M, Jouvenal K, Tripier D, Walter U. Identification, Purification, and Characterization of a Zyxin-Related Protein That Binds the Focal Adhesion and Microfilament Protein VASP (Vasodilator-Stimulated Phosphoprotein). *Proc Natl Acad Sci USA* (1995) 92(17):7956–60. doi: 10.1073/pnas.92.17.7956
38. Gertler FB, Niebuhr K, Reinhard M, Wehland J, Soriano P. Mena, a Relative of VASP and Drosophila Enabled, Is Implicated in the Control of Microfilament Dynamics. *Cell* (1996) 87(2):227–39. doi: 10.1016/S0092-8674(00)81341-0
39. Rottner K, Behrendt B, Small JV, Wehland J. VASP Dynamics During Lamellipodia Protrusion. *Nat Cell Biol* (1999) 1(5):321–2. doi: 10.1038/13040
40. Lambrechts A, Kwiatkowski AV, Lanier LM, Bear JE, Vandekerckhove J, Ampe C, et al. cAMP-Dependent Protein Kinase Phosphorylation of EVL, a Mena/VASP Relative, Regulates Its Interaction With Actin and SH3 Domains. *J Biol Chem* (2000) 275(46):36143–51. doi: 10.1074/jbc.M006274200
41. Svitkina TM, Bulanova EA, Chaga OY, Vignjevic DM, Kojima S, Vasiliev JM, et al. Mechanism of Filopodia Initiation by Reorganization of a Dendritic Network. *J Cell Biol* (2003) 160(3):409–21. doi: 10.1083/jcb.200210174

42. Bailly M. Ena/VASP Family: New Partners, Bigger Enigma. *Dev Cell* (2004) 7 (4):462–3. doi: 10.1016/j.devcel.2004.09.008
43. Benz PM, Blume C, Seifert S, Wilhelm S, Waschke J, Schuh K, et al. Differential VASP Phosphorylation Controls Remodeling of the Actin Cytoskeleton. *J Cell Sci* (2009) 122(Pt 21):3954–65. doi: 10.1242/jcs.044537
44. Bear JE, Svitkina TM, Krause M, Schafer DA, Loureiro JJ, Strasser GA, et al. Antagonism Between Ena/VASP Proteins and Actin Filament Capping Regulates Fibroblast Motility. *Cell* (2002) 109(4):509–21. doi: 10.1016/S0092-8674(02)00731-6
45. Damiano-Guercio J, Kurzawa L, Mueller J, Dimchev G, Schaks M, Nemethova M, et al. Loss of Ena/VASP Interferes With Lamellipodium Architecture, Motility and Integrin-Dependent Adhesion. *eLife* (2020) 9. doi: 10.7554/eLife.55351
46. Hu LD, Zou HF, Zhan SX, Cao KM. EVL (Ena/VASP-Like) Expression is Up-Regulated in Human Breast Cancer and Its Relative Expression Level Is Correlated With Clinical Stages. *Oncol Rep* (2008) 19(4):1015–20. doi: 10.3892/or.19.4.1015
47. Barone M, Müller M, Chiha S, Ren J, Albat D, Soicke A, et al. Designed Nanomolar Small-Molecule Inhibitors of Ena/VASP EVH1 Interaction Impair Invasion and Extravasation of Breast Cancer Cells. *Proc Natl Acad Sci USA* (2020) 117(47):29684–90. doi: 10.1073/pnas.2007213117
48. Krause M, Sechi AS, Konradt M, Monner D, Gertler FB, Wehland J. Fyn-Binding Protein (Fyb)/SLP-76-Associated Protein (SLAP), Ena/vasodilator-Stimulated Phosphoprotein (VASP) Proteins and the Arp2/3 Complex Link T Cell Receptor (TCR) Signaling to the Actin Cytoskeleton. *J Cell Biol* (2000) 149(1):181–94. doi: 10.1083/jcb.149.1.181
49. Estin ML, Thompson SB, Traxinger B, Fisher MH, Friedman RS, Jacobelli J. Ena/VASP Proteins Regulate Activated T-Cell Trafficking by Promoting Diapedesis During Transendothelial Migration. *Proc Natl Acad Sci USA* (2017) 114(14):E2901-e10. doi: 10.1073/pnas.1701886114
50. Miller MJ, Wei SH, Parker I, Cahalan MD. Two-Photon Imaging of Lymphocyte Motility and Antigen Response in Intact Lymph Node. *Sci (New York NY).* (2002) 296(5574):1869–73. doi: 10.1126/science.1070051
51. Hugues S, Fetler L, Bonifaz L, Helft J, Amblard F, Amigorena S. Distinct T Cell Dynamics in Lymph Nodes During the Induction of Tolerance and Immunity. *Nat Immunol* (2004) 5(12):1235–42. doi: 10.1038/ni1134
52. Katakai T, Hara T, Lee JH, Gonda H, Sugai M, Shimizu A. A Novel Reticular Stromal Structure in Lymph Node Cortex: An Immuno-Platform for Interactions Among Dendritic Cells, T Cells and B Cells. *Int Immunol* (2004) 16(8):1133–42. doi: 10.1093/intimm/dxh113
53. Henrickson SE, Mempel TR, Mazo IB, Liu B, Artyomov MN, Zheng H, et al. T Cell Sensing of Antigen Dose Governs Interactive Behavior With Dendritic Cells and Sets a Threshold for T Cell Activation. *Nat Immunol* (2008) 9 (3):282–91. doi: 10.1038/ni1559
54. Benson RA, Brewer JM, Garside P. Visualizing and Tracking T Cell Motility *In Vivo*. *Methods Mol Biol (Clifton NJ)* (2017) 1591:27–41. doi: 10.1007/978-1-4939-6931-9_3
55. Bousso P, Robey E. Dynamics of CD8+ T Cell Priming by Dendritic Cells in Intact Lymph Nodes. *Nat Immunol* (2003) 4(6):579–85. doi: 10.1038/ni928
56. Conley JM, Gallagher MP, Rao A, Berg LJ. Activation of the Tec Kinase ITK Controls Graded IRF4 Expression in Response to Variations in TCR Signal Strength. *J Immunol (Baltimore Md 1950).* (2020) 205(2):335–45. doi: 10.4049/jimmunol.1900853
57. Celli S, Lemaître F, Bousso P. Real-Time Manipulation of T Cell-Dendritic Cell Interactions *In Vivo* Reveals the Importance of Prolonged Contacts for CD4+ T Cell Activation. *Immunity* (2007) 27(4):625–34. doi: 10.1016/j.immuni.2007.08.018
58. Katzman SD, O'Gorman WE, Villarino AV, Gallo E, Friedman RS, Krummel MF, et al. Duration of Antigen Receptor Signaling Determines T-Cell Tolerance or Activation. *Proc Natl Acad Sci USA* (2010) 107(42):18085–90. doi: 10.1073/pnas.1010560107
59. Bromley SK, Peterson DA, Gunn MD, Dustin ML. Cutting Edge: Hierarchy of Chemokine Receptor and TCR Signals Regulating T Cell Migration and Proliferation. *J Immunol (Baltimore Md 1950).* (2000) 165(1):15–9. doi: 10.4049/jimmunol.165.1.15
60. Friedman RS, Jacobelli J, Krummel MF. Surface-Bound Chemokines Capture and Prime T Cells for Synapse Formation. *Nat Immunol* (2006) 7(10):1101–8. doi: 10.1038/ni1384
61. Dustin ML. Visualization of Cell-Cell Interaction Contacts: Synapses and Kinapses. *Self Nonself* (2011) 2(2):85–97. doi: 10.4161/self.2.2.17931
62. Dustin ML. Cell Adhesion Molecules and Actin Cytoskeleton at Immune Synapses and Kinapses. *Curr Opin Cell Biol* (2007) 19(5):529–33. doi: 10.1016/j.ceb.2007.08.003
63. Sims TN, Soos TJ, Xenias HS, Dubin-Thaler B, Hofman JM, Waite JC, et al. Opposing Effects of PKCtheta and WASp on Symmetry Breaking and Relocation of the Immunological Synapse. *Cell* (2007) 129(4):773–85. doi: 10.1016/j.cell.2007.03.037
64. Calvez R, Lafouresse F, De Meester J, Galy A, Valitutti S, Dupré L. The Wiskott-Aldrich Syndrome Protein Permits Assembly of a Focused Immunological Synapse Enabling Sustained T-Cell Receptor Signaling. *Haematologica* (2011) 96(10):1415–23. doi: 10.3324/haematol.2011.040204
65. Moreau HD, Lemaître F, Garrod KR, Garcia Z, Lennon-Duménil AM, Bousso P. Signal Strength Regulates Antigen-Mediated T-Cell Deceleration by Distinct Mechanisms to Promote Local Exploration or Arrest. *Proc Natl Acad Sci USA* (2015) 112(39):12151–6. doi: 10.1073/pnas.1506654112
66. Nordenfelt P, Elliott HL, Springer TA. Coordinated Integrin Activation by Actin-Dependent Force During T-Cell Migration. *Nat Commun* (2016) 7:13119. doi: 10.1038/ncomms13119
67. Mitchell JS, Burbach BJ, Srivastava R, Fife BT, Shimizu Y. Multistage T Cell-Dendritic Cell Interactions Control Optimal CD4 T Cell Activation Through the ADAP-SKAP55-Signaling Module. *J Immunol (Baltimore Md 1950).* (2013) 191(5):2372–83. doi: 10.4049/jimmunol.1300107
68. Wabnitz G, Balta E, Samstag Y. L-Plastin Regulates the Stability of the Immune Synapse of Naive and Effector T-Cells. *Adv Biol Regulation* (2017) 63:107–14. doi: 10.1016/j.jbior.2016.09.009
69. Wilton KM, Overlee BL, Billadeau DD. NKG2D-DAP10 Signaling Recruits EVL to the Cytotoxic Synapse to Generate F-Actin and Promote NK Cell Cytotoxicity. *J Cell Sci* (2019) 133(5). doi: 10.1242/jcs.230508
70. Lewis JB, Scangarello FA, Murphy JM, Eidell KP, Sodipo MO, Ophir MJ, et al. ADAP Is an Upstream Regulator That Precedes SLP-76 at Sites of TCR Engagement and Stabilizes Signaling Microclusters. *J Cell Sci* (2018) 131(21). doi: 10.1242/jcs.215517
71. Horstrup K, Jablonka B, Hönig-Liedl P, Just M, Kochsiek K, Walter U. Phosphorylation of Focal Adhesion Vasodilator-Stimulated Phosphoprotein at Ser157 in Intact Human Platelets Correlates With Fibrinogen Receptor Inhibition. *Eur J Biochem* (1994) 225(1):21–7. doi: 10.1111/j.1432-1033.1994.00021.x
72. Marangoni F, Murooka TT, Manzo T, Kim EY, Carrizosa E, Elpek NM, et al. The Transcription Factor NFAT Exhibits Signal Memory During Serial T Cell Interactions With Antigen-Presenting Cells. *Immunity* (2013) 38(2):237–49. doi: 10.1016/j.immuni.2012.09.012
73. Brodovitch A, Shenderov E, Cerundolo V, Bongrand P, Pierres A, van der Merwe PA. T Lymphocytes Need Less Than 3 Min to Discriminate Between Peptide MHCs With Similar TCR-Binding Parameters. *Eur J Immunol* (2015) 45(6):1635–42. doi: 10.1002/eji.201445214
74. Kwiatkowski AV, Rubinson DA, Dent EW, Edward van Veen J, Leslie JD, Zhang J, et al. Ena/VASP Is Required for Neuritogenesis in the Developing Cortex. *Neuron* (2007) 56(3):441–55. doi: 10.1016/j.neuron.2007.09.008
75. Aszódi A, Pfeifer A, Ahmad M, Glauner M, Zhou XH, Ny L, et al. The Vasodilator-Stimulated Phosphoprotein (VASP) Is Involved in cGMP- and cAMP-Mediated Inhibition of Agonist-Induced Platelet Aggregation, But Is Dispensable for Smooth Muscle Function. *EMBO J* (1999) 18(1):37–48. doi: 10.1093/emboj/18.1.37
76. Pope C, Kim S-K, Marzo A, Williams K, Jiang J, Shen H, et al. Organ-Specific Regulation of the CD8 T Cell Response to Listeria Monocytogenes Infection. *J Immunol* (2001) 166(5):3402–9. doi: 10.4049/jimmunol.166.5.3402
77. Humann J, Bjordahl R, Andreasen K, Lenz LL. Expression of the P60 Autolysin Enhances NK Cell Activation and Is Required for Listeria

Monocytogenes Expansion in IFN-γ-Responsive Mice. *J Immunol* (2007) 178 (4):2407–14. doi: 10.4049/jimmunol.178.4.2407
78. Gallagher MP, Conley JM, Berg LJ. Peptide Antigen Concentration Modulates Digital NFAT1 Activation in Primary Mouse Naive CD8+ T Cells as Measured by Flow Cytometry of Isolated Cell Nuclei. *ImmunoHorizons* (2018) 2(7):208–15. doi: 10.4049/immunohorizons.1800032
79. Jacobelli J, Friedman RS, Conti MA, Lennon-Dumenil AM, Piel M, Sorensen CM, et al. Confinement-Optimized Three-Dimensional T Cell Amoeboid Motility Is Modulated *via* Myosin IIA-Regulated Adhesions. *Nat Immunol* (2010) 11(10):953–61. doi: 10.1038/ni.1936
80. Bullen A, Friedman RS, Krummel MF. Two-Photon Imaging of the Immune System: A Custom Technology Platform for High-Speed, Multicolor Tissue Imaging of Immune Responses. *Curr topics Microbiol Immunol* (2009) 334:1–29. doi: 10.1007/978-3-540-93864-4_1
81. Markey KA, Gartlan KH, Kuns RD, MacDonald KP, Hill GR. Imaging the Immunological Synapse Between Dendritic Cells and T Cells. *J Immunol Methods* (2015) 423:40–4. doi: 10.1016/j.jim.2015.04.029

Conflict of Interest: The authors declare that the research was conducted in the absence of any commercial or financial relationships that could be construed as a potential conflict of interest.

Publisher's Note: All claims expressed in this article are solely those of the authors and do not necessarily represent those of their affiliated organizations, or those of the publisher, the editors and the reviewers. Any product that may be evaluated in this article, or claim that may be made by its manufacturer, is not guaranteed or endorsed by the publisher.

frontiers | Frontiers in Immunology

MINI REVIEW
published: 29 June 2022
doi: 10.3389/fimmu.2022.916137

Efficient T Cell Migration and Activation Require L-Plastin

Hemant Joshi[1,2] *and Sharon Celeste Morley*[1,2]*

[1] Division of Infectious Diseases, Department of Medicine, Washington University School of Medicine, St. Louis, MO, United States, [2] Division of Immunobiology, Department of Immunology and Pathology, Washington University School of Medicine, St. Louis, MO, United States

Rapid re-organization of the actin cytoskeleton supports T-cell trafficking towards immune sites and interaction with antigen presenting cells (APCs). F-actin rearrangement enables T-cell trafficking by stabilizing adhesion to vascular endothelial cells and promoting transendothelial migration. T-cell/APC immune synapse (IS) maturation also relies upon f-actin-anchored LFA-1:ICAM-1 ligation. Therefore, efficient T-cell responses require tight regulation of f-actin dynamics. In this review, we summarize how the actin-bundling protein L-plastin (LPL) regulates T-cell activation and migration. LPL enhances f-actin polymerization and also directly binds to the β2 chain of the integrin LFA-1 to support intercellular adhesion and IS formation in human and murine T cells. LPL- deficient T cells migrate slowly in response to chemo-attractants such as CXCL12, CCL19, and poorly polarize towards ICAM-1. Loss of LPL impairs thymic egress and intranodal motility. LPL is also required for T-cell IS maturation with APCs, and therefore for efficient cytokine production and proliferation. LPL$^{-/-}$ mice are less susceptible to T-cell mediated pathologies, such as allograft rejection and experimental autoimmune encephalomyelitis (EAE). LPL activity is regulated by its N-terminal "headpiece", which contains serine and threonine phosphorylation and calcium- and calmodulin-binding sites. LPL phosphorylation is required for lamellipodia formation during adhesion and migration, and also for LFA-1 clustering during IS formation. However, the precise molecular interactions by which LPL supports T-cell functional responses remain unclear. Future studies elucidating LPL-mediated regulation of T-cell migration and/or activation may illuminate pathways for therapeutic targeting in T-cell-mediated diseases.

Keywords: T cells, L-plastin, immune synapse formation, immune cell adhesion and migration, mechanotransduction, LFA-1 (CD11A/CD18; ITGAL/ITGB2), F-actin assembly, cytoskeleton

OPEN ACCESS

Edited by:
Manish Butte,
University of California,
Los Angeles, United States

Reviewed by:
Jeremie Rossy,
Biotechnology Institute Thurgau,
Switzerland

Tim Thauland,
University of California,
Los Angeles, United States

***Correspondence:**
Sharon Celeste Morley
morleys@wustl.edu

Specialty section:
This article was submitted to T Cell Biology, a section of the journal Frontiers in Immunology

Received: *08 April 2022*
Accepted: *02 June 2022*
Published: *29 June 2022*

Citation:
Joshi H and Morley SC (2022) Efficient T Cell Migration and Activation Require L-Plastin. Front. Immunol. 13:916137. doi: 10.3389/fimmu.2022.916137

INTRODUCTION

Activated T cells drive adaptive immune responses. Effective T cell responses require rapid migration towards immune sites, followed by engagement with antigen presenting cells (APCs) (1, 2). By supporting migration and adhesion, cytoskeletal rearrangements regulate the quality and magnitude of the T cell response. The cytoskeleton comprises filamentous proteins including microtubules, actin filaments, and intermediate filaments (3). Receptor engagement, internal organization of the cytoplasm, and stabilization against applied forces trigger cytoskeleton

rearrangement (4). For instance, chemokine receptor engagement promotes T-cell motility, shear flow activates T cell adhesion, and T cell receptor (TCR) engagement to peptide-major histocompatibility complex (pMHCs) on APCs triggers immune synapse (IS) formation (5–7).

Actin filaments are the most dynamic cytoskeletal proteins that respond to and direct T-cell biological processes. Actin filaments (f-actin) are formed by the rapid assembly of globular-actin (g-actin) monomers. Bundling, or cross-linking filaments, further remodels f-actin (8, 9). F-actin polymerization is ATP-dependent; ATP binding to monomeric g-actin enhances its affinity for f-actin association (polymerization), while hydrolysis of bound ATP to ADP triggers dissociation (depolymerization). An array of actin-binding proteins regulate actin turnover through g-actin sequestration, nucleation, ATP hydrolysis, nucleotide exchange, f-actin severing, capping, and bundling (10, 11). This review focus on how efficient T cell activation and migration rely on the f-actin bundling protein, leukocyte plastin (L-plastin; LPL).

LPL, also known as lcp1 or plastin-2, bundles f-actin (8, 12, 13). LPL belongs to the plastin family of actin-binding proteins, comprising three isotypes: LPL, T-plastin and I –plastin. Each isoform exhibits distinct tissue expression. Only LPL is expressed in immune cells. Consistent with its expression in hematopoietic cells, LPL specifically binds to β-actin, and does not interact with skeletal muscle α-actin or smooth muscle γ-actin (8). Physiologic LPL expression is restricted to replicating hematopoietic cells, but LPL is also ectopically overexpressed in multiple transformed cancer cells (14). LPL is a 66 kDa protein, consisting of an N-terminal regulatory "headpiece" and 2 actin-binding domains (ABDs); ABD1 and ABD2 (**Figure 1A**). LPL is distinguished from I- and T-plastin by its N-terminal regulatory sequence, as it is the only isoform containing two serine phosphorylation sites at Ser5 and Ser7. Each ABD contains tandem calponin homology (CH) domains (11, 15). How ABD1 and ABD2 of LPL coordinate to engage two actin filaments has not been fully described, because full-length LPL crystallization is unavailable. However, analysis of the available ABD2 structure along with available T-plastin and the *Arabidopsis thalinana* fimbrin (LPL orthologue) protein structures (16) suggests that binding of LPL-ABD2 to f-actin induces "closure" of the actin monomeric ATP binding site. The "closed" conformation inhibits hydrolysis to ADP, reducing depolymerization and stabilizing the actin filament (17). To stabilize bundles, LPL may adopt a twisted conformation, supporting the binding of ABD2 to one filament and activating ABD1 to bind another actin filament, generating cross-linked f-actin (17). Thus, LPL binding stabilizes polymerized actin, as well as altering the twist and tilt of each filament, while LPL bundling arranges filaments into parallel arrays (**Figure 1B**) (16, 18). LPL actin-binding is separable from its function in actin-bundling.

The actin-binding and actin-bundling activities are regulated by the N-terminal headpiece of LPL. The headpiece harbors at least three phosphorylation sites (Ser-5, Ser-7 and Thr-89), two calcium-binding EF-hand loops, and a consensus sequence for calmodulin binding (19–21). Under some conditions, phosphorylation of Ser-5 and Ser-7 enhances actin-bundling activity, and localizes LPL to sites of actin assembly (13, 22, 23). For example, IL-2 stimulation, CD3/CD28 or CD3/CD2 receptor engagement, and CXCL12 treatment all induce Ser-5 phosphorylation (24, 25). However, recent biochemical evidence suggests that single Ser-5 phosphorylation is irrelevant to LPL bundling activity (26), but enhances binding to f-actin structures in non-immune cells and under *in vitro* conditions (13). In T cells, LPL-mediated actin-bundling activity was first noted in a calcium-regulated manner (8). Calcium chelation by the high-affinity EF hands reduces the actin-bundling, but not the actin-binding, activity of LPL (9) (26). Jurkat T cells show increased actin-bundling activity in low intracellular Ca^{2+} concentration of 10^{-7} M, while incubation in higher concentrations, such as 10^{-6} M Ca^{2+}, destabilized f-actin bundles (8). Immune cells maintain 10^{-8}-10^{-7} M Ca^{2+} in resting phase while elevating to 10^{-6} upon activation, inducing f-actin rearrangement (e.g. intracellular Ca^{2+} is estimated to 50 nM in resting cells and > 1 mM in activated T cells) (27, 28). The physiological range of Ca^{2+} found in T cells correlates with the concentrations of Ca^{2+} that modulate LPL bundling activity. The spatiotemporal regulation of Ca^{2+} flux and LPL activity at the T cell immunological synapse (IS) is discussed in detail later.

In addition to bundling actin, LPL also directly binds to the cytoplasmic tail of the β1 or β2 subunits of integrins. The regulation of integrin affinity and/or avidity by LPL is poorly understood. In brief, integrins are transmembrane heterodimers that bind extracellular matrix proteins or receptors expressed on other cells and mediate cellular adhesion. The dominant integrin mediating T cell adhesion, LFA-1 ($\alpha_L\beta_2$; CD11a/CD18), exists in three affinity states: a low-affinity, "bent-closed" state, an intermediate affinity "extended-closed" state, and the high-affinity "extended-open" state (**Figure 1C**) (29). Conversion from the low- to intermediate-affinity state is induced by inside-out signaling; limited evidence suggests that LPL may be dispensable for this conversion (30, 31). However, studies in neutrophils indicated that binding of the β2 cytoplasmic tail by the isolated N-terminal peptide sequence of LPL converted the integrin to a high-affinity state (**Figure 1C**) (32). LPL was also required for integrin-mediated signaling to the oxidative burst in PMNs, though dispensable for integrin-mediated cell spreading (33), indicating that LPL participates in integrin-mediated signaling to downstream events beyond actin remodeling. LPL directly binds the β2 subunit of the integrin LFA-1 to connect with the actin cytoskeleton during migration and activation (34). Finally, LPL was shown to preferentially bind the "clasped" (or closed) cytoplasmic tail of CR3 (Mac-1; $\alpha_m\beta_2$; CD11b/CD18). Phosphomimetics of Ser5/Ser7 dual phosphorylation reduced the binding of LPL to β_2, and binding of LPL to β2 reduced CR3-mediated adhesion in the cell line RAW (35). The participation of LPL in T-cell activation and motility therefore extends beyond actin-bundling and into integrin signaling. LPL enables the actin cytoskeletal rearrangements and integrin-mediated adhesion that are core drivers of T-cell migration and T-cell adhesion to APCs and/or target cells. We review the increased knowledge about LPL in T-cell activation and motility, the heart of most adaptive immune responses.

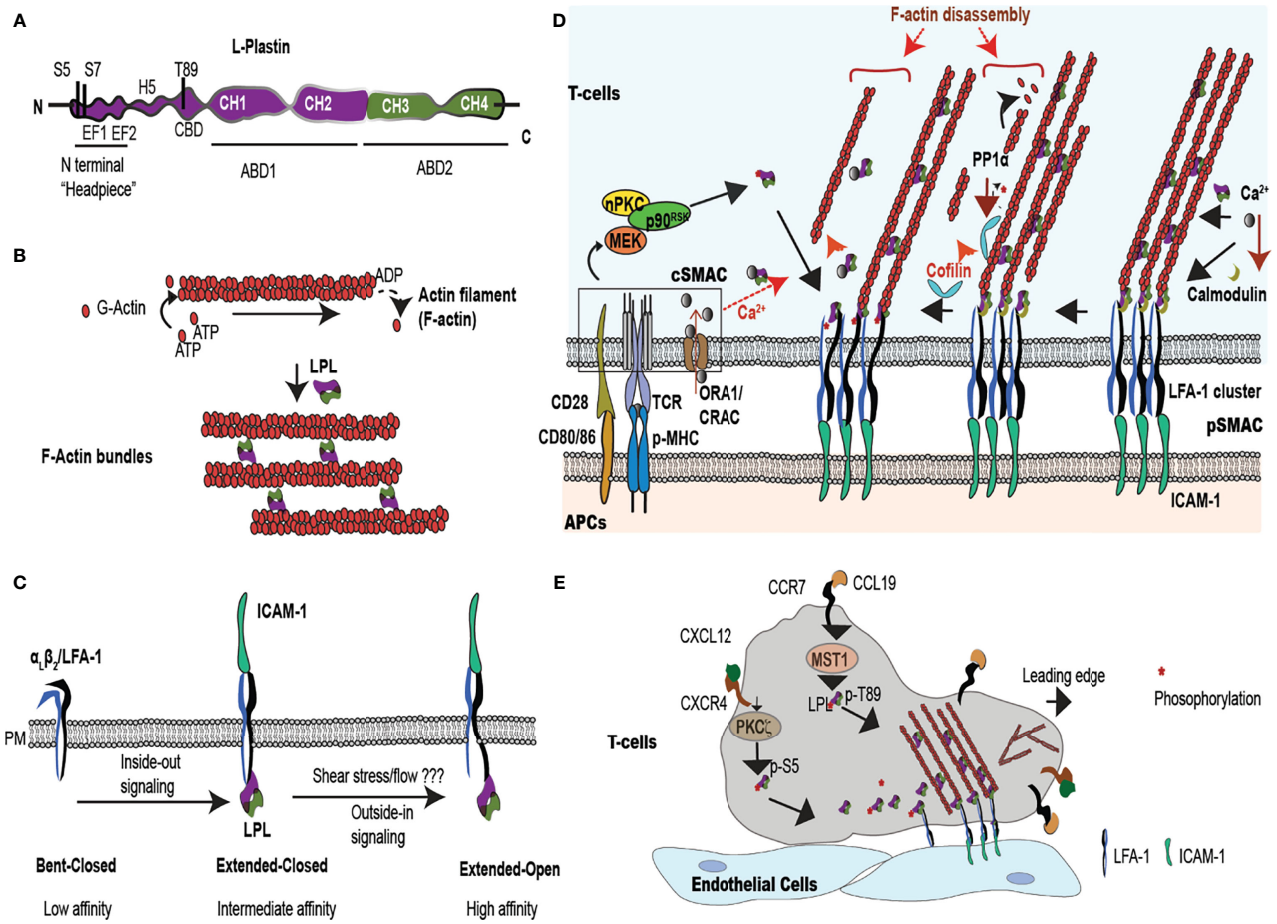

FIGURE 1 | LPL is an actin-bundling protein that supports T cell synapse maturation and migration. **(A)** LPL comprises a regulatory 'N-terminal headpiece' and two actin binding domains (ABDs). The regulatory headpiece includes three known phosphorylation sites (Ser-5, Ser-7, Thr89), two calcium binding EF domains, a regulatory H5 "switch helix," and a calmodulin binding domain (CBD). **(B)** LPL cross-links two actin filaments to generates f-actin bundles. **(C)** LPL interacts with the cytoplasmic tail of the β_2 subunit of the integrin LFA-1. In T cells, inside-out signaling induces a conformational change from low to intermediate affinity, whereas shear flow or ICAM-1 engagement triggers the high-affinity, extended-open conformation. **(D)** Multiple regulatory pathways converge upon LPL in the pSMAC, where LFA-1 mediates tight approximation to ICAM-expressing APCs. The IS, the interface at the site of T-cell:APC contact site, generates a cSMAC, pSMAC and a dSMAC (dSMAC not shown). In the IS, TCR ligation to peptide-loaded MHC (pMHC) and costimulatory CD28:CD80/86 interactions occur in the central super-molecular activation complex (cSMAC), which activates a kinase cascade [nPKC-MEK-ribosomal protein S6 kinase p90 ($p90^{RSK}$)]. This kinase cascade results in Ser-5 phosphorylation of LPL. LPL phosphorylation accelerates LFA-1 clustering in the peripheral SMAC (pSMAC). Phosphorylated LPL is largely associated with high affinity LFA-1, and may stabilize the IS. LPL can also bind to LFA-1 independently of phosphorylation. LPL-induced LFA-1 clusters further accumulate at IS by cofilin-mediated f-actin remodeling. Cofilin is activated by PP1α phosphatase. Simultaneously, LPL also recruits f-actin bundles to connect the IS to actin cytoskeleton. Ca^{2+} influx at cSMAC also regulates LPL. Ca^{2+} binding reduces the LPL bundling efficiency, perhaps allowing f-actin clearing at IS. However, lower Ca^{2+} in the pSMAC permits calmodulin binding to LPL, stabilizing actin bundles and maintainting LFA-1 clustering. **(E)** Intravascular T cells traffic to peripheral immunological sites *via* the binding of the integrin LFA-1 to the adhesion molecule, ICAM-1, expressed on vascular endothelial cells. In response to chemoattractants, such as CXCL12 and CCL19, T cells polarize the respective chemokine receptors CXCR4 and CCR7 to the leading edge and activate kinases such Mst1 and PKCζ. Mst1, PKCζ, and other kinases phosphorylate the regulatory headpiece of LPL. Phosphorylated LPL initiates LFA-1 clustering, sustaining ICAM-1 binding. Branched f-actin forms in the lamellipod, while the 'uropod' propels cells in a forward direction. The symbol "*" indicates the phosphate group during phosphorylation/dephosphorylation reaction.

REQUIREMENT FOR LPL IN T-CELL ACTIVATION

T cells mount adaptive immune responses by activating other immune cells through cytokine production and/or direct contact, and by direct killing of target cells. TCR engagement by APCs initiates T-cell activation through interaction at a specialized intercellular contact site, the IS. The IS is stabilized by cytoskeleton machinery *via* lamellipodia formation that enhances the contact area between APCs and T cells, increasing TCR signaling (5, 6). The T cell-APC contact site comprises three supramolecular activation clusters (SMAC) that organize signaling proteins into the central, peripheral, and distal SMACs (cSMAC, pSMAC, and dSMAC) (36). The four different actin formations that characterize the IS are extensively reviewed in (36). Notably, the f-actin network is "cleared," or hypodense, in the cSMAC,

where the TCR/CD3 signaling complexes accumulate (37). The pSMAC forms a ring around the centrally cleared area, and is marked by LFA-1 accumulation and generation of actomyosin arcs. These actomysoin arcs are force generating, enabling close approximation of the T cell to its target APC (**Figure 1D**). Larger molecules, such as CD43, localize to the outer dSMAC, where f-actin is organized in a branching network (36, 38, 39). Throughout the pSMAC and dSMAC are small actin foci, areas of integrin engagement that resemble macrophage podosomes. IS formation and T cell activation are absolutely dependent upon active actin rearrangements that create these varied actin structures (13, 40, 41).

Efficient IS formation also requires LPL. Murine T cells isolated from genetically-deficient LPL mice ($LPL^{-/-}$ mice) exhibited impaired IS formation (42), with reduced T-cell:APC contact area. Decreased T-cell activation in $LPL^{-/-}$ mice correlated with enhanced tolerance to T cell-mediated diseases such as skin allograft rejection and experimental autoimmune encephalomyelitis (EAE) (42). Furthermore, LPL supported T_{fh} cell-B cell interactions and was required for germinal center formation and subsequent T-dependent antibody production (43). In human T cells, LPL directly binds the β2 subunit (CD18) of LFA-1 to link the actin cytoskeleton to the IS (34, 44). Reduction of LPL (<10% normal expression through siRNA knockdown), impaired LFA-1 concentration to the pSMAC and generated smaller T-cell:APC contact zone, confirming a crucial need for LPL in IS formation (34).

The requirement for LPL Ser-5 phosphorylation during T-cell activation is unclear. CD3/CD2-mediated Ser-5 phosphorylation was first reported in 1994 (45). Subsequent extensive work using knock-down of LPL in human T cells, followed by re-expression of phosphomimetic or non-phosphorylatable LPL, has suggested a significant regulatory role for Ser-5. In human T cells, Ser-5 phosphorylation enabled translocation of the activation markers CD69 and CD25 to the cell surface after TCR/CD3, CD2 or CD28 engagement, although LPL localized to the IS independently of Ser-5 phosphorylation (24). In the IS, LPL maximizes accumulation of LFA-1 at pSMAC by directly interacting with LFA-1 (34). LPL localization to the pSMAC was stabilized by calmodulin binding and by ABD-mediated actin-bundling activity. LPL bound to LFA-1 equivalently in naive or CD3/CD28-activated T cells, independently of the EF-hand loops and Ser-5 phosphorylation (34). However, Ser-5 phosphorylation of LPL (LFA-1 bound) increased upon CD3/CD28 stimulation and at the IS generated after superantigen [*S. aureus* enterotoxin B (SEB)]-mediated cross-linking of Raji B cells and T cells (31).

Mechanistically, in CD3/CD28-costimulated T cells, activation of the nPKC-MEK- ribosomal protein S6 kinase p90 ($p90^{RSK}$) pathway phosphorylated LPL (Ser-5) to initiate LFA-1 clustering at the IS (31). Association of phosphorylated LPL with high affinity LFA-1 may sustain IS formation (31). Further, LPL-induced LFA-1 clustering was enhanced by another actin-binding protein, cofilin. Cofilin is an f-actin severing protein that promotes f-actin remodeling by generating new filament ends for addition or removal of g-actin monomers (46). Cofilin binds the ADP-bound actin monomer within an existing filament, increasing the likelihood of f-actin depolymerization, accelerating f-actin turn-over, untangling filaments, and facilitating re-arrangement (47). Cofilin enhances LFA-1 accumulation at the IS by accelerating f-actin remodeling (31). Cofilin is activated by PP1α-mediated dephosphorylation, while LPL is dephosphorylated by the serine/threonine phosphatase PP2A (31). LFA-1 clustering and accumulation at the IS enhances the interaction of LFA-1 with its ligand ICAM-1 (expressed by APCs), and amplifies T-cell activation (**Figure 1D**). Pharmacological inhibition of nPKC (Gö6983), MEK (U0126), or $p90^{RSK}$ (BI-D1870) reduced LPL phosphorylation and cofilin activation, which correlated with IS destabilization, diminished T cell-APC contact, and impaired T-cell activation (31). Similarly, blockade of LPL using nanobodies directed against the EF-hands or the ABDs impaired the binding of LPL to LFA-1, and subsequently inhibited IS formation and downstream T-cell proliferation (48). IS stabilization by LPL : LFA-1 binding is targeted by bacterial infections (*e.g. Bordetella pertussis* and *Bacillus anthracis*), in which cAMP production at the IS suppressed T-cell activation (49). Treatment with the glucocorticoid dexamethasone inhibited LPL Ser-5 phosphorylation after CD3/CD2 and CD3/CD28-mediated T cell activation, and dexamethasone also impaired IS formation (50). Thus, a major function of LPL during T cell activation is maintenance of the IS. LPL-mediated IS stabilization is further suggested by the observation that enhanced phosphorylation of LPL amplified LFA-1 clustering and inhibited serial killing by cytotoxic T cells (CTL). Amplified LFA-1 clustering prevented detachment from target cells, thereby prolonging IS maintenance, and thus reduced interactions with new target cells. The pro-oxidative drug WF-10 increased LPL phosphorylation, rigidified the cytolytic IS, and suppressed CTL activity (51). Thus, LPL phosphorylation activates naïve/effector T cells, while interrupting cytolytic activity, making it an important intrinsic modulator during critical immune reactions (44, 51).

Intriguingly, a murine model in which the Ser5 of LPL was converted to the non-phosphorylatable alanine, and thus ablated the Ser5 phosphorylation site, did not exhibit obvious defects in TCR-mediated activation (52). TCR-mediated activation was assessed by proliferation and upregulation of CD25 and CD69. Possible explanations for a lack of effect on T cell activation by ablation of Ser5 phosphorylation include the differences in experimental systems. These explanations will be discussed in detail later.

REQUIREMENT FOR LPL IN T-CELL RECRUITMENT (MIGRATION AND ADHESION)

T cells constantly migrate to scan APCs for foreign antigens, to activate immune responses, and to directly kill target cells. This rapid migration (average velocity of 8-15 μm/min) depends on the actin cytoskeleton (27). During chemotaxis, chemokine engagement induces lamellipodia formation and chemokine receptor concentration at the leading edges of cells. Contractile elements at

the rear edges, called "uropods," provide propulsive forces (53). LPL actin-bundling activity is essential for efficient T lymphocyte motility (34, 54, 55).

LPL was first identified as a critical component of T cell chemotaxis during CCL20-induced transwell migration (55). A more detailed analysis of the role of LPL in T cell migration was explored using $LPL^{-/-}$ mice (54). $LPL^{-/-}$ mice showed higher thymic retention of $CD4^+$ (3-fold increase) and $CD8^+$ (2-fold increase) single positive thymocytes, which resulted from impaired thymic egress. LPL-deficient mature T cells also exhibited impaired intranodal velocity and motility. During CCL19-mediated transwell migration, LPL-deficient T cells showed reduced polarization of CCR7 to the leading edge and reduced uropod formation (54). LPL phosphorylation at Thr-89 by Mst1 kinase (Ste20 kinase/STK4) supported T cell lamellipodia formation and thus T cell migration (21). Mst1 kinase had been previously shown to enable T-cell lamellipodia formation, polarization and migration (13, 56). Identification of a Mst1 consensus sequence in the regulatory headpiece of LPL provided a downstream molecular target by which Mst1 regulated T cell motility. Notably, expression of LPL-T89A, which ablated the Mst1 phosphorylation site (Thr-89), but not Ser-5, failed to restore CCL19-induced CCR7 polarization and transwell migration in LPL-deficient T cells, whereas expression of wild-type LPL did restore the chemokine-induced events. Furthermore, reconstitution of T cells in $LPL^{-/-}$ mice with lentivirally-expressed LPL-T89A showed greater accumulations of $CD4^+$ and $CD8^+$ single positive thymocytes than did $LPL^{-/-}$ mice, consistent with a requirement for Thr-89 phosphorylation during thymic egress (21).

Investigation in human T cells further confirmed a crucial role for LPL in migration (25). Reduction of LPL by 75-95% by siRNA knock-down caused impaired polarization of CXCR4 receptors in CXCL12 (SDF-1α)-stimulated T cells (25). In human T cells ($CD3^+$), CXCL12 activated atypical PKC-ζ to phosphorylate Ser-5 of LPL, triggering lamellipodial localization during polarization (25). However, T cell migration was not impaired in S5A mice, suggesting that Ser-5 phosphorylation of LPL correlates with, but may not be required for, T-cell migration (52). Chemokine signals induce a conformational change in LFA-1, through inside-out signaling, which converts LFA-1 to a moderate-affinity state. Moderate-affinity LFA-1 promotes cell adhesion to vascular endothelial cells *via* ICAM-1 binding (**Figure 1E**). LFA-1:ICAM-1 ligation reorganizes f-actin to initiate T-cell polarization, crawling and migration (57, 58). When LPL expression is reduced, unstimulated and effector (CD3/CD28 stimulated) T cells migrate more slowly and with higher migratory persistence on surfaces coated with immobilized CXCL12 and ICAM-1 (25). Thus, LPL-supported f-actin cytoskeletal polarization is essential for efficient T-cell migration (59).

DISCUSSION

A comprehensive model that reconciles apparently disparate observations regarding the regulation of LPL during T-cell migration and activation remains elusive. With multiple regulatory sites, and separable functions of actin-binding, actin-bundling, and integrin-association, too much remains unknown to formulate a complete description of the mechanism(s) by which LPL enables migration and IS formation. To provide a framework for future exploration, we suggest that the primary role of LPL is to stabilize multimolecular complexes that arise at sites of integrin-mediated adhesion, and thereby enhance or promote mechanotransduction at those sites. Mechanotransduction is the translation of external mechanical forces exerted upon the cell into intracellular biochemical signaling (60). For example, IS formation is strengthened by mechanosensation generated by interactions with mature APCs that actively increase cortical cytoskeletal stiffness, thereby boosting T-cell activation (61). Similarly, enhanced adhesion of T cells to stiffer culture surfaces (elastic modulus 25 kilopascal (kPa) to 100 kPa) triggers higher IL-2 production upon CD3 activation (62). Finally, T cells migrate faster on stiffer substrates, demonstrating that mechanotransduction also regulates T cell motility (63). A proposal that LPL supports formation of integrin-mediated adhesion sites and mechanotransduction through these sites provides a single mechanism common to both migration and IS formation (64), and explains how LPL deficiency could disrupt both these processes (**Figure 2**). As discussed below, this framework draws on studies of LPL in hematopoietic cell types including macrophages, B cells, and neutrophils, in addition to T cells.

LPL has been shown to regulate mechanotransduction in macrophages (65). WT macrophages incubated upon softer substrates produced more IL-1β in response to NLRP3 inflammasome activation. However, LPL-deficient macrophages produced the same, reduced amount of IL-1 β following NLRP3 activation, and were unresponsive to varying substrate stiffnesses (65). Mechanotransudction in LPL-deficient macrophages was disrupted due to the mislocalization of the kinase Pyk2. In macrophages, β2 integrin activation phosphorylates Pyk2 to induce podosome signaling (66). Macrophage podosomes are multimolecular signaling complexes generated by integrin-mediated adhesion and anchored by f-actin. Podosomes support macrophage adhesion, signaling and motility. Podosome stabilization requires LPL; thus, LPL also regulates macrophage motility (67). The f-actin foci described as one of the four actin structures present in the T-cell IS have been likened to macrophage podosomes (36). LPL is also required for CXCL12-induced migration and Pyk2 activation (Tyr-402 phosphorylation) in B cells (68). In T cells, Pyk2 regulates LFA-1:ICAM-1 signaling. $Pyk2^{-/-}$ T cells weakly adhere to ICAM-1 and migrate slowly upon CXCL12 stimulation (69), and thus are similar in phenotype to LPL-deficient T cells. While not yet experimentally determined in T cells, it is reasonable to propose that LPL serves to link sites of integrin-mediated adhesion to downstream Pyk2 activation and signaling in all hemaopoietic cells. However, the molecular mechanism by which LPL and Pyk2 interact is unclear, and further investigation in understanding of synergistic functioning of LPL and Pyk2 *via* f-actin cytoskeleton will help in understanding their role in T cell function and mechanotransduction.

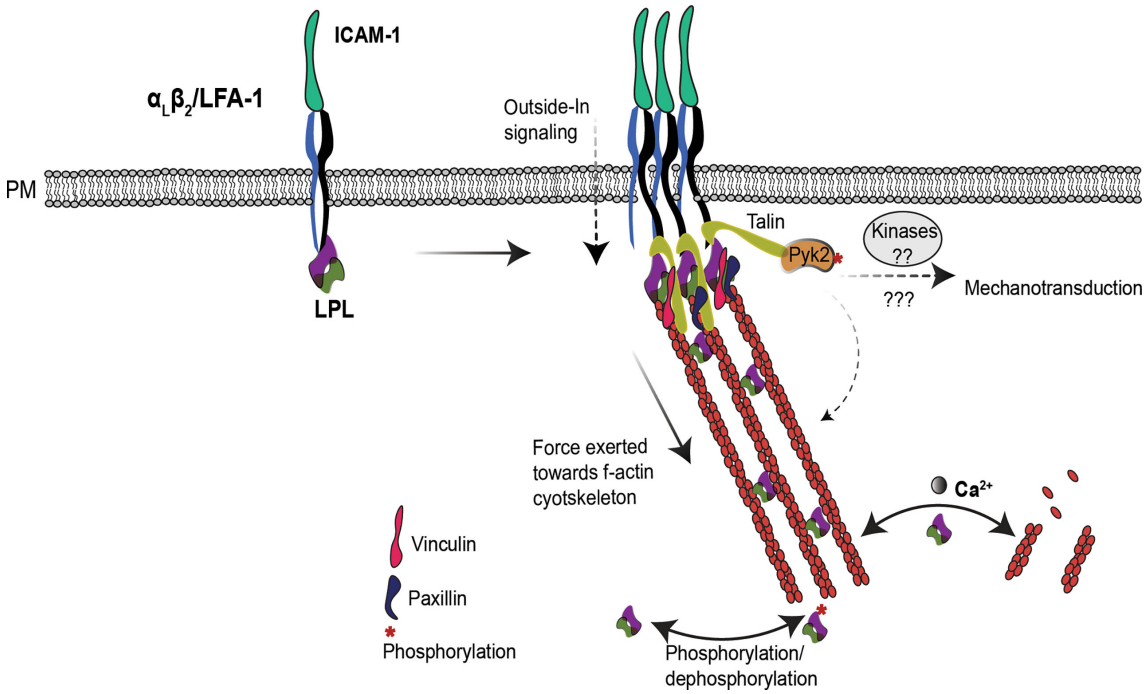

FIGURE 2 | LPL may regulate T cell integrins induced mechanotransduction. In T cells, LPL binds to LFA-1. Under certain conditions, e.g. shear flow or ICAM-1 engagement, LFA-1 shifts to the extended-open (high-affinity) conformation. LPL binding to LFA-1 recruits the mechanosensing protein Talin, and also connects it to the f-actin cytoskeleton. Talin recruits additional cytoskeleton-associated proteins, such as vinculin, paxillin and the tyrosine kinase Pyk2. Collectively, this cascade generates mechanotransduction through Pyk2 and other kinases, and triggers f-actin remodeling required for efficient T cell activation and migration. The separable activities of LPL–LFA-1 binding, f-actin binding, and f-actin-bundling—are coordinately regulated to support mechanotransduction. How the multiple regulatory sites on LPL (phosphorylation, Ca^{2+}, and calmodulin-binding) converge to modulate the varied activities of LPL are yet to be illuminated.

In T cells, LPL participates in the "inside-out" cascade for LFA-1 clustering to establish adhesion and IS formation (34). LFA-1 engagement also initiates an "outside -in" signal *via* linking to f-actin (60) to fine-tune T-cell migration, differentiation, and effector functions (70, 71). LPL helps recruit a mechanosensing protein, Talin, to LFA-1 clusters, connecting f-actin to the IS (34). Talin further recruits various cytoskeleton proteins, such as vinculin and paxillin and f-actin, by direct binding, and propagates mechanical signals (72, 73). Since the β_2-binding site also lies in ABDs (30), it has not yet been shown if a single molecule of LPL can bind both β2 integrin and f-actin, or if binding of one precludes binding of the other. Direct cross-linking of f-actin to the cytoplasmic tail of integrins by LPL would be one possible mechanism by which LPL could sustain integrin-mediated adhesion sites.

During T cell migration, LFA-1 binds to ICAM-1 on endothelial cells to enable transmigration (74). F-actin cytoskeleton retrograde flow aligns ICAM-1 bound integrins at the leading edge to reinforce cellular adhesions (75). While LPL appears to regulate the binding of integrins, such as LFA-1 and VLA-4, to their respective ligands, ICAM-1 and VCAM-1, during chemotaxis on immobilized CXCL12, LPL is dispensable under shear flow conditions (25). This differential requirement for LPL during static chemotaxis and under shear flow could be due to differential f-actin reorganization and/or recruitment of additional actin binding partners, such as Cofilin (31). LFA-1 changes from an inactive, clasped conformation to an active, open conformation to bind ICAM-1 (58, 76, 77). Perhaps the binding of LPL to the intracellular β2 integrin is conformation specific, and varies with T-cell migration under stasis versus shear flow. A recent study in human myeloid (PBL-985) cells showed preferential binding of LPL to the clasped αMβ2 (CD11β/CD18, also called CR3 or Mac-1) conformation to maintain the inactive state under flow (35). By analogy, LPL may likewise stabilize the inactive LFA-1 conformation when T cells are under flow, while under static conditions LPL promotes LFA-1 clustering to initiate adherence. However, conformation-specific binding of LPL to LFA-1 (CD11α/CD18) in T cells is unresolved and future studies will address this important open question.

Further studies are required to determine how signals from the multiple regulatory sites on the LPL N-terminal headpiece are integrated to modify the integrin-binding, actin-binding, and actin-bundling activities of LPL during T-cell activation and migration. Current studies have analyzed single regulatory sites without clearly defining how modulation at other sites impact LPL functioning. For instance, LPL Ser-5 phosphorylation is essential for activation and IS formation in human T cells, while Thr-89 phosphorylation supports T cell migration in murine cells (21). However, no studies have examined the combined effects of Ser5/Thr89 phosphorylation, or if phosphorylation at Ser5 prevents

Thr89 phosphorylation. Furthermore, no studies have examined the effect of Ca^{2+} binding on phosphorylated vs non-phosphorylated LPL (at any site). Thr-89 phosphorylation is not yet studied in human T cells, and may not function similarly as it does in mice. Regulation of LPL could vary between human and murine T cells during activation and migration because of different (and as yet undefined) pathways that phosphorylate Ser-5 and Thr-89, or because of different inter-molecular interactions. In human T cells, overexpression of non-phosphorylatable Ser-5 (S5A) LPL abrogated CD3-induced surface translocation of activation markers CD25 and CD69 (24), which was not observed in LPL-S5A reconstituted LPL deficient murine T cells (42). Similarly, our study in LPL-S5A mice showed no defect in CD25 and CD69 upregulation in CD3/CD28 activated T cells (52). However, the exact molecular cascade for LPL-dependent CD69 and CD25 upregulation is not known. Possibly, a dominant negative effect of the S5A mutant in overexpressing human T cells generated a different phenotype than endogenous expression of S5A-LPL-only expressing murine T- cells. Further detailed molecular studies are required to resolve the disparities of LPL regulation in human and mouse T cells.

In addition to phosphorylation, LPL activity is regulated by calcium influx in T cells. The LPL N-terminal headpiece possesses two EF-hand calcium-binding sites and a binding site for the calcium-binding protein calmodulin (15, 78). Calcium binding (increased intracellular calcium concentration above 10^{-7} M) at EF-hands induces a conformational change that inhibits LPL's bundling activity (8, 9). Recent NMR solution structures of the LPL EF-hand domains revealed a calcium sensor 'switch-helix' motif (H5) in-between EF-hand motifs and ABD1 (**Figure 1A**) (79). In the absence of Ca^{2+}, the H5 motif remains flexible and unstructured, which stabilizes the orientation of LPL-ABDs when bound to f-actin to promote efficient f-actin bundling. Whereas, when Ca^{2+} increases, the H5 motif changes conformation to a more rigid α-helix, which induces the release of the H5 motif from f-actin-ABD pocket and permits binding of H5 to EF hands. This helix switch in the H5 motif generates a conformation unfavorable to binding of LPL-ABDs to f-actin, thus reducing f-actin bundling (79). The coordinate spatial and temporal dynamics of Ca^{2+} flux and LPL activity during IS formation have not been fully defined. The Ca^{2+} channels ORA1 and CRAC are localized to the cSMAC, suggesting that Ca^{2+} flux is tightly spatially regulated, with increased flux in the cSMAC. Perhaps the higher levels of Ca^{2+} in the cSMAC inhibits LPL bundling activity, contributing to the decreased f-actin polymerization and f-actin density (actin "clearing") in the cSMAC (37). Lower levels of Ca^{2+} in the pSMAC may correlate with increased LPL-mediated actin-bundling and formation of actomyosin arcs. Calmodulin binding to LPL occurs in the absence of calcium. Calmodulin binding stabilizes LPL binding to LFA-1 clusters in the pSMAC to enhance T-cell/APC contact at IS (34) (**Figure 1D**). Additional studies are required to determine the spatiotemporal regulation of LPL phosphorylation, Ca^{2+} binding, and calmodulin binding during IS formation and maintenance.

The requirement for LPL in T-cell activation reveals new intrinsic regulators for therapeutic targeting to ameliorate T-cell-driven pathologies. For instance, reducing intracellular levels of LPL by genetic knock-down (48) or nanobody-mediated LPL inactivation (48) impair T cell activation and IS formation. Similarly, pharmacological inhibition of LPL directly using dexamethasone (50) or LPL kinase nPKC using Gö6983 (31) can be used to inhibit T-cell immune responses. Conversely, enhancing LPL phosphorylation using WF-10 could be employed to suppress T cell mediated cytotoxicity during allograft transplantation (51). In addition to activation, inhibiting cell migration by targeting kinases [e.g. Mst1 (21) and PKCζ (25)] could be explored to maximize T-cell retention in tumors microenvironment. The urgent need for therapies for autoimmune and oncologic processes compels further elucidation of the key T-cell migration and activation pathways dependent upon LPL.

AUTHOR CONTRIBUTIONS

HJ and SM both have equally contributed to idea conceptualization and manuscript writing. All authors contributed to the article and approved the submitted version.

FUNDING

This work was supported by National Institutes of Health grants R01- AI104732, R21EB030171, R01 AI118719, HL148033, R01AI139540, and R56 AI104732, National Science Foundation grants CBET-1900277 and CMMI1548571, American Lung Association grant ETRA 736343, Washington University in Saint Louis Children's Discovery Institute grants CDI-CORE-2019-813 and CDI-CORE-2015-505, Foundation for Barnes-Jewish Hospital grants 3770 and 4642, American Association of Immunologists AAI Careers in immunology fellowship. The content of this study is the authors' sole responsibility and does not necessarily represent official NIH views.

REFERENCES

1. Negulescu PA, Krasieva TB, Khan A, Kerschbaum HH, Cahalan MD. Polarity of T Cell Shape, Motility, and Sensitivity to Antigen. *Immunity* (1996) 4(5):421–30. doi: 10.1016/s1074-7613(00)80409-4
2. Iezzi G, Karjalainen K, Lanzavecchia A. The Duration of Antigenic Stimulation Determines the Fate of Naive and Effector T Cells. *Immunity* (1998) 8(1):89–95. doi: 10.1016/s1074-7613(00)80461-6
3. Thauland TJ, Hu KH, Bruce MA, Butt MJ. Cytoskeletal Adaptivity Regulates T Cell Receptor Signaling. *Sci Signal* (2017) 10(469):eaah3737. doi: 10.1126/scisignal.aah3737
4. Hu KH, Butte MJ. T Cell Activation Requires Force Generation. *J Cell Biol* (2016) 213(5):535–42. doi: 10.1083/jcb.201511053
5. Grakoui A, Bromley SK, Sumen C, Davis MM, Shaw AS, Allen PM, et al. The Immunological Synapse: A Molecular Machine Controlling T Cell Activation. *Science* (1999) 285(5425):221–7. doi: 10.1126/science.285.5425.221

6. Krummel MF, Davis MM. Dynamics of the Immunological Synapse: Finding, Establishing and Solidifying a Connection. *Curr Opin Immunol* (2002) 14 (1):66–74. doi: 10.1016/S0952-7915(01)00299-0
7. Dustin ML. Cell Adhesion Molecules and Actin Cytoskeleton at Immune Synapses and Kinapses. *Curr Opin Cell Biol* (2007) 19(5):529–33. doi: 10.1016/j.ceb.2007.08.003
8. Namba Y, Ito M, Zu Y, Shigesada K, Maruyama K. Human T Cell L-Plastin Bundles Actin Filaments in a Calcium-Dependent Manner. *J Biochem* (1992) 112(4):503–7. doi: 10.1093/oxfordjournals.jbchem.a123929
9. Miyakawa T, Shinomiya H, Yumoto F, Miyauchi Y, Tanaka H, Ojima T, et al. Different Ca^{2+}-Sensitivities Between the EF-Hands of T- and L-Plastins. *Biochem Biophys Res Commun* (2012) 429(3-4):137–41. doi: 10.1016/j.bbrc.2012.10.126
10. Al Tanoury Z, Schaffner-Reckinger E, Halavatyi A, Hoffmann C, Moes M, Hadzic E, et al. Quantitative Kinetic Study of the Actin-Bundling Protein L-Plastin and of its Impact on Actin Turn-Over. *PLoS One* (2010) 5(2):e9210. doi: 10.1371/journal.pone.0009210
11. Morley SC. The Actin-Bundling Protein L-Plastin: A Critical Regulator of Immune Cell Function. *Int J Cell Biol 2012* (2012) p:935173. doi: 10.1155/2012/935173
12. Lin CS, Aebersold R, Kent H S, Varma B M, Leavitt J. Molecular Cloning and Characterization of Plastin, a Human Leukocyte Protein Expressed in Transformed Human Fibroblasts. *Mol Cell Biol* (1988) 8(11):4659–68. doi: 10.1128/mcb.8.11.4659-4668.1988
13. Janji B, Giganti A, De Corte V, Catillon M, Bruyneel E, Lentz D, et al. Phosphorylation on Ser5 Increases the F-Actin-Binding Activity of L-Plastin and Promotes its Targeting to Sites of Actin Assembly in Cells. *J Cell Sci* (2006) 119(Pt 9):1947–60. doi: 10.1242/jcs.02874
14. Samstag Y, Klemke M. Ectopic Expression of L-Plastin in Human Tumor Cells: Diagnostic and Therapeutic Implications. *Adv Enzyme Regul* (2007) 47:118–26. doi: 10.1016/j.advenzreg.2006.12.008
15. Pacaud M, Derancourt J. Purification and Further Characterization of Macrophage 70-kDa Protein, a Calcium-Regulated, Actin-Binding Protein Identical to L-Plastin. *Biochemistry* (1993) 32(13):3448–55. doi: 10.1021/bi00064a031
16. Volkmann N, DeRosier D, Matsudaira P, Hanein D. An Atomic Model of Actin Filaments Cross-Linked by Fimbrin and Its Implications for Bundle Assembly and Function. *J Cell Biol* (2001) 153(5):947–56. doi: 10.1083/jcb.153.5.947
17. Galkin VE, Orlova A, Cherepanova O, Lebart MC, Egelman EH. High-Resolution Cryo-EM Structure of the F-Actin-Fimbrin/Plastin ABD2 Complex. *Proc Natl Acad Sci USA* (2008) 105(5):1494–8. doi: 10.1073/pnas.0708667105
18. Evans JG, Correia I, Krasavina O, Watson N, Matsudaira P. Macrophage Podosomes Assemble at the Leading Lamella by Growth and Fragmentation. *J Cell Biol* (2003) 161(4):697–705. doi: 10.1083/jcb.200212037
19. de Arruda MV. Fimbrin is a Homologue of the Cytoplasmic Phosphoprotein Plastin and has Domains Homologous With Calmodulin and Actin Gelation Proteins. *J Cell Biol* (1990) 111(3):1069–79. doi: 10.1083/jcb.111.3.1069
20. Shinomiya H, Hagi A, Fukuzumi M, Mizobuchi M, Hirata H, Utsumi S. Complete Primary Structure and Phosphorylation Site of the 65-kDa Macrophage Protein Phosphorylated by Stimulation With Bacterial Lipopolysaccharide. *J Immunol* (1995) 154(7):3471–8.
21. Xu X, Wang X, Todd EM, Jaeger ER, Vella JL, Mooren OL, et al. Mst1 Kinase Regulates the Actin-Bundling Protein L-Plastin To Promote T Cell Migration. *J Immunol* (2016) 197(5):1683–91. doi: 10.4049/jimmunol.1600874
22. Chellaiah MA, Ma T, Majumdar S. L-Plastin Phosphorylation Regulates the Early Phase of Sealing Ring Formation by Actin Bundling Process in Mouse Osteoclasts. *Exp Cell Res* (2018) 372(1):73–82. doi: 10.1016/j.yexcr.2018.09.014
23. Lin CS, Lau A, Lue TF. Analysis and Mapping of Plastin Phosphorylation. *DNA Cell Biol* (1998) 17(12):1041–6. doi: 10.1089/dna.1998.17.1041
24. Wabnitz GH, Köcher T, Lohneis P, Stober C, Konstandin MH, Funk B, et al. Costimulation Induced Phosphorylation of L-Plastin Facilitates Surface Transport of the T Cell Activation Molecules CD69 and CD25. *Eur J Immunol* (2007) 37(3):649–62. doi: 10.1002/eji.200636320
25. Freeley M, O'Dowd F, Paul T, Kashanin D, Davies A, Kelleher D. L-Plastin Regulates Polarization and Migration in Chemokine-Stimulated Human T Lymphocytes. *J Immunol* (2012) 188(12):6357–70. doi: 10.4049/jimmunol.1103242
26. Schwebach CL, Agrawal R, Lindert S, Kudryashova E, Kudryashov DS. The Roles of Actin-Binding Domains 1 and 2 in the Calcium-Dependent Regulation of Actin Filament Bundling by Human Plastins. *J Mol Biol* (2017) 429(16):2490–508. doi: 10.1016/j.jmb.2017.06.021
27. Krummel MF, Cahalan MD. The Immunological Synapse: A Dynamic Platform for Local Signaling. *J Clin Immunol* (2010) 30(3):364–72. doi: 10.1007/s10875-010-9393-6
28. Donnadieu E, Bismuth G, Trautmann A. Calcium Fluxes in T Lymphocytes. *J Biol Chem* (1992) 267(36):25864–72. doi: 10.1016/S0021-9258(18)35689-8
29. Walling BL, Kim M. LFA-1 in T Cell Migration and Differentiation. *Front Immunol* (2018) 9. doi: 10.3389/fimmu.2018.00952
30. Le Goff E, Vallentin A, Harmand PO, Aldrian-Herrada G, Rebière B, Roy C, et al. Characterization of L-Plastin Interaction With Beta Integrin and Its Regulation by Micro-Calpain. *Cytoskeleton (Hoboken)* (2010) 67(5):286–96. doi: 10.1002/cm.20442
31. Wabnitz GH, Honus S, Habicht J, Orlik C, Kirchgessner H, Samstag Y, et al. LFA-1 Cluster Formation in T-Cells Depends on L-Plastin Phosphorylation Regulated by P90(RSK) and PP2A. *Cell Mol Life Sci* (2021) 78(7):3543–64. doi: 10.1007/s00018-020-03744-z
32. Jones SL, Wang J, Turck CW, Brown EJ. A Role for the Actin-Bundling Protein L-Plastin in the Regulation of Leukocyte Integrin Function. *Proc Natl Acad Sci USA* (1998) 95(16):9331–6. doi: 10.1073/pnas.95.16.9331
33. Chen H, Mocsai A, Zhang H, Ding RX, Morisaki JH, Wh M, et al. Role for Plastin in Host Defense Distinguishes Integrin Signaling From Cell Adhesion and Spreading. *Immunity* (2003) 19(1):95–104. doi: 10.1016/s1074-7613(03)00172-9
34. Wabnitz GH, Lohneis P, Kirchgessner H, Jahraus B, Gottwald S, Konstandin M, et al. Sustained LFA-1 Cluster Formation in the Immune Synapse Requires the Combined Activities of L-Plastin and Calmodulin. *Eur J Immunol* (2010) 40(9):2437–49. doi: 10.1002/eji.201040345
35. Tseng HY, Samarelli AV, Kammerer P, Scholze S, Ziegler T, Immler R, et al. LCP1 Preferentially Binds Clasped Alphambeta2 Integrin and Attenuates Leukocyte Adhesion Under Flow. *J Cell Sci* (2018) 131(22):jcs218214. doi: 10.1242/jcs.218214
36. Hammer JA, Wang JC, Saeed M, Pedrosa AT. Origin, Organization, Dynamics, and Function of Actin and Actomyosin Networks at the T Cell Immunological Synapse. *Annu Rev Immunol* (2019) 37:201–24. doi: 10.1146/annurev-immunol-042718-041341
37. Hartzell CA, Jankowska KI, Burkhardt JK, Lewi RS. Calcium Influx Through CRAC Channels Controls Actin Organization and Dynamics at the Immune Synapse. *Elife* (2016) 5:e14850. doi: 10.7554/eLife.14850
38. Monks CR, Freiberg BA, Kupfer H, Sciaky N, Kupfer A. Three-Dimensional Segregation of Supramolecular Activation Clusters in T Cells. *Nature* (1998) 395(6697):82–6. doi: 10.1038/25764
39. Freiberg BA, Kupfer H, Maslanik W, Delli J, Kappler J, Zaller DM, et al. Staging and Resetting T Cell Activation in SMACs. *Nat Immunol* (2002) 3 (10):911–7. doi: 10.1038/ni836
40. Poenie M, Kuhn J, Combs J. Real-Time Visualization of the Cytoskeleton and Effector Functions in T Cells. *Curr Opin Immunol* (2004) 16(4):428–38. doi: 10.1016/j.coi.2004.05.016
41. Campi G, Varma R, Dustin ML. Actin and Agonist MHC-Peptide Complex-Dependent T Cell Receptor Microclusters as Scaffolds for Signaling. *J Exp Med* (2005) 202(8):1031–6. doi: 10.1084/jem.20051182
42. Wang C, Morley SC, Donermeyer D, Peng I, Lee WP, Devoss J, et al. Actin-Bundling Protein L-Plastin Regulates T Cell Activation. *J Immunol* (2010) 185 (12):7487–97. doi: 10.4049/jimmunol.1001424
43. Todd EM, Deady LE, Morley SC. Intrinsic T- and B-Cell Defects Impair T-Cell-Dependent Antibody Responses in Mice Lacking the Actin-Bundling Protein L-Plastin. *Eur J Immunol* (2013) 43(7):1735–44. doi: 10.1002/eji.201242780
44. Wabnitz G, Balta E, Samstag Y. L-Plastin Regulates the Stability of the Immune Synapse of Naive and Effector T-Cells. *Adv Biol Regul* (2017) 63:107–14. doi: 10.1016/j.jbior.2016.09.009
45. Henning SW, Meuer SC, Samstag Y. Serine Phosphorylation of a 67-kDa Protein in Human T Lymphocytes Represents an Accessory Receptor-Mediated Signaling Event. *J Immunol* (1994) 152(10):4808–15.
46. Tanaka K, Takeda S, Mitsuoka K, Oda T, Kimura-Sakiyama C, Maéda Y, et al. Structural Basis for Cofilin Binding and Actin Filament Disassembly. *Nat Commun* (2018) 9(1):1860. doi: 10.1038/s41467-018-04290-w

47. McCall PM, MacKintosh FC, Kovar DR, Gardel ML. Cofilin Drives Rapid Turnover and Fluidization of Entangled F-Actin. *Proc Natl Acad Sci USA* (2019) 116(26):12629–37. doi: 10.1073/pnas.1818808116
48. De Clercq S, Zwaenepoel O, Martens E, Vandekerckhove J, Guillabert A, Gettemans J. Nanobody-Induced Perturbation of LFA-1/L-Plastin Phosphorylation Impairs MTOC Docking, Immune Synapse Formation and T Cell Activation. *Cell Mol Life Sci* (2013) 70(5):909–22. doi: 10.1007/s00018-012-1169-0
49. Arumugham VB, Ulivieri C, Onnis A, Finetti F, Tonello F, Ladant D, et al. Compartmentalized Cyclic AMP Production by the Bordetella Pertussis and Bacillus Anthracis Adenylate Cyclase Toxins Differentially Affects the Immune Synapse in T Lymphocytes. *Front Immunol* (2018) 9:919. doi: 10.3389/fimmu.2018.00919
50. Wabnitz GH, Michalke F, Stober C, Kirchgessner H, Jahraus B, van denBoomen D, et al. L-Plastin Phosphorylation: A Novel Target for the Immunosuppressive Drug Dexamethasone in Primary Human T Cells. *Eur J Immunol* (2011) 41(11):3157–69. doi: 10.1002/eji.201041366
51. Wabnitz GH, Balta E, Schindler S, Kirchgessner H, Jahraus B, Meuer S, et al. The Pro-Oxidative Drug WF-10 Inhibits Serial Killing by Primary Human Cytotoxic T-Cells. *Cell Death Discovery* (2016) 2:16057. doi: 10.1038/cddiscovery.2016.57
52. Anaya EP, Lin X, Todd EM, Szasz TP, Morley SC. Novel Mouse Model Reveals That Serine Phosphorylation of L-Plastin Is Essential for Effective Splenic Clearance of Pneumococcus. *J Immunol* (2021) 206(9):2135–45. doi: 10.4049/jimmunol.2000899
53. Nieto M, Frade JM, Sancho D, Mellado M, Martinez AC, Sánchez-Madrid F, et al. Polarization of Chemokine Receptors to the Leading Edge During Lymphocyte Chemotaxis. *J Exp Med* (1997) 186(1):153–8. doi: 10.1084/jem.186.1.153
54. Morley SC, Wang C, Lo WL, Lio CW, Zinselmeyer BH, Miller MJ, et al. The Actin-Bundling Protein L-Plastin Dissociates CCR7 Proximal Signaling From CCR7-Induced Motility. *J Immunol* (2010) 184(7):3628–38. doi: 10.4049/jimmunol.0903851
55. Lin SL, Lin CW, Chien CL, Han ES, Chen SH, Kao YJ, et al. Temporal Proteomics Profiling of Lipid Rafts In CCR6-Activated T Cells Reveals the Integration of Actin Cytoskeleton Dynamics. *J Proteome Res* (2010) 9(1):283–97. doi: 10.1021/pr9006156
56. Katagiri K, Imamura M, Kinashi T. Spatiotemporal Regulation of the Kinase Mst1 by Binding Protein RAPL Is Critical for Lymphocyte Polarity and Adhesion. *Nat Immunol* (2006) 7(9):919–28. doi: 10.1038/ni1374
57. Hogg N, Patzak I, Willenbrock F. The Insider's Guide to Leukocyte Integrin Signalling and Function. *Nat Rev Immunol* (2011) 11(6):416–26. doi: 10.1038/nri2986
58. Alon R, Shulman Z. Chemokine Triggered Integrin Activation and Actin Remodeling Events Guiding Lymphocyte Migration Across Vascular Barriers. *Exp Cell Res* (2011) 317(5):632–41. doi: 10.1016/j.yexcr.2010.12.007
59. Morley SC. The Actin-Bundling Protein L-Plastin Supports T-Cell Motility and Activation. *Immunol Rev* (2013) 256(1):48–62. doi: 10.1111/imr.12102
60. Joshi H, Morley SC. Cells Under Stress: The Mechanical Environment Shapes Inflammasome Responses to Danger Signals. *J Leukoc Biol* (2019) 106(1):119–25. doi: 10.1002/JLB.3MIR1118-417R
61. Blumenthal D, Chandra V, Avery L, Burkhardt JK. Mouse T Cell Priming is Enhanced by Maturation-Dependent Stiffening of the Dendritic Cell Cortex. *Elife* (2020) 9:e55995. doi: 10.7554/eLife.55995
62. Judokusumo E, Tabdanov E, Kumari S, Dustin ML, Kam LC. Mechanosensing in T Lymphocyte Activation. *Biophys J* (2012) 102(2):L5–7. doi: 10.1016/j.bpj.2011.12.011
63. Saitakis M, Dogniaux S, Goudot C, Bufi N, Asnacios S, Maurin M, et al. Different TCR-Induced T Lymphocyte Responses are Potentiated by Stiffness With Variable Sensitivity. *Elife* (2017) 6:e23190. doi: 10.7554/eLife.23190
64. Rossy J, Laufer JM, Legler DF. Role of Mechanotransduction and Tension in T Cell Function. *Front Immunol* (2018) 9:2638. doi: 10.3389/fimmu.2018.02638
65. Joshi H, Almgren-Bell A, Anaya EP, Todd EM, Van Dyken SJ, Seth A, et al. L-Plastin Enhances NLRP3 Inflammasome Assembly and Bleomycin-Induced Lung Fibrosis. *Cell Rep* (2022) 38(11):110507. doi: 10.1016/j.celrep.2022.110507
66. Rodan GA, Duong LT. PYK2 Is an Adhesion Kinase in Macrophages, Localized in Podosomes and Activated by B2-Integrin Ligation. *Cell Motil Cytoskeleton* (2000) 47:15. doi: 10.1002/1097-0169(200011)47:3<174::AID-CM2>3.0.CO;2-N
67. Zhou JY, Szasz TP, Stewart-Hutchinson PJ, Sivapalan J, Todd EM, Deady LE, et al. L-Plastin Promotes Podosome Longevity and Supports Macrophage Motility. *Mol Immunol* (2016) 78:79–88. doi: 10.1016/j.molimm.2016.08.012
68. Todd EM, Deady LE, Morley SC. The Actin-Bundling Protein L-Plastin is Essential for Marginal Zone B Cell Development. *J Immunol* (2011) 187(6):3015–25. doi: 10.4049/jimmunol.1101033
69. Beinke S, Phee H, Clingan JM, Schlessinger J, Matloubian M, Weiss A. Proline-Rich Tyrosine Kinase-2 is Critical for CD8 T-Cell Short-Lived Effector Fate. *Proc Natl Acad Sci USA* (2010) 107(37):16234–9. doi: 10.1073/pnas.1011556107
70. Buxboim A, Ivanovska IL, Discher DE. Matrix Elasticity, Cytoskeletal Forces and Physics of the Nucleus: How Deeply do Cells 'Feel' Outside and in? *J Cell Sci* (2010) 123(Pt 3):297–308. doi: 10.1242/jcs.041186
71. Gérard A, Cope AP, Kemper C, Alon R, Köchl R. LFA-1 in T Cell Priming, Differentiation, and Effector Functions. *Trends Immunol* (2021) 42(8):706–22. doi: 10.1016/j.it.2021.06.004
72. Jankowska KI, Williamson EK, Roy NH, Blumenthal D, Chandra V, Baumgart T, et al. Integrins Modulate T Cell Receptor Signaling by Constraining Actin Flow at the Immunological Synapse. *Front Immunol* (2018) 9:25. doi: 10.3389/fimmu.2018.00025
73. Owen LM, Bax NA, Weis WI, Dunn AR. The C-Terminal Actin-Binding Domain of Talin Forms an Asymmetric Catch Bond With F-Actin. *Proc Natl Acad Sci USA* (2022) 119(10):e2109329119. doi: 10.1073/pnas.2109329119
74. Friedl P, Bröcker EB. T Cell Migration in Three-Dimensional Extracellular Matrix: Guidance by Polarity and Sensations. *Dev Immunol* (2000) 7(2-4):249–66. doi: 10.1155/2000/56473
75. Swaminathan V, Kalappurakkal JM, Mehta SB, Nordenfelt P, Moore TI, Koga N, et al. Actin Retrograde Flow Actively Aligns and Orients Ligand-Engaged Integrins in Focal Adhesions. *Proc Natl Acad Sci USA* (2017) 114(40):10648–53. doi: 10.1073/pnas.1701136114
76. Fischer RS, Myers KA, Gardel ML, Waterman CM. Stiffness-Controlled Three-Dimensional Extracellular Matrices for High-Resolution Imaging of Cell Behavior. *Nat Protoc* (2012) 7(11):2056–66. doi: 10.1038/nprot.2012.127
77. Alon R, Feigelson SW. Chemokine-Triggered Leukocyte Arrest: Force-Regulated Bi-Directional Integrin Activation in Quantal Adhesive Contacts. *Curr Opin Cell Biol* (2012) 24(5):670–6. doi: 10.1016/j.ceb.2012.06.001
78. Lin CS, Park T, Chen ZP, Leavitt J. Human Plastin Genes. Comparative Gene Structure, Chromosome Location, and Differential Expression in Normal and Neoplastic Cells. *J Biol Chem* (1993) 268(4):2781–92. doi: 10.1016/S0021-9258(18)53842-4
79. Ishida H, Jensen KV, Woodman AG, Hyndman ME, Vogel HJ. The Calcium-Dependent Switch Helix of L-Plastin Regulates Actin Bundling. *Sci Rep* (2017) 7:40662. doi: 10.1038/srep40662

Conflict of Interest: The authors declare that the research was conducted in the absence of any commercial or financial relationships that could be construed as a potential conflict of interest.

frontiers | Frontiers in Immunology

TYPE Review
PUBLISHED 28 July 2022
DOI 10.3389/fimmu.2022.898558

OPEN ACCESS

EDITED BY
Manish Butte,
University of California, Los Angeles, United States

REVIEWED BY
Jeremie Rossy,
Biotechnology Institute Thurgau, Switzerland
Kaushik Choudhuri,
Michigan Medicine, University of Michigan, United States
Jesse Goyette,
University of New South Wales, Australia

*CORRESPONDENCE
Pierre-Henri Puech
pierre-henri.puech@inserm.fr
Kheya Sengupta
kheya.sengupta@cnrs.fr

SPECIALTY SECTION
This article was submitted to T Cell Biology, a section of the journal Frontiers in Immunology

RECEIVED 17 March 2022
ACCEPTED 28 June 2022
PUBLISHED 28 July 2022

CITATION
Mustapha F, Sengupta K and Puech P-H (2022) May the force be with your (immune) cells: an introduction to traction force microscopy in immunology. *Front. Immunol.* 13:898558. doi: 10.3389/fimmu.2022.898558

May the force be with your (immune) cells: an introduction to traction force microscopy in Immunology

Farah Mustapha[1,2,3], Kheya Sengupta[2,3]* and Pierre-Henri Puech[1,3]*

[1]Laboratory Adhesion Inflammation (LAI), INSERM, CNRS, Aix Marseille University, Marseille, France, [2]Centre Interdisciplinaire de Nanoscience de Marseille (CINaM), CNRS, Aix Marseille University, Marseille, France, [3]Turing Center for Living Systems (CENTURI), Marseille, France

For more than a couple of decades now, "force" has been recognized as an important physical parameter that cells employ to adapt to their microenvironment. Whether it is externally applied, or internally generated, cells use force to modulate their various actions, from adhesion and migration to differentiation and immune function. T lymphocytes use such mechano-sensitivity to decipher signals when recognizing cognate antigens presented on the surface of antigen presenting cells (APCs), a critical process in the adaptive immune response. As such, many techniques have been developed and used to measure the forces felt/exerted by these small, solitary and extremely reactive cells to decipher their influence on diverse T cell functions, primarily activation. Here, we focus on traction force microscopy (TFM), in which a deformable substrate, coated with the appropriate molecules, acts as a force sensor on the cellular scale. This technique has recently become a center of interest for many groups in the "ImmunoBiophysics" community and, as a consequence, has been subjected to refinements for its application to immune cells. Here, we present an overview of TFM, the precautions and pitfalls, and the most recent developments in the context of T cell immunology.

KEYWORDS

traction force microscopy (TFM), immune cell, mechanics, force, mechanobiology

Introduction

The adult human body has approximately 10^{13} cells, and its fate, in terms of tissue and organ development and homeostasis, depends on how well these cells interact with one another and with their environment (see, for example (1–4) and references therein). A wealth of cell biology reports has documented the biochemical aspect of these interactions,

identifying the networks of secreted ligands, cell surface receptors, intracellular signaling pathways, and transcriptional factors at play. However, as cells live in a physical world, the mechanical aspect of such interactions cannot be neglected. Indeed, the last few decades of research have confirmed that cells do sense the mechanical forces arising from their environment; they actively respond to them through mechanically driven biological actions, such as adhesion, migration, division, differentiation, and even apoptosis - a process termed mechanotransduction (4). Mechanotransduction appears to be present in almost all interactions between a given cell and its environment, including immune cells.

For T lymphocytes, the initiation of an adaptive immune response necessitates the interaction of naive T cells with antigen presenting cells (APCs). This interaction starts with the T cell receptor (TCR) recognizing an antigenic peptide presented on the major histocompatibility complex (pMHC) of the APC. Once the TCR binds to a cognate pMHC, the T cell can be seen applying cycles of pushing and pulling forces on the APCs. These forces, generated from the rapid reorganization of the T cell cytoskeleton upon activating stimuli, may participate in the formation of a specialized cell-cell interface termed the "Immunological Synapse" (IS), encompassing additional receptor-ligand pairs. Through these interactions, the APC relays a highly orchestrated series of signals that drive T cell activation, proliferation, and eventual differentiation (3).

In recent years, it has become increasingly clear that the mechanical forces generated at the IS are essential for the proper activation of T cells; several of the cell surface receptors participating in the IS are mechanosensitive proteins, and the forces originating from the constant remodeling of the cytoskeleton play an important role in regulating them (5–7). It has been also proposed that both the amplitude and the time evolution of the forces applied through the TCR contribute to rapid discrimination of the antigenic peptides (8). Moreover, there is evidence suggesting that T cells and APCs use mechanical forces as a form of communication to transmit information across the synapse (2).

Thus, given the substantial impact of mechanical forces on the behavior of T cells, and knowing that even comparatively moderate defects in T cell activation can lead to autoimmune diseases on one hand, and immunodeficiency on the other, it comes as no real surprise that elucidating the precise mechanisms underpinning mechanotransduction is of significant interest to researchers in the area of fundamental and applied immunology, and biophysics. Clearly, a knowledge of both the intracellular and extracellular forces is required. Owing to this demand, the last two decades have witnessed a burst in novel experimental methods that have been employed to quantify cellular forces (4, 8, 9). These include, but are not limited to, Atomic Force Microscopy (AFM), Optical Tweezers (OT), Bio-membrane Force Probes (BFP), and Traction Force Microscopy (TFM) (Figure 1, and references within the caption).

This review will focus on methods that are now collectively known as Traction Force Microscopy (TFM). TFM is essentially a technique that permits the quantification of cellular traction forces *via* the non-invasive optical imaging of deformations induced by the cell. Though the term was initially used to refer to the forces exerted by adherent cells on 2D linear elastic substrates (37), it has since been adapted for quantification of three dimensional (tangential and normal) forces exerted onto 2D, 2.5D and 3D substrates.

Making invisible forces visible

Broadly speaking, forces are not an experimentally directly accessible quantity; they have to be inferred from the fact that they create some type of deformation or motion. The relation between deformation/motion and force is described by the classical laws of physics, one such example being Hooke's law for the deformation of a linear elastic spring: $F = k\,\Delta x$, where F is the force, k is the spring constant and Δx is the extension of the

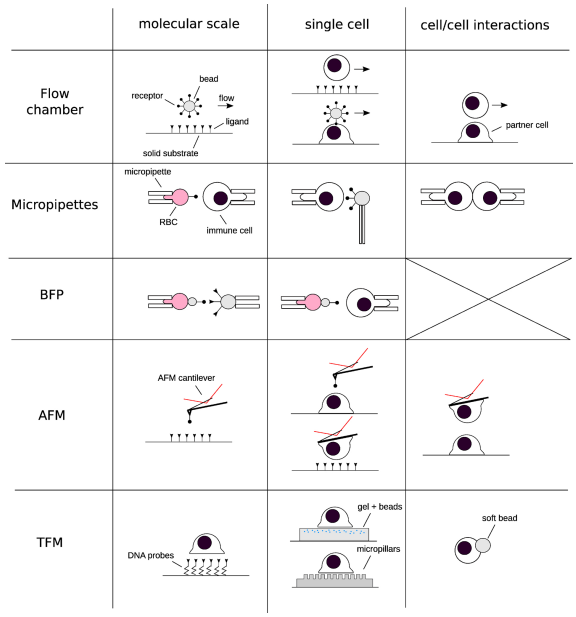

FIGURE 1
Schematics of the techniques that have been used for deciphering the implications of forces in immunology at different scales of space (from molecular to cell/cell interactions) and times. Each row represents a "group" of similar techniques, and each column a given spatial scale. A selection of references corresponding to each technique, *restricted to their application to immune cells:* Flow chamber: (10–12) Micropipettes: (13–16). Biomembrane Force Probe: (17–20). Atomic Force Microscopy: (21–26) Traction force microscopy and related techniques: (27–36).

spring. Without a measurement of Δx, no statement on F would be possible (k is a constant that can be obtained from a calibration experiment). In order to measure Δx, the relaxed reference state of the spring in the absence of any force has to be known.

Consequently, all measurements of cellular forces must start with the identification of a suitable strain gauge and incorporating it into a cell culture setup. One straightforward way of doing so is by replacing the traditional glass or plastic cell culture plates with a substrate capable of deforming under force. The earliest attempt at this was by Harris et al. who used a thin silicon rubber to show that fibroblasts generated elastic wrinkles when crawling (38). They named the force *"traction"*, comparing it to *"the traction an automobile's wheel exerts on the highway surface"*. However, because wrinkling is an inherently non-linear and complex process, the forces couldn't be accurately quantified.

Continuous versus discrete anchoring

Despite this seminal experiment remaining a rather qualitative observation, it inspired the design and development of alternative systems capable of quantitatively measuring traction forces. Nearly two decades later, in 1999, Dembo and Wang officially introduced "*Traction Force Microscopy*" – TFM - as a method to quantify forces exerted by adherent cells on compliant substrates (37). They replaced the silicon membranes with thicker, linearly elastic, hydrogels and adopted fluorescent beads as fiducial markers, instead of relying on wrinkles to report substrate deformation (Figure 2A). Above all, these changes replaced the generally nonlinear and mathematically complex description of wrinkle formation with a classical, linear, continuum mechanics model from material science (39, 40), thus opening the way for systematic force measurement.

In an attempt to further simplify the computationally intensive force calculations required for continuous hydrogels, Tan and colleagues introduced an elegant alternative system for TFM in 2003 (41). Theirs consisted of cylindrical polymeric pillar arrays, fabricated by soft lithography, where cellular forces can be laterally decoupled in a series of local strain gauges; once cells adhere to the protein-coated pillar tops, they bend them away from their unloaded position. By estimating this deformation and applying the classical beam bending theory, one can then calculate the local traction forces exerted by the cells (Figure 2B) (41, 42). Despite the obvious advantage of using such discrete adhesive surfaces (i.e., load-free reference position is readily available and the deflection of a given pillar only depends on the force applied to that particular pillar), the pillars themselves represent a major flaw in the system: They impose arbitrary restrictions on the size, shape, and location of cellular adhesions, and consequently control where and how cells transmit force (43, 44). In addition, if the cell makes adhesive protrusions that extend into the substrate beyond the very top of the pillars, the classical calculation is not applicable. Thus, even though forces can be elegantly calculated using such a system, it remains unclear how these calculations relate to those actually transmitted in the native cellular environment.

Though the pillar arrays system suffered from several intrinsic limitations, it is crucial to highlight that the concept behind it served as a foundation to build a number of new approaches that translated the "reference free" and "computationally easy" force reconstruction onto flat 2D TFM substrates. These include the micro-patterning of cell adhesive islands (45, 46), the lithographic photoresist of ordered arrays (47, 48), as well as the nano-patterning of quantum dots (QDs) on linearly elastic substrates (49). Using these technologies, a

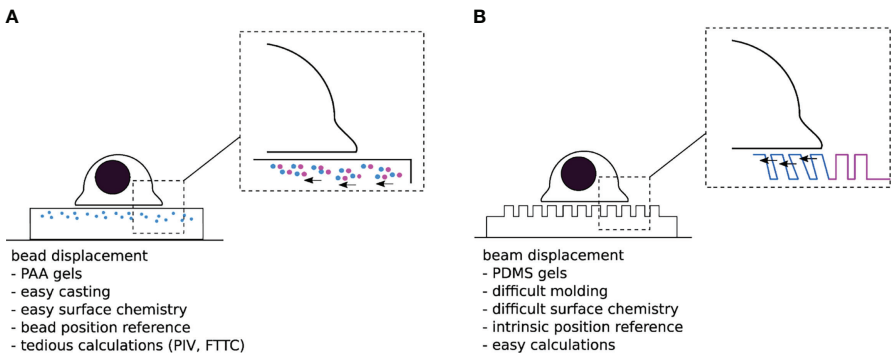

FIGURE 2
(A) "Traditional" TFM with PAA gels doped with sub-resolution fluorescent beads. One difficulty is to assess the non-perturbed bead position either at the beginning or the end of the experiment. **(B)** Micropillar based TFM. The typical size of a pillar is 1μm diameter over 10μm length, for a 1 μm interpillar distance, and a hexagonal compact 2D distribution-the numbers given here are typical orders of magnitude for these parameters). The unmolding step in the substrate fabrication process can be quite delicate, while the force localization and calculation are rather trivial.

regularized grid of reporter structures allows the determination of deformation of continuous 2D substrates without the need of a reference frame. However, as these patterns may represent the only sites where cells can exert force, similar to the pillars, the artificial constraint on cell force location will impact the physiological relevance.

From 2D to 3D TFM

Whether it's the continuous hydrogels from Dembo and Wang, or the pillar arrays from Tan and colleagues, both systems were originally developed with the aim of quantifying forces generated by *adherent* cells on 2D substrates. This was based on the assumption that cellular forces are predominantly tangential (in-plane, x, y), and that the forces normal to the substrate (out-of-plane, z) are negligible (50). However, since then, it has become evident that cells interacting with adherent substrates exert forces in 3D, and that the out-of-plane traction components are often comparable to the tangential ones (51, 52).

To account for these realizations, classical 2D TFM has been extended to 2.5D and 3D TFM (53–56).

2.5D TFM refers to the measurement of tangential and normal cellular forces exerted onto 2D substrates, not to be confused with "true 3D" TFM that quantifies forces exerted in 3D space (substrate). Nevertheless, in either case, by obtaining both the in- and out- of plane displacement fields of fiducial markers (e.g., fluorescent beads or patterns) using high-resolution image processing, for example through z-stack or astigmatic imaging (56), one can then reconstruct the "3D" force fields exerted by the cells.

While resolving normal traction forces is in itself difficult, given that it requires significant computational power, in addition to an appropriate imaging modality (discussed below), 3D TFM in specific comes with its unique set of challenges. Typically, in 3D TFM, cells (e.g., fibroblasts) are encapsulated *within* a deformable 3D extracellular matrix (ECM) scaffold material (e.g., collagen or fibrin fibers), pre-loaded with fluorescent beads (57). Unlike in 2D and 2.5D TFM, where the synthetic substrates can be fully characterized, biopolymers such as ECM materials are mechanically complex (57); they are constantly being synthesized, degraded and remodeled by cells. It is thus difficult to discern whether the recorded deformations are caused by one of those processes or by actual cellular forces. Besides, natural ECM is composed of fibers with highly non-linear force-extension relationships, meaning extracting traction forces from deformations is not possible using classical mechanics approaches. An innovative solution around these difficulties was put forth by Legant et al. who performed 3D-TFM with polyethylene glycol (PEG) hydrogels, incorporating domains that allowed for both adhesion (fibronectin RGD binding domain) and degradation (matrix metalloproteinase susceptible linkers) by the embedded cells (58). It is important to note that 3D TFM is not quite physiologically relevant when studying lymphocytes, potentially more so for other immune cells such as macrophages.

Another noteworthy innovative TFM adaptation involves the use of deformable hydrogel microparticles for force quantification (35). Though this approach does not follow the classical definition of either 2.5D or 3D TFM, since neither the substrates are 2D, nor are the cells encapsulated, it does allow the quantification of tangential and normal forces applied to a sphere of adjustable size, and can therefore be quite intriguing for the investigation of cell-cell interactions. For example, studying T cell-APC and cytotoxic T cell-infected cell interactions where membrane tension is essential for immune synapse stabilization (59) and perforin (a hydrophobic protein that forms pores in the target cell membrane) secretion (60).

Making the right material choices

Despite the many exciting developments in the broad field of TFM, the most commonly used system to measure cellular traction forces remains the one designed by Dembo and Wang in 1999: TFM on continuous and linearly elastic substrates embedded with fluorescent beads (37) (Figure 3). The most popular substrates used in this system are polyacrylamide gels (PAGs) and polydimethylsiloxane elastomers (PDMS, also called silicone). However, two unique features have given PAGs an edge over their counterparts. First, PAGs span an excellent range of elasticities (62). By simply varying the concentrations of acrylamide and N,N′-methylenebisacrylamide-the building blocks of PAGs- while retaining the same surface chemistry, the stiffness of the PAG can be adjusted to mimic that of most biological tissues (typically from 100 Pa to 100 kPa). Second, PAGs are generally non-fouling, meaning they are nearly inert as adhesive substrates. The same chemical stability and non-adherence that allows the usage of PAGs for the electrophoretic separation of nucleic acids and proteins, also guarantees that neither cell surface receptors nor adhesive proteins present in the serum can bind directly to the gel. Consequently, only molecules *covalently* grafted on the gel surface can act as ligands for the cells (29). In comparison, different formulations of PDMS are required for it to span a similar range [1 KPa- 1 MPa, 'Q-gel' is the more suitable choice for low elasticities and 'Sylgard' for the high ones; (63)]. Additionally, being extremely hydrophobic, PDMS requires supplementary passivation to prevent the non-specific adsorption of proteins onto its surface.

It is generally accepted that the experimental setup used for TFM has a great influence on the achievable result, both in accuracy and quality. Thus, regardless of the chosen material, a number of key considerations must be taken into account when designing a TFM substrate.

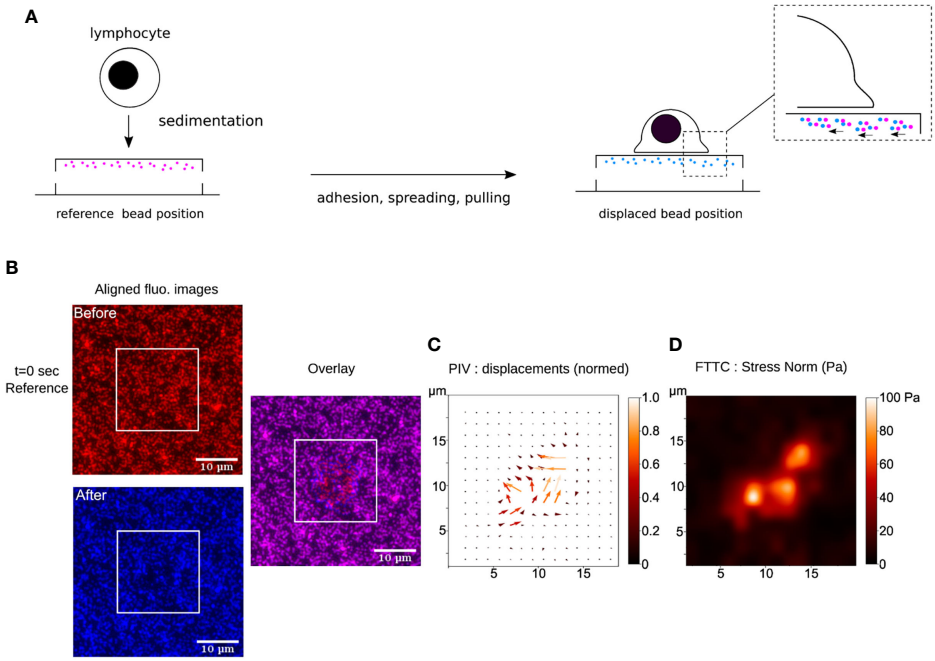

FIGURE 3
(A) Schematics of TFM for the study of early interactions of a primary human T lymphocyte with an ultra-soft APC-mimicking PAG doped with fluorescent nanobeads. **(B)** Raw fluorescence images, before and after the cell has landed, aligned to remove sample lateral drift. These ROIs are cut from original large field epifluorescence movies. The white squares indicate where a T lymphocyte has landed, as observed in bright-field transmission microscopy (not shown). The overlay shows the displacement of the beads due to cellular force. **(C)** Result of PIV calculation (over the zone delimited by the white square, where the cell sits) showing the constructed vector map of bead displacement field, taking t=0 sec frame (before the cell has landed) as the cell-/stress-free reference. The displacements have been normalized. **(D)** Result of FTTC calculation showing the gaussian smoothed map of stress norm. The data presented here has been processed using open-source softwares (Fiji/ImageJ (61), Python), following (29).

First, the thickness of the substrate needs to be sufficient. "Cells may not see or hear", but they can certainly "feel" their surroundings and sense a collective stiffness. Just like the princess in Hans Anderson's fairy tale who felt a small pea beneath a stack of soft mattresses, cells too can feel the stiffness of a rigid support buried beneath a soft layer, even if they're not in direct contact with it. The soft layer, in this case the substrate, must be sufficiently thick such that the cells feel and respond to its softness rather than the rigidity of the underlying glass.

Second, the stiffness of the substrate must be tuned to fit the biological system under investigation. Different cell types exert forces over a wide range, and thus the chosen stiffness must be able to manifest the exerted forces as an appropriate deformation. On one hand, if the substrate is too stiff, the cells will not be capable of effectively deforming it, resulting in insufficient bead displacement, and rendering the calculation of force impossible. On the other hand, if the substrate is too soft, then the bead displacement may be too large, thus breaching the linear-response regime and making the linear-elastic theory inapplicable. A starting point for cells hitherto unexplored in terms of force measurements, is to consider the elasticity data reported for cells or tissues that the cells under consideration interact with. For example, when working on T cells, a stiffness such as the one reported for antigen presenting cells may be the appropriate starting choice (64).

Third, considerations of roughness and porosity are important. Given the cross-linked nature of PAA and PDMS, their stiffness is related to the mesh size of their molecular polymer network; the stiffer they are, the smaller the mesh size. Thus, an additional restriction would be that the substrate must be stiff enough to grant the formation of a sufficiently small mesh size capable of trapping the beads inside of it. It is important to note that mesh size may also influence the surface density of the functionalized proteins (65).

Fourth, the density of the fiducial markers needs to be optimal. Bead density in the substrate, of course in conjunction with the optical technique chosen for observation, directly determines the accuracy of force recovery (61). Thus, it must be carefully chosen in accordance with the spatial scale, the magnitude of the forces being measured, and the image analysis method to be used later. The density of the beads must be high enough to capture the spatial intricacies of the traction force field. If the bead density is too low, then in certain areas the deformation may go unreported and thus the traction

information may be incomplete. Alternatively, if the bead density is too high, the image of the beads may overlap and nearby beads may not be resolved, thus concealing details of their relative displacement.

Quantifying displacements

The fundamental principle behind TFM has remained the same since its conception: when cells adhere or migrate over sufficiently compliant substrates, they exert traction forces that can deform said substrate. These deformations are spatially and temporally mapped by monitoring the changes in lateral position of sub-resolution fluorescent beads embedded just below the cell accessible, functionalized surface.

In order to measure cell traction forces, (at least) two images of the substrate have to be acquired: One image of the bead field while the substrate is subjected to cellular forces (i.e., the stressed state) and another image of the bead field in the absence of cellular forces (i.e., the relaxed state). The image of the beads in their relaxed state can either be obtained *before* cell engagement (28, 66) or *after* cell detachment using EDTA or cocktails of proteolytic enzymes such as Trypsin or Accutase (67). Provided that the substrate is linearly elastic, the beads should return back to their relaxed state once the cells, and therefore the exerted forces, have been removed. The displacement caused by the cells can then be computed by comparing the bead positions in the stressed state to that in the relaxed state.

There are currently two main approaches to perform this comparison, either by localizing and tracking each individual bead, also known as single-particle tracking (SPT, (68, 69)), or by correlating displacements with regions of an image, also known as particle image velocimetry (PIV, (70)).

SPT identifies and tracks individual bead centroids by utilizing single particle localization algorithms. Basically, these algorithms scan all the pixels in the relaxed image to identify the pixel coordinates of the fluorescent beads (referred to as pixel intensity maxima). For each bead that is tracked, a box of pixels centered around the maximum intensity pixel is designated. The relative pixel intensities in that box serve as a "fingerprint" for the tracked bead, which is then used to find the coordinates of the corresponding "fingerprint" in the stressed image. This process is repeated for every bead in the image. Usually such procedures are able to track the bead displacements with submicron resolution (71).

Alternatively, one can forgo identifying and tracking individual bead centroids, and instead use PIV to calculate and project displacements on a grid, using image cross-correlation. To do that, both rest and stressed images have to be first partitioned into small interrogation windows. The pattern of an interrogation window in the first image is correlated with a region of equal size in the second image that is shifted pixel-wise in the vicinity of the location of the interrogation window of the first image. The result of this operation is a local correlation map of a specific bead pattern. The position of the maximum correlation value within this map is the most probable displacement of the bead pattern of this specific interrogation window.

Because PIV requires the image to be divided into smaller regions, some of the displacement occurring in the sub-regions might be lost. To minimize this loss, the selection of a "correct" PIV window is critical. If the window is too large, fine detail regarding the bead displacement will be lost, and the overall resolution of the force will be compromised. Alternatively, if the window is too small, such that it contains no distinguishable features (eg. a too small number of beads or even no beads to the extreme limit), the correlation between frames will be unreliable and prone to error due to the creation of non-existing displacement. Such a choice is influenced by the density of beads but also by the scale of the features one expects to record.

Both of these approaches have their own limitations, and they can also be combined (30, 69). SPT potentially yields higher accuracy but may introduce incorrect bead matches between the relaxed and stressed images which contaminate the true displacement data. PIV on the other hand is robust against mismatches as well as sample drift in the z direction, however, it is doubtful to obtain comparable lateral accuracy and resolution. Nevertheless, they have both been utilized in 2D TFM with minimal modifications. The question of which approach to use depends on the expected nature of the forces. For example, in the case of focal adhesion forming cells where forces are likely to result in a collective motion of a group of beads, it would probably be more appropriate and practical to use an approach that depends on image cross correlation instead of individual bead displacement.

Mapping forces

The final step in TFM is to convert displacements into a map of cellular traction stresses or forces. In other words, a relationship, derived from the physics of materials, is needed to describe the deformation of a material in response to a force applied onto its surface. Although this conversion fundamentally requires solving a stress-strain problem, several approaches have been developed to do so, the two main ones being the forward approach and the inverse approach.

The forward approach is more straightforward and computationally efficient. As the name suggests, the stress tensor is calculated directly from a three-dimensional displacement field, using the constitutive law of the material, and the surface traction is calculated from the 3D stress field (72). One major advantage for this method is that it can be easily applied to nonlinear, viscoelastic, or other material constitutive properties without having to modify the general mathematical framework. Nevertheless, there are two major trade-offs to using

it. First, a 3D or quasi 3D displacement field is needed and second, noise effects may become very important. In traditional 2D TFM where fluorescent beads are embedded in the substrate, the stress field is not known immediately at the cell-substrate interface, it's rather measured at the layer of beads closest to the interface. Consequently, in order to calculate the forces experienced at the true substrate interface, some method of extrapolation must be implemented to estimate the stress field at the interphase from that at bead level. This estimation might introduce significant error if one can't ensure that a large enough number of beads is present quite near to the substrate surface.

One way to address this concern is to adopt the inverse approach. In this approach, the traction field becomes a convolution of the displacement field and Green's function. It's important to note that the utilization of Green's function imposes several key assumptions. First, forces are mainly exerted along the substrate surface rather than normal to it. Second, the substrate is estimated to be a 2D elastic plane extending laterally to infinity (a semi-infinite half space). Third, the strains are small and thus the substrate deforms under a linear elastic regime. Lastly, the substrate material remains homogeneous in both relaxed and stressed states. Even if all these assumptions are experimentally met, the inverse approach still suffers from two major limitations. First, upon inversion, the calculated forces become very sensitive to high frequency fluctuations (i.e., noise) in the displacement data. To solve this problem, a pre-smoothing, also known as regularization, must be implemented to obtain a reasonable solution (73)). The regularization coefficient must be carefully chosen so as to provide a balance between how well the solution fits the noise-distorted experimental displacement data and the overall magnitude of the traction forces. If the solution is over-regularized, the data will become over-smoothed and the resolution of the recovered forces will be lost. Alternatively, if the data is under-regularized, the solution will overfit the noise in the displacement and will thus be a false representative of the traction forces. Secondly, the computation needed to solve the inverse problem and implement the additional regularization steps is quite time-consuming and computationally expensive. The most common and general way to solve this problem is by using Fourier Transform Traction Cytometry (FTTC) whereby, essentially the integrated displacements are transformed into Fourier Space and the calculations are performed using matrix multiplications.

Improving detection in 2D (and 3D)

The accuracy and resolution of TFM ultimately depend on the spatio-temporal resolution of the optical microscopy technique with which it is accompanied. The spatial resolution is a limit imposed by the resulting finite size of the point spread function (PSF) associated with each fluorescent bead. At high densities, the PSF of the beads begin to overlap, hindering the reliable tracking of their displacement. Similarly, the temporal resolution also influences the ability to reference and track individual beads over time. Not to mention that at low time resolutions, dynamic processes are concealed, whereas at higher time resolution, requiring more frequent imaging, phototoxicity as well as photobleaching become a concern. As such, experimentalists often find themselves forced into a trade-off between spatial and temporal resolution.

The first straightforward attempt to partially overcome these limitations came from Sabass et al. who proposed to incorporate fluorescent beads of two different colors to increase the allowed bead density while decreasing the noise and irregularities in bead tracking (69, 74). To further improve the spatial resolution of TFM from the micron to the submicron scale, Colin-York et al. combined super-resolution stimulated emission depletion (STED) microscopy with TFM (2D STED-TFM) (75). STED-TFM allowed a 5-fold improvement in the resolution of the tracked bead displacement field, yielding a much finer recovery of force compared to standard laser scanning confocal microscopy. This step forward however, came at the expense of increasing the image acquisition time to a few minutes for each field of view due to the STED scanning. Additionally, the high laser intensity required for fluorescence depletion diminished the biocompatibility of this approach. The same group later addressed these problems by developing live-cell super-resolution 3D SIM-TFM, a technique combining structured illumination microscopy (SIM) and TFM. Because SIM is a wide-field technique, it does not rely on image raster scanning, and thus, unlike STED, allowed faster acquisition times (11 ms per frame, 15 frames per super-resolution image in 3D mode), and at a significantly lower fluorescence excitation light, thus increasing the number of images that can be a acquired at a given time frame while minimizing the effects of photobleaching (76, 77).

To overcome the need for the axial scanning required for the 3D imagining of the beads using 3D SIM-TFM, and further increase the speed of acquisition, they later combined TFM with 2.5D astigmatic imaging (aTFM) and SIM in total internal reflection fluorescence microscopy mode (TIRF-SIM) (56). Astigmatic imaging allowed the 3D information in the ~1 μm zone surrounding the focal plane to be inferred from a single wide-field image, rather than having to perform multi-frame z-stack acquisitions, thus increasing image acquisition to up to 90 ms per SIM image frame, while the use of TIRF reduced the contribution of out-of-plane fluorescence and enhanced the overall quality (contrast) of the images. In their most recent work, they extended TIRF-SIM to 2D (2D TIRF-SIM-TFM), demonstrating a >2 fold

increase in spatial resolution and >10 fold increase in temporal resolution in comparison to traditional TFM (78).

There are two main limitations that appear when using 3D SIM-TFM and TIRF-SIM-TFM (2.5D and 2D). Firstly, they necessitate the use of high numerical aperture objectives with narrow working distances which consequently diminishes the imaging depth and limits the thickness of the substrate that can be used. This is particularly problematic in TFM since, as mentioned previously, the substrate must be sufficiently thick to eliminate any mechanical influence coming from the underlying glass. Secondly, imaging the substrate-cell interface requires that the substrate has a refractive index similar to that of glass, such as PDMS (variety Qgel for example, (63)), which in itself comes with its own set of constraints, primarily the limited elasticity range that can be achieved. PAGs, having a refractive index similar to that of water, are therefore not directly amenable to such refined techniques.

It is also noteworthy that the availability of such advanced microscopy systems is likely limited by prohibitively high costs, either on the material side or on the development time needed to set them up, which often limits experimentalists to more classical fluorescence (epi or confocal) and phase-contrast microscopy. Normally, this would rule out the possibility of recovering 3D traction forces since traditional 2D imaging systems suffer from a relatively high degree of out-of-focus light-scattering. However, Hazlett et al. found an interesting strategy to get around that difficulty (54). They embedded a single dense layer of fluorescent beads on the PAG surface, and then obtained volumetric images of the beads by deconvolving the experimental epifluorescence images acquired using the PSF collected from a single bead in the images. Using SPT, they managed to quantify 3D volumetric bead displacements, and consequently, 3D stress fields.

Insights into T cell biology from TFM data

In this section, we present a few prominent examples of recent insights gained into the workings of T cells thanks to TFM studies.

One of the earliest experiments implementing TFM for T cell studies examined the complementary roles of CD3 (parts of the TCR complex, responsible for signal transmission across the membrane) and CD28 (a costimulatory molecule participating T cell activation) in mechanosensing during primary human CD4+ T cell activation. Using PDMS pillar arrays presenting activating antibodies against CD3/or pMHCs and/or CD28, Bashour et al. confirmed that antigen recognition does in fact involve force exertion. They recorded traction forces of around 100 pN, exerted specifically through the TCR-CD3 complex, and which could be augmented with co-stimulation through the engagement of PI3K signaling pathways (27).

To examine the interplay between activation and adhesion, Tabdanov et al. also employed PDMS pillar arrays, but functionalized with activating anti-CD3 antibody +/- ICAM-1 instead (79). Their experiments showed that the incorporation of ICAM-1 significantly increased the cellular contractile stresses exerted by Jurkat T cells, in comparison to those recorded when only the TCR/CD3 complex was engaged. Combined with their experiments on micropatterned surfaces, their work highlighted a mechanical cooperation between the TCR/CD3 and LFA-1-ICAM-1 systems, whereby actin nucleation (governed by Arp2/3) downstream of TCR signaling sustained the growth of the LFA-1 dependent actin network, which in turn then provided the cytoskeletal tension to allow mechanical sensing, T-cell spreading and enhanced TCR activation.

Focusing further on the influence of the T cell cytoskeleton, Hui et al. used enhanced green fluorescent protein (eGFP)–actin expressing Jurkat T cells and poly-L-lysine-anti-CD3-coated polyacrylamide gels, to demonstrate the contribution of actin polymerization and myosin contractility in force generation and maintenance during T cell activation (28). With this system, they recorded peak stresses reaching 20–30 Pa and a total force of a few nanonewtons and showed that the EGFP-actin Jurkat T cells exerted larger forces on polyacrylamide gels of increased stiffness. This came in contrast to Bashour et al.'s work (27), where no change in traction force per pillar as a function of pillar stiffness was observed. Building on these results, the same group later utilized the same system to showcase the role of dynamic microtubules in regulating force generation at the T cell-substrate interface, through suppressing Rho contractility and actin flow (80).

Another study highlighting the role of actin in T cell force generation, was that of Savinko et al. (81) employing silicone-based gel substrates coated solely with ICAM-1. In these experiments, knocking out the actin-binding protein filamin A dropped the traction stresses exerted by mouse CD4+ effector T cells by approximately 50% (from $\simeq$ 50 Pa to $\simeq$ 25 Pa).

Linking cytoskeletal forces and effector function, Tamazalit et al. used PDMS pillar arrays presenting cognate p-MHC-I to show that CD8+ T lymphocytes employ F-actin rich protrusions, generated by Wiskott-Aldrich Syndrome protein (WASP) and the Arp2/3 actin nucleation complex, for synaptic force exertion and cytotoxic function (perforin and granzyme release; granzymes are proteases that induce cell apoptosis) - A process they termed as "mechano-potentiation" (82).

In an innovative approach, Vorselen et al. studied the interaction of eGFP-actin expressing cytotoxic T lymphocytes (CTLs) with activating (quantified as Ca^{2+} influx) soft (~ 300 Pa) deformable polyacrylamide microparticles (DAAM-particles, $\simeq$ 15 μm in diameter) functionalized with cognate pMHCs and

ICAM-1. Interestingly, using this technique, the shear stresses (~ 100 Pa) detected in the contact area (8 μm in diameter) between the CTLs and the microparticles were directed outwards, and as time progressed, localized indentations i.e., normal traction forces (up to 200 Pa, 0.5 nN total force) started forming within that area (35).

Similarly, Aramesh et al. also adopted an unconventional strategy to study both tangential and normal forces generated by T cells. Instead of using microparticles-doped gels however, they performed a functionalized bead assay whereby anti-CD3 and/or anti-CD28-functionalized 200 nm neutravidin-conjugated beads were bound onto the surface of biotinylated poly(ethylene glycol)diacrylate (PEGDA) gels or PDMS-based QGel, and Jurkat T cells were left to interact with them (55). In accordance with Bashour et al.'s observations (27), their experiments also showed that co-stimulation by CD28 does in fact enhance T cell forces, reaching up to 10 nN forces, and not surprisingly, the increased force generated correlated with increased Ca^{2+} influx, i.e., increased activation. However, what was truly intriguing about their data was that single T cell microvilli were targeting single beads, and within that T cell-microvilli contact, actin was forming a vortex-like ring structure where the TCR was enriched and CD45 was excluded. This comes in line with previous reports suggesting that the size-mediated exclusion of CD45 from the IS shifts the ITAM phosphorylation–dephosphorylation balance, thereby triggering TCR signaling (83).

Though this section has focused on the existing literature regarding T lymphocytes studies using TFM, several other immune cell types have been investigated using the same methodologies, often though to a lesser extent. These include neutrophils (31), B cells (30, 66), dendritic cells (84) and macrophages (36).

Molecular sensors for force measurements

All the techniques mentioned thus far represent macroscopically large strain gauges that measure force maps generated by the cell, at the (sub)cellular scale. The same principle can be implemented at the nanoscale to measure the force borne by a specific molecule, through the interaction of a single receptor and ligand: provided that mechanical properties can be evaluated at the molecular scale, deformations of individual molecules, such as the extension of protein domains or DNA molecules, can be converted into forces. To this end, a great deal of effort has been dedicated over the last decade into the development of molecular force sensors (32, 85–87). These may not formally qualify as TFM but are included here because of their immense importance and potential.

The principal components of these sensors are deformable molecules that are sensitive to molecular tension, and that are labeled with a dye, a dye–quencher pair, or a dye-dye pair. Once force is applied onto the construct, its configuration will change, and consequently the fluorescent activity of the sensor will change as well. Thus, the experienced molecular force will eventually be reported as surface fluorescence loss, fluorescence gain, or Förster resonance energy transfer (FRET) efficiency change (88). Note that, similar to the substrates used in classical TFM, the responsivity range of the deformable molecule should match the range of the molecular force transmitted by the molecule under investigation.

While most common molecular force sensors are coated onto surfaces and are thus used to report the forces applied by cells onto said surfaces, another type can be used to measure forces *inside* cells. Typically, these constitute mechanosensitive proteins that have been engineered with fluorophore pairs and expressed in living cells; As they experience force, the separation distance between the fluorophores, and consequently the FRET efficiency, is altered, allowing for the real time measurement of intracellular forces across single molecules (89, 90).

Although such sensors provide an immediate readout of molecular forces, for several reasons, interpreting the obtained signals might not be as straightforward. First the effective spring constant of the elastic linker might depend on the local environment in the cell, even if previously calibrated by single-molecule force spectroscopy experiments (by Atomic Force Microscopy, Optical or magnetic Tweezers (91). Second, the fluorescent signal is a sensitive function of domain separation and relative orientation, thus, a direct conversion into force can be problematic (92, 93). Third, it is difficult to control the number of engaged sensors, consequently, the fluorescent signal cannot easily be integrated over a larger region. Not to mention that using such a technique allows the recovery of only the norm of the force exerted and not the exact direction of said force. Therefore, advanced molecular force sensors can be expected to complement, but not fully replace, traditional TFM in the future.

Conclusions and perspectives

The last two decades have witnessed an upsurge in the development of a wide variety of techniques for probing cell generated forces. Though they have not been discussed in this review, they have been described in great detail elsewhere (See for example, for immune cells, (2, 8)). Despite their growing availability, such advanced biophysical techniques still require specialized skills and often expensive tools that are still far from becoming routine laboratory equipment in biology labs, unlike conventional molecular biology tools for examining gene expression and protein concentration. Perhaps the simplest of

these techniques, and the one that is rapidly leading its way towards standardization, is TFM. Most likely, TFM has gained such wide adoption by the mechanobiology community because of its ease of implementation and longstanding history.

However, if we disregard for a brief moment its attractive simplicity, we will see that TFM suffers from very serious caveats. Primarily, the computational analysis required for tracking displacements and recovering force maps is quite complex, nuanced and difficult to validate. Even marginal errors in retrieving bead displacement will introduce large errors into the final stress and force fields. Moreover, as explained above, extracting force fields from displacement fields is a mathematically ill-posed problem that will introduce noise into the final measurements, and will thus necessitate regularization. Since there is not a "standard" regularization factor, which is quite logical since this value will depend on several experimental and numerical parameters, which are not uniform (e.g., bead size, bead density, substrate stiffness, cellular forces, and imaging parameters, methodology for calculating the beads displacements …), one could end up with either over-smoothed, or alternatively, under-regularized data, which does not faithfully represent the exerted cellular traction forces. Given such variable experimental and analysis protocols, comparing experimental values obtained in different laboratories becomes very difficult, especially, as is the case for any quantification of living systems, since biological diversity, such as cell culture conditions and cell passage number, may also impact the scatter in measured values.

Potentially, the only way to overcome these challenges is by utilizing reproducible and accessible standardized protocols, as well as implementing open source softwares for data analysis. Several startup companies that sell prefabricated substrates exist today, which is a partial step towards standardization - though in our experience their rigidities need to be verified by the end user. Python, ImageJ/Fiji, and even Matlab scripts are now available online for calculating stresses, force maps and energies from bead images (see for example https://sites.google.com/site/qingzongtseng/tfm, https://github.com/topics/traction-force-microscopy, https://github.com/MBPPlab/TFM_v1). Though this does not completely solve the problem, it is a step in the right direction towards standardization.

To further complexify the picture, the generation of mechanical forces by biological systems are space and time scales dependent, from cells, down to single molecules and up to entire organisms, lasting less than a few seconds up to hours and even over their whole lifetime. For example, looking at T cell activation, certain processes such as actin turn-over occur at the order of seconds, while others may take several minutes, such as the building of the IS, or more. Another important point is that, *in-vivo*, cells are interacting with different substrates/other cells and are constantly integrating the myriad of biochemical and physical signals rising from their microenvironment. Trying to recapitulate such intricate physiological conditions is extremely challenging, and so it remains difficult to understand how forces measured *in-vitro*, on mechanically simplified substrates, relate to those existing in living tissues or organs. A prominent example in T cell studies is that every interaction of a T cell with APCs will be made under different mechanical conditions as pointed out by Bufi et al. (64) leading to adaptation in experimental parameters, such as the substrate rigidity in TFM to accommodate for a precise encounter to be studied.

Therefore, before opting for one technique or the other, an investigator needs to make several critical decisions: (1) *in-vivo* or *in-vitro* (2) 2D, 2.5D or 3D, (3) spatial resolution- nanoscale or microscale- and/or temporal resolution-sub second, second, or minutes, (4) molecular scale forces or cellular scale forces. Another key point is deciding whether one time point quantification, and thus one force value, will suffice, or whether the process is dynamic and will require time-lapse measurements. We have specifically highlighted this point in our recent work using TFM on ultra-soft PAGs which showed that T cells exhibit distinct dynamic stress and energy patterns (29).

With the pace at which the field of mechanobiology is growing, it is not unreasonable to imagine that the next-generation tools for quantifying cellular forces will exhibit an extended range of measurable forces, an improved spatio-temporal resolution, and will re-create a more complex cellular microenvironment that will allow cells to experience a dynamically changing set of biochemical and physical conditions, more representative of that occurring in *in-vivo* settings. Though this may sound quite alluring, one has to keep in mind that the more complex our questions and experiments become, the more difficult it will be to extract meaningful correlations and determine clear cause–effects relations. There will always be a series of more or less arbitrary trade-offs.

Perhaps the most exciting and currently achievable experimental approach in the world of TFM revolves around combining simultaneous measurement techniques. This could be through merging fluorescent molecular force sensors with classical 2D TFM, to have a better understanding of how forces propagate between the molecular and cellular scales. It could also be through the simultaneous quantification of cellular/molecular forces with signaling cascades, eg. using live phosphorylation (94) or calcium reporters (95, 96), to yield a more complete picture of how force generation and biochemical events are integrated across different scales. Ultimately, studying the mechanobiology of cells in general, but of immune cells and T cells in particular, will be the route to enhancing our understanding of the role of mechanobiology in health and disease (2, 4), and hopefully we will one day be able to translate this wealth of knowledge into next-generation diagnoses and treatments.

Author contributions

All authors listed have made a substantial, direct, and intellectual contribution to the work and approved it for publication.

Acknowledgments

The project leading to this publication has received some funding from France 2030, the French Government program managed by the French National Research Agency (ANR-16-CONV-0001) and from Excellence Initiative of Aix-Marseille University - A*MIDEX. Part of this work was also supported by institutional grants from Inserm, CNRS and Aix-Marseille University to the LAI and from CNRS and Aix-Marseille University to the CINAM.

FM was supported as a PhD grant by the European Union's Horizon 2020 research and innovation programme under the Marie Skłodowska-Curie grant agreement No713750, with the financial support of the Regional Council of Provence- Alpes-Côte d'Azur and with of the A*MIDEX (n° ANR- 11-IDEX-0001-02), funded by the Investissements d'Avenir project funded by the French Government, managed by the French National Research Agency (ANR).

Conflict of interest

The authors declare that the research was conducted in the absence of any commercial or financial relationships that could be construed as a potential conflict of interest.

Publisher's note

References

1. Hannezo E, Heisenberg C-P. Mechanochemical feedback loops in development and disease. *Cell* (2019) 178(1):12–255. doi: 10.1016/j.cell.2019.05.052

2. Huse M. Mechanical forces in the immune system. *Nat Rev Immunol* (2017) 17(11):679–90. doi: 10.1038/nri.2017.74

3. Basu R, Huse M. Mechanical communication at the immunological synapse. *Trends Cell Biol* (2017) 27(4):241–545. doi: 10.1016/j.tcb.2016.10.005

4. Puech P-H, Bongrand P. Mechanotransduction as a major driver of cell behaviour: Mechanisms, and relevance to cell organization and future research. *Open Biol* (2021) 11(11):2102565. doi: 10.1098/rsob.210256

5. Comrie WA, Burkhardt JK. Action and traction: Cytoskeletal control of receptor triggering at the immunological synapse. *Front Immunol* (2016) 7:68. doi: 10.3389/fimmu.2016.00068

6. Blumenthal D, Burkhardt JK. Multiple actin networks coordinate mechanotransduction at the immunological synapse. *J Cell Biol* (2020) 219(2): e201911058. doi: 10.1083/jcb.201911058

7. Chabaud Mélanie, Paillon Noémie, Gaus K, Hivroz C. Mechanobiology of antigen-induced T cell arrest. *Biol Cell* (2020) 112(7):196–2125. doi: 10.1111/boc.201900093

8. Liu B, Kolawole EM, Evavold BD. Mechanobiology of T cell activation: To catch a bond. *Annu Rev Cell Dev Biol* (2021) 37(1):65–875. doi: 10.1146/annurev-cellbio-120219-055100

9. Limozin L, Puech P-H. Membrane organization and physical regulation of lymphocyte antigen receptors: A biophysicist's perspective. *J Membrane Biol* (2019) 252(4–5):397–412. doi: 10.1007/s00232-019-00085-2

10. Limozin L, Bridge M, Bongrand P, Dushek O, Merwe PAvd, Robert P. TCR-PMHC kinetics under force in a cell-free system show no intrinsic catch bond, but a minimal encounter duration before binding. *Proc Natl Acad Sci United States America* (2019) 116(34):16943–485. doi: 10.1073/pnas.1902141116

11. Vitte J, Pierres A, Benoliel A-M, Bongrand P. Direct quantification of the modulation of interaction between cell- or surface-bound LFA-1 and ICAM-1. *J Leukoc Biol* (2004) 76(3):594–6025. doi: 10.1189/jlb.0204077

12. Vitte J, Benoliel A-M, Eymeric P, Bongrand P, Pierres A. Beta-1 integrin-mediated adhesion may be initiated by multiple incomplete bonds, thus accounting for the functional importance of receptor clustering. *Biophys J* (2004) 86(6):4059–745. doi: 10.1529/biophysj.103.038778

13. Husson J, Chemin K, Bohineust A, Hivroz C, Henry N. Force generation upon T cell receptor engagement'. edited by javed n. agrewala. *PloS One* (2011) 6 (5):e196805. doi: 10.1371/journal.pone.0019680

14. Sawicka A, Babataheri A, Dogniaux Stéphanie, Barakat AI, Gonzalez-Rodriguez D, Hivroz C, et al. Micropipette force probe to quantify single-cell force generation: Application to T-cell activation. *Mol Biol Cell* (2017) 28 (23):3229–395. doi: 10.1091/mbc.E17-06-0385

15. Sung K-LP, Sung LA, Crimmins M, Burakoff SJ, Chien S. Determination of junction avidity of cytolytic T cell and target cell. *Sci New Ser* (1986) 234 (4782):1405–8. doi: 10.1126/science.3491426

16. Chen W, Zarnitsyna VI, Sarangapani KK, Huang J, Zhu C. Measuring receptor–ligand binding kinetics on cell surfaces: From adhesion frequency to thermal fluctuation methods. *Cell Mol Bioengineering* (2008) 1(4):276–885. doi: 10.1007/s12195-008-0024-8

17. Chen W, Evans EA, McEver RP, Zhu C. Monitoring receptor-ligand interactions between surfaces by thermal fluctuations. *Biophys J* (2008) 94 (2):694–7015. doi: 10.1529/biophysj.107.117895

18. Evans E, Kinoshita K. Using force to probe single-molecule receptor-cytoskeletal anchoring beneath the surface of a living cell. *Methods Cell Biol* (2007) 83(07):373–965. doi: 10.1016/S0091-679X(07)83016-0

19. Kinoshita K, Leung A, Simon S, Evans E. Long-lived, high-strength states of ICAM-1 bonds to B2 integrin, II: Lifetimes of LFA-1 bonds under force in leukocyte signaling. *Biophys J* (2010) 98(8):1467–755. doi: 10.1016/j.bpj.2009.12.4316

20. Liu B, Chen W, Evavold BD, Zhu C. Accumulation of dynamic catch bonds between TCR and agonist peptide-MHC triggers T cell signaling. *Cell* (2014) 157 (2):357–685. doi: 10.1016/j.cell.2014.02.053

21. Marshall BT, Long M, Piper JW, Yago T, McEver RP, Zhu C. Direct observation of catch bonds involving cell-adhesion molecules. *Nature* (2003) 423 (6936):190–93. doi: 10.1038/nature01605

22. Puech P-H, Nevoltris D, Robert P, Limozin L, Boyer C, Bongrand P. Force measurements of TCR/PMHC recognition at T cell surface. *PloS One* (2011) 6(7): e223445. doi: 10.1371/journal.pone.0022344

23. Rico Félix, Chu C, Abdulreda MH, Qin Y, Moy VT. Temperature modulation of integrin-mediated cell adhesion. *Biophys J* (2010) 99(5):1387–965. doi: 10.1016/j.bpj.2010.06.037

24. Hu KH, Butte MJ. T cell activation requires force generation. *J Cell Biol* (2016) 213(5):535–425. doi: 10.1083/jcb.201511053

25. Lim TS, Mortellaro A, Lim CT, Hämmerling GünterJ, Ricciardi-Castagnoli P. Mechanical interactions between dendritic cells and T cells correlate with T cell responsiveness. *J Immunol (Baltimore Md.: 1950)* (2011) 187(1):258–655. doi: 10.4049/jimmunol.1100267

26. Zak A, Merino-Cortés SV, Sadoun Anaïs, Mustapha F, Babataheri A, Dogniaux Stéphanie, et al. Rapid viscoelastic changes are a hallmark of early leukocyte activation. *Biophys J* (2021) 120(9):1692–704. doi: 10.1016/j.bpj.2021.02.042

27. Bashour KT, Gondarenko A, Chen H, Shen K, Liu X, Huse M, et al. CD28 and CD3 have complementary roles in T-cell traction forces. *Proc Natl Acad Sci* (2014) 111(6):2241–465. doi: 10.1073/pnas.1315606111

28. Hui KL, Balagopalan L, Samelson LE, Upadhyaya A. Cytoskeletal forces during signaling activation in jurkat T-cells. *Mol Biol Cell* (2015) 26(4):685–955. doi: 10.1091/mbc.E14-03-0830

29. Mustapha F, Sengupta K, Puech P-H. Protocol for measuring weak cellular traction forces using well-controlled ultra-soft polyacrylamide gels. *STAR Protoc* (2022) 3(1):1011335. doi: 10.1016/j.xpro.2022.101133

30. Kumari A, Pineau J, Sáez PJ, Maurin M, Lankar D, Roman MS, et al. Actomyosin-driven force patterning controls endocytosis at the immune synapse. *Nat Commun* (2019) 10(1):2870. doi: 10.1038/s41467-019-10751-7

31. Henry SJ, Chen CS, Crocker JC, Hammer DA. Protrusive and contractile forces of spreading human neutrophils. *Biophys J* (2015) 109(4):699–7095. doi: 10.1016/j.bpj.2015.05.041

32. Blanchard AT, Salaita K. Emerging uses of DNA mechanical devices. *Science* (2019) 365(6458):1080–81. doi: 10.1126/science.aax3343

33. Hong J, Ge C, Jothikumar P, Yuan Z, Liu B, Bai Ke, et al. A TCR mechanotransduction signaling loop induces negative selection in the thymus. *Nat Immunol* (2018) 19(12):1379–90. doi: 10.1038/s41590-018-0259-z

34. Spillane KM, Tolar P. DNA-based probes for measuring mechanical forces in cell-cell contacts: Application to b cell antigen extraction from immune synapses. *Methods Mol Biol* (2018) 1707:69–80. doi: 10.1007/978-1-4939-7474-0_5

35. Vorselen D, Wang Y, de Jesus MM, Shah PK, Footer MJ, Huse M, et al. Microparticle traction force microscopy reveals subcellular force exertion patterns in immune cell–target interactions. *Nat Commun* (2020) 11(1). doi: 10.1038/s41467-019-13804-z

36. Vorselen D, Barger SR, Wang Y, Cai W, Theriot JA, Gauthier NC, et al. Phagocytic "Teeth" and myosin-II "Jaw" power target constriction during phagocytosis. *ELife* (2021) 10:e68627. doi: 10.7554/eLife.68627

37. Dembo M, Wang YL. Stresses at the cell-to-Substrate interface during locomotion of fibroblasts. *Biophys J* (1999) 76(4):2307–16. doi: 10.1016/S0006-3495(99)77386-8

38. Harris AK, Wild P, Stopak D. Silicone rubber substrata: A new wrinkle in the study of cell locomotion. *Sci (New York N.Y.)* (1980) 208(4440):177–79. doi: 10.1126/science.6987736

39. Style RW, Boltyanskiy R, German GK, Hyland C, MacMinn CW, Mertz AF, et al. Traction force microscopy in physics and biology. *Soft Matter* (2014) 10 (23):4047–555. doi: 10.1039/C4SM00264D

40. Ferrari A. Recent technological advancements in traction force microscopy. *Biophys Rev* (2019) 11(5):679–81. doi: 10.1007/s12551-019-00589-0

41. Tan JL, Tien J, Pirone DM, Gray DS, Bhadriraju K, Chen CS. Cells lying on a bed of microneedles: An approach to isolate mechanical force. *Proc Natl Acad Sci* (2003) 100(4):1484–89. doi: 10.1073/pnas.0235407100

42. Hur SS, Jeong JiH, Ban MJ, Park JH, Yoon JK, Hwang Y. Traction force microscopy for understanding cellular mechanotransduction. *BMB Rep* (2020) 53 (2):74–815. doi: 10.5483/BMBRep.2020.53.2.308

43. Schoen I, Hu W, Klotzsch E, Vogel V. Probing cellular traction forces by micropillar arrays: Contribution of substrate warping to pillar deflection. *Nano Lett* (2010) 10(5):1823–305. doi: 10.1021/nl100533c

44. Schwarz US, Soiné JérômeRD. Traction force microscopy on soft elastic substrates: A guide to recent computational advances. *Biochim Biophys Acta - Mol Cell Res* (2015) 1853(11):3095–104. doi: 10.1016/j.bbamcr.2015.05.028

45. Polio SR, Rothenberg KE, Stamenović D, Smith ML. A micropatterning and image processing approach to simplify measurement of cellular traction forces. *Acta Biomaterialia* (2012) 8(1):82–885. doi: 10.1016/j.actbio.2011.08.013

46. Canović EP, Seidl DT, Polio SR, Oberai AA, Barbone PE, Stamenović D, et al. Biomechanical imaging of cell stiffness and prestress with subcellular resolution. *Biomechanics Modeling Mechanobiol* (2014) 13(3):665–785. doi: 10.1007/s10237-013-0526-8

47. Balaban NQ, Schwarz US, Riveline D, Goichberg P, Tzur G, Sabanay I, et al. Force and focal adhesion assembly: A close relationship studied using elastic micropatterned substrates. *Nat Cell Biol* (2001) 3(5):466–72. doi: 10.1038/35074532

48. Merkel R, Kirchgeßner N, Cesa CM, Hoffmann B. Cell force microscopy on elastic layers of finite thickness. *Biophys J* (2007) 93(9):3314–235. doi: 10.1529/biophysj.107.111328

49. Bergert M, Lendenmann T, Zündel M, Ehret AE, Panozzo D, Richner P, et al. Confocal reference free traction force microscopy. *Nat Commun* (2016) 7 (1):12814. doi: 10.1038/ncomms12814

50. Vogel V, Sheetz M. Local force and geometry sensing regulate cell functions. *Nat Rev Mol Cell Biol* (2006) 7(4):265–755. doi: 10.1038/nrm1890

51. Delanoë-Ayari H, Rieu JP, Sano M. 4D traction force microscopy reveals asymmetric cortical forces in migrating *Dictyostelium* cells. *Phys Rev Lett* (2010) 105(24):248103. doi: 10.1103/PhysRevLett.105.248103

52. Bastounis E, Meili R, Álvarez-González Begoña, Francois J, del Álamo JC, Firtel RA, et al. Both contractile axial and lateral traction force dynamics drive amoeboid cell motility. *J Cell Biol* (2014) 204(6):1045–615. doi: 10.1083/jcb.201307106

53. Burnette DT, Shao L, Ott C, Pasapera AM, Fischer RS, Baird MA, et al. A contractile and counterbalancing adhesion system controls the 3D shape of crawling cells. *J Cell Biol* (2014) 205(1):83–96. doi: 10.1083/jcb.201311104

54. Hazlett L, Landauer AK, Patel M, Witt HA, Yang J, Reichner JS, et al. Epifluorescence-based three-dimensional traction force microscopy. *Sci Rep* (2020) 10(1):165995. doi: 10.1038/s41598-020-72931-6

55. Aramesh M, Mergenthal S, Issler M, Plochberger B, Weber F, Qin X-H, et al. Functionalized bead assay to measure three-dimensional traction forces during T-cell activation. *Nano Lett* (2021) 21(1):507–14. doi: 10.1021/acs.nanolett.0c03964

56. Li Di, Colin-York H, Barbieri L, Javanmardi Y, Guo Y, Korobchevskaya K, et al. Astigmatic traction force microscopy (ATFM). *Nat Commun* (2021) 12 (1):21685. doi: 10.1038/s41467-021-22376-w

57. Song D, Dong Li, Gupta M, Li L, Klaas O, Loghin A, et al. Recovery of tractions exerted by single cells in three-dimensional nonlinear matrices. *J Biomechanical Eng* (2020) 142(8):0810125. doi: 10.1115/1.4046974

58. Legant WR, Choi CK, Miller JS, Shao L, Gao L, Betzig E, et al. Multidimensional traction force microscopy reveals out-of-Plane rotational moments about focal adhesions. *Proc Natl Acad Sci USA* (2013) 110(3):881–65. doi: 10.1073/pnas.1207997110

59. Kumari S, Mak M, Poh Y-C, Tohme M, Watson N, Melo M, et al. Cytoskeletal tension actively sustains the migratory T-cell synaptic contact. *EMBO J* (2020) 39(5):e102783. doi: 10.15252/embj.2019102783

60. Basu R, Whitlock BM, Husson J, Lieberman J, Kam LC, Huse M, et al. Cytotoxic T cells use mechanical force to potentiate target cell killing cytotoxic T cells use mechanical force to potentiate target cell killing. *Cell* (2016) 165(1):100–10. doi: 10.1016/j.cell.2016.01.021

61. Martiel J-L, Leal A, Kurzawa L, Balland M, Wang I, Vignaud Timothée, et al. Measurement of cell traction forces with ImageJ. *Methods Cell Biol* (2015) 125:269–87. doi: 10.1016/bs.mcb.2014.10.008

62. Tse JR, Engler AJ. Preparation of hydrogel substrates with tunable mechanical properties. *Curr Protoc Cell Biol* (2010) 47(1):105.16.1–10.16.16. doi: 10.1002/0471143030.cb1016s47

63. Wahl A, Dinet Céline, Dillard P, Nassereddine A, Puech P-H, Limozin L, et al. Biphasic mechanosensitivity of T cell receptor-mediated spreading of lymphocytes. *Proc Natl Acad Sci* (2019) 116(13):5908–135. doi: 10.1073/pnas.1811516116

64. Bufi N, Saitakis M, Dogniaux Stéphanie, Buschinger O, Bohineust A, Richert A, et al. Human primary immune cells exhibit distinct mechanical properties that are modified by inflammation. *Biophys J* (2015) 108(9):2181–905. doi: 10.1016/j.bpj.2015.03.047

65. Wen JH, Vincent LG, Fuhrmann A, Choi YuS, Hribar KC, Taylor-Weiner H, et al. Interplay of matrix stiffness and protein tethering in stem cell differentiation. *Nat Mater* (2014) 13(10):979–875. doi: 10.1038/nmat4051

66. Kumari A, Pineau J, Lennon-Duménil A-M, Balland M, Pierobon P. Traction force microscopy to study b lymphocyte activation. *JoVE (Journal Visualized Experiments)* (2020) 161:e60947. doi: 10.3791/60947

67. Charrier EE, Asnacios A, Milloud R, Mets RDe, Balland M, Delort F, et al. Desmin mutation in the c-terminal domain impairs traction force generation in myoblasts. *Biophys J* (2016) 110(2):470–805. doi: 10.1016/j.bpj.2015.11.3518

68. Sergé A, Bertaux N, Rigneault Hervé, Marguet D. Dynamic multiple-target tracing to probe spatiotemporal cartography of cell membranes. *Nat Methods* (2008) 5(8):687–945. doi: 10.1038/nmeth.1233

69. Sabass B, Gardel ML, Waterman CM, Schwarz US. High resolution traction force microscopy based on experimental and computational advances. *Biophys J* (2008) 94(1):207–5. doi: 10.1529/biophysj.107.113670

70. Fu S, Biwolé P-H, Mathis C. A comparative study of particle image velocimetry (PIV) and particle tracking velocimetry (PTV) for airflow measurement. *ICFDT 2015 : 17th International Conference on Fluid Dynamics and Thermodynamics* (2015) 9(1):6.

71. Kraning-Rush CM, Carey SP, Califano JP, Reinhart-King CA. Quantifying traction stresses in adherent cells. *Methods Cell Biol* (2012) 110:139–78. doi: 10.1016/B978-0-12-388403-9.00006-0

72. Blumberg JW, Schwarz US. Comparison of direct and inverse methods for 2.5D traction force microscopy. *PloS One* (2022) 17(1):e02627735. doi: 10.1371/journal.pone.0262773

73. Mulligan JA, Bordeleau François, Reinhart-King CA, . Adie SG. Traction force microscopy for noninvasive imaging of cell forces. *Adv Exp Med Biol* (2018) 1092:319–49. doi: 10.1007/978-3-319-95294-9_15

74. Plotnikov SV, Sabass B, Schwarz US, Waterman CM. High-resolution traction force microscopy. *Methods Cell Biol* (2014) 123:367–94. doi: 10.1016/B978-0-12-420138-5.00020-3

75. Colin-York H, Eggeling C, Fritzsche M. Dissection of mechanical force in living cells by super-resolved traction force microscopy. *Nat Protoc* (2017) 12 (4):783–965. doi: 10.1038/nprot.2017.009

76. Colin-York H, Javanmardi Y, Skamrahl M, Kumari S, Chang VT, Khuon S, et al. Cytoskeletal control of antigen-dependent T cell activation. *Cell Rep* (2019) 26 (12):3369–3379.e5. doi: 10.1016/j.celrep.2019.02.074

77. Colin-York H, Javanmardi Y, Barbieri L, Li Di, Korobchevskaya K, Guo Y, et al. Spatiotemporally super-resolved volumetric traction force microscopy. *Nano Lett* (2019) 19(7):4427–34. doi: 10.1021/acs.nanolett.9b01196

78. Barbieri L, Colin-York H, Korobchevskaya K, Li Di, Wolfson DL , Karedla N, et al. Two-dimensional TIRF-SIM–traction force microscopy (2D TIRF-SIM-TFM). *Nat Commun* (2021) 12(1):2169. doi: 10.1038/s41467-021-22377-9

79. Tabdanov E, Gondarenko S, Kumari S, Liapis A, Dustin ML, Sheetz MP, et al. Micropatterning of TCR and LFA-1 ligands reveals complementary effects on cytoskeleton mechanics in T cells. *Integr Biol (United Kingdom)* (2015) 7(10):1272–845. doi: 10.1039/c5ib00032g

80. Hui KL, Upadhyaya A. Dynamic microtubules regulate cellular contractility during T-cell activation. *Proc Natl Acad Sci* (2017) 114(21):E4175–835. doi: 10.1073/pnas.1614291114

81. Savinko T, Guenther C, Uotila LM, Asens ML, Yao S, Tojkander S, et al. Filamin a is required for optimal T cell integrin-mediated force transmission, flow adhesion, and T cell trafficking. *J Immunol (Baltimore Md.: 1950)* (2018) 200 (9):3109–165. doi: 10.4049/jimmunol.1700913

82. Tamzalit F, Wang MS, Jin W, Tello-Lafoz M, Boyko V, Heddleston JM, et al. Interfacial actin protrusions mechanically enhance killing by cytotoxic T cells. *Sci Immunol* (2019) 4(33):eaav5445. doi: 10.1126/sciimmunol.aav5445

83. Aramesh M, Stoycheva D, Sandu I, Ihle SJ, Zünd T, Shiu J-Y, et al. Nanoconfinement of microvilli alters gene expression and boosts T cell activation. *Proc Natl Acad Sci* (2021) 118(40):e2107535118. doi: 10.1073/pnas.2107535118

84. Bendell AC, Williamson EK, Chen CS, Burkhardt JK, Hammer DA. The Arp2/3 complex binding protein HS1 is required for efficient dendritic cell random migration and force generation. *Integr Biol* (2017) 9(8):695–7085. doi: 10.1039/c7ib00070g

85. Jurchenko C, Salaita KS. Lighting up the force: Investigating mechanisms of mechanotransduction using fluorescent tension probes. *Mol Cell Biol* (2015) 35 (15):2570–825. doi: 10.1128/MCB.00195-15

86. Liu Y, Galior K, Ma VP-Y, Salaita K. Molecular tension probes for imaging forces at the cell surface. *Accounts Chem Res* (2017) 50(12):2915–245. doi: 10.1021/acs.accounts.7b00305

87. Liu Z, Liu Y, Chang Y, Seyf HR, Henry A, Mattheyses AL, et al. Nanoscale optomechanical actuators for controlling mechanotransduction in living cells. *Nat Methods* (2016) 13(2):143–465. doi: 10.1038/nmeth.3689

88. Schmid J, Birbach A. Fluorescent proteins and fluorescence resonance energy transfer (FRET) as tools in signaling research. *Thromb Haemostasis* (2007) 97(03):378–845. doi: 10.1160/TH06-08-0472

89. Grashoff C, Hoffman BD, Brenner MD, Zhou R, Parsons M, Yang MT, et al. Measuring mechanical tension across vinculin reveals regulation of focal adhesion dynamics. *Nature* (2010) 466(7303):263–66. doi: 10.1038/nature09198

90. Nordenfelt P, Elliott HL, Springer TA. Coordinated integrin activation by actin-dependent force during T-cell migration. *Nat Commun* (2016) 7(1):13119. doi: 10.1038/ncomms13119

91. Zhong BL, Vachharajani VT, Dunn AR. STReTCh: A strategy for facile detection of mechanical forces across proteins in cells. *Preprint Bioengineering* (2022). doi: 10.1101/2021.12.31.474658

92. Gayrard Charlène, Borghi N. FRET-based molecular tension microscopy. *Methods* (2016) 94:33–42. doi: 10.1016/j.ymeth.2015.07.010

93. Kong HJ, Polte TR, Alsberg E, Mooney DJ. FRET measurements of cell-traction forces and nano-scale clustering of adhesion ligands varied by substrate stiffness. *PNAS* (2005) 102(12):4300-5. doi: 10.1073/pnas.0405873102

94. Cadra S, Gucciardi A, Valignat M-P, Theodoly O, Vacaflores A, Houtman JCD, et al. ROZA-XL, an improved FRET based biosensor with an increased dynamic range for visualizing zeta associated protein 70 KD (ZAP-70) tyrosine kinase activity in live T cells. *Biochem Biophys Res Commun* (2015) 459(3):405–105. doi: 10.1016/j.bbrc.2015.02.117

95. Sadoun Anaïs, Biarnes-Pelicot M, Ghesquiere-Dierickx L, Wu A, Théodoly O, Limozin L, et al. Controlling T cells spreading, mechanics and activation by micropatterning. *Sci Rep* (2021) 11(1):67835. doi: 10.1038/s41598-021-86133-1

96. Mank M, Griesbeck O. Genetically encoded calcium indicators. *Chem Rev* (2008) 108(5):1550–645. doi: 10.1021/cr078213v

frontiers | Frontiers in Immunology

TYPE Review
PUBLISHED 02 August 2022
DOI 10.3389/fimmu.2022.938004

OPEN ACCESS

EDITED BY
Jerome Delon,
INSERM U1016 Institut Cochin, France

REVIEWED BY
Susana Minguet,
University of Freiburg, Germany
Askar M. Akimzhanov,
University of Texas Health Science Center at Houston, United States
Jeremie Rossy,
Biotechnology Institute Thurgau, Switzerland

*CORRESPONDENCE
Barbara Molon
barbara.molon@unipd.it

SPECIALTY SECTION
This article was submitted to T Cell Biology, a section of the journal Frontiers in Immunology

RECEIVED 06 May 2022
ACCEPTED 08 July 2022
PUBLISHED 02 August 2022

CITATION
Molon B, Liboni C and Viola A (2022) CD28 and chemokine receptors: Signalling amplifiers at the immunological synapse. *Front. Immunol.* 13:938004. doi: 10.3389/fimmu.2022.938004

CD28 and chemokine receptors: Signalling amplifiers at the immunological synapse

Barbara Molon[1,2]*, Cristina Liboni[1,2] and Antonella Viola[1,2]

[1]Pediatric Research Institute "Città della Speranza", Corso Stati Uniti, Padova, Italy, [2]Department of Biomedical Sciences, University of Padova, Padova, Italy

T cells are master regulators of the immune response tuning, among others, B cells, macrophages and NK cells. To exert their functions requiring high sensibility and specificity, T cells need to integrate different stimuli from the surrounding microenvironment. A finely tuned signalling compartmentalization orchestrated in dynamic platforms is an essential requirement for the proper and efficient response of these cells to distinct triggers. During years, several studies have depicted the pivotal role of the cytoskeleton and lipid microdomains in controlling signalling compartmentalization during T cell activation and functions. Here, we discuss mechanisms responsible for signalling amplification and compartmentalization in T cell activation, focusing on the role of CD28, chemokine receptors and the actin cytoskeleton. We also take into account the detrimental effect of mutations carried by distinct signalling proteins giving rise to syndromes characterized by defects in T cell functionality.

KEYWORDS

immune synapse, Chemokine receptors, CD28, costimulation, lipid raft

Signalling compartmentalization: surrounding molecules to integrate and amplify signals

Cells must be able to sense, decode and integrate a plethora of environmental stimuli. For many years, an outstanding question for cell biologists was how different signalling cascades, exploiting common intracellular effectors, could trigger distinct cellular responses. It is now clear that to allow the proper progress of specific cellular responses, signalling effectors must be locally confined in space and time, a concept referred as signalling compartmentalization. The tight control of the location, duration and frequency of signalling molecules indeed contributed to the relevant functional specificity that enables receptors to encode distinct cellular responses.

Protein compartmentalization is integral to achieving effective and controlled T cell responses, which are drivers of the adaptive branch of the immune system (1, 2). Over the

last years, multiple studies have shed light on both the mechanisms by which signals are compartmentalized in T cells and the physiological role played by such compartmentalization (3). Both lymphocyte migration and activation indeed rely on the selective and transient segregation of signalling molecules and membrane receptors that localized in specific cell locations with different kinetics.

The dynamic molecular compartmentation of signalling players in T cells is ensured by the interplay between the plasma membrane (PM), cytoskeleton networks, and intracellular organelles.

Collectively, such events lead to the establishment of a morphological and molecular asymmetry know as lymphocyte polarization which is crucial for T cell migration and activation.

In resting conditions, T lymphocytes present a spherical shape retained by the cytoskeleton tension and, in particular, by the intermediate filaments and the cortical actin (4, 5). T lymphocyte surface is "decorated" with microvilli sustained by parallel bundles of highly dynamic actin filaments (6, 7) (Figure 1). These structures allow T cells to sense the surrounding microenvironment and, importantly, they promote signalling compartmentalization at their tips, leading to the coalescence of proteins and receptors involved in T cell adhesion and activation, as integrin $\alpha_4\beta_7$-Very Late Antigen 4 (VLA-4), L-selectin, chemokines receptors as CXCR4 (8, 9) and T cell receptor (TCR) complexes (6, 10–14). At the tip of microvilli, proteins are found in close proximity thus prompting an easier and more efficient "scanning" of the APC surface in search of the peptide-major histocompatibility complex (pMHC) and, at the same time, increasing the avidity for subsequent interaction of the two cells. Indeed, following T cells adhesion and activation, microvilli are resorbed and integrin avidity is upregulated in a process mediated by ERMs proteins (ezrin, radixin and moesin), acting as a bridge between the PM and the actin cytoskeleton (15–17). Notably, it has been recently proposed that membrane curvature could also promote signalling compartmentalization within microvilli tip (18). This topic has been extensively discussed elsewhere (19).

In this landscape, a particular focus should be made on the actin cytoskeleton bearing a ubiquitous but fundamental role in multiple cellular processes. As for T cells, the actin cytoskeleton has a key importance in their activation, mainly during the formation and maintenance of a specialized junction named the Immunological Synapse (IS). In accordance to this, recently, it has become clear that mechanical and biochemical signals at the IS are integrated by actin dynamics (20).

Besides cytoskeleton, signalling compartmentalization in T cells is orchestrated also by "small (10–200 nm), heterogeneous, highly dynamic, sterol- and sphingolipid-enriched domains that compartmentalize cellular processes" (21, 22), defined as lipid rafts. Even if, due to technical issues, their description and existence has been debated for years, it has been clear from the beginning that their main feature is the ability to promote signalling *via* proteins juxtaposition (controlling the inclusion/exclusion of proteins) thus generating "signalling hubs". Giving their limited size, lipid rafts can welcome only a limited number of proteins which probably stand among 10-30 proteins (22, 23). The partitioning of molecules within their structure can be regulated by multiple factors including the intrinsic molecule state, the signalling state of the cell and post-translational modifications (PTMs). Interestingly, lipid rafts are not stand alone structure by they are connected to the cytoskeleton *via* actin-binding proteins as ezrin and filamin acquiring then the definition of "floating island" or "flying kites" (21, 24).

The advancements in imaging techniques, with the introduction of single molecule and scanning confocal imaging, have overcome this primordial separation of these compartments. For instance, the "Picket and Fence Model" postulated by Kusumi and colleagues defined confinements area within the membrane (between 30 and 700nm) where transmembrane proteins are anchored and lined up along a fence of cytoskeletal proteins (25). This model arises from the evidence that transmembrane proteins can also move within confined areas and they have to "hop" when changing it. This concept was expanded by the definition of the "proteins island model" in the PM. Protein islands (both rafts and non-rafts islands) are actin-rich areas where membrane-associated proteins are clustered (26, 27) surrounded by a "sea" on protein-free regions. It has been observed that, in activated membranes, rafts and non-rafts regions presented more frequent contacts, a feature that probably shapes and influences their functionality and morphology (26). Interestingly, actin cytoskeleton is mandatory for their establishment, while cholesterol depletion does not impair proteins distribution between rafts and non-rafts regions, implying a superior organization order (26). Even if reports in this direction are still missing, it could not be excluded that protein islands may also have a role in cell-cell communication, membrane trafficking and membrane fusion.

Compelling evidence also indicates that the endocytic compartment works as a signalling hub within the cell (Figure 1). As elegantly revised by Scita and Di Fiore (18), endosomes sustain the signal originated by the PM and, at the same time, allow the generation of unique signals. This is possible thanks to their small volume which favors the coincidence of detectors, the specific enrichment of some lipids, the rapid microtubule-mediated transport of molecules; moreover, the endosome acidic pH might trigger and regulate specific enzymatic functions. Even if additional studies are required to model and experimentally validate endosome dynamics, it is clear how endocytosis provides a controlled spatial and temporal dimension for distinct signaling pathways.

Overall, the spatial ordering of molecular players in distinct cellular compartment enables the complexity of multiple signaling events, a feature which is mandatory for a proficient T cell migration and activation (28).

10.3389/fimmu.2022.938004

Signalling compartmentalization in T cells

Even if in resting conditions T cells present a round-shaped morphology, they acquire functional polarity upon stimulation by a variety of ligands. This is particularly evident during T cell migration and priming, when the definition of a cellular polarity allows the maintenance of active and distinct signalling compartments. In the past, our laboratory has analyzed the mechanisms responsible for signaling amplification and compartmentalization during these two processes, focusing on the role of CD28 and chemokine receptors governed by the actin cytoskeleton. In this manuscript, we will focus on the contribution of the aforementioned players in T cell migration and activation.

CD28 at the crossroad of cytoskeleton and lipid rafts

T cell priming starts in lymph nodes (LNs) with the formation of a stable interaction between naive T cells and antigen presenting dendritic cells (DCs). This represents a very sensitive process ultimately leading to multiple cellular responses, including T cell proliferation and the secretion of a wide range of cytokines, chemokines and cytotoxic mediators. By the use of two-photon microscopy, seminal studies unveiled the kinetics of this event *in vivo* by proposing the 3-stage paradigm: upon antigen encounter, T cells engaged first transient serial interactions (phase 1) and next stable contacts (phase 2) with antigen-loaded DCs; finally they increased their motility, detached and proliferate (phase 3) (29). In particular, the interactions between T cells and APCs are transient between 2 and 8h following the first encounters, stable between 8 and 24h, and again transient by 24–36h (30, 31).

The stability of T cell-DC interaction is determined by multiple interconnected signals, from TCRs as well as stimulatory and inhibitory receptors that are integrated in a specialized membrane junction named the "immunological synapse"-IS (32, 33) (Figure 1). In T lymphocytes, signalling events occurring at this platform cause multiple downstream effects ranging from the dynamic rearrangement of the actin cytoskeleton, and the initiation of a gene expression cascade ultimately leading to the generation of effector and memory T cells (34–36). At the IS, the duration of distinct molecular signals including the amplitude and kinetics of intracellular Ca^{2+} waves ranges between few minutes to hours (37).

The formation of the IS is initiated with the extension of filopodia and lamellipodia from the T cell toward the APC. The interaction of the two cells leads to the establishment of a F-actin rich interface. Then, TCR and co-stimulatory molecules, including CD28, trigger the reorganization of the cytoskeleton with the recruitment of the actin polymerization machinery and its regulatory proteins at the IS where, in a positive-feedback loop, they promote the maintenance of the TCR signalling (38, 39). Actin segregates into radial asymmetric zones defined as the supramolecular activation clusters (SMACs) (34, 40–42). We can distinguish the cSMAC (central SMAC), comprising the TCR and co-stimulation molecules; an outer ring named as pSMAC (peripheral SMAC) containing the LFA-1 (41, 43) and a distal SMAC (dSMAC) including the CD43 and CD45 (44, 45).

Mechanistically, several protein tyrosine kinases (PTKs), including Src family PTKs such as Lck and Fyn and the Syk family PTK zeta chain of TCR-associated protein 70 (ZAP-70) are brought into proximity of the CD3 complex upon TCR engagement (46). There, Lck or Fyn causes the phosphorylation of the immunoreceptor tyrosine-based activation motifs (ITAM) in the CD3 subunits. Tyrosine phosphorylation of CD3 provides the binding site for ZAP-70 *via* its SH2 domain, and then Lck or Fyn activates ZAP-70 by phosphorylation (47, 48). ZAP-70 activation in turn favored the phosphorylation of downstream adaptors, including the linker for activation of T cells (LAT) and SH2 domain-containing leukocyte phosphoprotein of 76 kDa (SLP-76) acting as scaffolds to recruit additional signalling molecules. As a consequence, multiple signalling pathways are activated at the IS eventually leading to T-cell activation, proliferation, and differentiation (49).

Importantly, in naïve T cells, the outcome of TCR stimulation is regulated by costimulatory signals. Among them, the CD28-mediated signalling strongly influences T cell priming. At the IS, CD28 signals lower T cell activation threshold by enabling an effective priming by few antigenic complexes (40, 50, 51). When CD28 is recruited at the IS, it promotes the recruitment of multiple downstream interactors at its cytoplasmic tail. Among them, the phosphoinositide 3-kinase (PI3K) (52), Lck (53, 54), growth factor receptor-bound protein 2 (Grb2) (55), Grb2-related adaptor protein (Gads) (56), IL2-inducible T cell kinase (Itk), the guaninenucleotide exchange factor Vav (57), Akt (58), protein phosphatase 2A (PP2A) (59, 60), and protein kinase C theta (PKCθ) (57). With respect to PKCθ, it has been reported that CD28-mediated signals are required for the specific localization of this kinase to the center region of the IS through its V3 motif (61).

As well, CD28 attends the selective sorting of molecular interactors in lipid membrane domains, acting as privileged sites in which signals are protected and amplified. Indeed, we showed that the CD28 co-stimulation of the TCR signaling cascade is based on lipid rafts (62). Next, we found that the kinase Lck is recruited into CD28-signaling rafts and directed to the IS upon CD28 engagement by a process requiring the CD28 COOH-terminal PxxPP motif and Vav-1, key regulator of the actin cytoskeleton rearrangements (63). Of note, IS lipid microdomains are also enriched in TCR signalling proteins, including the Src-family kinase Fyn, the adapter protein LAT, phosphoprotein associated with glycosphingolipid-enriched

domains (PAG) or Csk-activating protein (Cbp) and Lck-interacting molecule (LIME) (33, 64). Interestingly, the partitioning of Lck and LAT at the IS lipid microdomains is dictated by the post-translational modifications (PTM, including protein S-acylation) (65–67). In this regard, a recent report showed that S-acylation of the plasma membrane channel ORAI1 is crucial for the selective trapping of this channel in cholesterol-rich lipid microdomains at the IS where it controls the local Ca^{2+} fluxes leading to T cell activation (68).

Furthermore, according to the protein islands theory, LAT clusters appear to aggregate with CD3/CD28 complexes in the activating surface of T cells (26). LAT acts a central mediator for T cell activation dictating, once phosphorylated, the co-clustering of CD2 and Lck in membrane discrete microdomains *via* protein-protein interactions in a process initiated by F-actin and actin-associated proteins. Beside this, LAT also regulate calcium dynamics at the IS and Ras signalling (28). As mentioned before, CD28 acts as a master regulator of actin cytoskeleton rearrangements during T cell activation by tuning the actin polymerization machinery. This process is under the control of several interactors: upon TCR-engagement, the kynase ZAP-70 phosphorylates the adaptors SLP-76 that then binds Nck and the guanine nucleotide exchange factor Vav-1. More, Nck constitutively associated with WASp (69, 70) thus acting as a bridge to recruit WASp itself to the SLP-76 signaling complex. In association with SLP-76, Vav-1 mediates the exchange of GDP- to GTP-bound Cdc42, Rho family GTPases that interacts with the conserved VCA domain of WASp allowing its binding to the Arp2/3 complex. Once bound to the VCA domain, Arp2/3 promotes the branching of the actin polymerization and rearrangement at the T cell-APC contact site (71). Arp2/3 cooperates with filamins that are actin crosslinking proteins. In this landscape of interactors, we pointed out the actin-binding protein Filamin-A (FLNa) as the molecular partner of CD28 both in the reshaping of the actin cytoskeleton and in the lipid rafts recruitment at the IS (72). In this study, we showed that the COOH-terminal PxxPP motif of CD28 is required for CD28–FLNa association, and that FLNa has a direct role in CD28 signalling by recruiting Cdc42 at the site of Vav-1 activation. Vav-1 plays a crucial role in the regulation of the CD28 costimulation. Indeed, it has been shown that the adaptor molecule Cbl-b controls the CD28 dependence of T-cell activation by selectively suppressing TCR-mediated Vav activation (73). Cytoskeletal actin dynamics are also regulated by the phosphatidylinositol bisphosphate (PIP2) produced by the activity of the PIP5K enzymes. In this regard, we and other showed that, in collaboration with PIP5Kα and Vav1, PIP5Kβ promotes actin polymerization and CD28 signaling in human T cells (74, 75). Other reports further support the relevance of the dynamic regulation of actin in CD28-mediated costimulation by linking the actin-uncapping proteins Rltpr (76) and CapZIP (77) to the CD28 costimulatory signalling.

More recently, a phenomenological agent-based model has been developed for assessing the contribution of actin-driven forces to IS formation and CD28 localization. By applying this model, authors proposed that although CD28 can reach the IS center by passively following TCR clusters, the ring-like pattern of CD28 at the synapse is determined by the coupling to the actin cytoskeleton (78).

Taken together this evidence endorses the outstanding role of CD28 as a signalling hub in T cells finely tuning cytoskeletal dynamics and lipid rafts reorganization.

Beside CD28, which positively regulates T cell activation, other inhibitory molecules are present on the T cell surface. Among these, the most characterized are CTLA4 and PD1, whose importance rapidly increased in recent years as targets for immune-mediated therapies. These are recruited within the cSMAC together with their downstream mediators and here they compete with CD28 ligands (B7-1/CD80 and B7-2/CD86) for binding, thus promoting the establishment of T cell anergy (5, 34, 79). Interestingly, most of CTLA4 seems to reside within endocytic vesicles, a mechanism facilitating its signalling with a fine compartmentalization (5, 79). Similarly to CTLA4, also PD-1 presents a minimal expression in resting conditions, further increased after T cell activation (79). Thanks to the binding to PD-L1 and PD-L2, it abolishes IL-2 production in T cells and, albeit only in some settings, it also induce T cells apoptosis (79). As was recently revised, both these molecules affect T cell motility reducing its ability to "pause" when encountering the cognate APC thus raising the threshold for IS formation in the "reverse-stop signal model" (80, 81). This effect seems to be mediated by phosphatidylinositol 3-kinase, Vav-1, Cdc42, and myosin light chain MLC kinase (82) which also affect T cell motility to inflamed sites (80). In addition, in was reported that PD-1 mediates the inhibition of T cell function acting mostly on CD28 rather than on TCR (83).

Chemokine receptors

In T cells, the activation of chemokine receptor signalling contributes to the spatial and temporal repositioning ofwfi 2 intracellular and membrane-bound players, ultimately defining T cell polarity. During migration, polarity refers to the ability of cells to change their morphology in response to chemoattractants, and to maintain a stable asymmetric shape with two poles: the leading edge, which protrudes at the cell front, and the rear edge (termed uropod in leukocytes), at the back (84). This process, which is initiated by chemokine receptor signalling and adhesive interactions with the extracellular matrix (ECM), increases the sensitivity toward chemokine gradients, by the selective recruitment of chemokine receptors at the T cell front (85) (Figure 1). Compartmentalization of the PM into distinct lipid microdomains is pivotal in establishing and maintaining leukocyte polarity and perturbation of lipid

10.3389/fimmu.2022.938004

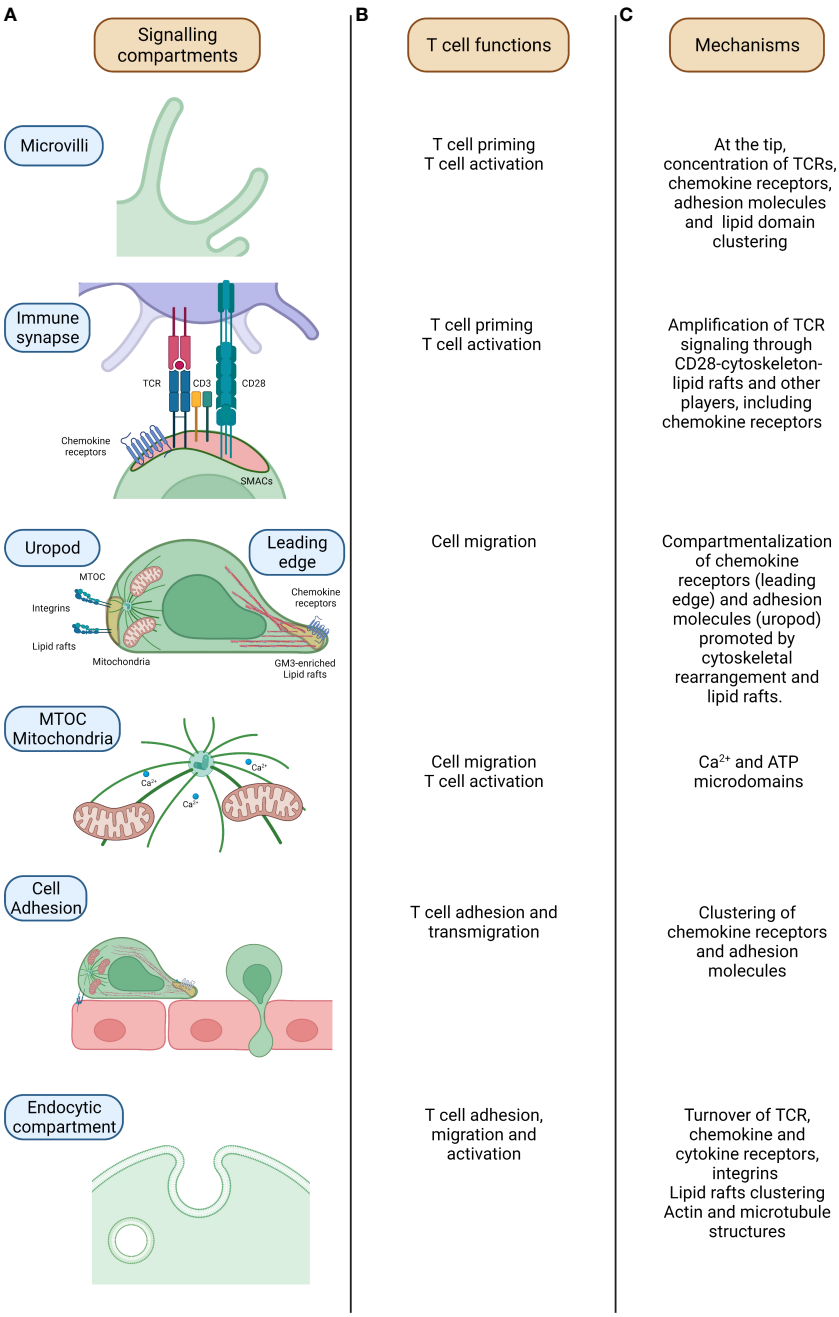

FIGURE 1
Mechanisms of signalling compartmentalization in T cells. From the left, relevant compartments which regulate signalling compartmentalization in T cells **(A)**, related T cell activities **(B)** and mechanisms underpinning signalling compartmentalization at these sites are outlined **(C)**. In microvilli, parallel actin filaments allow the sustainment of the structure which assure the concentration of proteins and molecules and signalling compartmentalization in naïve T cells. In the immune synapse (IS), where the formation of the couple between the T cell and the APC is assured by the specific recognition of the Ag recognized on the MHCII molecules by the TCR, the binding of the two cells is further sustained by the CD3 and co-stimulatory molecules (CD28/B7-1/CD80-B7-2/CD86). Here, the compartmentalization of the signalling is mediated by the concerted action of cytoskeletal components, lipid rafts and endocytic compartment. During T cell migration, the T cell acquires an intrinsic polarity mandatory for the definition of a leading edge and a rear pole (uropod). The differential segregation of proteins at these two poles (cytokines and chemokines receptors at the front side while mitochondria and integrins of the rear one) assures the functional motility of the T cell. Mitochondria relocation within the T cell is mediated by microtubules in a Ca^{2+} dependent fashion. This process is orchestrated by the MTOC (microtubules organizing center) which controls microtubules polymerization and then mitochondria localization in a Ca^{2+} -dependent fashion. The definition of T cell polarity is mandatory for a proficient T cell migration with, on one side, chemokine receptors guiding the movement at the leading edge while, on the other side, adhesion molecules controlling T cell adhesion hence providing an antithetic force. Lastly, the endocytic compartment, apart from the recycling of molecules, promotes the fine compartmentalization and the amplification of the signal with the juxtapositioning of molecules and proteins. TCR-T cell receptor; MTOC-MicroTubule Organizing Center; ATP-Adenosine TriPhosphate.

microdomains inhibits both cell polarization and migration (85, 86).

The spatial organization of chemokine receptors into dimers and higher-ordered oligomers further adds to the complexity of possible GPCR arrangements, and consequently modulation of signaling (87). Recent studies shed light on how cholesterol dictates the spatial organization of GPCRs within the PM. in particular, it has been proposed that cholesterol promotes the oligomerization of chemokine receptors at the PM that ultimately enabling the integration of distinct signaling pathways at the receptor-membrane interface (88). Previously, it has been shown that the CXCR4 and CCR5 receptors associate to GM3-enriched lipid rafts and are consequently redistributed to the leading edge of moving cells. Interestingly, both CXCR4 and CCR5 directly interact with FLNa, that actively modulates their signalling pathways. Indeed, the specific blockade of CXCR4–FLNa interaction inhibited CXCL12-induced chemotaxis in T cells. As for CXCR4, filamin-A expression did not affect CCR5-mediated Ca^{2+} flux, but regulated F-actin remodelling (89).

Chemokine receptors play a pivotal role during T cell activation, too. Long-lasting interactions between T cells and APCs are dependent on antigens (90, 91), but antigen-specific interactions are preceded by antigen-independent, chemokine-promoted adhesive contacts in the T cell-APC pair, enabling T cells to scan the surface of their cellular partners (92–94). Although the induction of cell polarity at the IS was thought to be dependent on TCR triggering, we have shown that CXCR4-induced activation of LFA-1 at the contact site with APCs starts MTOC and mitochondria relocation towards the upcoming IS (95). Importantly, we found that, by recruiting mitochondria to the IS, LFA-1 sustains and amplifies the upcoming TCR-induced Ca^{2+} signalling, indicating that establishment of T-cell polarity is pivotal to a prompt and sustained T cell activation (95) (Figure 1). Interestingly, by bringing mitochondria and ORAI channels into close proximity and by re-organizing plasma membrane calcium ATPases (PMCAs) into discrete regions co-localizing with mitochondria, the IS prevents Ca^{2+} -dependent channel inactivation and reduce local Ca^{2+}-dependent PMCA modulation (96).

The tight spatial and temporal regulation of cytosolic calcium (Ca^{2+}) is of paramount importance for multiple T cell effector functions as differentiation, proliferation, metabolism, cytokine release and cytotoxicity. The IS indeed controls Ca^{2+} microdomains by bringing mitochondria and ORAI channels into close proximity and favoring the segregation of PMCA into distinct PM domains. The proteins and organelles re-distribution allows mitochondria to rapidly take up the inflowing Ca^{2+}, thereby avoiding high Ca^{2+} microdomains close to ORAI channels, which prevents Ca^{2+}-dependent channel inactivation and reduce local Ca^{2+}-dependent PMCA modulation. This optimizes net Ca^{2+} influx at the IS (96).

The mechanisms responsible for Ca^{2+} signal compartmentalization in T cells have been extensively explored and described (97). Early recruitment of mitochondria at the T-cell IS occurs independently of TCR stimulation and through a mechanism requiring chemokine receptor signalling (95). Interestingly, we had also shown that chemokine receptor signaling induces accumulation of mitochondria at the uropode of migrating cells, where they are required to sustain phosphorylation of the MLC, a key step in high-speed moving cells (98).

In addition to shaping T cells for effective signaling, chemokine receptors directly support the IS stabilization and indeed and T cell activation. We had demonstrated that CXCR4 and CCR5 are stably recruited into the IS by APC-secreted chemokines (70). In this context, chemokine receptors contribute to the amplification of the TCR signalling acting as powerful costimulatory molecules (99). Indeed, their recruitment at the IS prolong the duration of the T cell–APC interaction and strengthen T cell–APC pair attraction ultimately avoiding premature splitting due to chemoattractant sources (99).

Of note, TCR engagement significantly impacts on chemokine receptor signaling properties by favoring the selective triggering of distinct downstream players (79). Canonically, chemokine signaling, initiated following ligand binding, causes the dissociation of the Gai and Gbg subunits of the heterotrimeric G proteins, leading to calcium flux, PI3K triggering and the activation of the small Rho GTPases signaling. However, alternative signalling pathways resulting from the coupling with other G proteins have also been reported for these receptors (100). Importantly, we showed that at the IS chemokines promote the preferential association of the receptor CCR5 with the Gq/11 subunit instead of Gi one (99).

The functional versatility of chemokine receptors in the context of T cell activation may depend on their ability to heterodimerize with other GPCRs. For example, we showed that CXCR4/CCR5-mediated costimulation grounded on their ability to form heterodimers at the IS (101).

In addition, inhibitory molecules (as CTLA4) have been demonstrated to alter the motility both *via* the up-regulation of chemokine receptors (CCR5 and CCR7) and by the increase in the sensitivity to their respective chemokines (CCL4 (MIP-1β), CXCL12 (SDF1α) and CCL19). This evidence leads to the proposal of a model for chemotaxis integrating CD28 and CTLA-4 signals *via* the G protein-coupled receptor kinase GRK. CD28 triggers CCR5 phosphorylation *via* GRK, while CTLA-4 engagement inactivates GRK2 counteracting this mechanism (80).

More recently, an additional mechanism elucidating CXCL12-induced T cell co-stimulation has been proposed. Smith and colleagues showed that the chemokine enhances the number, stability, and phosphorylation of SLP-76 microclusters formed in response to stimulation of the TCR. This results in proximity of SLP-76 and ZAP-70 clusters and in enhanced TCR-dependent gene expression (102).

Multiple studies worked to clarify whether other chemokines preferentially act as co-stimulatory partners for the TCR ultimately promoting T-cell activation. Recently, it has been proposed that CCR7, which drives T cell and DC migration and trafficking in LNs, colocalizes with the TCR at the IS, within subsynaptic vesicles. There, CCR7 promotes and prolongs ZAP70 activity, resulting in T cell costimulation (103).

All these data, together with many more that we could not include in our discussion, suggest that T cell priming results from a timely and spatially regulated interplay between adhesive and chemoattractant forces mainly occurring in LNs, enabling T cell scanning for the cognate antigen and the formation of long-lasting interaction upon recognition (104).

Congenital defects in cytoskeletal proteins lead to impairment of T cell activation

Perturbations in the equilibrium between adhesive and chemotactic forces leads to defects in the formation of a productive IS, due to the instability of the T cell-APC mating (105). Of note, different inborn errors in genes encoding for proteins controlling these functions, lead to syndromes linked to defects in T cell motility and/or activation (106).

The Warts, Hypogammaglobulinemia, Infections, and Myelokathexis (WHIM) syndrome is a primary immunodeficiency disorder in which a genetic mutation impairs CXCR4 internalization and enhances its responsiveness to CXCL12. WHIM patients experience a wide range of symptoms, including recurring infections, human papillomavirus (HPV)-induced warts, reduced long-term immunoglobulin G (IgG) titers, myelokathexis, and leukopenia (107). The dominant mutations in the chemokine receptor CXCR4 lead to the truncation of its carboxy-terminal domain, ultimately resulting in a defective ability of the receptor to internalize after binding its ligand. As a consequence, immune cells bearing the WHIM-mutant receptor display increased signalling and enhanced migration in response to chemokine stimulation (108). We observed that, in contrast to the wild-type CXCR4, the WHIM-mutant CXCR4 failed to be recruited into the IS and impaired the formation of long-lasting T-APC interactions, thus limiting T cell priming and immune responses to antigens (109). Thus, the hyperfunctional WHIM-mutant CXCR4 favors motility over formation of stable IS, resulting in aberrant T cell activation (109).

The Wiskott-Aldrich syndrome (WAS) is a primary immunodeficiency determined by mutations in the WAS-protein (WASp), a member of a larger family of proteins (WASP family) that functions as nucleation-promoting factors for the Arp2/3 complex, which drives the generation of branched actin filaments (110). WASp is exclusively expressed in cells of the haematopoietic lineage and its loss-of-function mutations cause a syndrome characterized by a broad range of clinical signs, with patients showing an increased susceptibility to infections, haemorrhages, eczema and different autoimmune disorders (111). Upon TCR engagement, WASP is recruited to the IS where it interacts with VAV, RAC and Cdc42 and is activated by VAV effectors (6, 112, 113). WAS patients present alterations in T cell actin cytoskeleton dynamics (114, 115). $WASp^{-/-}$ T cells fail to polymerize actin in response to anti-CD3 stimulation, and show defective IS. The disorganized signaling platforms of $WASp^{-/-}$ T cells do not allow complete and efficient cellular activation and, consequently, T cells from WAS patients show decreased cell proliferation and cell survival (111). Interestingly, this is linked with a severe impairment in CD28 internalization possibly caused by the formation of the functional complex WASp/SNX9/p85/CD28 (116).

Mutations in the WASp-interacting protein (WIP) can also determine a syndrome with clinical signs similar to WAS. WIP is involved in the regulation of WASp activity by promoting its stability, activation and localization to sites of active actin polymerization. Moreover, independently from WASp, WIP regulates actin cytoskeleton in lymphocytes affecting the homing of T cells to infected tissues (117).

Additional immunodeficiencies caused by defects in actin-binding proteins and leading to T cell synapse instability have been described. Among them, the deficiency of the ARPC1B protein, part of the Arp2/3 complex, caused the emission of aberrant actin-rich structures, including spikes and long filopodia-like structures, both in the context of 2D IS and contact with APC (118). Thus, patients suffering of ARPC1B deficiency show defects in T cell proliferation and cytotoxic activity. Interestingly, ARPC1B also contributes to the recycling of the TCR, CD8 and GLUT1 (119), thus causing reduced expression of these molecules in ARPC1B-deficient $CD8^+$ T cells. In addition, as a result of an impaired endosome-to-membrane recycling processes caused by a deficient actin remodeling, T cells lacking the Arp2/3 activator WASH also fail to maintain surface levels of the TCR, CD28, LFA-1 and GLUT1 molecules (120).

Although relevant for T cell activity, other defects, including HEM1 and WDR1 deficiencies, might not be solely explained by defective IS and have been reviewed elsewhere (121). Further investigations are needed to mechanistically explore the role of CD28 and other costimulatory molecules in these disorders.

Future directions

Although here we focused our discussion on chemical signaling, it must be noted that mechanical signals control T cell functions and are required for cell polarization, migration and activation. In particular, membrane curvature seems to initiate signaling events resulting in the organization of larger signaling platforms (122, 123). In both neutrophils and CD8+ T cells, cell polarization was shown to be dependent on local increase of plasma membrane curvature induced by initial adhesion (122). The curved

membrane can orchestrate the formation of signaling platforms through the Bin-Amphiphysin-Rvs (BAR) superfamily. BAR proteins induce, regulate and detect membrane curvature (124) and recruit to the curved membrane other proteins, including regulators of actin dynamics.

While the N-BAR and the F-BAR proteins are generally associated with membrane invaginations, the I-BAR are present in various membrane protrusions (125) and involved in microvilli formation (126). Little is known about the role of BAR proteins in T cell functions. The I-BAR IRSp53 is expressed in T cells and essential for the release of HIV particles through a pathway involving Rac1, Wave2 and Arp2/3 (127, 128), but its role in microvilli formation and TCR signaling is unknown. On the other hand, sorting nexin 9 (SNX9), which belongs to the N-BAR subfamily but regulates filopodia formation (129), forms a signaling complex on endocytic vesicles with CD28, WASp and p85 in T cells triggered by CD3/CD28 antibodies (116). In a feed-forward fashion, SNX9 itself was recently shown, once recruited to the IS, to generate membrane tubulation out of CD28 clusters with these dynamic structures regulating both CD28 phosphorylation status and IL-2 production (130).

Further studies will be required to shed light on the role of BAR domain proteins and the membrane curvature in signaling compartmentalization and T cell functions. However, it seems conceivable that cells employ a combination of physical and biochemical forces to tune the formation of structures and domains on the plasma membrane (131). How the integration of the different forces occurred in T cells will be an interesting subject for future investigations.

In addition, accumulating evidence suggests that mechanical forces are key determinants in initiating signaling through the TCR that clearly acts as a membrane mechanoreceptor. In this regard, very recently a new model for TCR triggering has been proposed (132). Indeed, the TCR Bending Mechanosignal (TBM) model predicts that mechanical forces might cause membrane curvature around engaged pMHC/TCR complexes; such mechanical cue is necessary to reach the energy threshold required for the triggering of the signalling cascade ultimately activating T responses (132).

Of note, the investigation of whether and how mechanical signals control costimulatory molecules, as CD28 and chemokine receptors, would be an interesting advancement in this field.

Signalling compartmentalization is essential for immune cells to respond with high specificity and sensitivity. Thus, achieving a deeper understanding of the mechanisms regulating the generation of signalling compartments during T cell migration and activation will be important to modulate immune responses with future therapeutics and will be vital to design effective CAR-T cells.

Author contributions

BM, CL, AV conceived and wrote the manuscript. CL drew the figure. All authors contributed to the article and approved the submitted version.

Funding

BM and AV received research grant from Istituto di Ricerca pediatrica Fondazione Città della Speranza

Conflict of interest

The authors declare that the research was conducted in the absence of any commercial or financial relationships that could be construed as a potential conflict of interest.

Publisher's note

References

1. Jun JE, Goodnow CC. Scaffolding of antigen receptors for immunogenic versus tolerogenic signaling. *Nat Immunol* (2003) 4(11):1057–64. doi: 10.1038/ni1001.

2. Abraham RT, Weiss A. Jurkat T cells and development of the T-cell receptor signalling paradigm. *Nat Rev Immunol* (2004) 4(4):301–8. doi: 10.1038/nri1330

3. Russell S, Oliaro J. Compartmentalization in T-cell signalling: Membrane microdomains and polarity orchestrate signalling and morphology. *Immunol Cell Biol* (2006) 84(1):107–13. doi: 10.1111/j.1440-1711.2005.01415.x

4. Etienne-Manneville S. Cytoplasmic intermediate filaments in cell biology. *Annu Rev Cell Dev Biol* (2018) 34(1):1–28. doi: 10.1146/annurev-cellbio-100617-062534

5. Mastrogiovanni M, Juzans M, Alcover A, Di Bartolo V. Coordinating cytoskeleton and molecular traffic in T cell migration, activation, and effector functions. *Front Cell Dev Biol* (2020) 8:1138. doi: 10.3389/fcell.2020.591348

6. Burkhardt JK, Carrizosa E, Shaffer MH. The actin cytoskeleton in T cell activation. *Annu Rev Immunol* (2008) 26:233–59. doi: 10.1146/annurev.immunol.26.021607.090347

7. Majstoravich S, Zhang J, Nicholson-Dykstra S, Linder S, Friedrich W, Siminovitch KA, et al. Lymphocyte microvilli are dynamic, actin-dependent structures that do not require wiskott-Aldrich syndrome protein (WASp) for their morphology. *Blood* (2004) 104(5):1396–403. doi: 10.1182/blood-2004-02-0437

8. Berlin C, Bargatze RF, Campbell JJ, von Andrian UH, Szabo MC, Hasslen SR, et al. Alpha 4 integrins mediate lymphocyte attachment and rolling under physiologic flow. *Cell* (1995) 80(3):413–22. doi: 10.1016/0092-8674(95)90491-3

9. Singer II, Scott S, Kawka DW, Chin J, Daugherty BL, DeMartino JA, et al. CCR5, CXCR4, and CD4 are clustered and closely apposed on microvilli of human macrophages and T cells. *J Virol* (2001) 75(8):3779–90. doi: 10.1128/JVI.75.8.3779-3790.2001

10. Bretscher MS, Aguado-Velasco C. Membrane traffic during cell locomotion. *Curr Opin Cell Biol* (1998) 10(4):537–41. doi: 10.1016/S0955-0674(98)80070-7

11. Cai E, Marchuk K, Beemiller P, Beppler C, Rubashkin MG, Weaver VM, et al. Visualizing dynamic microvillar search and stabilization during ligand detection by T cells. *Science* (2017) 356(6338):eaal3118. doi: 10.1126/science.aal3118

12. Griffiths GM, Tsun A, Stinchcombe JC. The immunological synapse: a focal point for endocytosis and exocytosis. *J Cell Biol* (2010) 189(3):399–406. doi: 10.1083/jcb.201002027

13. Niedergang F, Di Bartolo V, Alcover A. Comparative anatomy of phagocytic and immunological synapses. *Front Immunol* (2016) 7:18. doi: 10.3389/fimmu.2016.00018

14. Stein JV, Cheng G, Stockton BM, Fors BP, Butcher EC, von Andrian UH. L-selectin-mediated leukocyte adhesion *in vivo*: microvillous distribution determines tethering efficiency, but not rolling velocity. *J Exp Med* (1999) 189(1):37–50. doi: 10.1084/jem.189.1.37

15. Alon R, Feigelson S. From rolling to arrest on blood vessels: leukocyte tap dancing on endothelial integrin ligands and chemokines at sub-second contacts. *Semin Immunol* (2002) 14(2):93–104. doi: 10.1006/smim.2001.0346

16. Brown MJ, Nijhara R, Hallam JA, Gignac M, Yamada KM, Erlandsen SL, et al. Chemokine stimulation of human peripheral blood T lymphocytes induces rapid dephosphorylation of ERM proteins, which facilitates loss of microvilli and polarization. *Blood* (2003) 102(12):3890–9. doi: 10.1182/blood-2002-12-3807

17. Nijhara R, van Hennik PB, Gignac ML, Kruhlak MJ, Hordijk PL, Delon J, et al. Rac1 mediates collapse of microvilli on chemokine-activated T lymphocytes. *J Immunol* (2004) 173(8):4985–93. doi: 10.4049/jimmunol.173.8.4985

18. Scita G, Di Fiore PP. The endocytic matrix. *Nature* (2010) 463(7280):464–73. doi: 10.1038/nature08910

19. McMahon HT, Gallop JL. Membrane curvature and mechanisms of dynamic cell membrane remodelling. *Nature* (2005) 438(7068):590–6. doi: 10.1038/nature04396

20. Roy NH, Burkhardt JK. The actin cytoskeleton: A mechanical intermediate for signal integration at the immunological synapse. *Front Cell Dev Biol* (2018) 6:116. doi: 10.3389/fcell.2018.00116

21. Mayor S, Viola A, Stan RV, del Pozo MA. Flying kites on slippery slopes at keystone. symposium on lipid rafts and cell function. *EMBO Rep* (2006) 7 (11):1089–93. doi: 10.1038/sj.embor.7400836

22. Pike LJ. Lipid rafts: bringing order to chaos. *J Lipid Res* (2003) 44(4):655–67. doi: 10.1194/jlr.R200021-JLR200

23. Subczynski WK, Kusumi A. Dynamics of raft molecules in the cell and artificial membranes: approaches by pulse EPR spin labeling and single molecule optical microscopy. *Biochim Biophys Acta* (2003) 1610(2):231–43. doi: 10.1016/S0005-2736(03)00021-X

24. Viola A, Gupta N. Tether and trap: regulation of membrane-raft dynamics by actin-binding proteins. *Nat Rev Immunol* (2007) 7(11):889–96. doi: 10.1038/nri2193

25. Ritchie K, Iino R, Fujiwara T, Murase K, Kusumi A. The fence and picket structure of the plasma membrane of live cells as revealed by single molecule techniques (Review). *Mol Membr Biol* (2003) 20(1):13–8. doi: 10.1080/0968768021000055698

26. Lillemeier BF, Pfeiffer JR, Surviladze Z, Wilson BS, Davis MM. Plasma membrane-associated proteins are clustered into islands attached to the cytoskeleton. *Proc Natl Acad Sci USA* (2006) 103(50):18992–7. doi: 10.1073/pnas.0609009103

27. Goyette J, Gaus K. Mechanisms of protein nanoscale clustering. *Curr Opin Cell Biol* (2017) 44:86–92. doi: 10.1016/j.ceb.2016.09.004

28. Douglass AD, Vale RD. Single-molecule microscopy reveals plasma membrane microdomains created by protein-protein networks that exclude or trap signaling molecules in T cells. *Cell* (2005) 121(6):937–50. doi: 10.1016/j.cell.2005.04.009

29. Mempel TR, Henrickson SE, von Andrian UH. T-Cell priming by dendritic cells in lymph nodes occurs in three distinct phases. *Nature* (2004) 427(6970):154–9. doi: 10.1038/nature02238

30. Gérard A, Khan O, Beemiller P, Oswald E, Hu J, Matloubian M, et al. Secondary T cell-T cell synaptic interactions drive the differentiation of protective CD8+ T cells. *Nat Immunol* (2013) 14(4):356–63. doi: 10.1038/ni.2547

31. Ueda H, Morphew MK, McIntosh JR, Davis MM. CD4+ T-cell synapses involve multiple distinct stages. *Proc Natl Acad Sci USA* (2011) 108(41):17099–104. doi: 10.1073/pnas.1113703108

32. Davis MM, Boniface JJ, Reich Z, Lyons D, Hampl J, Arden B, et al. Ligand recognition by alpha beta T cell receptors. *Annu Rev Immunol* (1998) 16:523–44. doi: 10.1146/annurev.immunol.16.1.523

33. Mazzon C, Viola A. From tango to quadrilla. *Cell Adhes Migr* (2007) 1(1):7–12. doi: 10.4161/cam.3982

34. Dustin ML, Choudhuri K. Signaling and polarized communication across the T cell immunological synapse. *Annu Rev Cell Dev Biol* (2016) 32:303–25. doi: 10.1146/annurev-cellbio-100814-125330

35. Shah K, Al-Haidari A, Sun J, Kazi JU. T Cell receptor (TCR) signaling in health and disease. *Signal Transduct Target Ther* (2021) 6(1):1–26. doi: 10.1038/s41392-021-00823-w

36. Werlen G, Palmer E. The T-cell receptor signalosome: a dynamic structure with expanding complexity. *Curr Opin Immunol* (2002) 14(3):299–305. doi: 10.1016/S0952-7915(02)00339-4

37. Friedmann KS, Bozem M, Hoth M. Calcium signal dynamics in T lymphocytes: Comparing *in vivo* and *in vitro* measurements. *Semin Cell Dev Biol* (2019) 94:84–93. doi: 10.1016/j.semcdb.2019.01.004

38. Lasserre R, Charrin S, Cuche C, Danckaert A, Thoulouze MI, de Chaumont F, et al. Ezrin tunes T-cell activation by controlling Dlg1 and microtubule positioning at the immunological synapse. *EMBO J* (2010) 29(14):2301–14. doi: 10.1038/emboj.2010.127

39. Nguyen K, Sylvain NR, Bunnell SC. T Cell costimulation *via* the integrin VLA-4 inhibits the actin-dependent centralization of signaling microclusters containing the adaptor SLP-76. *Immunity* (2008) 28(6):810–21. doi: 10.1016/j.immuni.2008.04.019

40. Grakoui A, Bromley SK, Sumen C, Davis MM, Shaw AS, Allen PM, et al. The immunological synapse: a molecular machine controlling T cell activation. *Science* (1999) 285(5425):221–7. doi: 10.1126/science.285.5425.221

41. Monks CRF, Freiberg BA, Kupfer H, Sciaky N, Kupfer A. Three-dimensional segregation of supramolecular activation clusters in T cells. *Nature* (1998) 395(6697):82–6. doi: 10.1038/25764

42. Shaw AS, Dustin ML. Making the T cell receptor go the distance: a topological view of T cell activation. *Immunity* (1997) 6(4):361–9. doi: 10.1016/S1074-7613(00)80279-4

43. Lee KH, Holdorf AD, Dustin ML, Chan AC, Allen PM, Shaw AS. T Cell receptor signaling precedes immunological synapse formation. *Science* (2002) 295 (5559):1539–42. doi: 10.1126/science.1067710

44. Delon J, Kaibuchi K, Germain RN. Exclusion of CD43 from the immunological synapse is mediated by phosphorylation-regulated relocation of the cytoskeletal adaptor moesin. *Immunity* (2001) 15(5):691–701. doi: 10.1016/S1074-7613(01)00231-X

45. Freiberg BA, Kupfer H, Maslanik W, Delli J, Kappler J, Zaller DM, et al. Staging and resetting T cell activation in SMACs. *Nat Immunol* (2002) 3(10):911–7. doi: 10.1038/ni836

46. June CH, Fletcher MC, Ledbetter JA, Schieven GL, Siegel JN, Phillips AF, et al. Inhibition of tyrosine phosphorylation prevents T-cell receptor-mediated signal transduction. *Proc Natl Acad Sci USA* (1990) 87(19):7722–6. doi: 10.1073/pnas.87.19.7722

47. Zhang W, Sloan-Lancaster J, Kitchen J, Trible RP, Samelson LE. LAT: the ZAP-70 tyrosine kinase substrate that links T cell receptor to cellular activation. *Cell* (1998) 92(1):83–92. doi: 10.1016/S0092-8674(00)80901-0

48. Chan AC, Iwashima M, Turck CW, Weiss A. ZAP-70: a 70 kd protein-tyrosine kinase that associates with the TCR zeta chain. *Cell* (1992) 71(4):649–62. doi: 10.1016/0092-8674(92)90598-7

49. Wang H, Kadlecek TA, Au-Yeung BB, Goodfellow HES, Hsu LY, Freedman TS, et al. ZAP-70: An essential kinase in T-cell signaling. *Cold Spring Harb Perspect Biol* (2010) 2(5):a002279. doi: 10.1101/cshperspect.a002279

50. Viola A, Lanzavecchia A. T Cell activation determined by T cell receptor number and tunable thresholds. *Science* (1996) 273(5271):104–6. doi: 10.1126/science.273.5271.104

51. Andres PG, Howland KC, Dresnek D, Edmondson S, Abbas AK, Krummel MF. CD28 signals in the immature immunological synapse. *J Immunol* (2004) 172 (10):5880–6. doi: 10.4049/jimmunol.172.10.5880

52. Harada Y, Ohgai D, Watanabe R, Okano K, Koiwai O, Tanabe K, et al. A single amino acid alteration in cytoplasmic domain determines IL-2 promoter activation by ligation of CD28 but not inducible costimulator (ICOS). *J Exp Med* (2003) 197(2):257–62. doi: 10.1084/jem.20021305

53. Holdorf AD, Green JM, Levin SD, Denny MF, Straus DB, Link V, et al. Proline residues in Cd28 and the src homology (Sh)3 domain of lck are required for T cell costimulation. *J Exp Med* (1999) 190(3):375–84. doi: 10.1084/jem.190.3.375

54. Liu P, Aitken K, Kong YY, Opavsky MA, Martino T, Dawood F, et al. The tyrosine kinase p56 lck is essential in coxsackievirus B3-mediated heart disease. *Nat Med* (2000) 6(4):429–34. doi: 10.1038/74689

55. Raab M, Cai YC, Bunnell SC, Heyeck SD, Berg LJ, Rudd CE. p56Lck and p59Fyn regulate CD28 binding to phosphatidylinositol 3-kinase, growth factor receptor-bound protein GRB-2, and T cell-specific protein-tyrosine kinase ITK: implications for T-cell costimulation. *Proc Natl Acad Sci USA* (1995) 92(19):8891–5. doi: 10.1073/pnas.92.19.8891

56. Watanabe R, Harada Y, Takeda K, Takahashi J, Ohnuki K, Ogawa S, et al. Grb2 and gads exhibit different interactions with CD28 and play distinct roles in CD28-mediated costimulation. *J Immunol* (2006) 177(2):1085–91. doi: 10.4049/jimmunol.177.2.1085

57. Villalba M, Coudronniere N, Deckert M, Teixeiro E, Mas P, Altman A. A novel functional interaction between vav and PKCtheta is required for TCR-induced T cell activation. *Immunity* (2000) 12(2):151–60. doi: 10.1016/S1074-7613(00)80168-5

58. Kane LP, Andres PG, Howland KC, Abbas AK, Weiss A. Akt provides the CD28 costimulatory signal for up-regulation of IL-2 and IFN-gamma but not TH2 cytokines. *Nat Immunol* (2001) 2(1):37–44. doi: 10.1038/83144

59. Chuang E, Fisher TS, Morgan RW, Robbins MD, Duerr JM, Vander Heiden MG, et al. The CD28 and CTLA-4 receptors associate with the serine/threonine phosphatase PP2A. *Immunity* (2000) 13(3):313–22. doi: 10.1016/S1074-7613(00)00031-5

60. Alegre ML, Frauwirth KA. Thompson CB. T-cell regulation by CD28 and CTLA-4. *Nat Rev Immunol* (2001) 1(3):220–8. doi: 10.1038/35105024

61. Brzostek J, Gascoigne NRJ, Rybakin V. Cell type-specific regulation of immunological synapse dynamics by B7 ligand recognition. *Front Immunol* (2016) 7:24. doi: 10.3389/fimmu.2016.00024

62. Viola A, Schroeder S, Sakakibara Y, Lanzavecchia A. T Lymphocyte costimulation mediated by reorganization of membrane microdomains. *Science* (1999) 283(5402):680–2. doi: 10.1126/science.283.5402.680

63. Tavano R, Gri G, Molon B, Marinari B, Rudd CE, Tuosto L, et al. CD28 and lipid rafts coordinate recruitment of lck to the immunological synapse of human T lymphocytes. *J Immunol Baltim Md* (2004) 173(9):5392–7. doi: 10.4049/jimmunol.173.9.5392

64. Mañes S, Viola A. Lipid rafts in lymphocyte activation and migration. *Mol Membr Biol* (2006) 23(1):59–69. doi: 10.1080/09687860500430069

65. Harder T, Kuhn M. Selective accumulation of raft-associated membrane protein LAT in T cell receptor signaling assemblies. *J Cell Biol* (2000) 151(2):199–208. doi: 10.1083/jcb.151.2.199

66. Zhang W, Trible RP, Samelson LE. LAT palmitoylation: its essential role in membrane microdomain targeting and tyrosine phosphorylation during T cell activation. *Immunity* (1998) 9(2):239–46. doi: 10.1016/S1074-7613(00)80606-8

67. Resh MD. Myristylation and palmitylation of src family members: the fats of the matter. *Cell* (1994) 76(3):411–3. doi: 10.1016/0092-8674(94)90104-X

68. Carreras-Sureda A, Abrami L, Ji-Hee K, Wang WA, Henry C, Frieden M, et al. Acylation by ZDHHC20 targets ORAI1 channels to lipid rafts for efficient Ca2 + signaling by jurkat T cell receptors at the immune synapse. Lewis RS, Swartz KJ, editors. *eLife* (2021) 10:e72051. doi: 10.7554/eLife.72051

69. Rivero-Lezcano OM, Marcilla A, Sameshima JH, Robbins KC. Wiskott-Aldrich syndrome protein physically associates with nck through src homology 3 domains. *Mol Cell Biol* (1995) 15(10):5725–31. doi: 10.1128/MCB.15.10.5725

70. Paensuwan P, Ngoenkam J, Khamsri B, Preechanukul K, Sanguansermsri D, Pongcharoen S. Evidence for inducible recruitment of wiskott-Aldrich syndrome protein to T cell receptor-CD3 complex in jurkat T cells. *Asian Pac J Allergy Immunol* (2015) 33(3):189–95. doi: 10.12932/AP0544.33.3.2015

71. Matalon O, Reicher B, Barda-Saad M. Wiskott-Aldrich syndrome protein–dynamic regulation of actin homeostasis: from activation through function and signal termination in T lymphocytes. *Immunol Rev* (2013) 256(1):10–29. doi: 10.1111/imr.12112

72. Tavano R, Contento RL, Baranda SJ, Soligo M, Tuosto L, Manes S, et al. CD28 interaction with filamin-a controls lipid raft accumulation at the T-cell immunological synapse. *Nat Cell Biol* (2006) 8(11):1270–6. doi: 10.1038/ncb1492

73. Chiang YJ, Kole HK, Brown K, Naramura M, Fukuhara S, Hu RJ, et al. Cbl-b regulates the CD28 dependence of T-cell activation. *Nature* (2000) 403(6766):216–20. doi: 10.1038/35003235

74. Kallikourdis M, Trovato AE, Roselli G, Muscolini M, Porciello N, Tuosto L, et al. Phosphatidylinositol 4-phosphate 5-kinase β controls recruitment of lipid rafts into the immunological synapse. *J Immunol Baltim Md* (2016) 196(4):1955–63. doi: 10.4049/jimmunol.1501788

75. Porciello N, Kunkl M, Viola A, Tuosto L. Phosphatidylinositol 4-phosphate 5-kinases in the regulation of T cell activation. *Front Immunol* (2016) 7:186. doi: 10.3389/fimmu.2016.00186

76. Liang Y, Cucchetti M, Roncagalli R, Yokosuka T, Malzac A, Bertosio E, et al. The lymphoid lineage-specific actin-uncapping protein rltpr is essential for costimulation *via* CD28 and the development of regulatory T cells. *Nat Immunol* (2013) 14(8):858–66. doi: 10.1038/ni.2634

77. Tian R, Wang H, Gish GD, Petsalaki E, Pasculescu A, Shi Y, et al. Combinatorial proteomic analysis of intercellular signaling applied to the CD28 T-cell costimulatory receptor. *Proc Natl Acad Sci USA* (2015) 112(13):E1594–1603. doi: 10.1073/pnas.1503286112

78. Siokis A, Robert PA, Demetriou P, Dustin ML, Meyer-Hermann M. F-Actin-Driven CD28-CD80 localization in the immune synapse. *Cell Rep* (2018) 24(5):1151–62. doi: 10.1016/j.celrep.2018.06.114

79. Intlekofer AM, Thompson CB. At The bench: Preclinical rationale for CTLA-4 and PD-1 blockade as cancer immunotherapy. *J Leukoc Biol* (2013) 94(1):25–39. doi: 10.1189/jlb.1212621

80. Brunner-Weinzierl MC, Rudd CE. CTLA-4 and PD-1 control of T-cell motility and migration: Implications for tumor immunotherapy. *Front Immunol* (2018) 9:2737. doi: 10.3389/fimmu.2018.02737

81. Rudd CE. The reverse stop-signal model for CTLA4 function. *Nat Rev Immunol* (2008) 8(2):153–60. doi: 10.1038/nri2253

82. Wei B, Dias S da R, Wang H, Rudd CE. CTL-associated antigen-4 ligation induces rapid T cell polarization that depends on phosphatidylinositol 3-kinase, vav-1, Cdc42, and myosin light chain kinase. *J Immunol* (2007) 179(1):400–8. doi: 10.4049/jimmunol.179.1.400

83. Hui E, Cheung J, Zhu J, Su X, Taylor MJ, Wallweber HA, et al. T Cell costimulatory receptor CD28 is a primary target for PD-1-mediated inhibition. *Science* (2017) 355(6332):1428–33. doi: 10.1126/science.aaf1292

84. Sánchez-Madrid F, del Pozo MA. Leukocyte polarization in cell migration and immune interactions. *EMBO J* (1999) 18(3):501–11. doi: 10.1093/emboj/18.3.501

85. Gómez-Móuton C, Abad JL, Mira E, Lacalle RA, Gallardo E, Jiménez-Baranda S, et al. Segregation of leading-edge and uropod components into specific lipid rafts during T cell polarization. *Proc Natl Acad Sci USA* (2001) 98(17):9642–7. doi: 10.1073/pnas.171160298

86. Mañes S, Ana Lacalle R, Gómez-Moutón C, Martínez-A C. From rafts to crafts: membrane asymmetry in moving cells. *Trends Immunol* (2003) 24(6):320–6. doi: 10.7554/eLife.72051

87. Mellado M, Martínez-A C, Rodríguez-Frade JM. Analysis of G-protein-coupled receptor dimerization following chemokine signaling. *Methods* (2002) 27(4):111–24. doi: 10.1016/s1046-2023(02)00093-2

88. Legler DF, Matti C, Laufer JM, Jakobs BD, Purvanov V, Uetz-von Allmen E, et al. Modulation of chemokine receptor function by cholesterol: New prospects for pharmacological intervention. *Mol Pharmacol* (2017) 91(4):331–8. doi: 10.1124/mol.116.107151

89. Jiménez-Baranda S, Gómez-Moutón C, Rojas A, Martínez-Prats L, Mira E, Ana Lacalle R, et al. Filamin-a regulates actin-dependent clustering of HIV receptors. *Nat Cell Biol* (2007) 9(7):838–46. doi: 10.1038/ncb1610

90. Skokos D, Shakhar G, Varma R, Waite JC, Cameron TO, Lindquist RL, et al. Peptide-MHC potency governs dynamic interactions between T cells and dendritic cells in lymph nodes. *Nat Immunol* (2007) 8(8):835–44. doi: 10.1038/ni1490

91. Henrickson SE, Mempel TR, Mazo IB, Liu B, Artyomov MN, Zheng H, et al. T Cell sensing of antigen dose governs interactive behavior with dendritic cells and sets a threshold for T cell activation. *Nat Immunol* (2008) 9(3):282–91. doi: 10.1038/ni1559

92. Revy P, Sospedra M, Barbour B, Trautmann A. Functional antigen-independent synapses formed between T cells and dendritic cells. *Nat Immunol* (2001) 2(10):925–31. doi: 10.1038/ni713

93. Montoya MC, Sancho D, Vicente-Manzanares M, Sánchez-Madrid F. Cell adhesion and polarity during immune interactions. *Immunol Rev* (2002) 186:68–82. doi: 10.1034/j.1600-065X.2002.18607.x

94. Friedman RS, Jacobelli J, Krummel MF. Mechanisms of T cell motility and arrest: deciphering the relationship between intra- and extracellular determinants. *Semin Immunol* (2005) 17(6):387–99. doi: 10.1016/j.smim.2005.09.006

95. Contento RL, Campello S, Trovato AE, Magrini E, Anselmi F, Viola A. Adhesion shapes T cells for prompt and sustained T-cell receptor signalling. *EMBO J* (2010) 29(23):4035–47. doi: 10.1038/emboj.2010.258

96. Quintana A, Pasche M, Junker C, Al-Ansary D, Rieger H, Kummerow C, et al. Calcium microdomains at the immunological synapse: how ORAI channels, mitochondria and calcium pumps generate local calcium signals for efficient T-cell activation. *EMBO J* (2011) 30(19):3895–912. doi: 10.1038/emboj.2011.289

97. Trebak M, Kinet JP. Calcium signalling in T cells. *Nat Rev Immunol* (2019) 19(3):154–69. doi: 10.1038/s41577-018-0110-7

98. Campello S, Lacalle RA, Bettella M, Mañes S, Scorrano L, Viola A. Orchestration of lymphocyte chemotaxis by mitochondrial dynamics. *J Exp Med* (2006) 203(13):2879–86. doi: 10.1084/jem.20061877

99. Molon B, Gri G, Bettella M, Gómez-Moutón C, Lanzavecchia A, Martínez-A C, et al. T Cell costimulation by chemokine receptors. *Nat Immunol* (2005) 6 (5):465–71. doi: 10.1038/ni1191

100. Thelen M, Stein JV. How chemokines invite leukocytes to dance. *Nat Immunol* (2008) 9(9):953–9. doi: 10.1038/ni.f.207

101. Contento RL, Molon B, Boularan C, Pozzan T, Manes S, Marullo S, et al. CXCR4–CCR5: A couple modulating T cell functions. *Proc Natl Acad Sci* (2008) 105(29):10101–6. doi: 10.1073/pnas.0804286105

102. Smith X, Schneider H, Köhler K, Liu H, Lu Y, Rudd CE. The chemokine CXCL12 generates costimulatory signals in T cells to enhance phosphorylation and clustering of the adaptor protein SLP-76. *Sci Signal* (2013) 6(286):ra65. doi: 10.1126/scisignal.2004018

103. Laufer JM, Kindinger I, Artinger M, Pauli A, Legler DF. CCR7 is recruited to the immunological synapse, acts as Co-stimulatory molecule and drives LFA-1 clustering for efficient T cell adhesion through ZAP70. *Front Immunol* (2019) 9:3115. doi: 10.3389/fimmu.2018.03115

104. Viola A, Contento RL, Molon B. T Cells and their partners: The chemokine dating agency. *Trends Immunol* (2006) 27(9):421–7. doi: 10.1016/j.it.2006.07.004

105. Dustin ML. Stop and go traffic to tune T cell responses. *Immunity* (2004) 21(3):305–14. doi: 10.1016/j.immuni.2004.08.016

106. Kallikourdis M, Viola A, Benvenuti F. Human immunodeficiencies related to defective APC/T cell interaction. *Front Immunol* (2015) 6:433. doi: 10.3389/fimmu.2015.00433

107. Hernandez PA, Gorlin RJ, Lukens JN, Taniuchi S, Bohinjec J, Francois F, et al. Mutations in the chemokine receptor gene CXCR4 are associated with WHIM syndrome, a combined immunodeficiency disease. *Nat Genet* (2003) 34(1):70–4. doi: 10.1038/ng1149

108. Balabanian K, Lagane B, Pablos JL, Laurent L, Planchenault T, Verola O, et al. WHIM syndromes with different genetic anomalies are accounted for by impaired CXCR4 desensitization to CXCL12. *Blood* (2005) 105(6):2449–57. doi: 10.1182/blood-2004-06-2289

109. Kallikourdis M, Trovato AE, Anselmi F, Sarukhan A, Roselli G, Tassone L, et al. The CXCR4 mutations in WHIM syndrome impair the stability of the T-cell immunologic synapse. *Blood* (2013) 122(5):666–73. doi: 10.1182/blood-2012-10-461830

110. Derry JM, Ochs HD, Francke U. Isolation of a novel gene mutated in wiskott-Aldrich syndrome. *Cell* (1994) 78(4):635–44. doi: 10.1016/0092-8674(94)90528-2

111. Albert MH, Notarangelo LD, Ochs HD. Clinical spectrum, pathophysiology and treatment of the wiskott-Aldrich syndrome. *Curr Opin Hematol* (2011) 18(1):42–8. doi: 10.1097/MOH.0b013e32834114bc

112. Barda-Saad M, Braiman A, Titerence R, Bunnell SC, Barr VA, Samelson LE. Dynamic molecular interactions linking the T cell antigen receptor to the actin cytoskeleton. *Nat Immunol* (2005) 6(1):80–9. doi: 10.1038/ni1143

113. Zeng R, Cannon JL, Abraham RT, Way M, Billadeau DD, Bubeck-Wardenberg J, et al. SLP-76 coordinates nck-dependent wiskott-Aldrich syndrome protein recruitment with vav-1/Cdc42-dependent wiskott-Aldrich syndrome protein activation at the T cell-APC contact site. *J Immunol Baltim Md* (2003) 171(3):1360–8. doi: 10.4049/jimmunol.171.3.1360

114. Snapper SB, Meelu P, Nguyen D, Stockton BM, Bozza P, Alt FW, et al. WASP deficiency leads to global defects of directed leukocyte migration in vitro and *in vivo*. *J Leukoc Biol* (2005) 77(6):993–8. doi: 10.1189/jlb.0804444

115. Lafouresse F, Cotta-de-Almeida V, Malet-Engra G, Galy A, Valitutti S, Dupré L. Wiskott-Aldrich syndrome protein controls antigen-presenting cell-driven CD4+ T-cell motility by regulating adhesion to intercellular adhesion molecule-1. *Immunology* (2012) 137(2):183–96. doi: 10.1111/j.1365-2567.2012.03620.x

116. Badour K, McGavin MKH, Zhang J, Freeman S, Vieira C, Filipp D, et al. Interaction of the wiskott–Aldrich syndrome protein with sorting nexin 9 is required for CD28 endocytosis and cosignaling in T cells. *Proc Natl Acad Sci* (2007) 104(5):1593–8. doi: 10.1073/pnas.0610543104

117. Massaad MJ, Oyoshi MK, Kane J, Koduru S, Alcaide P, Nakamura F, et al. Binding of WIP to actin is essential for T cell actin cytoskeleton integrity and tissue homing. *Mol Cell Biol* (2014) 34(23):4343–54. doi: 10.1128/MCB.00533-14

118. Brigida I, Zoccolillo M, Cicalese MP, Pfajfer L, Barzaghi F, Scala S, et al. T-Cell defects in patients with ARPC1B germline mutations account for combined immunodeficiency. *Blood* (2018) 132(22):2362–74. doi: 10.1182/blood-2018-07-863431

119. Randzavola LO, Strege K, Juzans M, Asano Y, Stinchcombe JC, Gawden-Bone CM, et al. Loss of ARPC1B impairs cytotoxic T lymphocyte maintenance and cytolytic activity. *J Clin Invest* (2019) 129(12):5600–14. doi: 10.1172/JCI129388

120. Piotrowski JT, Gomez TS, Schoon RA, Mangalam AK, Billadeau DD. WASH knockout T cells demonstrate defective receptor trafficking, proliferation, and effector function. *Mol Cell Biol* (2013) 33(5):958–73. doi: 10.1128/MCB.01288-12

121. Dupré L, Boztug K, Pfajfer L. Actin dynamics at the T cell synapse as revealed by immune-related actinopathies. *Front Cell Dev Biol* (2021) 9:665519. doi: 10.3389/fcell.2021.665519

122. Ren C, Yuan Q, Braun M, Zhang X, Petri B, Zhang J, et al. Leukocyte cytoskeleton polarization is initiated by plasma membrane curvature from cell attachment. *Dev Cell* (2019) 49(2):206–219.e7. doi: 10.1016/j.devcel.2019.02.023

123. Orbach R, Su X. Surfing on membrane waves: Microvilli, curved membranes, and immune signaling. *Front Immunol* (2020) 11:2187. doi: 10.3389/fimmu.2020.02187

124. Kessels MM, Qualmann B. Interplay between membrane curvature and the actin cytoskeleton. *Curr Opin Cell Biol* (2021) 68:10–9. doi: 10.1016/j.ceb.2020.08.008

125. Saarikangas J, Zhao H, Pykäläinen A, Laurinmäki P, Mattila PK, Kinnunen PKJ, et al. Molecular mechanisms of membrane deformation by I-BAR domain proteins. *Curr Biol* (2009) 19(2):95–107. doi: 10.1016/j.cub.2008.12.029

126. Postema MM, Grega-Larson NE, Neininger AC, Tyska MJ. IRTKS (BAIAP2L1) elongates epithelial microvilli using EPS8-dependent and independent mechanisms. *Curr Biol* (2018) 28(18):2876–88.e4. doi: 10.1016/j.cub.2018.07.022

127. Inamdar K, Tsai FC, Dibsy R, de Poret A, Manzi J, Merida P, et al. Full assembly of HIV-1 particles requires assistance of the membrane curvature factor IRSp53. *eLife* (2021) 10:e67321. doi: 10.7554/eLife.67321

128. Thomas A, Mariani-Floderer C, López-Huertas MR, Gros N, Hamard-Péron E, Favard C, et al. Involvement of the Rac1-IRSp53-Wave2-Arp2/3 signaling pathway in HIV-1 gag particle release in CD4 T cells. *J Virol* (2015) 89(16):8162–81. doi: 10.1128/JVI.00469-15

129. Jarsch IK, Gadsby JR, Nuccitelli A, Mason J, Shimo H, Pilloux L, et al. A direct role for SNX9 in the biogenesis of filopodia. *J Cell Biol* (2020) 219(4):e201909178. doi: 10.1083/jcb.201909178

130. Ecker M, Schregle R, Kapoor-Kaushik N, Rossatti P, Betzler VM, Kempe D, et al. SNX9-induced membrane tubulation regulates CD28 cluster stability and signalling. *eLife* (2022) 11:e67550.

131. Sens P, Plastino J. Membrane tension and cytoskeleton organization in cell motility. *J Phys Condens Matter Inst Phys J* (2015) 27(27):273103. doi: 10.1088/0953-8984/27/27/273103

132. Al-Aghbar MA, Jainarayanan AK, Dustin ML, Roffler SR. The interplay between membrane topology and mechanical forces in regulating T cell receptor activity. *Commun Biol* (2022) 5(1):1–16. doi: 10.1038/s42003-021-02995-1

Advantages of publishing in Frontiers

OPEN ACCESS
Articles are free to read for greatest visibility and readership

FAST PUBLICATION
Around 90 days from submission to decision

HIGH QUALITY PEER-REVIEW
Rigorous, collaborative, and constructive peer-review

TRANSPARENT PEER-REVIEW
Editors and reviewers acknowledged by name on published articles

Frontiers
Avenue du Tribunal-Fédéral 34
1005 Lausanne | Switzerland

Visit us: www.frontiersin.org
Contact us: frontiersin.org/about/contact

REPRODUCIBILITY OF RESEARCH
Support open data and methods to enhance research reproducibility

DIGITAL PUBLISHING
Articles designed for optimal readership across devices

FOLLOW US
@frontiersin

IMPACT METRICS
Advanced article metrics track visibility across digital media

EXTENSIVE PROMOTION
Marketing and promotion of impactful research

LOOP RESEARCH NETWORK
Our network increases your article's readership